

Investigating Phosphopantothenoylcysteine Synthetase
as a Potential Antibacterial Target

by

James D. Patrone

A dissertation submitted in partial fulfillment
of the requirements for the degree of
Doctor of Philosophy
(Medicinal Chemistry)
in The University of Michigan
2010

Doctoral Committee:

Assistant Professor Garry D. Dotson, Chair
Professor John Montgomery
Professor David H. Sherman
Associate Professor George A. Garcia
Research Professor Hollis D. Showalter

To Oscar
.....for everything you do

Acknowledgements

I wish to thank and acknowledge Dr. Garry D. Dotson, my mentor, for all that he has given me over the past five years. Garry has enabled me to grow and mature as a scientist and as a person. I thank him for challenging me and holding to high standards as well as giving me the freedom to grow and test out my own ideas. I will always be grateful for the mentorship, patience, and support he has given me over the years. I would like to acknowledge and thank Dr. George Garcia, Dr. John Montgomery, Dr. David Sherman, and Dr. Hollis Showalter for giving their time and serving on my committee. My committee has been extremely supportive in my research efforts over the past years as well as instrumental in allowing me to move forward to the next phase of my career and for that I am very thankful. I would also like to thank and acknowledge Dr. Ron Woodard for always having an open door or stopping in the Dotson Lab to talk to me and provide guidance and advice throughout my graduate career. My conversations with Dr. Woodard were always entertaining and informative and he was one of the only people to spend as much time as me in CC Little. I thank Heather Carlson for expanding my knowledge beyond the wet lab and for challenging me as well as for always having time to talk. Lastly, I would like to thank and acknowledge Dr. Jeanne Stuckey and Dr. Jennifer Meagher for their collaboration with me on my project and teaching me all I know about crystallography. Jeanne and Jennifer were not only fantastic collaborators, but really great friends and I would be willing to take a road trip to Chicago anytime.

I would like to thank the members of the Dotson Lab; Kyle Heslip, Ron Jenkins, Nicole Scott, and Jiangwei Yao. It has been a pleasure to work with these individuals over the years. I would like to thank Kyle, Nicole, and Jiangwei for their contributions to my research project. Each of these Dotson Lab members was instrumental in the completion of my research. I would like thank the Med Chem students in particular Caleb

Bates, Katrina Lexa, Ron Jenkins, Allen Brooks, Kyle Heslip, Doug Hansen, and Scott Barraza for their friendship and scholarship.

I would like to thank the beautiful Stefanie Stachura for always being there and putting up with my long work hours and craziness. Stefanie has always been there to support me emotionally and making me take a break and enjoy the real world for a while. Stefanie truly deserves all the credit for supporting me and getting me through my graduate career. I would like to thank Oscar for being a great roommate and the best friend a guy could ask for. I thank my friends here in Michigan; Caleb Bates, Jon Mortison, Nick Deprez, Katrina Lexa, Ron Jenkins, and Kyle Heslip for being the best friend a guy could ask for. You guys have always been there for me and have always kept things interesting.

Lastly, I thank the Chemistry Biology Interface (CBI) Training Grant and the Fred Lyons Fellowship for their financial support over the course of my graduate studies.

Table of Contents

Dedication	ii
Acknowledgements	iii
List of Figures	vi
List of Schemes	ix
List of Tables	x
Abstract	xi
Chapter	
1. Introduction	1
2. Synthesis and Evaluation of Intermediate Mimics of Bacterial PPCS	16
3. Co-Crystallization of Intermediate Mimics with <i>E. coli</i> PPCS	68
4. Probes of individual half Reactions of PPCS	90
5. Difluorophosphonate Mechanistic Probe	123
6. Conclusion	140

List of Figures

Figure	
1.1 Timeline of antibacterial deployment and resistance observed	1
1.2 Sales of antimicrobials by company in millions (2006)	2
1.3 Structure of phosphopantetheine	3
1.4 Phosphopantetheine and its location in acyl carrier protein and coenzyme A	4
1.5 CoA biosynthetic pathway	5
1.6 Differences in PPCS Type	6
1.7 Sequence Similarity of CoA enzymes	8
1.8 Mechanism of PPCS	9
1.9 Possible mechanisms of cysteine attack during second half reaction of PPCS	10
1.10 Proposed intermediate mimics	11
1.11 Proposed PPA analogs	12
1.12 Mechanism of nucleophilic PPA analogs	12
1.13 Mechanism of action of cysteine trap	13
2.1 Mechanism of PPCS	18
2.2 Design of Intermediate Mimics	19
2.3 Retrosynthetic Analysis of the phosphodiester mimic	19
2.4 The pyrophosphate reagent coupled assay system	26
2.5 Representative IC ₅₀ curve	27
2.6 Inhibition curves for phosphodiester 8	29
2.7 Slow-onset binding modes	30
2.8 k_{obs} versus concentration of compound 8	31
2.9 IC ₅₀ plot for phosphodiester 8 vs. ecPPCS	49
2.10 IC ₅₀ plot for phosphodiester 8 vs. efPPCS	50
2.11 IC ₅₀ plot for phosphodiester 8 vs. spPPCS	51
2.12 IC ₅₀ plot for phosphodiester 8 vs. hPPCS	52

2.13 IC ₅₀ plot for cyclic phosphodiester 10 vs. ecPPCS	53
2.14 IC ₅₀ plot for cyclic phosphodiester 10 vs. efPPCS	54
2.15 IC ₅₀ plot for cyclic phosphodiester 10 vs. spPPCS	55
2.16 IC ₅₀ plot for cyclic phosphodiester 10 vs. hPPCS	56
2.17 IC ₅₀ plot for sulfamate 17 vs. ecPPCS	57
2.18 IC ₅₀ plot for sulfamate 17 vs. efPPCS	58
2.19 IC ₅₀ plot for sulfamate 17 vs. spPPCS	59
2.20 IC ₅₀ plot for sulfamate 17 vs. hPPCS	60
2.21 IC ₅₀ plot for sulfamate 19 vs. ecPPCS	61
2.22 IC ₅₀ plot for sulfamate 19 vs. efPPCS	62
2.23 IC ₅₀ plot for sulfamate 19 vs. spPPCS	63
2.24 IC ₅₀ plot for sulfamate 19 vs. hPPCS	64
3.1 First Inhibitors of PPCS	69
3.2 Co-crystals of PPCS [15mg/ml] and Inhibitor 8 from Nextall PEG screen	70
3.3 Phosphodiester mimic 8 bound to PPCS domain	72
3.4 Overlay of phosphodiester 8 and PPCS (blue) with 1U7Z (yellow)	72
3.5 Nucleotide binding pocket of PPCS with phosphodiester 8	73
3.6 Asn210Asp mutation in the active site	74
3.7 Phosphopantothenate binding pocket of PPCS with phosphodiester 8	74
3.8 Co-crystals of PPCS and 10 (left) and PPCS (right) and 17	76
3.9 Emerald Wizard Screen	76
3.10 Sulfamate mimic 17 bound to PPCS domain	78
3.11 Overlay of phosphodiester 8 and sulfamate 17	78
3.12 Nucleotide binding pocket of PPCS with sulfamate 17	79
3.13 Phosphopantothenate binding pocket of PPCS with sulfamate 17	79
3.14 Cyclic phosphodiester 10 bound to PPCS domain	81
3.15 Overlay of cyclic phosphodiester 10 and phosphodiester 8	82
3.16 Nucleotide binding pocket with cyclic phosphodiester 10	82
3.17 Phosphopantothenate binding pocket with cyclic phosphodiester 10	83
4.1 Mechanism of both half reactions of PPCS	90
4.2 Known inhibitors of bacterial and malarial growth	91

4.3 Proposed PPA analogs	91
4.4 Mechanism of proposed PPA analog inhibitors	92
4.5 Examples of vinyl sulfones in literature	92
4.6 Mechanism of vinyl sulfone intermediate mimic	93
4.7 Kinase assay	96
4.8 Kinase assay results	96
4.9 Velocity versus PPA concentration	97
4.10 K_m^{app} versus [I]	98
4.11 Retrosynthetic analysis of vinyl sulfone intermediate mimic	99
5.1 Difluorophosphonate inhibitor of ASA-DH	123
5.2 Proposed difluorophosphonate electrophilic trap and its mechanism of action	124
5.3 Retrosynthetic analysis of proposed difluorophosphonate mimic	125
5.4 Alternative esters	127
5.5 Synthesis of phosphonates	129
5.6 TBAF method of installing difluorophosphonate	132
6.1 Mechanism of intermediate mimic inhibition	140
6.2 Selective inhibitors of PPCS	141

List of Schemes

Scheme	
2.1 Synthesis of phosphite 2	20
2.2 Synthesis of tribenzoyl cytidine 4	21
2.3 Synthesis of diol 6	21
2.4 Synthesis of phosphodiester mimics 8 & 10	22
2.5 Synthesis of NHS ester 13	24
2.6 Synthesis of Diol 15	24
2.7 Synthesis of sulfamate mimics	25
4.1 Synthesis of proposed thiol PPA analog	94
4.2 Synthesis of amine PPA analog	95
4.3 Synthesis of Boc protected vinyl sulfone	99
4.4 Synthesis of phthaloyl protected vinyl sulfone	100
4.5 Synthesis of PMB protected vinyl sulfone	100
4.6 Synthesis of tribenzoyl cytidine amine	101
4.7 Coupling of two fragments	101
4.8 Synthesis of N-Boc sulfones	102
4.9 Synthesis of vinyl sulfone PPA analog	104
5.1 Synthesis of NHS ester	125
5.2 Model reaction of DCC coupling	126
5.3 C-C bond forming reaction	126
5.4 Model reaction of phosphonate linkage	127
5.5 Synthesis of β -alanine fragments	128
5.6 Alternative difluorophosphonate strategy	130

List of Tables

Table	
2.1 IC ₅₀ values of intermediate mimics	28
3.1 Data collection statistics for structure of phosphodiester 8 bound PPCS	71
3.2 Data collection statistics for structure of sulfamate 17 bound PPCS	77
3.3 Data collection statistics for structure of phosphodiester 10 bound PPCS	81
5.1 Attempts to install electrophilic fluorine	130

Abstract

Phosphopantothenoylcysteine synthetase (PPCS) is the second enzyme in the universal Coenzyme A (CoA) biosynthetic pathway. PPCS is responsible for catalyzing the condensation of 4'-phosphopantothenate (PPA) and L-cysteine via nucleotide triphosphate activation of PPA. PPCSs have been broadly classified into three types (Type I-III) based upon expression profile and nucleotide triphosphate specificity. Type I PPCSs are found in a majority of bacteria and archaea, utilize CTP for activation of PPA in the first half reaction, and are expressed as the C-terminal domain of a fusion protein with phosphopantothenoylcysteine decarboxylase (PPCDC). Type II PPCSs are in eukaryotes, utilize both CTP and ATP, and expressed separately from PPCDC as a monofunctional enzyme. Type III PPCSs are found in certain bacteria, utilize CTP, and are expressed as a monofunctional enzyme. Based upon the difference in nucleotide triphosphate specificity and PPCS type between human and bacteria, PPCS was chosen for exploration as a possible novel antibacterial target.

Four mimics of the activated intermediate produced from the first half reaction catalyzed by PPCS were synthesized in twelve steps in average of 18% overall yield. These four intermediate mimics were tested in vitro for PPCS inhibition against PPCS from *E. coli*, *E. faecalis*, *S. pneumoniae*, and human. IC_{50} s were obtained for all four intermediate mimics and the best mimic had a K_i of 24 nM against efPPCS. The best intermediate mimic displayed low nanomolar potency versus the bacterial forms of PPCS while displaying 100-1000 fold selectivity for the bacterial PPCS over human PPCS. Further, three of the intermediate mimics were used in a structural study to elucidate how they bind within the PPCS active site. The co-crystal structures of PPCS and the three intermediate mimics were solved to 2.11-2.37 Å. Analogs of PPA where the carboxylate was replaced with either an amine or thiol. The phosphorylated thiol PPA mimic was found to act as a competitive inhibitor of PPCS with respect to PPA with a K_i of 12 μM. This study shows that it is possible to selectively inhibit bacterial PPCS

over human PPCS and thus PPCS represents an antibacterial target worthy of further investigation.

Chapter 1

Introduction

Since the discovery of the sulfa drugs in the mid 1930s, antibacterial research has provided society with unprecedented improvements in quality of life in dealing with a very wide range of pathogens.¹ Despite the tremendous benefits gained from antibacterial agents, antibacterial resistant strains of bacteria are emerging at a rapid pace due to questionable and unnecessary antibiotic usage, and pose a major threat to public health.² Nowhere is this phenomenon more apparent than in hospitals and more specifically intensive care units (ICUs).³ Due to this current state of antibiotic resistance in the public health sector it is imperative that alternative antibiotic targets be investigated in hopes of producing novel antibacterial agents with new targets and mechanisms of action.

Unfortunately, in response to this emerging crisis the pace at which novel antibiotics with new targets have been entering the market has slowed.³ Only two new chemical classes of antibacterial agents, the oxazolidinones and lipopeptides, have been introduced since 1970 and resistance to these agents has already been observed (**Figure 1.1**).⁴ Currently, only nine of the fifteen major pharmaceutical companies in the United

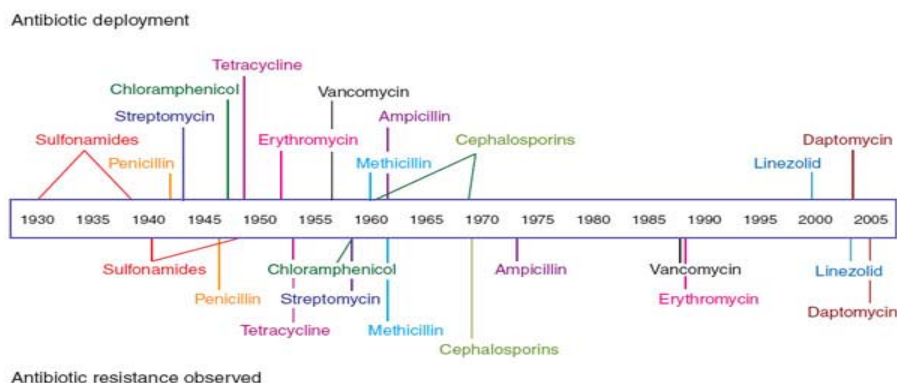


Figure 1.1: Timeline of antibacterial deployment and resistance observed⁴

States have active research programs in antimicrobial agents. There are several contributing factors that have led to the major pharmaceutical sector shifting its research focus from antimicrobials to other areas of interest.

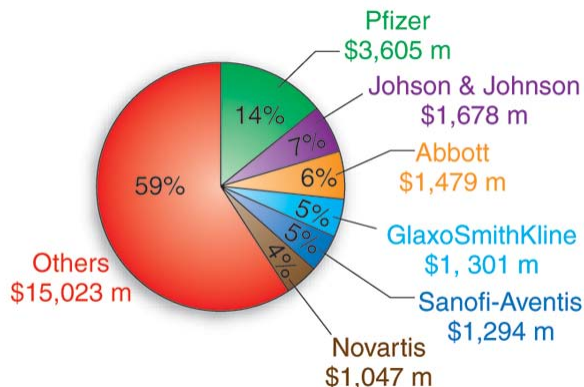


Figure 1.2: Sales of antimicrobials by company in millions (2006)⁵

This shift in research focus is in part due to the fact that antimicrobial agents are not very profitable commodities as compared to agents in other therapeutic areas. Despite the antimicrobial market being quite substantial as a whole with sales of \$25.5 billion in 2007, only three individual antimicrobial agents generated more than \$1 billion in sales in 2007.⁶ One cause of this low profitability for antimicrobials is the short duration of administration. An effective antimicrobial agent would have an acute dosing regimen, usually lasting only two weeks, which is in stark contrast to the chronic dosing regimen of an erectile dysfunction or cholesterol lowering agent, which are regularly taken over the course of years and thus create a disparity in profit window. Another factor limiting the profitability of an antimicrobial agent is the heavily saturated antimicrobial market. As of 2006, there were 21 total classes of antimicrobials of which 4 classes represented 72% of the market.⁶ In order to gain a foothold in the antibacterial market, a novel agent would not only be competing against these already established antimicrobials, but it would also be competing against their overwhelming number of less expensive generic alternatives.⁶ Further evidence of the saturated antimicrobial market can be seen by looking at the market sales of the large pharmaceutical companies (**Figure 1.2**).⁵ While several large pharmaceutical companies such as Pfizer and Johnson and Johnson still have a moderate market share, 59% of the market is comprised of various smaller companies.⁵

Another factor that has driven many major pharmaceutical companies out of antimicrobial research is the stringent FDA regulations associated with bringing a new antimicrobial agent to the market. Despite antibacterial agents requiring relatively short clinical trials, the FDA is requiring data to prove that a new anti-infective agent is superior to the current treatment rather than just equivalent. Since 2008, the FDA has denied four of six New Drug Applications (NDA) for antibacterial agents based upon the results from the Phase III trial.⁷ Failure from a costly Phase III trial is a huge deterrent for pharmaceutical companies to continue anti-infective research programs. The average Phase III trial costs \$21,000 per patient and as the FDA requirements are becoming more stringent the cost rises because more patients are necessary to meet the rising demands.⁸

As major pharmaceutical companies reduce antibacterial research, the onus has been placed on smaller biotech companies and the academic sector. While small biotech companies and academia cannot conduct large phase II and phase III trials, they can continue to explore novel chemical scaffolds and targets. To this end, my research project has been studying phosphopantothencysteine synthetase (PPCS) as a new antibacterial target.

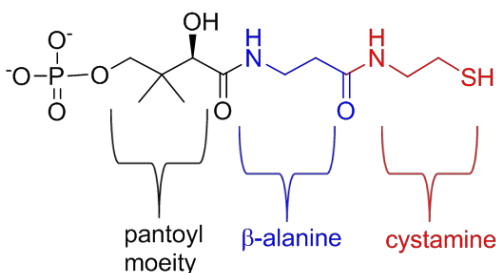


Figure 1.3: Structure of phosphopantetheine

Phosphopantetheine-containing compounds are essential cofactors across all kingdoms of life. Phosphopantetheine is a dipeptide composed of cystamine and β -alanine modified with a phosphorylated pantoic acid group, which is derived from α -ketoisovalerate (**Figure 1.3**). Phosphopantetheine-containing biomolecules are responsible for carbonyl activation and transfer in a variety of biological reactions through the thiol group on the terminal cystamine portion. Phosphopantetheine is found attached to the 5' phosphate in Coenzyme A (CoA) and to a post-translationally

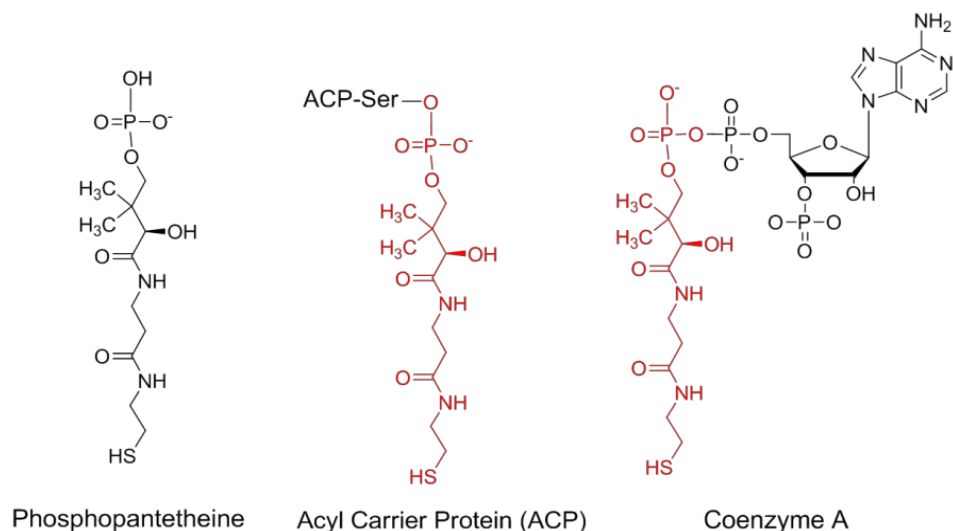


Figure 1.4: Phosphopantetheine and its location in acyl carrier protein and coenzyme A modified, conserved serine in acyl carrier protein (ACP) (**Figure 1.4**). It has been estimated through a survey of the Braunschweig enzyme database (BRENDA) that up to 8-12% of all known cellular enzymatic activity utilizes phosphopantetheine in the form of CoA, ACP, or one of their thioesters.⁹ Among these, phosphopantetheine plays an important role in the bacterial fatty acid synthase Type II (FAS II) and tricarboxylic acid cycle (TCA), which are both essential for bacterial growth.^{10, 11}

Pantothenate (vitamin B₅), discovered in 1933 by Williams et al., is the common precursor for the synthesis of phosphopantetheine across all kingdoms of life. Humans and animals rely on the uptake of exogenous pantothenate via a Na⁺ coupled multivitamin transporter.¹² Conversely, most bacteria, fungi, and plants are able to synthesize pantothenate from α -ketoisovalerate and β -alanine. *E. coli* can produce up to 15 times the pantothenate required for CoA biosynthesis, and enough pantothenate to sustain a mammal without further vitamin B₅ supplementation.¹² Whether taken up or synthesized de novo, pantothenate is converted to phosphopantetheine and eventually CoA by the universal CoA biosynthetic pathway (**Figure 1.5**).

The CoA biosynthetic pathway consists of five enzymatic steps starting from pantothenate.¹³⁻¹⁸ Brown and Abiko were responsible for the early elucidation of the pathway in the late 1950's and 1960's.¹³⁻¹⁸ The first step in the pathway is the ATP-dependent phosphorylation of the 4' position hydroxyl group on pantothenate by pantothenate kinase (PanK) to yield 4'-phosphopantothenic acid (PPA).¹³ The second

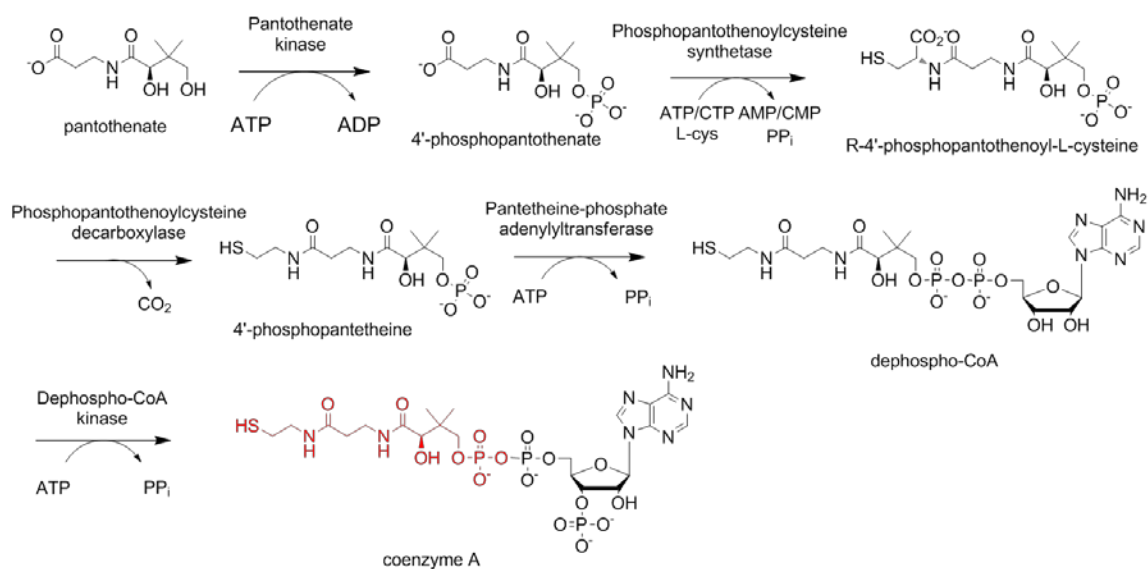


Figure 1.5: CoA biosynthetic pathway

step is the formation of an amide bond between L-cysteine and PPA to form 4'-phosphopantothenoylcysteine, which is catalyzed using a nucleotide triphosphate co-substrate by PPCS.^{13, 19} 4'-phosphopantothenoylcysteine is then oxidatively decarboxylated by phosphopantothenoylcysteine decarboxylase (PPCDC) to yield 4'-phosphopantetheine. The fourth step is the condensation of 4'-phosphopantetheine with the α phosphate of ATP, adding an AMP moiety to 4'-phosphopantetheine to produce dephospho CoA. Lastly, de-phospho CoA is phosphorylated on the 3' alcohol of the ribose ring by de-phospho CoA kinase (DPCK). Importantly, Brown established that in order for PPA to be converted into CoA using isolates from *Proteus morgani*, cytidine triphosphate (CTP) was required.¹³ Specifically, CTP was needed for PPCS to catalyze the amide bond formation in the second step of the pathway.¹³

Despite this pioneering work conducted in the 1950's and 1960's, it was not until the early 2000's that all of the genes for the CoA pathway in human and bacteria were cloned and characterized.¹⁹ With the ability to clone, overexpress, and purify all the enzymes in the pathway, the CoA biosynthetic pathway has been fully elucidated. Recent studies have also focused on studying the differences between human and bacterial CoA biosynthesis and ways to exploit these differences in order to find novel antibacterial targets.²⁰⁻²⁵

PPCS, which is responsible for the condensation of L-cysteine and PPA, was chosen as the target to explore in this study. Due to the differences in PPCSs across the various species of life, PPCSs have been put into three different classes (Types I-III). Type I PPCSs are found in a majority of bacteria and archaea, utilize CTP for activation of PPA in the first half reaction, and are expressed as the C-terminal domain of a fusion protein with PPCDC (Figure 1.6). Type II PPCSs are found in eukaryotes, utilize both CTP and ATP, and expressed separately from PPDC as a monofunctional enzyme. Type III PPCSs are found in certain bacteria, utilize CTP in the first half reaction of PPCS, and are expressed as a monofunctional enzyme. In *E. coli*, a prototypical Type I PPCS, the PPCS domain and PPCDC domain are encoded on the same gene and expressed as a homododecamer. The PPCDC domain consists of serine 2 through asparagine 190, while the PPCS domain consists of the C-terminal amino acids from isoleucine 191 to arginine 406 (Figure 1.6). In humans, PPCS (Type II) and PPCDC are encoded on two separate genes and PPCS is expressed as dimer.

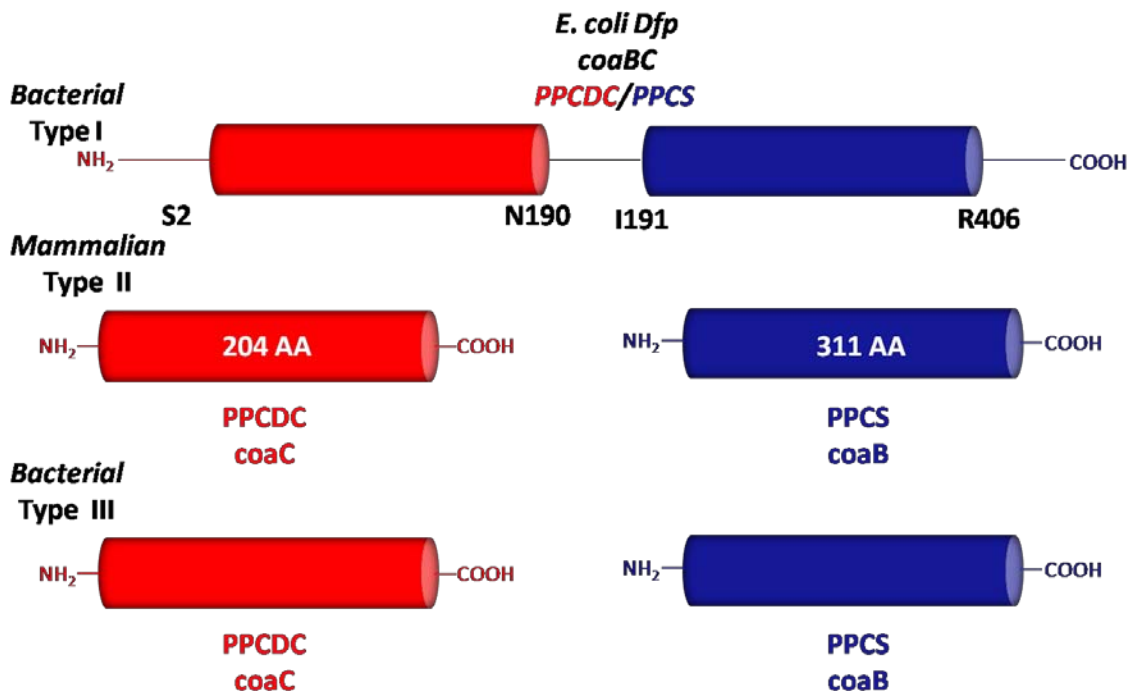


Figure 1.6: Differences in PPCS Type

PPCS was chosen for exploration as a novel antibacterial target because it was a well validated target based upon previous studies. In the mid 1980s, Spitzer and coworkers characterized a conditional lethal *E. coli* mutant which was auxotrophic for

pantothenate at 30°C and at non-permissive temperatures (42°C) did not grow even in media supplemented with pantothenate.²⁶ The affected gene locus was designated *dfp* (dna flavoprotein). Recently, the *dfp* gene product was identified as a bifunctional protein composed of PPCS and PPCDC, and the temperature sensitive allele characterized as a mutation within the PPCDC domain of the protein leading to decreased solubility of the PPCDC/PPCS protein at non-permissive temperatures.²⁷ It has also been shown using genome-wide transposon mutagenesis studies in *E. coli* that the gene responsible for PPCS/PPCDC is essential for bacterial growth.²⁶ In this study, transposable elements were allowed to randomly insert into the *E. coli* genome in the presence and absence of extra-chromosomal copies of genes involved in mammalian CoA biosynthesis. In the absence of the extra-chromosomal copies, no viable mutants were isolated containing transposon insertions in genes associated with the biosynthesis of phosphopantetheine-containing molecules from pantothenate. However, when the extra-chromosomal copies were present, they were able to complement the lethal insertions and cells were isolated containing transposable elements in genes associated with CoA biosynthesis. Therefore, each catalytic step in the vitamin B₅ to CoA pathway has been shown to be required. Furthermore, the absence of a transport system for the phosphorylated intermediates in the pathway eliminates the possibility of extra-cellular CoA uptake or transport of phosphorylated precursors from the growth medium.

Further, an amino acid sequence similarity analysis revealed low sequence similarity between human PPCS and most bacterial PPCSs (**Figure 1.7**).²⁸ When comparing human PPCS to the various bacterial PPCSs in **Figure 1.7** (right column), there is less than 20% similarity between human PPCS and ecPPCS and the other Type I PPCSs and only 20-30% similarity with *E. faecalis* and *S. pneumoniae* PPCSs (Type III).²⁸ This low sequence similarity between bacterial and human PPCSs provides evidence that the selective inhibition of bacterial PPCS by a therapeutic agent is possible.²⁸ ecPPCS shows 20% or greater similarity when compared to every other bacteria in **Figure 1.7** (left column) and in most cases greater than 40%, which suggests that targeting PPCS should lead to a molecule with broad spectrum antibacterial properties.²⁸

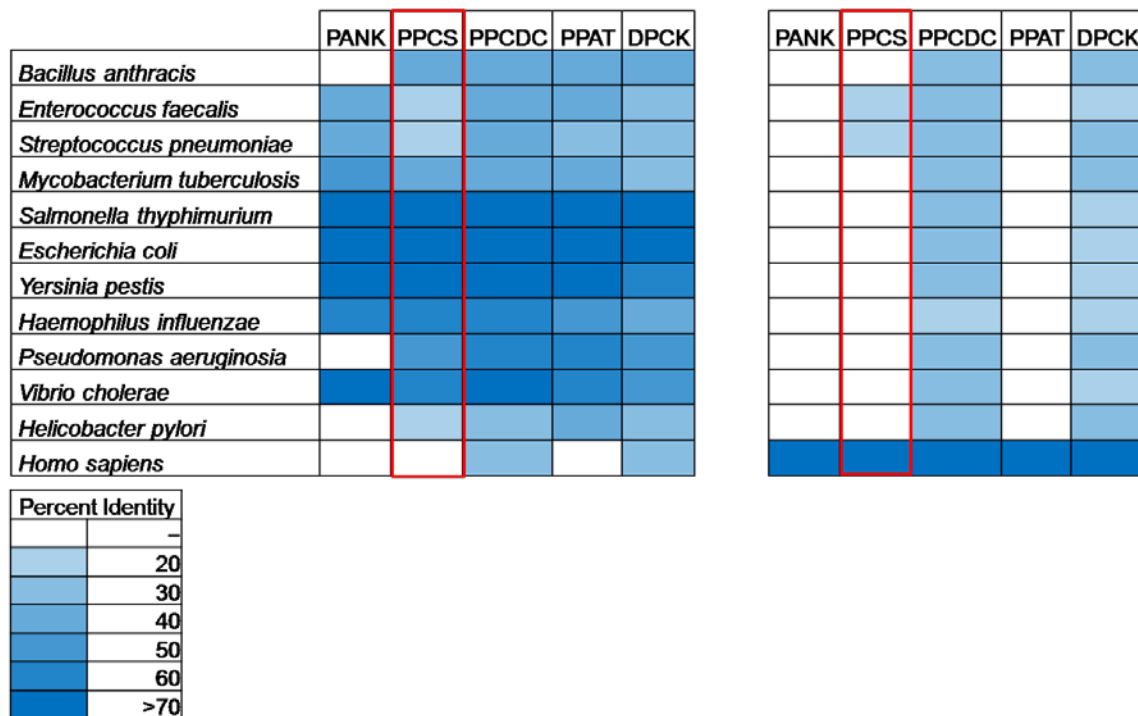


Figure 1.7: Sequence Similarity of CoA enzymes. Left column is sequence similarity relative to *E. coli* PPCS. Right column is sequence similarity relative to human PPCS.²⁸

Another attractive feature of PPCS as a possible drug target is that the structure for both a mutant *E. coli* PPCS and human PPCS have been solved in literature.^{19, 24} The crystal structure of a mutant PPCS from *E. coli* provides us with information on the important binding contacts within the active site. The conditions used within this study provide us with a foundation to begin our own structural study of PPCS with our proposed inhibitors bound in the active site. The crystal structure can be used as a model and allow for the solving of any future crystal structures using molecular replacement, which is easier and less time consuming than having to use multiple isomorphous replacement. Our studies would allow us to look at the differences between the structure of the intermediate mimic and its binding mode in order to glean information that will allow for the design of second generation inhibitors.

Mechanistically, bacterial PPCS (Type I & III) is responsible for binding PPA and catalyzing its reaction with CTP to form the active acyl-cytidylate intermediate in the first half reaction (**Figure 1.7**).^{22, 29} Cysteine then enters the active site of the enzyme and initiates a nucleophilic displacement of the cytidine monophosphate (CMP) to form a peptide bond and release the product, 4'-phosphopantothenoylcysteine (PPC) in the

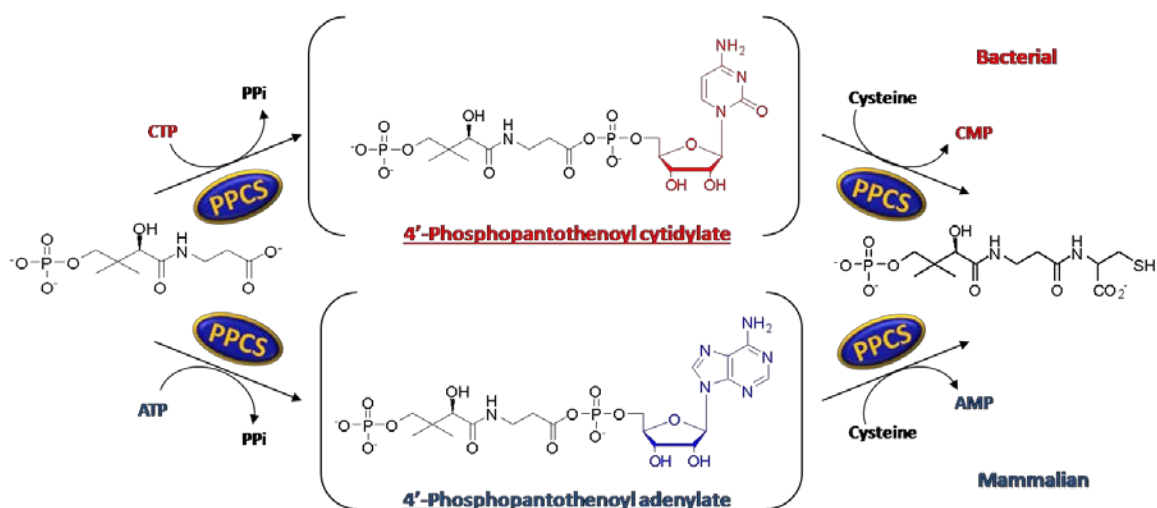


Figure 1.8: Mechanism of PPCS

second half reaction.²² The 4'-phosphopantothenoylcysteine is oxidatively decarboxylated by PPCDC to form 4'-phosphopantetheine.²² Conversely, Human PPCS (Type II) can utilize both CTP and ATP in catalyzing the first half reaction of PPCS and had been reported to display a 4:1 preference for ATP over CTP, which presented an opportunity for differential inhibition of bacterial and human PPCS.^{30, 31} Utilizing ATP in the first half reaction of human PPCS catalysis leads to the formation of an activated adenylate intermediate, this differs drastically in the size and binding contacts of the nucleobase as compared to the activated cytidylate intermediate formed in bacterial PPCS catalysis (**Figure 1.8**). By designing inhibitors to mimic the activated cytidylate intermediate of bacterial PPCS catalysis, one should be able to utilize a majority of the binding contacts of the activated intermediate resulting in tight binding, while maintaining selectivity based upon the differences in the nucleotide binding pockets between human and bacterial PPCS.

It is known that cysteine attacks the carbonyl on the mixed anhydride of the activated intermediate, forms the amide bond in PPA and releases CMP, it is not known whether the amine of cysteine simply attacks the activated intermediate and forms the amide bond in PPA or if the more nucleophilic thiol of cysteine initiates the attack on the activated intermediate to form a labile thioester that rearranges to form the more thermodynamically stable amide bond of PPA (**Figure 1.9**). Identification of the cysteine binding site and the orientation of cysteine binding to the PPCS-acyl cytidylate complex,

have yet to be ascertained and have mechanistic implications toward the ability of PPCS to discriminate between cysteine and serine.²¹ This discrimination has critical biological implications, since incorporation of serine would lead to the production of potentially toxic CoA antimetabolites. Attempts by other researchers at obtaining PPCS with cysteine bound at the active site have not been successful due to product formation upon adding cysteine to the intermediate-bound enzyme. A definitive answer to the mechanism of selective cysteine incorporation awaits a PPCS structure with a substrate analog bound at the active site.

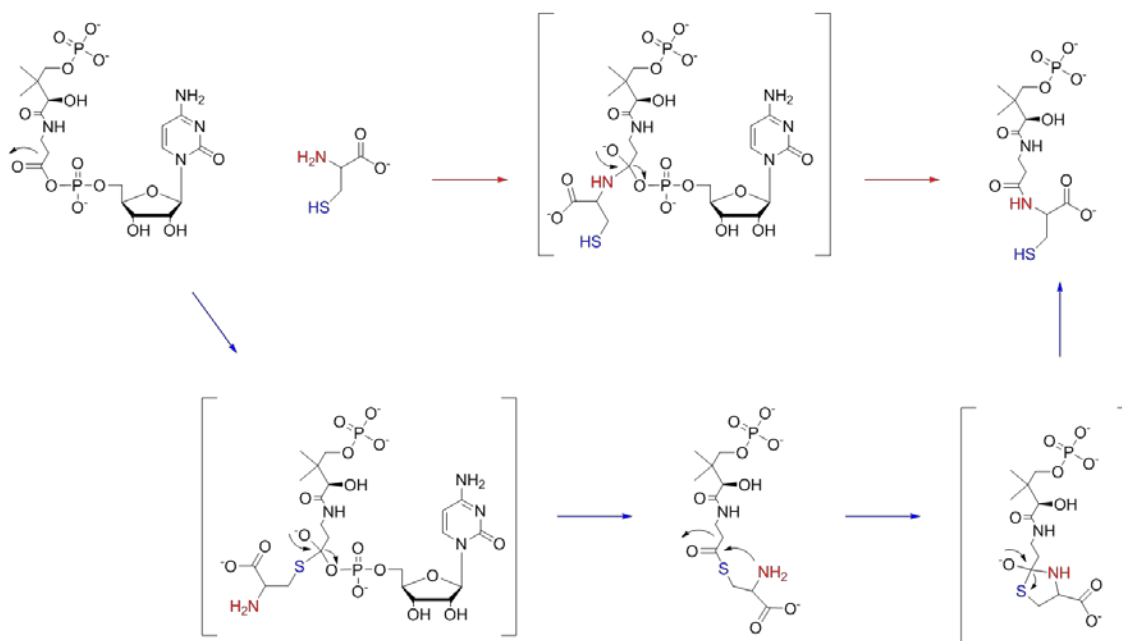


Figure 1.9: Possible mechanisms of cysteine attack during second half reaction of PPCS

Synthesize and evaluate phosphodiester and sulfamate PPCS intermediate mimics against PPCS from *E. coli*, *E. faecalis*, *S. pneumoniae*, and Human

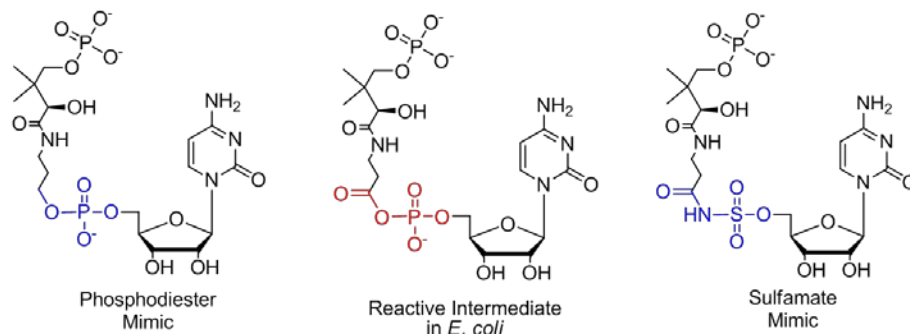


Figure 1.10: Proposed intermediate mimics

Based on this strategy, phosphodiester and sulfamate intermediate mimics were designed (**Figure 1.10**). The phosphodiester mimic was designed by removing the electrophilic carbonyl attacked during the second half reaction from the activated intermediate. This proposed inhibitor should be able to utilize the binding contacts of the intermediate mimic within PPCS's active site, but is not enzymatically competent due to the inability of cysteine to attack an activated carbonyl, form an amide bond, and release CMP. The sulfamate mimic replaces the internal mixed anhydride of the activated intermediate with a less chemically labile sulfamate linkage. The proposed sulfamate inhibitor maintains the electrophilic carbonyl attacked during the second half reaction, but the negative charge of the phosphate has been replaced. This strategy should provide information about the ability of PPCS to accommodate differences in charge and geometry in the internal linkage of the intermediate mimics.

Structural study of PPCS from *E. coli* co-crystallized with intermediate mimics to elucidate the differences in binding contacts for selectivity and potency

Beyond using these first generation inhibitors to selectively inhibit bacterial PPCS, the intermediate mimics can be used in structural studies. Obtaining IC₅₀ values for the inhibitors will give us a relative idea of how structural changes to the intermediate mimic are accommodated by PPCS, but a structural study will show us which binding contacts are most important when targeting PPCS. This information will be vital in designing second generation inhibitors for designing potency and selectivity.

Synthesize and evaluate mechanistic probes of PPCS

In an alternative strategy, PPCS can be studied using mechanistic probes designed to be reactive with the other substrates within the enzyme active site. The first set of mechanistic probes is a pair of analogs of PPA (**Figure 1.11**). These molecules were designed by replacing the carboxylic acid of PPA with either a thiol or an amine. Upon incubation of the nucleophilic PPA mimic with CTP and PPCS, the PPA mimic should

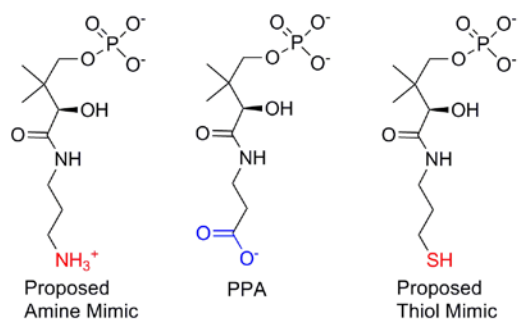


Figure 1.11: Proposed PPA analogs

attack the α phosphate of CTP displacing pyrophosphate and concurrently forming an intermediate mimic analogous to the proposed phosphodiester inhibitor in the PPCS active site (**Figure 1.12**).

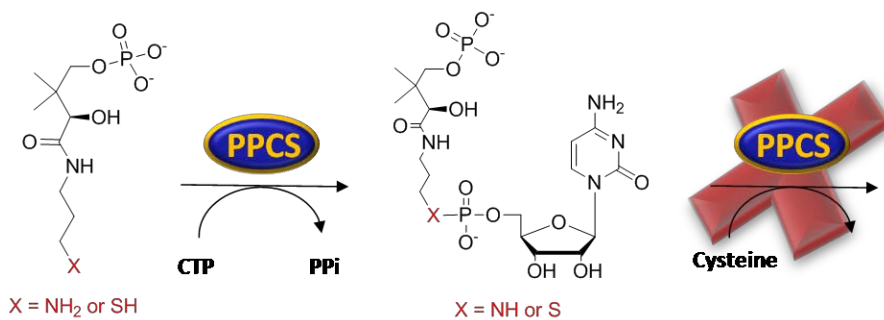


Figure 1.12: Mechanism of nucleophilic PPA analogs

The alternative mechanistic probe was designed to study the mechanism of the cysteine attack during the second half reaction. To study the mechanism of the nucleophilic attack during the second half reaction, a vinyl sulphone intermediate mimic was designed to trap the cysteine nucleophile (**Figure 1.13**).

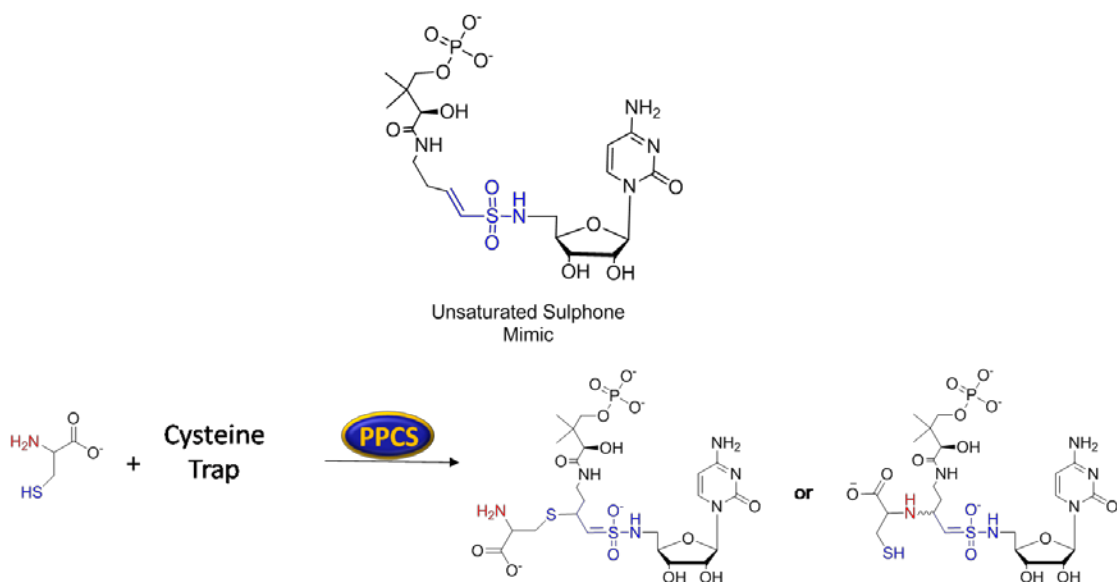


Figure 1.13: Mechanism of action of cysteine trap

PPCS is an interesting and attractive target for possible novel antibacterial agents. To date PPCS has not been studied as a potential antibacterial target and as such there is little information about how to specifically target bacterial PPCS over human PPCS. This study represents the first time probes or inhibitors have been synthesized and evaluated, based upon their action on PPCS to gather information about how to specifically inhibit bacterial PPCS. These probes represent the first attempt to prove PPCS is a viable antibacterial target. While these molecules are not potential drug candidates due to their physiochemical property, these probes are the first inhibitors of PPCS and can be used as a proof of concept and to gather information about PPCS for the design of later generation inhibitors.

References

1. Levin, S. A.; Andreasen, V., Disease transmission dynamics and the evolution of antibiotic resistance in hospitals and communal settings - Commentary. *Proceedings of the National Academy of Sciences of the United States of America* **1999**, 96, (3), 800-801.
2. Beovic, B., The issue of antimicrobial resistance in human medicine. *International Journal of Food Microbiology* **2006**, 112, (3), 280-287.
3. Levin, B. R.; Bonten, M. J. M., Cycling antibiotics may not be good for your health. *Proceedings of the National Academy of Sciences of the United States of America* **2004**, 101, (36), 13101-13102.
4. Clatworthy, A. E.; Pierson, E.; Hung, D. T., Targeting virulence: a new paradigm for antimicrobial therapy. *Nat Chem Biol* **2007**, 3, (9), 541-548.
5. Christoffersen, R. E., Antibiotics--an investment worth making? *Nature Biotechnology* **2006**, 24, (12), 1512(3).
6. Kresse, H.; Belsey, M. J.; Rovini, H., The antibacterial drugs market. *Nature Reviews Drug Discovery* **2007**, 6, (1), 19(2).
7. Jarvis, L. M., Antibiotics Yo-Yo. *Chemical and Engineering News* 2010, pp 30-33.
8. Fletcher, L., Cubist highlights FDA's antibiotic resistance. *Nat Biotech* **2002**, 20, (3), 206-207.
9. Spry, C.; Kirk, K.; Saliba, K. J., Coenzyme A biosynthesis: an antimicrobial drug target. *Fems Microbiology Reviews* **2008**, 32, (1), 56-106.
10. Zhang, Y.-M.; White, S. W.; Rock, C. O., Inhibiting Bacterial Fatty Acid Synthesis. *Journal of Biological Chemistry* **2006**, 281, (26), 17541-17544.
11. Strauss, E.; Kinsland, C.; Ge, Y.; McLafferty, F. W.; Begley, T. P., Phosphopantothenoylcysteine Synthetase from *Escherichia coli*. Identification and characterization of the last unidentified Coenzyme A biosynthetic enzyme in bacteria. *J. Biol. Chem.* **2001**, 276, (17), 13513-13516.
12. Leonardi, R.; Zhang, Y. M.; Rock, C. O.; Jackowski, S., Coenzyme A: Back in action. *Progress in Lipid Research* **2005**, 44, (2-3), 125-153.
13. Brown, G. M., The Metabolism of Pantothenic Acid. *Journal of Biological Chemistry* **1959**, 234, (2), 370-378.
14. Abiko, Y., Investigations on Pantothenic Acid and Its Related Compounds: X. Biochemical Studies (5). Purification and Substrate Specificity of Phosphopantothenoylcysteine Decarboxylase from Rat Liver. *J Biochem* **1967**, 61, (3), 300-308.
15. Abiko, Y., Investigations on Pantothenic Acid and Its Related Compounds: IX. Biochemical Studies (4). Separation and Substrate Specificity of Pantothenate Kinase and Phosphopantothenoylcysteine Synthetase. *J Biochem* **1967**, 61, (3), 290-299.
16. Abiko, Y.; Suzuki, T.; Shimizu, M., Investigations on Pantothenic Acid and Its Related Compounds XI. Biochemical Studies (6). A Final Stage in the Biosynthesis of CoA. *J Biochem* **1967**, 61, (3), 309-312.
17. Abiko, Y.; Tomikawa, M.; Shimizu, M., Further Studies on Phosphopantothenoylcysteine Synthetase. *J Biochem* **1968**, 64, (1), 115-117.
18. Suzuki, T.; Abiko, Y.; Shimizu, M., Investigations on Pantothenic Acid and Its Related Compounds XII. Biochemical Studies (7). Dephospho-CoA Pyrophosphorylase and Dephospho-CoA Kinase as a Possible Bifunctional Enzyme Complex. *J Biochem* **1967**, 62, (6), 642-649.

19. Stanitzek, S.; Augustin, M. A.; Huber, R.; Kupke, T.; Steinbacher, S., Structural Basis of CTP-Dependent Peptide Bond Formation in Coenzyme A Biosynthesis Catalyzed by Escherichia coli PPC Synthetase. *Structure* **2004**, 12, (11), 1977-1988.
20. Strauss, E.; Begley, T. P., The Antibiotic Activity of N-Pentylpantothenamide Results from Its Conversion to Ethyldeithia-Coenzyme A, a Coenzyme A Antimetabolite. *Journal of Biological Chemistry* **2002**, 277, (50), 48205-48209.
21. Kupke, T., Active-site residues and amino acid specificity of the bacterial 4'-phosphopantothenoylcysteine synthetase CoaB. *European Journal of Biochemistry* **2004**, 271, (1), 163-172.
22. Kupke, T., Molecular Characterization of the 4'-Phosphopantothenoylcysteine Synthetase Domain of Bacterial Dfp Flavoproteins. *J. Biol. Chem.* **2002**, 277, (39), 36137-36145.
23. Strauss, E.; Tadhg, P. B., The Selectivity for Cysteine over Serine in Coenzyme A Biosynthesis. *ChemBioChem* **2005**, 6, (2), 284-286.
24. Manoj, N.; Strauss, E.; Begley, T. P.; Ealick, S. E., Structure of Human Phosphopantothenoylcysteine Synthetase at 2.3 Å Resolution. *Structure* **2003**, 11, (8), 927-936.
25. Zhao, L.; Allanson, N. M.; Thomson, S. P.; Maclean, J. K. F.; Barker, J. J.; Primrose, W. U.; Tyler, P. D.; Lewendon, A., Inhibitors of phosphopantetheine adenylyltransferase. *European Journal of Medicinal Chemistry* **2003**, 38, (4), 345-349.
26. Spitzer, E. D.; Weiss, B., dfp Gene of Escherichia coli K-12, a locus affecting DNA synthesis, codes for a flavoprotein. *J. Bacteriol.* **1985**, 164, (3), 994-1003.
27. Blaesse, M.; Kupke, T.; Huber, R.; Steinbacher, S., Crystal structure of the peptidyl-cysteine decarboxylase EpiD complexed with a pentapeptide substrate. *EMBO J* **2000**, 19, (23), 6299-6310.
28. Genschel, U., Coenzyme A Biosynthesis: Reconstruction of the Pathway in Archaea and an Evolutionary Scenario Based on Comparative Genomics. *Mol Biol Evol* **2004**, 21, (7), 1242-1251.
29. Yao, J.; Patrone, J. D.; Dotson, G. D., Characterization and Kinetics of Phosphopantothenoylcysteine Synthetase from Enterococcus faecalis. *Biochemistry* **2009**, 48, (12), 2799-2806.
30. Yao, J. W.; Dotson, G. D., Kinetic characterization of human phosphopantothenoylcysteine synthetase. *Biochimica Et Biophysica Acta-Proteins and Proteomics* **2009**, 1794, (12), 1743-1750.
31. Daugherty, M.; Polanuyer, B.; Farrell, M.; Scholle, M.; Lykidis, A.; de Crecy-Lagard, V.; Osterman, A., Complete Reconstitution of the Human Coenzyme A Biosynthetic Pathway via Comparative Genomics. *Journal of Biological Chemistry* **2002**, 277, (24), 21431-21439.

Chapter 2

Synthesis and Evaluation of Intermediate Mimics of Bacterial PPCS

Introduction

Phosphopantetheine ((*R*)-3-hydroxy-4-(3-(2-mercapto-ethylamino)-3-oxopropylamino)-2,2-dimethyl-4-oxobutyl dihydrogen phosphate) is a fundamental feature in many biological acyl transfer reactions. The molecule is found embedded within coenzyme A (CoA), as well as on a post-translationally modified, conserved serine of acyl carrier protein (ACP). Both CoA and ACP play essential roles as acyl group donor substrates in several reactions associated with intermediary metabolism and cell membrane assembly in living organisms.¹ Additionally, CoA has been determined to be the major low molecular weight thiol in non-glutathione producing bacteria, and is responsible for maintaining thiol/disulfide homeostasis in several human pathogens, such as *Staphylococcus aureus*, *Borrelia burgdorferi*, and *Bacillus anthracis*.² The critical nature of phosphopantetheine-containing molecules to the integrity and viability of cells makes the biosynthetic pathway leading to the production of these compounds an intriguing target for antimicrobial development.

In 1959, Brown showed that in addition to pantothenate, cysteine, and ATP, bacterial phosphopantetheine biosynthesis had an additional requirement for cytidine triphosphate (CTP), which was needed for the coupling of phosphopantothenate and cysteine by phosphopantothenoylcysteine synthetase (PPCS) in partially purified extracts of *Proteus morganii*.³ The CTP-dependence of bacterial PPCS, in contrast to its ATP-utilizing mammalian counterpart, has been recently confirmed using purified protein from *E. coli*.⁴ In most bacteria PPCS and phosphopantothenoylcysteine decarboxylase (PPCDC) are expressed as a single bifunctional polypeptide (~46 kDa; *coaBC* gene

product, formerly known as *dfp*), consisting of a N-terminal flavin mononucleotide (FMN) binding domain (PPCDC; ~21 kDa), and C-terminal PPCS domain (~25 kDa).^{5, 6} This is in contrast to their mammalian counterparts which are expressed as separate polypeptides (PPCS, 34 kDa; PPCDC, 22 kDa). The exceptions in the list of bacterial pathogens expressing bifunctional PPCS-PPCDC are *Streptococci* and *Enterococci* species, which contain two separate ORFs, *coaB* and *coaC*, in one operon. In addition, *Bacillus anthracis* (as well as *Bacillus cereus*) contains both a bifunctional PPCDC/PPCS and a monofunctional PPCS ortholog, but no monofunctional PPCDC.⁷ Monofunctional PPCSs from *Enterococcus faecalis*, *Streptococcus pneumoniae*, and *B. anthracis* reveal very high sequence similarity to each other, but they are quite divergent from the PPCS domain of the bifunctional PPCDC/PPCS proteins. In contrast to other bacterial orthologs, they produce a low but reliable similarity score compared with the human monofunctional PPCS. Thus, PPCS exists in nature in three types: Type I PPCS are found in a majority of bacteria and archaea, are CTP specific, and are expressed as the C-terminal domain of a bifunctional protein fusion in conjunction with phosphopantothenoylcysteine decarboxylase (PPCDC),^{8, 9} Type II PPCS are found mainly in eukaryotes, can utilize both ATP and CTP to support catalysis, and are expressed as a monofunctional enzyme,^{10, 11} and Type III PPCS are found in a smaller subset of bacteria, and are expressed as monofunctional enzymes and have been shown to be CTP specific.¹²

PPCS utilizes three substrates and catalysis proceeds through two half reactions, consisting of the formation of a nucleotide-activated phosphopantothenate intermediate in the first half reaction, followed by an acylation reaction in the second half reaction, resulting in amide bond formation yielding phosphopantothenoylcysteine (Figure 2.1). PPCS is a member of the aminoacyl-tRNA synthetase superfamily and the mechanism for formation of the phosphopantothenoyl cytidylate is similar to that for formation of the aminoacyl adenylate intermediate. It is of interest to note that the topical antibiotic mupirocin inhibits bacterial isoleucyl tRNA synthetase by mimicking binding contacts of the isoleucyl adenylate intermediate.^{13, 14}

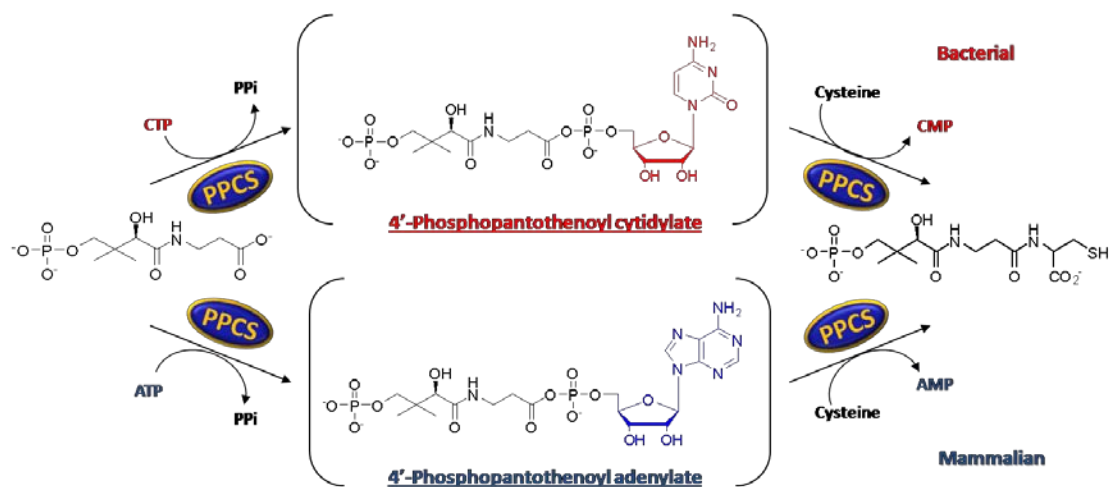


Figure 2.1: Mechanism of PPCS

As stated, one of the main differences between bacterial and human PPCS is the nucleotide triphosphate specificity, where bacterial PPCSs are CTP specific and thus generate an activated cytidylate intermediate for amide bond formation (**Figure 2.1**). Kinetic and structural studies have shown that the nucleobase binding sites of bacterial PPCS (Types I and III) differ greatly from that of the human Type II enzyme. We have therefore employed a strategy to achieve selective bacterial inhibition by exploiting the differences in the nucleobase binding pocket between the bacterial and human enzymes by basing the inhibitor design on the activated cytidylate intermediate. The proposed inhibitors should bind tightly to the bacterial nucleotide binding pocket, and less tightly to the human PPCS based upon the difference in the nucleobase binding pocket and the nucleotide triphosphate specificity. The proposed phosphodiester intermediate mimic was designed to mimic the activated intermediate, except that the electrophilic carbonyl on the phosphopantothenate portion of the molecule has been completely removed (**Figure 2.2**). Changing the chemically labile mixed anhydride to a chemically stable phosphodiester should allow the phosphodiester mimic to take advantage of the binding contacts of the activated intermediate in the PPCS active site while eliminating the possibility for cysteine attack and amide bond formation of the second half reaction. The proposed sulfamate intermediate mimic was designed by replacing the mixed anhydride linkage of the activated intermediate with a sulfamate linkage. The non-hydrolysable sulfamate linkage was chosen based upon recent success using it as a phosphate isostere

for activated intermediates in systems such as asparagine biosynthesis in humans and siderophore biosynthesis in *Mycobacterium tuberculosis* and *Yersinia pestis* to give inhibitors with IC₅₀s ranging from low μM to nM.¹⁵⁻¹⁸

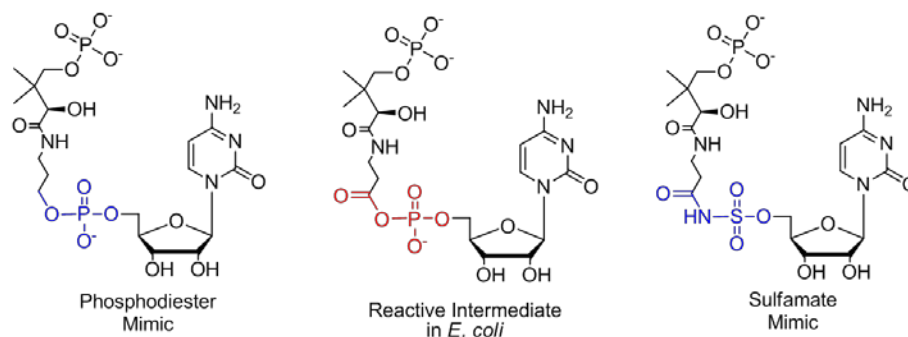


Figure 2.2: Design of Intermediate Mimics

Synthesis of Intermediate Mimics

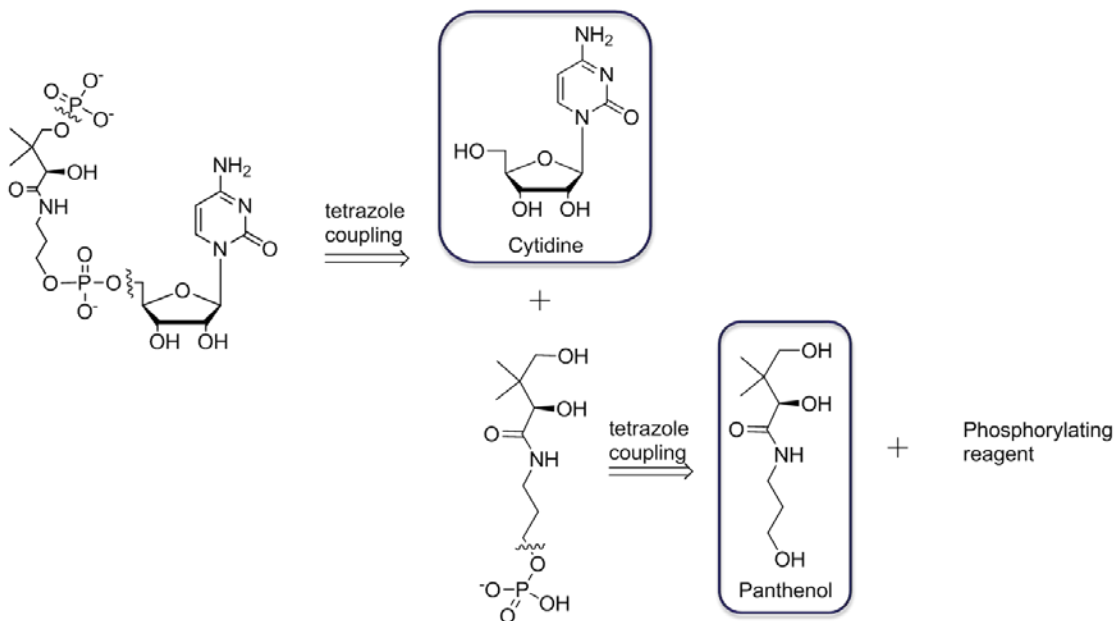
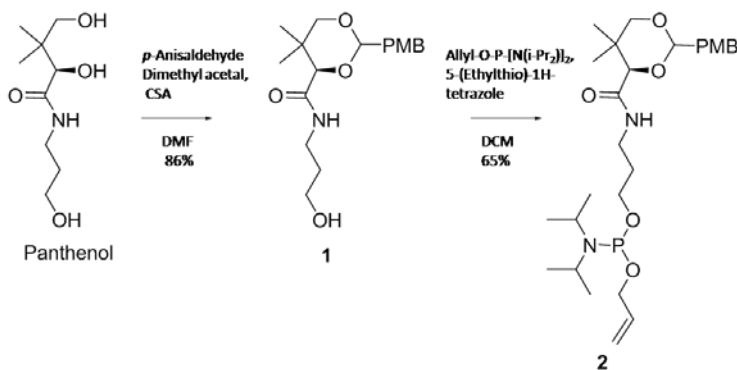


Figure 2.3: Retrosynthetic Analysis of the phosphodiester mimic

After retrosynthetic analysis of the phosphodiester mimic, one can envision the first disconnection is the terminal phosphate from the primary alcohol of the 1,3 diol of the panthenol portion of the mimic, which may be installed synthetically late in the synthesis by phosphorylation and in situ oxidation (**Figure 2.3**). The second disconnection of the molecule dissects the molecule into the two major fragments: a commercially available cytidine portion, and the N-3 phosphorylated panthenol fragment. The N-3

panthenol fragment can simply be disconnected to panthenol, a commercially available triol and a phosphate group, which may be installed via an appropriately substituted phosphitylating reagent using a tetrazole mediated coupling and oxidation.

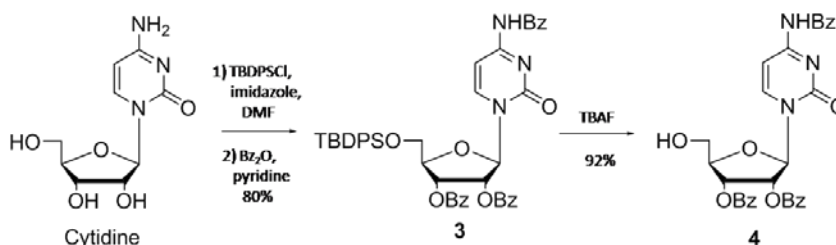


Scheme 2.1: Synthesis of phosphite 2

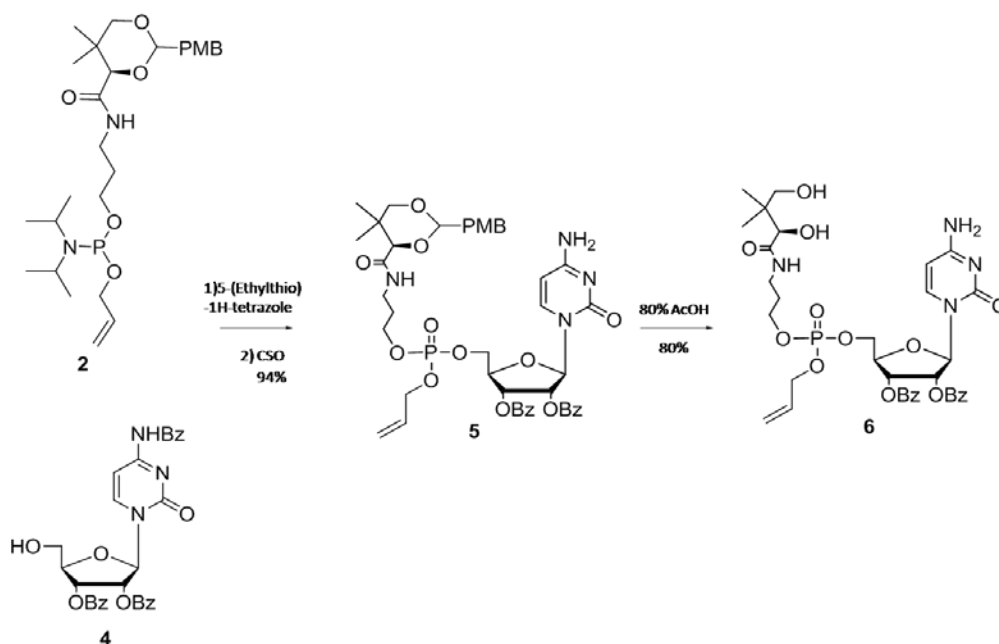
The synthesis of the phosphodiester mimic begins with the protection of the 1,3 diol of panthenol as the *p*-methoxybenzylidene (PMB) acetal **1** (Scheme 2.1).^{19, 20} The PMB acetal was chosen as the protecting group because it is more readily removed under acidic conditions than other acetals such as the benzylidene or acetonide due to the electron donating capability of the *p*-methoxy group.^{21, 22} Also, the acid labile PMB acetal provides the ability to utilize an orthogonal base labile protecting group strategy on the cytidine portion. This is a key feature because it allows for the installation of the terminal phosphate on the panthenol portion of the molecule later in the synthetic scheme. The PMB acetal **1** was then phosphitylated on the open N-3 alcohol using O-allyl-*N,N,N,N*-tetraisopropylphosphoramidite and 5-(ethylthio)-1H-tetrazole as the activating agent to yield the phosphite **2** in 65% yield.^{23, 24} The P(III) phosphoramidite chemistry was chosen as the method to install the phosphate moieties in the proposed inhibitors due to the increased reactivity of the activated P(III) species generated *in situ* and the stability of the phosphitylated intermediates unless treated with an activator. The P(III) chemistry was also advantageous because it allowed for asymmetric substitution of the phosphorous species based upon the order of addition and equivalents of the desired substituting nucleophile.²⁴

The cytidine fragment of the phosphodiester mimic was selectively protected at the 2' and 3' alcohol positions on the ribose ring and the N⁵ exocyclic amine on cytosine moiety with base labile benzoate esters following the procedures of Cohen et

al.²³ The first step is to selectively protect the 5' alcohol as the *tert*-butyldiphenylsilyl (TBDPS) ether (**Scheme 2.2**).²³ The 2' and 3' secondary alcohols and the N⁵ exocyclic amine were then protected as benzoate esters to give the fully protected cytidine **3** in 80%.²³ The silyl ether **3** was then treated with 1.1 equivalents of tetrabutylammonium fluoride (TBAF) to selectively deprotect the 5' alcohol and give the tribenzoyl cytidine **4**.²³



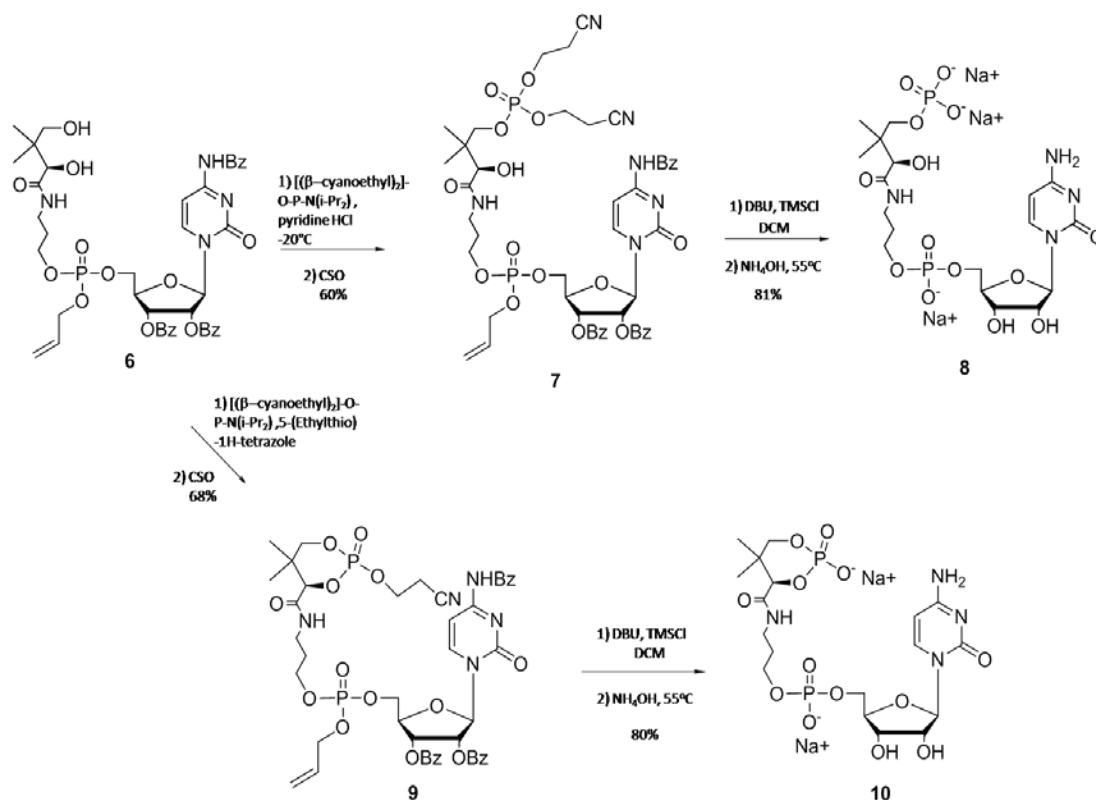
Scheme 2.2: Synthesis of tribenzoyl cytidine **4**



Scheme 2.3: Synthesis of diol **6**

The phosphite **2** and tribenzoyl cytidine **4** were then linked via 5-(ethylthio)-1H-tetrazole activation and displacement of the diisopropyl group of the phosphoramidite on **2** followed by *in situ* oxidation using (1*S*)-(+)-(10-camphorsulfonyl)oxaziridine (CSO) to yield the phosphodiester **5** in 94% (**Scheme 2.3**).²³⁻²⁵ Phosphodiester **5** was then treated

with 80% acetic acid, which selectively deprotected the PMB acetal on the 1,3 diol on the panthenol fragment to yield diol **6**.^{21, 22}



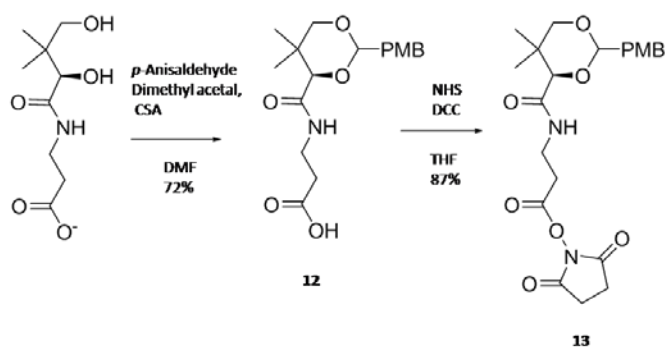
Scheme 2.4: Synthesis of phosphodiester mimics **8** & **10**

The final phosphorylation of the primary alcohol of the 1,3 diol proved to be more synthetically challenging than initially anticipated. Initial strategies utilized P(V) chemistry to install a phosphate protected with ethyl, benzyl, and allyl groups. In all cases phosphorylation of the 4' hydroxyl of the panthenol portion was accomplished in low to moderate yields. Deprotection of the phosphate esters proved to be problematic leading either to decomposition of the molecule due to harsh reaction conditions or ineffective deprotection of the terminal phosphate. Finally, a strategy utilizing P(III) phosphoramidate chemistry with β-cyanoethyl protecting groups on the phosphate was employed (**Scheme 2.4**). Initially, Diol **6** was phosphitylated using 5-(ethylthio)-1H-tetrazole as the activator at room temperature and oxidized *in situ* using CSO.^{23, 25} However, in the presence of the 1,3 diol, these conditions actually yielded the protected cyclic phosphodiester **9**. While not the desired product, the protected phosphate **9** was

taken forward due to its interesting cyclic phosphate on the panthenol portion in order to conduct an initial SAR study. The protected phosphate **9** was deprotected over two steps. First, the β -cyanoethyl phosphate ester was removed in the presence of DBU and TMSCl.²⁶ The β -cyanoethyl protecting groups were chosen because deprotection is accomplished under mild conditions using DBU to deprotonate the β hydrogen and eliminate acrylonitrile and expose the negative charge on the phosphate. The TMSCl temporarily protects the negative charge on the phosphate and allows for complete deprotection. Next, the benzoate esters and the allyl group on the internal phosphate linkage were removed upon treatment with NH_4OH and β -mercaptoethanol (allyl scavenger) at 55°C for 1 hour.²⁷ The cyclic phosphate mimic **10** was purified by anion exchange column chromatography, followed by salt removal using gel filtration chromatography (BioGel P2) to yield the disodium salt in 80% yield.

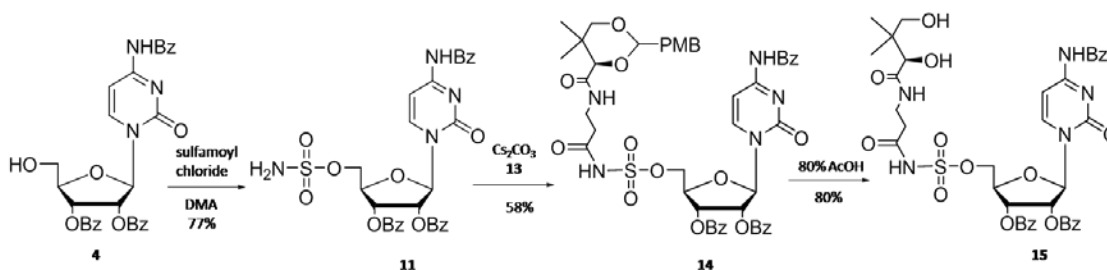
In order to give the desired terminal phosphate mimic, alternative phosphitylating procedures were explored. Initial attempts to conduct the phosphitylation at temperatures below -40°C yielded unreacted diol **6**. Next, **6** was phosphitylated at -20°C , using *O,O*-bis β -cyanoethyl-*N,N*-diisopropyl phosphoramidite and pyridinium HCl as the activator, for 1 hour followed by *in situ* oxidation to yield the protected phosphate in 60%.²⁸ These conditions were chosen to suppress the unwanted cyclization based upon the hypothesis that the less acidic activator (pyridinium HCl), lower temperature, and shorter reaction time would not allow formation of the thermodynamically more stable six membered phosphorous containing ring before the reaction was quenched by *in situ* oxidation of the phosphite to the less reactive phosphate. Phosphate **7** was globally deprotected in the aforementioned two step sequence used to deprotect **9**, and the resulting phosphodiester **8** was purified via anion exchange chromatography and desalted by gel filtration chromatography to give the trisodium salt in an overall yield of 19%.²³

The proposed sulfamate mimic was synthesized using a similar convergent synthetic strategy. The first step involves the protonation of the calcium salt of pantothenate followed by the selective protection of the 1,3 diol to give PMB acetal **12** (Scheme 2.5).^{19, 20} In order to facilitate the coupling of the two fragments of the sulfamate mimic, the carboxylic acid of PMB acetal **12** was activated as the NHS ester via the procedure of Burkart et al.^{15, 19, 20, 29}



Scheme 2.5: Synthesis of NHS ester **13**

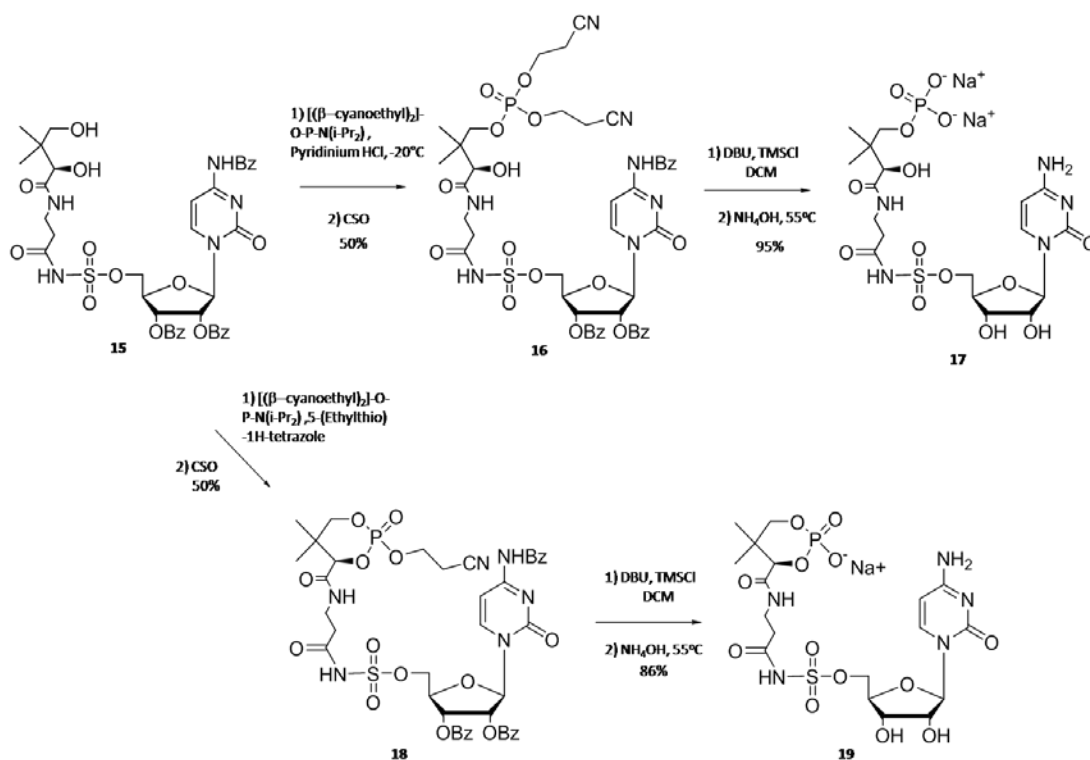
The sulfamoyl moiety of the molecule was generated by treating tribenzoyl cytidine **4** with freshly prepared sulfamoyl chloride in *N,N*-dimethylacetamide (DMA) to yield sulfamoyl tribenzoyl cytidine **11** (**Scheme 2.6**).^{15, 30, 31} The internal sulfamate linkage between the cytidine and pantothenate portions of the molecule was installed by combining activated NHS ester **13** and sulfamoyl tribenzoyl cytidine **11** in the presence of Cs_2CO_3 to yield acetal **14** in 58%.¹⁵ PMB acetal **14** was selectively deprotected using 80% acetic acid to yield the desired diol **15**.^{21, 22}



Scheme 2.6: Synthesis of Diol **15**

The final stages of the synthesis of the sulfamate mimic involved selective phosphitylation of the primary alcohol of the 1,3 diol at -20°C using pyridinium HCl as the activator and in situ oxidation to the phosphate **16** (**Scheme 2.7**). Global deprotection was accomplished over two steps using DBU and TMSCl followed by NH_4OH at 55°C for 1 hour to afford the sulfamate mimic **17** after purification using anion exchange and size exclusion chromatography. Alternatively, diol **15** was phosphitylated at room temperature using 5-(ethylthiol)-1H-tetrazole as the activating agent and in situ oxidation to the cyclic phosphate **18**. The protected cyclic phosphate **18** was deprotected over two steps using DBU and TMSCl followed by NH_4OH at 55°C for 1 hour and purification via

anion exchange and size exclusion chromatography to yield the desired sulfamate mimic **19** with the cyclic phosphate in 86%.



Scheme 2.7: Synthesis of sulfamate mimics

Biochemical Evaluation of Intermediate Mimics

The initial biochemical studies carried out with intermediate mimics **8**, **10**, **17** and **19** were to obtain the IC₅₀ values against PPCS from human (Type II), *E. coli* (Type I), *S. pneumonia* (Type III), and *E. faecalis* (Type III). PPCS activity was monitored using the commercially available pyrophosphate reagent (**Figure 2.4**). The pyrophosphate reagent is a coupled assay, which actually monitors the pyrophosphate liberated during the activation of PPA by CTP during the first half reaction of PPCS. The assay couples four enzymes from the glycolysis pathway and results in the oxidation of two molecules of NADH to NAD⁺ for every PPi generated. The oxidation of NADH is monitored by the disappearance of the UV absorbance at 340 nm. The pyrophosphate reagent is advantageous due to the fact it is a continuous assay. The continuous monitoring of PPCS activity over time is more efficient for data collection over the time course of the

enzymatic reaction than an end point assay, and is amenable to a 96 well or 384 well format giving the assay the capacity to be used in a high throughput fashion.

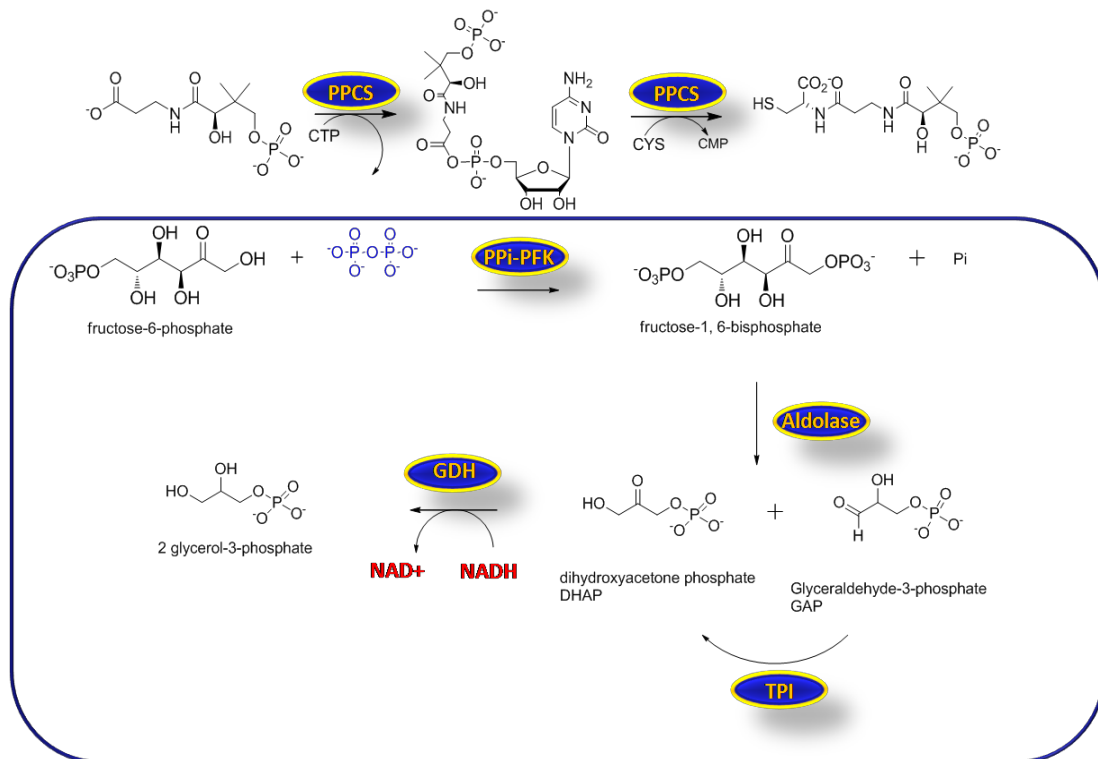


Figure 2.4: The pyrophosphate reagent coupled assay system

However, due to the fact the pyrophosphate reagent is coupled to four enzymes in order to elicit the signal actually being monitored, several controls had to be run. The first control was to ensure that any and all enzymes in the pyrophosphate reagent were faster than PPCS itself and thus the signal measured at 340 nm would be a measure of PPCS activity and not a measure of an enzyme in the pyrophosphate reagent. This control was run by varying the concentration of PPCS and verifying the linearity of the PPCS velocity versus concentration (data not shown). The second control was to ensure that the intermediate mimics were inhibiting PPCS and not simply inhibiting one of the coupled enzymes of the pyrophosphate reagent. This control was run by adding known concentrations of pyrophosphate into the assay after PPCS activity had been inhibited by phosphodiester **8**. In this case, the varying concentrations of pyrophosphate produced a nearly instantaneous disappearance of signal at 340 nm thus proving that the reporter enzymes were not inhibited by the intermediate mimic **8** (data not shown).

IC₅₀ values were generated by pre-incubating PPCS with varying concentrations of the desired inhibitor and initiating the enzyme reaction upon the addition of a fixed concentration of CTP (0.6 mM), PPA (0.6 mM), and cysteine (1 mM). All assays were run in triplicate monitoring the first 10% of PPCS activity (initial rates). The inhibition data was plotted as percent activity of PPCS versus inhibitor concentration with a representative graph in **Figure 2.5** and all graphs contained in the **Appendix to Chapter 2**. Then the IC₅₀ values were determined using the equation:

$$Y = \frac{1}{1 + \frac{[I]}{IC_{50}}} \cdot 100 \quad (1)$$

and solving for IC₅₀.

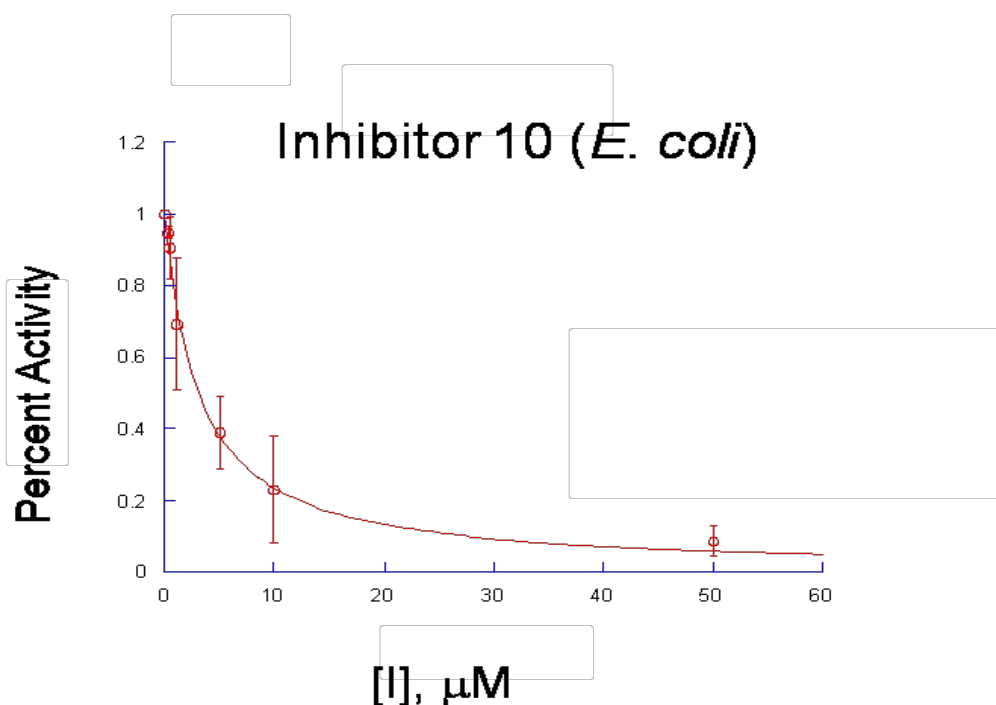


Figure 2.5: Representative IC₅₀ curve

The phosphodiester mimic **8**, which most closely mimics the activated intermediate, was the most potent inhibitor with an IC₅₀ ranging from 10-68 nM across the bacterial PPCSs (Types I & III) (**Table 2.1**). Phosphodiester **8** was able to achieve a 150 fold selectivity *E. coli* and *E. faecalis* (Types I & III) and a 1000 fold selectivity for *S. pneumoniae* (Type III) over human (Type II). Cyclic phosphodiester **10** was less potent across all types of PPCS as compared to phosphodiester **8** displaying IC₅₀s ranging from

3-18 μM . The cyclic inhibitor **10** displayed its most potent IC_{50} against ecPPCS (Type I) and was 4-6 fold less potent against Type III PPCSs. Despite being less potent against all PPCSs, the cyclic phosphate **10** maintained its selectivity for types I and III over Type II, PPCS with its most potent IC_{50} of 3 μM against *E. coli* and a 3 mM IC_{50} against human PPCS (Type II) and thus 1000 fold selectivity.

	<i>E. coli</i> (I)	<i>E. faecalis</i> (III)	<i>S. pneumoniae</i> (III)	Human (II)
8	68 nM (9)	65 nM (9)	10 nM (2)	10 μM (1)
10	3.0 μM (0.3)	18 μM (5)	13 μM (4)	3 mM (0.2)
17	270 nM (3)	2.7 μM (0.3)	3.9 μM (0.2)	200 μM (11)
19	16 μM (5)	180 μM (7)	280 μM (27)	5.9 mM (0.6)

Table 2.1: IC_{50} values of intermediate mimics. Standard error shown in parentheses.

The sulfamate mimics **17** and **19** displayed a similar pattern in their IC_{50} s relative to their phosphodiester analogs **8** and **10**. The non-cyclic phosphate mimic **17** was the more potent of the sulfamate inhibitors with an IC_{50} of 270 nM against *E. coli* (Type I) and 10-14 fold less potent against Type III PPCSs. Furthermore, inhibitor **17** displayed 50-740 fold selectivity as compared to human (Type II) PPCS. The cyclic phosphate mimic **19** displayed IC_{50} values analogous to the phosphodiester mimic **10** being the least potent inhibitor across all PPCSs with IC_{50} s ranging from 16-280 μM for bacterial PPCSs and a 5.9 mM IC_{50} against human (Type II) PPCS.

Upon further investigation of the IC_{50} values, there are several trends between inhibitor structure and inhibition of PPCS type. *E. coli* (Type I) PPCS accommodates structural changes to both the internal linkage and terminal phosphate more readily than *E. faecalis* and *S. pneumoniae* (Type III) PPCS, with inhibitors **10**, **17**, and **19** all showing their most potent IC_{50} against *E. coli* PPCS and a 4-17 fold drop in potency against Type III PPCSs. The terminal phosphate on the panthenol portion of the inhibitor is more important in binding as compared to the internal linker and/or its binding contacts are less accommodating to structural change. This trend was evidenced by sulfamate inhibitor **17** displaying IC_{50} values 3-15 fold more potent across all PPCSs (Types I-III) than the cyclic phosphodiester **10**.

The IC_{50} values of inhibitor **8** were on the same order of magnitude with the PPCS concentration, which by definition meant that inhibitor **8** was a tight-binding

inhibitor. Care must be taken when determining the K_i for a tight binding inhibitor because the assumption that concentration of free inhibitor is approximately equal the total concentration of total inhibitor is no longer valid. In order to determine the mechanism and obtain the inhibition constant of inhibitor **8**, we chose to use efPPCS based upon the recent full steady state kinetic characterization.¹²

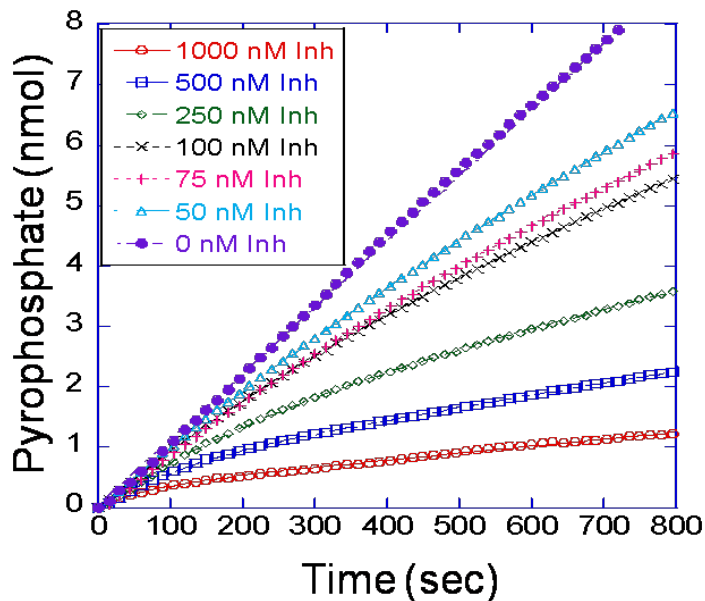


Figure 2.6: Inhibition curves for phosphodiester **8**

Using the aforementioned pyrophosphate reagent assay as the monitoring system for PPCS activity, varying amounts of phosphodiester **8** were added to PPCS without pre-incubation, in the presence of fixed concentrations of CTP, PPA, and cysteine. Plotting reaction progress versus time for the varying concentrations of inhibitor **8**, the slow-onset binding mode can be seen from the time-dependent decrease in PPCS reaction rate (**Figure 2.6**).

Since phosphodiester **8** shows slow-onset, tight binding inhibition, we chose to use the method of Morrison et al. to determine the mode of binding. In slow-onset inhibition there are generally three modes of binding: simple reversible slow binding, enzyme isomerization, and mechanism-based inhibition (**Figure 2.7**).

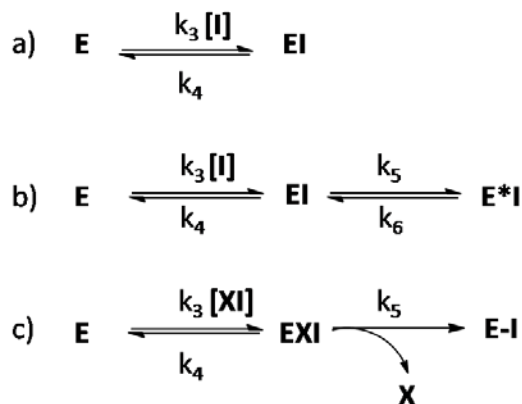


Figure 2.7: Slow-onset binding modes. a) simple reversible b) enzyme isomerization c) mechanism-based inhibition

The reaction progress curves from **Figure 2.6** were fit to obtain the apparent first-order rate constant k_{obs} , using the software KaleidaGraph (Synergy Software, Inc.) using equation 1, where P is the amount of pyrophosphate produced during a period of time t , v_i and v_s are the initial and equilibrium rates, $[E]$ is the concentration of efPPCS in the assay, and $[I]$ is the concentration of inhibitor in the assay.

$$P = v_s t + \frac{(v_i - v_s)(1 - \gamma)}{k_{obs} \gamma} \ln \left\{ \frac{[1 - \gamma \exp(k_{obs} t)]}{1 - \gamma} \right\} \quad (2)$$

where

$$\gamma = \frac{[E]}{[I]} \left(1 - \frac{v_s}{v_i} \right)^2 \quad (3)$$

The obtained k_{obs} were then plotted against inhibitor concentration to investigate the kinetic mechanism of inhibition (**Figure 2.8**). The linear relationship of the data in **Figure 2.8** proved that inhibitor **8** was a single-step inhibition mechanism with a slow association and disassociation step and that there was no isomerization step of PPCS upon binding of compound **8**. This result was unexpected as most slow-onset inhibitors have an isomerization step; however, based upon the linear fit in **Figure 2.8**, phosphodiester **8** is in the smaller subset of slow-onset inhibitors that are simply reversible inhibitors.

Beyond proving the binding mode of phosphodiester **8**, **Figure 2.8** can be used to solve for the K_i . Based upon the equation:

$$k_{obs} = k_3^{app} [I] + k_4 \quad (4)$$

k_3^{app} and k_4 can be interpolated from the slope of the line and the y-intercept in **Figure 2.8**, respectively, giving a $k_3^{app} = 1.42 \times 10^4 \text{ M}^{-1}\text{s}^{-1}$, and a $k_4 = 7.02 \times 10^{-4}\text{s}^{-1}$. K_i^{app} for compound **8** was solved using equation 5 and was found to be 49 nM. Since phosphodiester **8** is a noncompetitive inhibitor (data not shown), K_i^{app} was converted to K_i via equation 6 ($\alpha = 2.9$).³² After rearranging equation 6, phosphodiester **8** was shown to have $K_i = 24 \text{ nM}$.

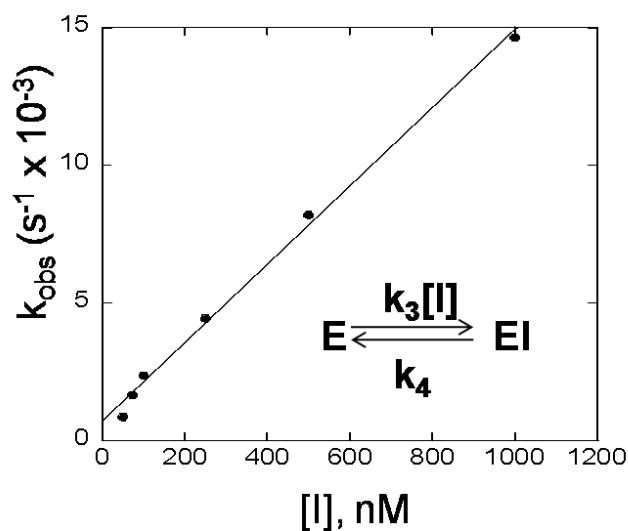


Figure 2.8: k_{obs} versus concentration of compound **8**

$$K_i^{app} = k_4/k_3^{app} \quad (5)$$

$$K_i^{app} = \frac{[S] + K_m}{\frac{K_m}{K_i} + \frac{[S]}{\alpha K_i}} \quad (6)$$

Conclusion

The phosphodiester mimics **8** and **10** and sulfamate mimics **17** and **19** represent the first selective bacterial inhibitors of PPCS. The most potent inhibitor **8** displayed low nM IC_{50} values ranging from 10-68 nM for both Types I and III bacterial PPCSs and 140-

1000 fold selectivity compared to human PPCS (Type II). Further characterization of inhibitor **8** established it as a slow-onset, tight binding inhibitor with a simple one step mode of inhibition and a K_i of 24 nM against efPPCS. This set of four inhibitors has given us a foundation for inhibiting bacterial PPCS and the structural changes to the inhibitor in the linker and terminal phosphate regions that are allowed by the various types of PPCS. It has been established that changes to the linker region are tolerated 4-17 fold more than perturbing the terminal phosphate. Also, *E. coli* (Type I) PPCS showed the greatest tolerance for structural change to the inhibitor with the best IC₅₀ values for inhibitors **10**, **17**, and **19**.

Despite these molecules' effectiveness against isolated PPCS in the in vitro assay, they displayed no effect against *E. coli* in a zone of inhibition assay (data not shown). This lack of effect was not surprising and is most likely a consequence of the physiochemical properties of the molecules preventing cellular entry with all of the molecules having at least one negative charge and most possessing multiple negative charges. These molecules, however, are an important first step in exploring PPCS as an antibacterial target and will be used in future structural studies to gather more detailed information on binding contacts necessary for potency and selectivity against bacterial PPCSs. The information gleaned from these studies will be used to aid in the design of the second generation inhibitors into more drug-like molecules with maximized potency and selectivity.

Acknowledgements

This work was previously published as Patrone, J. D.; Yao, J.; Scott, N. E.; Dotson, G. D., Selective Inhibitors of Bacterial Phosphopantothenoylecysteine Synthetase. *Journal of the American Chemical Society* **2009**, 131, (45), 16340-16341. I would like to thank and acknowledge Nicole Scott for cloning of ecPPCS and Jiangwei Yao for cloning and expressing efPPCS, spPPCS, and hPPCS, and performing the assay to determine the α value used in K_i determination.

Materials & Methods

General Methods: All chemicals were used as purchased from Acros, Fisher, Fluka, Sigma-Aldrich, or Specialty Chemicals Ltd. and used without further purification unless otherwise noted. ^1H NMR, ^{13}C NMR, and ^{31}P NMR spectra were recorded on a Bruker Avance DRX 500MHz spectrometer or Bruker Avance DPX 300MHz spectrometer. Proton assignments are reported in ppm from an internal standard of TMS (0.0ppm), and phosphorous assignments are reported relative to an external standard of 85% H_3PO_4 (0.0ppm). Proton chemical data are reported as follows: chemical shift, multiplicity (ovlp = overlapping, s = singlet, d = doublet, t = triplet, q = quartet, p = pentet, m = multiplet, br = broad), coupling constant in Hz, and integration. All high resolution mass spectra were acquired from the Mass Spectrometry facility in the Chemistry Department at The University of Michigan using either positive-ion or negative-ion mode ESI-MS. Thin layer chromatography was performed using Analtech GHLF 250 micron silica gel TLC plates. All flash chromatography was performed using grade 60 Å 230-400 mesh silica purchased from Fisher.

(4R)-N-(3-hydroxypropyl)-2-(4-methoxyphenyl)-5,5-dimethyl-1,3-dioxane-4-

carboxamide (1) D-panthenol (1.0 g, 5 mmol) was rendered anhydrous by evaporation from ethanol stock (5 mL) followed by evaporation from toluene (2 x 5 mL) and dissolved in anhydrous DMF (20 mL). Camphor sulfonic acid (CSA) (0.0116 g, 0.05 mmol) was added and stirred at room temperature for 15 min. *p*-Methoxybenzaldehyde dimethyl acetal (2.55 mL, 15 mmol) was added and the reaction was stirred at room temperature for 24 h. The solvents were removed *in vacuo* and then the resulting syrup was purified over silica (100 mL) eluting with 10% EtOAc in hexanes (300 mL), 25% EtOAc in hexanes (300 mL), and 50% EtOAc in hexanes yielding a white crystalline solid (1.4 g, 86%). Mixture of diastereomers (55%/45%), ^1H NMR (DMSO- d_6 major diastereomer): δ 7.55 (s, 1H), 7.44 (d, $J = 7.05$ Hz, 2H), 6.93 (d, $J = 7.15$ Hz, 2H), 5.50 (s, 1H), 4.52 (t, $J = 4.55$ Hz, 1H), 4.08 (s, 1H), 3.75 (s, 3H), 3.61 (q, $J = 9.74$ Hz, 2H), 3.41 (d, $J = 5.40$ Hz, 2H), 3.28-3.06 (m, 2H), 1.56 (t, $J = 5.75$ Hz, 2H), 0.98 (s, 3H), 0.96 (s, 3H). ^{13}C NMR (DMSO- d_6): δ 168.63, 160.01, 130.98, 128.24, 113.79, 100.88, 83.76,

77.87, 59.39, 55.59, 36.34, 32.99, 32.62, 22.05, 19.59. HR-ESI-MS: calcd for [M+Na]⁺, 346.1625; found 346.1622.

Allyl 3-((4R)-2-(4-methoxyphenyl)-5,5-dimethyl-1,3-dioxane-4-carboxamido)propyl diisopropyl-phosphoramidite (2) The protected alcohol **1** (3.1 g, 9.59 mmol) and 5-(ethylthiol)-1H-tetrazole (0.836 g, 6.42 mmol) were dissolved in anhydrous DCM. Allyl-*N,N,N,N*-tetraisopropylphosphoramidite (5.2 mL, 16.3 mmol) was added dropwise to the solution over a period of 5 minutes. The reaction was allowed to stir at room temperature for 6 hours, at which time solvents were removed *in vacuo*. The syrup was then purified over silica (150 mL) eluting with 30% EtOAc in hexanes (450 mL), 50% EtOAc in hexanes (450 mL), and 100% EtOAc (450 mL). Product eluted in 30% EtOAc and was obtained as colorless oil (3.2 g, 65%). ¹H NMR (DMSO-*d*₆): δ 7.47-7.42 (ovlp, d,t, 3H), 6.93 (d, *J* = 8.75 Hz, 2H), 5.91-5.78 (m, 2H), 5.53 (s, 1H), 5.26 (d, *J* = 17.15 Hz, 1H), 5.10 (d, *J* = 10.20 Hz, 1H), 4.09 (s, 3H), 3.67-3.61 (m, 2H), 3.55-3.47 (m, 4H), 3.27-3.25 (m, 2H), 3.15-3.12 (m, 2H), 1.70 (t, *J* = 6.65 Hz, 2H), 1.19 (s, 6H), 1.10 (s, 6H), 1.03 (s, 3H), 0.95 (s, 3H). ¹³C NMR (DMSO-*d*₆): δ 168.76, 160.00, 134.39, 130.95, 128.31, 116.85, 113.73, 100.97, 83.84, 77.88, 63.55, 55.58, 46.53, 45.73, 35.27, 32.98, 30.52, 22.75, 22.02, 19.60. ³¹P NMR (DMSO-*d*₆): δ 145.82 (s, 1P). HR-ESI-MS: calcd for [M+Na]⁺, 533.2751; found 533.2764.

2'-3'-*O,N*⁴-Tribenzoyl-5'-*O*-*tert*-butyldiphenylsilyl cytidine (3)²³ Cytidine (6.0 g, 25 mmol, 1.0 equiv) and imidazole (4.2 g, 63 mmol) were dissolved in DMF (45 mL). *tert*-Butyldiphenylsilyl chloride (7.0 mL, 27 mmol) was added dropwise over 10 min. The reaction was stirred at room temperature for 1 h and then quenched by addition of methanol (10 mL). The solvents were removed *in vacuo* and the resulting syrup was partitioned between H₂O and DCM. The aqueous layer was further washed with DCM (2x) and then the organic extracts were combined and upon standing the product crystallized out within 10 min. The crystals were dried under vacuum and then dissolved in pyridine (40 mL). Benzoic anhydride (56 g, 250 mmol, 10 equiv) was added and the reaction was stirred at room temperature for 2 days. The reaction was quenched with H₂O (20 mL). The solvents were removed *in vacuo* and the resulting syrup was partitioned between water and DCM. The aqueous layer was further extracted with DCM (2x), and the combined organic extracts were washed with 5% aqueous HCl, saturated aqueous

sodium bicarbonate, and brine solution. The organic layer was then dried over Na_2SO_4 and then the solvent was removed *in vacuo* and the product was purified over silica (300 mL) eluting with 10% EtOAc in hexanes (900 mL), 25% EtOAc in hexanes (900 mL), and 50% EtOAc in hexanes (900 mL). The product was obtained as a white solid (15.4 g, 76%). ^1H NMR (DMSO-*d*6): δ 11.38 (s, 1H), 8.31 (d, $J = 6.85$ Hz, 1H), 8.02 (d, $J = 7.55$ Hz, 2H), 7.87-7.80 (m, 3H), 7.68-7.60 (m, 7H), 7.54-7.30 (m, 14H), 6.28 (d, $J = 2.30$ Hz, 1H), 5.93-5.90 (m, 2H), 4.61 (q, $J = 4.52$ Hz, 1H), 4.11 (dd, $J = 3.25, 11.70$ Hz, 1H), 3.97 (dd, $J = 4.10, 11.55$ Hz, 1H), 1.01 (s, 9H). ^{13}C NMR (DMSO-*d*6): δ 168.05, 165.07, 165.02, 164.09, 154.62, 146.22, 135.59, 135.52, 134.41, 134.34, 133.55, 133.31, 132.88, 132.58, 130.54, 129.84, 129.77, 129.24, 129.00, 128.93, 128.50, 128.41, 97.18, 90.56, 82.28, 74.67, 70.82, 63.54, 27.07, 19.23. HR-ESI-MS: calcd for $[\text{M}+\text{Na}]^+$, 816.2712; found 816.2740.

2'-3'-O,*N*⁴-Tribenzoyl cytidine (4)²³ The protected cytidine derivative **3** (15.5 g, 19.5 mmol) was dissolved in THF (30 mL). Acetic acid (1.7 mL, 29 mmol) was added followed by tetrabutylammonium fluoride solution (1.0 M, 59 mL, 59 mmol). The reaction was stirred at room temperature for 1 h and then the solvents were removed *in vacuo*. The resulting syrup was partitioned between saturated aqueous sodium bicarbonate and DCM, and the aqueous layer was further extracted using DCM (2x). The combined organic extracts were washed with a brine solution, and dried over Na_2SO_4 . The product was purified over silica (150 mL) eluting with 50% EtOAc in hexanes (450 mL), 75% EtOAc in hexanes (450 mL), and 100% EtOAc (450 mL) with the product obtained in 100% EtOAc as a white solid (9.9 g, 90%). ^1H NMR (DMSO-*d*6): δ 11.31 (s, 1H), 8.52 (d, $J = 7.00$ Hz, 1H), 8.02 (d, $J = 7.25$ Hz, 2H), 7.93 (d, $J = 8.05$ Hz, 2H), 7.83 (d, $J = 7.15$, 2H), 7.68-7.58 (m, 3H), 7.53-7.39 (m, 7H), 6.38 (d, $J = 4.95$ Hz, 1H), 5.85 (t, $J = 5.31$ Hz, 1H), 5.79 (t, $J = 5.64$ Hz, 1H), 5.50 (t, $J = 5.11$ Hz, 1H), 4.53 (q, $J = 3.65$ Hz, 1H), 3.88 (m, 1H), 3.81 (m, 1H). ^{13}C NMR (DMSO-*d*6): δ 167.33, 164.68, 164.43, 163.54, 154.46, 145.65, 133.82, 133.78, 133.00, 132.74, 129.24, 129.23, 128.76, 128.67, 128.45, 128.39, 96.82, 88.38, 83.15, 74.39, 71.44, 60.47. HR-ESI-MS: calcd for $[\text{M}+\text{Na}]^+$, 578.1534; found 578.1538.

(2R,3R,4R,5R)-2-(((allyloxy)(3-((4R)-2-(4-methoxyphenyl)-5,5-dimethyl-1,3-dioxane-4-carboxamido)propoxy)phosphoryl)oxy)methyl)-5-(4-benzamido-2-oxopyrimidin-1(2H)-yl)tetrahydrofuran-3,4-diyl dibenzoate (5) The tribenzoyl cytidine **4** (858 mg, 1.45 mmol) and the *p*-methoxybenzylidene panthenol phosphoramidite **2** (1.26 g, 2.47 mmol) were dissolved in toluene (2 x 5 mL) and evaporated, then dissolved in anhydrous acetonitrile (10 mL) along with 3 Å molecular sieves (0.5 g). Concurrently, in a separate flask 5-ethylthiol-1*H*-tetrazole (566 mg, 4.35 mmol) was dissolved in anhydrous acetonitrile (3 mL) and both flasks were stirred at room temperature for 1 hour. The content of the tetrazole and acetonitrile mixture (~ 3.5 mL) was then added dropwise over 10 minutes to the first flask and the reaction was stirred at room temperature for 4 hours. The phosphite was then oxidized *in situ* upon the addition of (1*R*)-(-)-(8,8-dichloro-10-camphor-sulfonyl) oxaziridine (CSO) (736 mg, 2.47 mmol) in ethyl acetate (3 mL) dropwise over 5 minutes and then allowed to stir for 2 hours. The reaction was quenched upon the addition of dimethyl sulfide (0.2 mL), the reaction was filtered, and then solvents were removed *in vacuo*. The reaction was purified over silica (50 mL) eluting with 25% EtOAc in hexanes (150 mL), 50% EtOAc in hexanes (150 mL), 75% EtOAc in hexanes (150 mL) with the product eluting as white crystalline solid (1.43 g, 94%). ¹H NMR (DMSO-*d*₆): δ 11.41 (s, 1H), 8.31 (d, *J* = 7.12, 1H), 8.03 (d, *J* = 7.25 Hz, 2H), 7.93 (d, *J* = 7.55, 2H), 7.87 (d, *J* = 7.45 Hz, 2H), 7.67-7.64 (m, 4H), 7.55-7.38 (m, 9H), 6.91 (d, *J* = 7.60, Hz, 2H), 6.25 (s, 1H), 5.93 (s, 3H), 5.82 (t, *J* = 6.08 Hz, 1H), 5.50 (s, 1H), 5.36-5.31 (m, 1H), 5.20 (t, *J* = 9.45 Hz, 1H), 4.69 (s, 1H), 4.35 (s, 3H), 4.50-4.42 (m, 1H), 4.40-4.35 (m, 1H), 3.75 (s, 3H), 3.64-3.58 (m, 2H), 1.80-1.72 (m, 2H), 1.01 (s, 3H), 0.92 (s, 3H). ¹³C NMR (DMSO-*d*₆): δ 168.82, 167.88, 165.02, 164.36, 160.02, 154.78, 147.35, 134.42, 134.35, 133.40, 133.35, 130.99, 130.93, 129.81, 129.22, 129.00, 128.93, 128.23, 118.37, 113.74, 100.97, 97.28, 91.45, 83.83, 80.63, 77.91, 74.17, 70.95, 68.19, 66.65, 66.17, 55.57, 35.17, 32.96, 30.46, 21.99, 19.57. ³¹P NMR (DMSO-*d*₆): δ -0.96 (s, 1P). HR-ESI-MS: calcd for [M+Na]⁺, 1003.3138; found 1003.3148.

(2R,3R,4R,5R)-2-(((allyloxy)(3-((R)-2,4-dihydroxy-3,3-dimethylbutanamido)propoxy)phosphoryl)oxy)methyl)-5-(4-benzamido-2-oxopyrimidin-1(2H)-yl)tetrahydrofuran-3,4-diyl dibenzoate (6) The acetal **5** (710 mg, 0.72 mmol) was dissolved in 80% acetic acid (8 mL) and was stirred at room temperature for 20 hours. The solvents were removed *in vacuo* and the syrup was partitioned between DCM and H₂O. The H₂O layer was washed with DCM (2 x 20 mL) and then the organic extracts were dried (Na₂SO₄) and evaporated *in vacuo*. The syrup was purified over silica (50 mL) eluting with 50% EtOAc in hexanes (150 mL), 75% EtOAc in hexanes (150 mL), and 100% EtOAc with the product obtained as white crystalline solid (610 mg, 95%). ¹H NMR (DMSO-*d*₆): δ 11.41 (s, 1H), 8.32 (d, *J* = 7.40 Hz, 1H), 8.03 (d, *J* = 7.41 Hz, 2H), 7.94 (d, *J* = 7.11 Hz, 2H), 7.94 (d, *J* = 7.12 Hz, 2H), 7.86 (d, *J* = 7.15 Hz, 2H), 7.55-7.44 (m, 9H), 6.25 (s, 1H), 5.96-5.90 (m, 2H), 5.83 (t, *J* = 6.35 Hz, 1H), 5.38-5.33 (m, 2H), 5.23-5.19 (m, 1H), 4.70 (s, 1H), 4.56-4.53 (m, 3H), 4.47-4.39 (ovlp, m, 2H), 4.06-4.01 (m, 2H), 3.71 (d, *J* = 5.55 Hz, 1H), 3.20-3.11 (m, 4H), 1.80-1.74 (m, 2H), 0.80 (s, 3H), 0.78 (s, 3H). ¹³C NMR (DMSO-*d*₆): δ 173.56, 167.89, 165.09, 165.01, 164.39, 154.81, 147.43, 134.42, 134.36, 133.38, 133.35, 129.82, 129.22, 129.00, 128.93, 128.28, 118.39, 113.73, 97.25, 83.72, 80.67, 75.56, 74.17, 70.95, 68.49, 68.21, 66.67, 66.10, 35.05, 30.51, 21.44, 20.80. ³¹P NMR (DMSO-*d*₆): δ -0.99 (s, 1P). HR-ESI-MS: calcd for [M+Na]⁺, 885.2719; found 885.2733.

(2R,3R,4R,5R)-2-(((allyloxy)(3-((R)-4-((bis(2-cyanoethoxy)phosphoryl)oxy)-2-hydroxy-3,3-dimethylbutanamido)propoxy)phosphoryl)oxy)methyl)-5-(4-benzamido-2-oxopyrimidin-1(2H)-yl)tetrahydrofuran-3,4-diyl dibenzoate (7) The diol **6** (75 mg, 0.087 mmol), *O,O*-bis(cyanoethyl)-*N*-diisopropylamine phosphoramidite (36 mg, 0.131 mmol), and 3 Å molecular sieves were dissolved in anhydrous pyridine (0.5 mL) and cooled to -20°C. Pyridinium HCl (15 mg, 0.131 mmol) was dissolved in anhydrous pyridine (1 mL) and then added dropwise to the reaction mixture. The reaction was allowed to stir at -20°C for 2 h. At this point CSO (39 mg, 0.131 mmol) in DCM (1 mL) was added to the reaction and allowed to stir for 1 h. Solvents were removed *in vacuo* and resulting syrup was purified over silica (5 mL) eluting with 50% EtOAc in hexanes (25 mL), 75% EtOAc in hexanes (25 mL), 100% EtOAc (25 mL), and 10% MeOH in EtOAc (25 mL) to yield 55.6 mg of white crystalline solid (61%). ¹H NMR

(DMSO- d_6): δ 11.40 (s, 1H), 8.31 (d, $J = 7.90$ Hz, 1H), 8.21-8.19 (m, 1H), 8.03 (d, $J = 7.45$ Hz, 2H), 7.93 (d, $J = 7.90$ Hz, 2H), 7.87 (d, $J = 7.50$ Hz, 2H), 7.69-7.66 (m, 4H), 7.55-7.44 (ovlp, m, 6H), 6.25 (s, 1H), 5.97-5.91 (m, 2H), 5.83 (t, $J = 6.55$, 1H), 5.77 (s, 1H), 5.71 (d, $J = 5.50$ Hz, 1H), 5.35 (dd, $J = 6.20, 15.90$ Hz, 2H), 5.21 (t, $J = 9.15$ Hz, 1H), 4.70 (br,s, 1H), 4.54 (s, 2H), 4.44-4.41 (m, 1H), 4.41-4.39 (m, 1H), 4.25-4.18 (m, 4H), 3.95 (m, 1H), 3.85 (m, 1H), 3.75 (m, 1H), 3.70 (d, $J = 5.6$ Hz, 1H), 3.60 (t, $J = 6.6$ Hz, 1H), 2.92 (t, $J = 5.2$ Hz, 4H), 1.84-1.78 (m, 2H), 1.03 (s, 3H), 0.96 (s, 3H). ^{13}C NMR (DMSO- d_6): δ 173.12, 167.45, 164.64, 164.57, 163.94, 154.36, 147.02, 133.99, 133.93, 132.98, 132.89, 129.38, 128.78, 128.57, 128.49, 127.84, 118.47, 117.95, 113.29, 96.83, 91.22, 80.24, 80.14, 75.09, 73.72, 70.50, 68.03, 67.79, 66.24, 65.68, 60.40, 34.60, 30.08, 29.99, 22.24, 21.00, 20.35. HR-ESI-MS: calcd for $[\text{M}+\text{Na}]^+$, 1071.2913; found 1071.2937.

Trisodium (R)-4-((3-((((2R,3S,4R,5R)-5-(4-amino-2-oxopyrimidin-1(2H)-yl)-3,4-dihydroxytetrahydrofuran-2-yl)methoxy)oxidophosphoryl)oxy)propyl)amino)-3-hydroxy-2,2-dimethyl-4-oxobutyl phosphate (8) The protected phosphate **7** (56 mg, 0.0537 mmol) was dissolved in anhydrous DCM (1 mL). DBU (0.077 mL, 0.429 mmol) and TMSCl (0.023 mL, 0.215 mmol) were added dropwise to the solution and allowed to stir at rt for 6h. Solvents were removed *in vacuo*, and then the resulting syrup was dissolved in NH_4OH (2 mL). β -mercaptoethanol (0.1 mL) was added and the reaction was stirred at 55°C for 1 h. The reaction was then placed on a C-18 prep sep column and eluted with H_2O . The UV active fractions (fractions 3-5) were collected and manually loaded onto a 15 mL AMGP anion exchange column. The anion exchange column was washed with H_2O (30 mL) and then eluted with a 0-60% gradient of 1M NaCl. The fractions were monitored at 254 nm and the UV active fractions at 22% 1M NaCl were collected and lyophilized. The powder was then dissolved in H_2O and purified over a 300 mL sephadex size exclusion column. The UV active fractions (16-20) were collected and lyophilized to yield desired trisodium salt as a fluffy white solid (28.5 mg, 80.8%). ^1H NMR ($\text{D}_2\text{O}-d_2$): δ 7.84 (d, $J = 7.55$ Hz, 1H), 6.00 (d, $J = 7.65$ Hz, 1H), 5.88 (d, $J = 3.45$ Hz, 1H), 4.21-4.16 (m, 2H), 4.16 (s, 1H), 4.09 (d, $J = 10.10$ Hz, 1H), 4.00-3.07 (m, 1H), 3.94 (s, 1H), 3.85-3.81 (m, 2H), 3.68 (dd, $J = 5.32, 9.85$ Hz, 1H), 3.40 (dd, $J = 4.84, 9.92$ Hz, 1H), 3.23 (t, $J = 6.70$ Hz, 2H), 1.78 (t, $J = 6.52$ Hz, 2H), 0.87 (s, 3H), 0.76 (s, 3H).

^{13}C NMR ($\text{D}_2\text{O}-d_2$): δ 174.84, 165.99, 157.23, 141.27, 96.35, 89.45, 82.39, 74.54, 74.11, 70.83, 69.14, 64.07, 63.69, 38.23, 35.69, 29.49, 20.99, 18.25. ^{31}P NMR ($\text{D}_2\text{O}-d_2$): δ 1.78 (s, 1P), 0.35 (s, 1P). HR-ESI-MS: calcd for $[\text{M}+\text{H}]^+$, 657.0922; found 657.0936.

Allyl **(((2R,3S,4R,5R)-5-(4-amino-2-oxopyrimidin-1(2H)-yl)-3,4-dihydroxytetrahydrofuran-2-yl)methyl) (3-((4R)-2-(2-cyanoethoxy)-5,5-dimethyl-2-oxido-1,3,2-dioxaphosphinane-4-carboxamido)propyl) phosphate (9)** The diol **6** (190 mg, 0.22 mmol) and 5-(ethylthiol)-1H-tetrazole (86 mg, 0.66 mmol) along with 3 Å molecular sieves were dissolved in anhydrous CH_3CN (5 mL). *O,O*-bis(cyanoethyl)-*N*-diisopropylamine phosphoramidite (119 mg, 0.44 mmol) in anhydrous CH_3CN (0.5 mL) was added dropwise and the reaction was stirred at rt for 4 h. CSO (131 mg, 0.44 mmol) in anhydrous CH_3CN (3mL) was added dropwise and allowed to stir for 2 h. The solvents were removed *in vacuo* and the resulting syrup was purified over silica (5 mL) eluting with 50% EtOAc in hexanes (25 mL), 75% EtOAc in hexanes (25 mL), 100% EtOAc (25 mL) to yield 135.6 mg of white crystalline solid (59%). ^1H NMR ($\text{DMSO}-d_6$): δ 11.41 (s, 1H), 8.31 (d, $J = 7.45$ Hz, 1H), 8.21-8.19 (m, 1H), 8.03 (d, $J = 7.60$ Hz, 2H), 7.93 (d, $J = 7.45$ Hz, 2H), 7.88 (d, $J = 7.35$ Hz, 2H), 7.69-7.64 (m, 4H), 7.54 (t, $J = 7.72$ Hz, 2H), 7.47 (ovlp,d,t 6H), 6.26 (d, $J = 2.53$ Hz, 1H), 5.97-5.91 (m, 2H), 5.35 (dd, $J = 5.05, 15.62$ Hz, 2H), 4.72-4.70 (m, 1H), 4.61 (s, 1H), 4.55 (br,s, 3H), 4.47-4.45 (m, 1H), 4.41-4.38 (m, 1H), 4.18 (q, $J = 5.27$ Hz, 2H), 4.13 (d, $J = 11.35$, 1H), 4.395 (m, 1H), 3.85 (m, 1H), 3.60 (t, $J = 6.6$ Hz, 1H), 2.97 (t, $J = 5$ Hz, 2H), 1.82-1.78 (m, 2H), 1.03 (s, 3H), 0.96 (s, 3H). ^{13}C NMR ($\text{DMSO}-d_6$): δ 167.65, 165.83, 165.69, 164.65, 164.58, 163.83, 154.22, 146.91, 133.99, 133.93, 133.08, 132.97, 132.89, 129.38, 128.78, 128.57, 128.49, 128.03, 118.42, 117.95, 96.87, 91.16, 84.38, 80.20, 78.00, 73.73, 70.50, 68.06, 67.78, 66.25, 65.59, 62.75, 61.78, 34.29, 29.78, 26.47, 19.98, 19.14, 19.03, 17.64, 15.02. ^{31}P NMR ($\text{DMSO}-d_6$): δ -1.01 (s, 1P), -9.44 (s, 1P). HR-ESI-MS: calcd for $[\text{M}+\text{Na}]^+$, 1000.2542; found 1000.2576.

Disodium **(((2R,3S,4R,5R)-5-(4-amino-2-oxopyrimidin-1(2H)-yl)-3,4-dihydroxytetrahydrofuran-2-yl)methyl (3-((R)-5,5-dimethyl-2,2-dioxido-1,3,2-dioxaphosphinane-4-carboxamido)propyl) phosphate (10)** The protected phosphate **9** (15 mg, 0.0155 mmol) was dissolved in anhydrous DCM (1 mL). DBU (0.02 mL, 0.115 mmol) and TMSCl (0.006 mL, 0.057 mmol) were added dropwise to the solution and

allowed to stir at rt for 6h. Solvents were removed *in vacuo*, and then the resulting syrup was dissolved in NH₄OH (2 mL). β-mercaptoethanol (0.1 mL) was added and the reaction was stirred at 55°C for 1 h. The reaction was then placed on a C-18 prep sep column and eluted with H₂O. The UV active fractions (fractions 3-5) were collected and manually loaded onto a 15 mL AGMP1 anion exchange column. The anion exchange column was washed with H₂O (30 mL) and then eluted with a 0-60% gradient of 1 M NaCl. The fractions were monitored at 254 nm and the UV active fractions at 18% 1 M NaCl were collected and lyophilized. The powder was then dissolved in H₂O and desalted over a 300 mL sephadex size exclusion column. The UV active fractions (15-19) were collected and lyophilized to yield desired disodium salt as a fluffy white solid (7.6 mg, 81.1%). ¹H NMR (D₂O-*d*₂): δ 7.82 (d, *J* = 7.10 Hz, 1H), 5.99 (d, *J* = 7.70 Hz, 1H), 5.88 (s, 1H) 4.40 (s, 1H) 4.23-4.21 (m, 2H) 4.17-4.15 (m, 1H), 4.07 (d, *J* = 4.15 Hz, 1H) 3.99 (d, *J* = 11.50 Hz, 2H), 3.82 (q, *J* = 6.05 Hz, 2H), 3.63 (dd, *J* = 11.10, 23.15 Hz, 1H), 3.23 (dm, 2H), 1.75 (t, *J* = 6.20 Hz), 0.91 (s, 3H), 0.86 (s, 3H). ¹³C NMR (D₂O-*d*₂): δ 170.48, 166.07, 157.62, 141.24, 96.34, 89.39, 82.49, 82.42, 76.38, 74.12, 69.144, 64.11, 63.58, 35.73, 34.54, 29.51, 19.94, 17.38. ³¹P NMR (D₂O-*d*₂): δ -0.367 (s, 1P), -4.21 (s, 1P). HR-ESI-MS: calcd for [M-H]⁻, 571.1206, found 571.1213.

Sulfamoyl chloride³⁰ Chlorosulfonyl isocyanate (1.2 mL, 14.1 mmol) was dissolved in anhydrous DCM (7 mL) and cooled to 0°C. 88% Formic acid (0.65 mL, 14.7 mmol) was added dropwise and stirred at 0°C for 15 min. The reaction was stirred at rt for 45 min and then heated to reflux for 45 min. The reaction mixture was then placed in the -20°C freezer overnight. The next day the mixture was cooled to -48°C and the sulfamoyl chloride crystallized out. The crystals were vacuumed filtered and washed with DCM to yield the desired product (1.6 g, 96%).

2'-3'-*O,N*⁴-Tribenzoyl-5'-*O*-sulfamoyl cytidine (11)³¹ Tribenzoyl cytidine **4** (1.54 g, 2.7 mmol) was dissolved in anhydrous DMA (5 mL). A solution of freshly made sulfamoyl chloride (940 mg, 8.11 mmol) dissolved in anhydrous DMA (2 mL) was added dropwise at 0°C. The ice bath was removed and the reaction was stirred at rt for 3 h. The reaction was quenched with H₂O (1 mL) and the solvents were removed *in vacuo*. The resulting syrup was partitioned between EtOAc (250 mL) and brine (50 mL). The brine layer was washed with EtOAc (2 x 50 mL) and then the organic extracts were combined, dried

(Na₂SO₄), and concentrated *in vacuo*. The crude mixture was then purified over silica (50 mL) eluting with 50% EtOAc in hexanes to yield the desired product as a white solid (1.32 g, 77%). ¹H NMR (DMSO-*d*₆): δ 11.41 (s, 1H), 8.29 (d, *J* = 7.50 Hz, 1H), 7.87 (d, *J* = 8.10 Hz, 2H) 8.03 (d, *J* = 8.00 Hz, 2H), 7.95 (d, *J* = 8.20 Hz, 2H), 7.75 (s, 2H), 7.70-7.65 (m, 3H), 7.52-7.40 (m, ovlp, 7H), 6.27 (d, *J* = 3.65 Hz, 1H), 5.91 (t, *J* = 5.05 Hz, 1H) 5.81 (t, *J* = 6.10 Hz, 1H), 4.77 (s, 1H), 4.50-4.44 (m, 1H), 4.43-4.41 (m, 1H). ¹³C NMR (DMSO-*d*₆): δ 167.53, 164.57, 164.47, 163.70, 154.19, 146.54, 133.91, 133.87, 133.00, 132.80, 129.30, 128.72, 128.70, 128.47, 128.41, 128.36, 96.93, 90.66, 79.46, 73.64, 70.64, 67.88. HR-ESI-MS: calcd for [M-H]⁻, 635.1448, found 635.1445.

2,5-Dioxopyrrolidin-1-yl-3-((4*R*)-2-(4-methoxyphenyl)-5,5-dimethyl-1,3-dioxane-4-carboxamido)propanoate (13)²⁹ Pantothenic acid hemicalcium salt (5 g, 20.98 mmol) was dissolved in anhydrous DMF (50 mL). Concentrated H₂SO₄ (0.65 mL, 20.98 mmol) was added dropwise and stirred for 30 min. *p*-Anisaldehyde dimethyl acetal (3.6 mL, 20.98 mmol) and CSA (244 mg, 1.05 mmol) were added and the reaction was stirred for 16 h. Solvents were removed *in vacuo* and the resulting syrup was portioned between EtOAc (500 mL) and H₂O (50 mL). The organic layer was washed with H₂O (2 x 50 mL). The organic layer is then dried (Na₂SO₄) and evaporated. The resulting white solid is then washed with DCM to remove any remaining *p*-anisaldehyde dimethyl acetal to yield the desired product as a white crystalline product (5.1 g, 72%).

The PMB protected pantothenic acid (750 mg, 2.10 mmol) and *N*-hydroxysuccinimide (242 mg, 2.10 mmol) were dissolved in anhydrous THF (5 mL). A solution of DCC (433 mg, 2.10 mmol) in anhydrous THF (3 mL) was added dropwise and the reaction was stirred for 6h. The reaction mixture was then filtered over celite to remove the white precipitate. The white precipitate was then washed with EtOAc (10 mL). The organic filtrate was then concentrated *in vacuo* to yield the desired product as a glassy clear solid (885 mg, 93%). ¹H NMR (DMSO-*d*₆): δ 7.59 (s, 1H), 7.45 (d, *J* = 8.40 Hz, 2H), 6.94 (d, *J* = 8.80 Hz, 2H), 5.53 (s, 1H), 4.12 (s, 1H), 3.76 (s, 1H), 3.33 (s, 3H), 2.88 (t, *J* = 7.10 Hz, 2H), 2.81 (s, 4H), 2.42-2.40 (m, ovlp, 2H), 1.00 (s, 3H), 0.96 (s, 3H). ¹³C NMR (DMSO-*d*₆): δ 170.59, 169.07, 167.84, 160.00, 130.95, 128.27, 113.80, 100.91, 83.63, 77.85, 55.61, 34.30, 33.02, 30.94, 25.90, 21.97, 19.50. HR-ESI-MS: calcd for [M+Na]⁺, 457.1582; found 457.1589.

5'-O-(N-(3-((4R)-2-(4-Methoxyphenyl)-5,5-dimethyl-1,3-dioxane-4-carboxamido)propanoyl)sulfamoyl)-2',3'-O,N⁴-tribenzoylcytidine (14)¹⁵ NHS ester **13** (442 mg, 0.97 mmol) was dissolved in anhydrous DMF (8 mL). Sulfamoyl cytidine **11** (307 mg, 0.485 mmol) was added and the solution was cooled to 0°C. Cs₂CO₃ (316 mg, 0.97 mmol) was added and stirred at 0°C for 30 min. The ice bath was removed and the reaction was stirred at rt for 16 h. The solvents were removed *in vacuo* and the resulting paste was taken up in EtOAc (50 mL) and filtered. The white precipitate was washed thoroughly with EtOAc (100 mL). The combined filtrate was purified over silica (25 mL) eluting with 75% EtOAc in hexanes (100 mL), 100% EtOAc (100 mL), and 10% MeOH in EtOAc (100 mL) to yield the desired product as a white solid (270 mg, 58%). ¹H NMR (DMSO-*d*₆): δ 11.33 (s, 1H), 8.02 (d, *J* = 7.20 Hz, 2H), 7.94 (d, *J* = 7.20 Hz, 2H), 7.83 (d, *J* = 7.10 Hz, 2H), 7.64 (t, *J* = 7.55 Hz, 3H), 7.55-7.41 (m, ovlp, 12H), 6.90 (d, *J* = 8.81 Hz, 2H), 6.30 (d, *J* = 4.30 Hz, 1H), 5.83 (t, *J* = 5.15 Hz, 1H), 5.75 (t, *J* = 5.49 Hz, 1H), 5.48 (s, 1H), 4.69 (m, 1H), 4.47-4.38 (m, 2H), 4.12-3.96 (m, ovlp, 1H), 4.05 (s, 1H), 3.73 (s, 3H), 3.59 (d, *J* = 2.72 Hz, 1H), 3.29-3.26 (m, 2H), 2.39-2.84 (m, 2H), 0.98 (s, 3H), 0.92 (s, 3H). ¹³C NMR (DMSO-*d*₆): δ 167.92, 167.23, 164.49, 164.31, 163.63, 159.39, 154.35, 146.33, 133.80, 133.76, 132.96, 132.68, 130.32, 129.23, 128.67, 128.63, 128.52, 128.40, 128.33, 127.61, 113.21, 100.26, 96.83, 83.08, 80.00, 77.29, 73.94, 71.04, 54.96, 34.48, 32.40, 21.43, 18.91. HR-ESI-MS: calcd for [M+H]⁺, 954.2863; found 954.2906.

5'-O-(N-(3-((R)-2,4-Dihydroxy-3,3-dimethylbutanamido)propanoyl)sulfamoyl)-2',3'-O,N⁴-tribenzoylcytidine (15) The *p*-methoxy benzyl acetal **14** (92.5 mg, 0.097 mmol) was dissolved in 80% AcOH (5 mL) and stirred at rt for 12 h. Solvents were removed *in vacuo* and the resulting syrup was purified over silica (10 mL) eluting with 75% EtOAc in hexanes (25 mL), 100% EtOAc (25 mL), and 10% MeOH in EtOAc (25 mL) to yield the desired product as a white solid (65 mg, 80%). ¹H NMR (DMSO-*d*₆): δ 11.33 (s, 1H), 8.50 (s, 1H), 8.02 (d, *J* = 7.53 Hz, 2H), 7.95 (d, *J* = 7.29 Hz, 2H), 7.83 (d, *J* = 7.65 Hz, 2H), 7.67-7.61 (m, 5H), 7.55-7.41 (m, 8H), 6.32 (s, 1H), 5.84-5.82 (m, 1H), 5.75 (t, *J* = 5.52 Hz, 1H), 5.35 (d, *J* = 5.61 Hz, 1H), 4.74-4.70 (m, 1H), 4.44-4.31 (m, 2H), 4.10 (d, *J* = 5.22 Hz, 1H), 3.67 (d, *J* = 5.52 Hz, 1H), 3.30-3.26 (m, 2H), 2.30-2.27 (m, 2H), 0.77 (s, 3H), 0.75 (s, 3H). ¹³C NMR (DMSO-*d*₆): δ 176.72, 173.03, 165.10, 164.84, 147.23, 147.00, 134.39, 134.34, 133.62, 133.24, 129.82, 129.31, 129.22, 129.00, 128.92, 97.50,

88.70, 81.15, 75.50, 74.77, 72.05, 68.58, 66.71, 66.16, 39.27, 35.75, 21.27, 20.96. HR-ESI-MS: calcd for [M+Na]⁺, 858.2263; found 858.2286.

5'-O-(N-(((R)-Bis(2-cyanoethyl) 3-hydroxy-4-(3-oxopropylamino)-2,2-dimethyl-4-oxobutyl) phosphoryl)oxy)sulfamoyl)-2',3'-O,N⁴-tribenzoylcytidine (16) The diol **15** (65 mg, 0.077 mmol), *O,O*-bis(cyanoethyl)-*N*-diisopropylamine phosphoramidite (32 mg, 0.117 mmol), and 3 Å molecular sieves were dissolved in anhydrous pyridine (0.5 mL) and cooled to -20°C. Pyridinium HCl (13.5 mg, 0.117 mmol) was dissolved in anhydrous pyridine (1 mL) and then added dropwise to the reaction mixture. The reaction was allowed to stir at -20°C for 2 h. At this point CSO (35 mg, 0.117 mmol) in DCM (1 mL) was added to the reaction and allowed to stir for 1 h. Solvents were removed *in vacuo* and resulting syrup was purified over silica (5 mL) eluting with 50% EtOAc in hexanes (25 mL), 75% EtOAc in hexanes (25 mL), 100% EtOAc (25 mL), and 10% MeOH in EtOAc (25 mL) to yield 38 mg of white solid (50%). ¹H NMR (DMSO-*d*₆): δ 11.34 (s, 1H), 8.46 (s, 1H), 8.04 (d, *J* = 7.20 Hz, 2H), 7.96 (d, *J* = 7.17 Hz, 2H), 7.86 (d, *J* = 7.14 Hz, 2H), 7.66 (t, *J* = 7.53 Hz, 3H), 7.57-7.43 (m, 8H), 6.34 (d, *J* = 6.30 Hz, 1H), 5.86-5.81 (m, 1H), 5.79-5.70 (ovlp, m, 2H), 4.75 (s, 1H), 4.46-4.40 (m, 2H), 4.28-4.21 (m, 4H), 4.04 (q, *J* = 11.92, 1H), 3.94-3.92 (m, 1H), 3.88-3.86 (m, 1H), 3.29-3.26 (m, 2H), 2.95 (t, *J* = 8.74 Hz, 4H), 2.28-2.23 (m, 2H), 0.89 (s, 3H), 0.85 (s, 3H). ¹³C NMR (DMSO-*d*₆): δ 176.42, 174.02, 165.12, 161.98, 134.36, 133.25, 129.81, 129.21, 128.90, 103.80, 97.52, 75.49, 74.65, 68.56, 62.89, 60.87, 30.65, 26.95, 23.87, 21.28, 20.91, 19.61. ³¹P NMR (DMSO-*d*₆): δ -2.13 (s, 1P). HR-ESI-MS: calcd for [M+Na]⁺, 1044.2458; found 1044.2482.

5'-O-(N-(((R)-3-hydroxy-4-(3-oxopropylamino)-2,2-dimethyl-4-oxobutyl)phosphoryl)oxy) sulfamoyl) cytidine disodium salt (17) The protected phosphate **16** (61 mg, 0.0597 mmol) was dissolved in anhydrous DCM (1 mL). DBU (0.086 mL, 0.478 mmol) and TMSCl (0.026 mL, 0.239 mmol) were added dropwise to the solution and allowed to stir at rt for 6h. Solvents were removed *in vacuo*, and then the resulting syrup was dissolved in NH₄OH (2 mL). β-mercaptoethanol (0.1 mL) was added and the reaction was stirred at 55°C for 1 h. The reaction was then placed on a C-18 prep column and eluted with H₂O. The UV active fractions (fractions 3-5) were collected and manually loaded onto a 15 mL AGMP1 anion exchange column. The anion exchange column was washed with H₂O (30 mL) and then eluted with a 0-60% gradient of 1M

NaCl. The fractions were monitored at 254 nm and the UV active fractions at 58% 1M NaCl were collected and lyophilized. The powder was then dissolved in H₂O and desalted over a 300 mL sephadex size exclusion column. The UV active fractions (15-20) were collected and lyophilized to yield desired trisodium salt as a fluffy white solid (36 mg, 95%). ¹H NMR (D₂O-*d*₂): δ 7.75 (d, *J* = 7.10 Hz, 1H), 5.99 (d, *J* = 7.70 Hz, 1H), 5.86 (s, 1H), 4.31 (d, *J* = 9.60 Hz, 1H), 4.23-4.21 (m, 2H), 4.15 (s, 1H), 3.67-3.64 (m, 1H), 3.37 (t, *J* = 6.80 Hz, 2H), 3.30 (dd, *J* = 4.00, 9.20 Hz, 1H), 2.38 (t, *J* = 6.58 Hz, 2H), 0.88 (s, 3H), 0.72 (s, 3H). ¹³C NMR (D₂O-*d*₂): δ 180.70, 174.99, 166.14, 157.66, 141.25, 96.38, 89.51, 81.35, 74.62, 73.99, 70.70, 69.22, 67.57, 38.38, 37.97, 35.70, 21.34, 17.96. ³¹P NMR (D₂O-*d*₂): δ 1.42 (s, 1P). HR-ESI-MS: calcd for [M+Na]⁺, 670.0779; found 670.0780.

5'-O-(N-(((R)-2-(2-cyanoethoxy)-5,5-dimethyl-N-(3-oxopropyl)-1,3,2-

dioxaphosphinane-4-carboxamide 2-oxy)sulfamoyl)-2',3'-O,N4-tribenzoyl cytidine (18) The diol **15** (115 mg, 0.14 mmol) and 5-(ethylthiol)-1H-tetrazole (54 mg, 0.411 mmol) along with 3 Å molecular sieves were dissolved in anhydrous CH₃CN (5 mL). *O,O*-bis(cyanoethyl)-*N*-diisopropylamine phosphoramidite (75 mg, 0.275 mmol) in anhydrous CH₃CN (0.5 mL) was added dropwise and the reaction was stirred at rt for 4 h. CSO (82 mg, 0.275 mmol) in anhydrous CH₃CN (3mL) was added dropwise and allowed to stir for 2 h. The solvents were removed *in vacuo* and the resulting syrup was purified over silica (5 mL) eluting with 50% EtOAc in hexanes (25 mL), 75% EtOAc in hexanes (25 mL), 100% EtOAc (25 mL), and 10% MeOH in EtOAc (25 mL) to yield the desired product as a white solid (68 mg, 52%). ¹H NMR (DMSO-*d*₆): δ 11.34 (s, 1H), 8.55 (s, 1H), 8.20 (s, 1H), 8.03 (d, *J* = 7.25 Hz, 2H), 7.96 (d, *J* = 7.15 Hz, 2H), 7.84 (d, *J* = 8.0 Hz, 2H), 7.69 (t, *J* = 7.35 Hz, 2H), 7.65 (t, *J* = 7.35 Hz, 2H), 7.52 (q, *J* = 8.15 Hz, 4H), 7.45 (t, *J* = 7.90 Hz, 3H), 6.35 (d, *J* = 4.50 Hz, 1H), 5.83 (t, *J* = 5.40 Hz, 1H) 5.76 (ovlp,m, 2H), 4.73 (s, 1H), 4.51 (d, *J* = 7.75 Hz, 1H), 4.37-4.31 (m, 2H), 4.23-4.18 (m, 2H), 3.88 (t, *J* = 4.65 Hz, 1H), 3.18 (m, 1H), 3.15 (q, *J* = 7.35 Hz, 1H), 2.94 (t, *J* = 4.30Hz, 2H), 2.28-2.23 (m, 2H), 1.02 (s, 3H), 0.95 (s, 3H). ¹³C NMR (DMSO-*d*₆): δ 186.17, 165.12, 164.88, 164.00, 154.90, 146.31, 134.35, 133.24, 129.80, 129.22, 129.00, 128.92, 128.31, 119.28, 118.71, 95.78, 89.01, 82.35, 74.32, 73.23, 65.71, 63.22,

60.88, 26.91, 19.62, 15.50. ³¹P NMR (DMSO-*d*₆): δ -9.46 (s, 1P). HR-ESI-MS: calcd for [M+Na]⁺, 973.2087; found 973.2098.

Sodium 5'-O-(N-(((R)-5,5-dimethyl-4-((3-oxopropyl)carbamoyl)-1,3,2-dioxaphosphinan-2-olate 2-oxy)sulfamoyl) cytidine (19) The protected phosphate **18** (38 mg, 0.0402 mmol) was dissolved in anhydrous DCM (1 mL). DBU (0.058 mL, 0.322 mmol) and TMSCl (0.015 mL, 0.16 mmol) were added dropwise to the solution and allowed to stir at rt for 6h. Solvents were removed *in vacuo*, and then the resulting syrup was dissolved in NH₄OH (2 mL). β-mercaptoethanol (0.1 mL) was added and the reaction was stirred at 55°C for 1 h. The reaction was then placed on a C-18 prep sep column and eluted with H₂O. The UV active fractions (fractions 3-5) were collected and manually loaded onto a 15 mL AMGP anion exchange column. The anion exchange column was washed with H₂O (30 mL) and then eluted with a 0-60% gradient of 1M NaCl. The fractions were monitored at 254 nm and the UV active fractions at 54% 1M NaCl were collected and lyophilized. The powder was then dissolved in H₂O and purified over a 300 mL sephadex size exclusion column. The UV active fractions (15-20) were collected and lyophilized to yield desired trisodium salt as a fluffy white solid (21 mg, 86%). ¹H NMR (D₂O-*d*₂): δ 8.61 (s, 1H), 7.82 (d, *J* = 7.70 Hz, 1H), 6.03 (d, *J* = 7.70 Hz, 1H), 5.85 (d, *J* = 3.35 Hz, 1H), 4.40 (s, 1H), 4.31 (d, *J* = 10.10 Hz, 1H), 4.23 (s, 2H), 4.21-4.17 (m, 2H), 3.98 (d, *J* = 11.20 Hz, 1H), 3.62 (dd, *J* = 11.42, 22.83 Hz, 1H), 3.45-3.35 (m, 2H), 2.40 (t, *J* = 6.70 Hz, 2H), 0.93 (s, 3H), 0.87 (s, 3H). ¹³C NMR (D₂O-*d*₂): δ 180.55, 174.77, 166.12, 160.40, 141.23, 96.36, 89.54, 82.26, 81.30, 74.66, 73.92, 69.23, 67.65, 39.23, 38.31, 37.94, 35.66, 21.44, 17.85. ³¹P NMR (D₂O-*d*₂): δ -4.26 (s, 1P). HR-ESI-MS: calcd for [M-H]⁻, 606.0883; found 606.0901.

Purification of *E. faecalis* PPCS: *E. coli* BL21 AI/pUMGD1 was used to express *E. faecalis* PPCS and the enzyme purified by previously published methods.¹²

Purification of C-terminal Hexa-Histidine Tagged Human PPCS: *E. coli* BL21 (DE3)/pUMJY120ho was used to express human PPCS and the enzyme purified by previously published methods.³³

Cloning, Overexpression, and Purification of *E. coli* PPCS: The *coaB* coding region of the *dfp* gene (encoding ser181-arg406 of the *E. coli* CoaBC protein)^{4, 34} was PCR amplified using *E. coli* MG1655 genomic DNA as a template, and the primers,

coabec1(forward primer), 5' – CGCGCATA TGTCGCCCCGTCAACGACCTGAAACATCTG-3' and dfp3 (reverse primer), 5'- GCGCCTCGAGACGTCGATTTTTTTCATCATAACGGG-3'. The forward primer introduces an *NdeI* site (shown underlined) to provide a start codon for the *coaB* coding region, and the reverse primer creates a *XhoI* site (shown underlined) downstream of the stop codon of the open reading frame. The PCR products were digested with *NdeI* and *XhoI*, and ligated into pET23a(+) (Novagen) cut with *NdeI* and *XhoI*. The resulting plasmid was designated pUMDOT3 and the insert was confirmed by DNA sequencing.

E. coli BL21 AI (Invitrogen) harboring the plasmid pUMDOT3 were grown in 500 mL LB-ampicillin media (5 g of NaCl, 5 g of yeast extract, 10 g of tryptone, and 100 mg of ampicillin per L) at 37°C and 250 rpm to a OD600 of 0.6. The cells were then cooled by shaking at 16°C for 10-15 min, induced with 0.07% L-arabinose, and continued to grow at 16°C and 250 rpm for 12-16 hours. The cells were harvested at 6000 x g for 10 minutes at 4°C, washed, and then suspended in 12 ml of 20 mM HEPES pH 8.0. Cells were lysed by French Press and crude cytosol obtained by centrifugation at 20,000 x g for 25 minutes at 4°C.

ecPPCS was purified using a tandem anion exchange column (Source 15Q (GE Healthcare); 20 mL) and cation exchange column (Source 15S (GE Healthcare); 8 mL). The 12 mL of crude cytosol was loaded onto the tandem chromatography columns which had been pre-equilibrated with 20 mM HEPES pH 8.0. The columns were then washed with another 40 mL of equilibration buffer and the anion exchange column was removed. Under these conditions the ecPPCS does not bind to the anion exchange resin, but does bind to the cation exchange resin. The cation exchange column was eluted with a linear gradient of 0-0.4 M NaCl in 20 mM HEPES pH 8.0, with a total gradient volume of 100 mL. ecPPCS eludes as a single peak at 75 mM NaCl and was greater than 98 % pure as determined by SDS-PAGE.

Cloning, Overexpression, and Purification of the C-terminal Hexa-Histidine Tagged

***Streptococcus pneumoniae* PPCS:** The *coaB* gene was amplified from *S. pneumoniae* TIGR4 genomic DNA via PCR, using the forward primer CATATGAAAATTTTAGTTACATC and reverse primer CTCGAGAGAATGATAGGCTTGAATTTTTTC to introduce a *NdeI* site before and

XhoI site after the gene. The PCR product from the amplification was digested with *NdeI* and *XhoI*, and then ligated into pET23a(+) (Novagen) also digested with *NdeI* and *XhoI*. The desired plasmid was designated pUMJY140h, and the sequence of the inserted *coaB* gene was confirmed by DNA sequencing. Since the reverse primer was designed to exclude the stop codon of the gene, the linker and hexa-histidine tag encoded by the pET23a(+) vector is expressed with the gene to generate the C-terminal hexa-histidine tagged PPCS.

E. coli strain BL21 AI, transformed with plasmid pUMJY140h, was incubated in four 1 L flasks containing 250 ml each of LB-ampicillin media at 37°C and 250 rpm to an OD600 of 0.6-0.8. Then, the culture was cooled to 16°C and induced with L-arabinose (0.065% w/v final concentration). Incubation at 16°C and 250 rpm shaking was continued for 16 hours. Cells from 1 L of culture were harvested via centrifugation at 6,000 x g, washed with 20 mM HEPES pH 8.0, and resuspended in 60 ml of 20 mM HEPES pH 8.0. The harvested cells were lysed via French Press, and the lysed mixture was centrifuged at 20,000 x g for 30 minutes to spin down the cellular debris as the pellet.

The resulting supernatant was shaken gently with Ni-NTA resin (4 mL per 1 L culture) in a solution of 10 mM imidazole and 20 mM HEPES pH 8.0 for 10 minutes. Then, the mixture was poured into a 20 mL column and the resin was collected in the column. The column was washed with 5 column volumes of 50 mM imidazole, 20 mM HEPES pH 8.0, followed by 5 column volumes of 50 mM imidazole, 500 mM NaCl, 20 mM HEPES pH 8.0. The column was pre-equilibrated prior to elution by flowing through 2 column volumes of 50 mM imidazole, 20 mM HEPES pH 8.0, and then eluted with a 250 mM imidazole, 20 mM HEPES pH 8.0 solution. The elution was collected as 1 mL fractions, until proteins were no longer eluted. The fractions containing protein were collected, diluted 4 fold with 20 mM HEPES pH 8.0, and chromatographed on a Mono Q 5/50 GL column pre-equilibrated with 20 mM HEPES pH 8.0 buffer. The column was eluted over a 10 column volume linear gradient of 0 – 0.5 M NaCl buffered with 20 mM HEPES pH 8.0. Approximately 30 mg of spPPCS was purified per liter of culture.

PPCS inhibition assays: The PPCS reaction was observed in the forward reaction via an enzyme coupled assay.^{12, 33} The coupled assay measured production of pyrophosphate from PPCS activity via the oxidation of NADH, which could be monitored as a

disappearance of absorption at 340 nm. For each mole of pyrophosphate produced, two moles of NADH are oxidized. The commercially available Pyrophosphate Reagent (PR) from Sigma-Aldrich was used as the pyrophosphate detection system and each vial of the PR was initially suspended in 4.5 mL of 100 mM Tris-HCl pH 7.6. Assays were performed on a SpectraMax M5 (Molecular Devices) microplate reader using 96-well half-area plates (Costar UV), with a final assay volume of 100 μ L. The pre-incubation mixture consisted of 30 μ L PR, 20 μ L PPCS (20-400 nM final assay concentration), and 20 μ L of varying concentrations of inhibitor in a total volume of 70 μ L. These solutions were preincubated at 37°C for 15 minutes. The enzymatic reaction was initiated by addition of the substrates (also pre-incubated at 37°C for 15 minutes) to the assay mixture, to a final concentration of 0.6 mM MgCTP (or MgATP with the human enzyme), 1.0 mM L-cysteine, and 0.6 mM PPA. The oxidation of NADH, monitored by a decreasing UV absorbance at 340 nm ($\epsilon = 6.22 \text{ mM}^{-1} \text{ cm}^{-1}$), is monitored over the course of the assay. Assays were run in triplicate with the average IC_{50} being reported. As a control, pre-incubation of the PR (in the absence of PPCS) with the highest concentrations of inhibitors (1000 nM) showed no inhibition of the coupling enzymes when assayed as above with the addition of magnesium pyrophosphate (0.1 mM).

K_i Determination³⁵: Assays were performed on a SpectraMax M5 (Molecular Devices) microplate reader using 96-well half-area plates (Costar UV), with a final assay volume of 100 μ L. The assay mixture consisted of 30 μ L of PR, 0.86 mM MgCTP, 0.86 mM PPA, 1.43 mM L-cysteine, 14 mM DTT, and 19 μ L of varying concentrations of inhibitor in a total volume of 70 μ L. The assay mixture was preincubated at 37°C for 15 minutes. The enzymatic reaction was initiated by addition of 30 μ L of efPPCS (also pre-incubated at 37°C for 15 minutes) to the assay mixture, to a final concentration of 27 nM. The oxidation of NADH, monitored by a decreasing UV absorbance at 340 nm ($\epsilon = 6.22 \text{ mM}^{-1} \text{ cm}^{-1}$), is monitored over the course of the assay (assays ran in triplicate).

Appendix to Chapter 2

IC₅₀ Plots for Intermediate Mimics

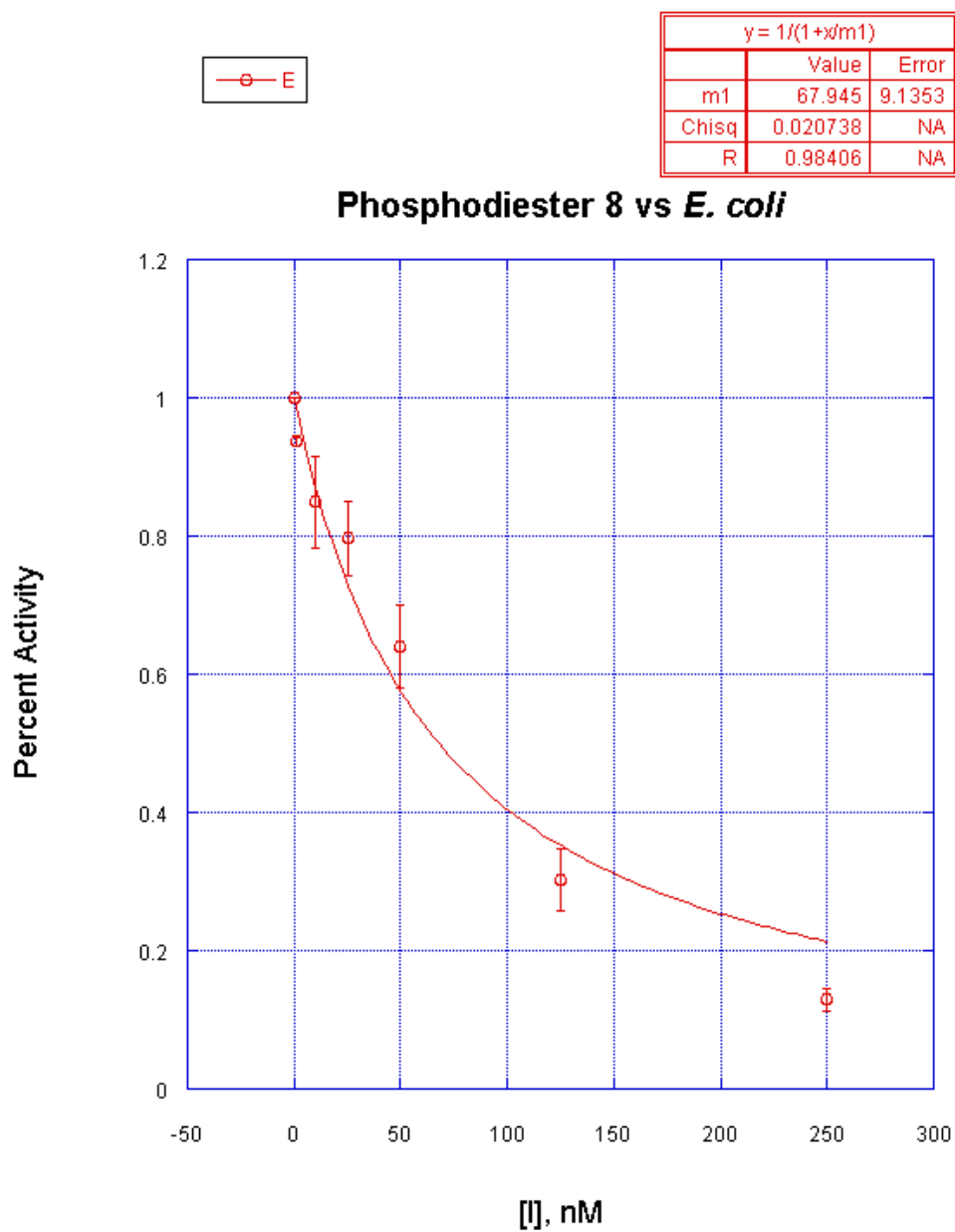


Figure 2.9: IC₅₀ plot for phosphodiester **8** vs. ecPPCS

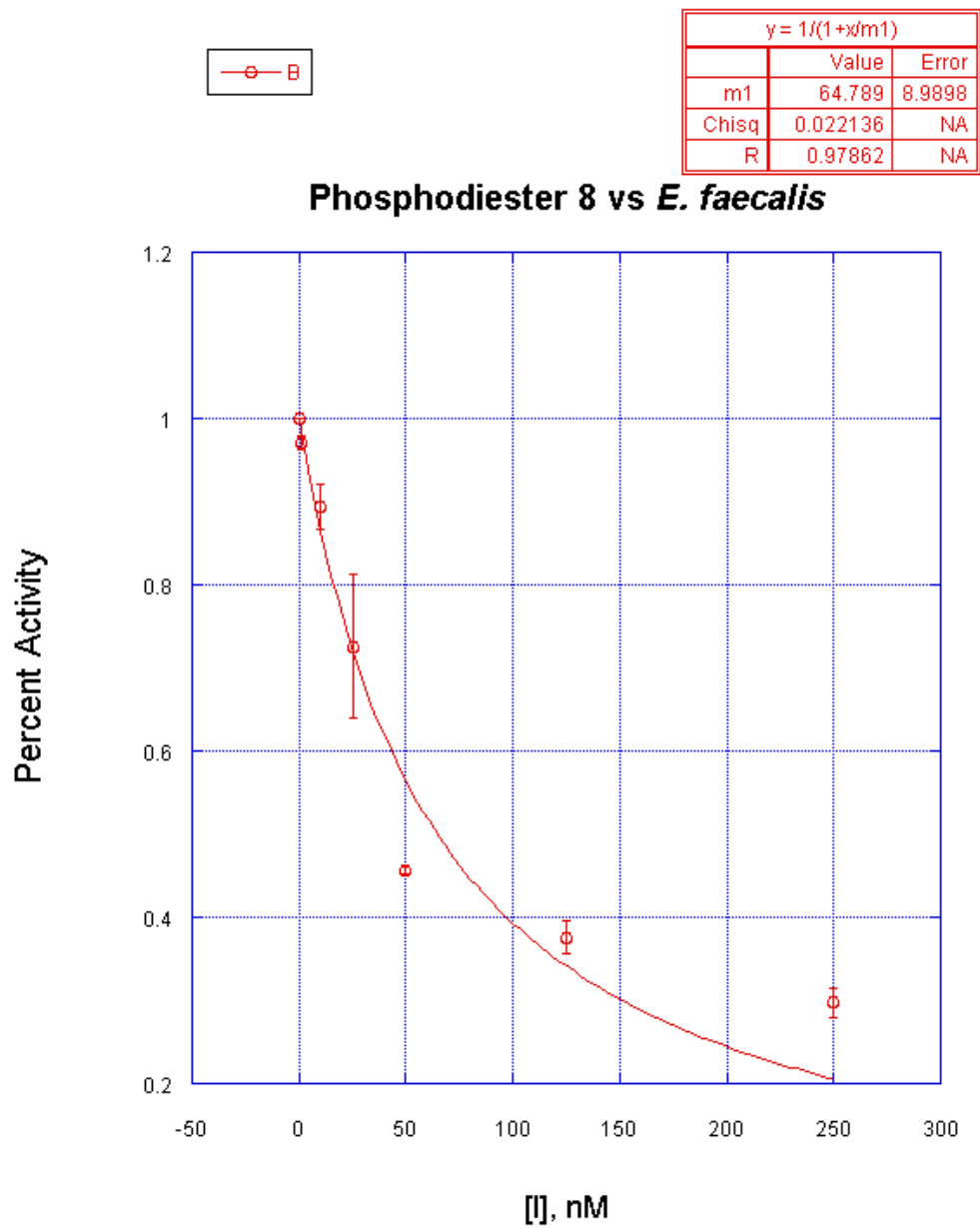


Figure 2.10: IC₅₀ plot for phosphodiester **8** vs. efPPCS

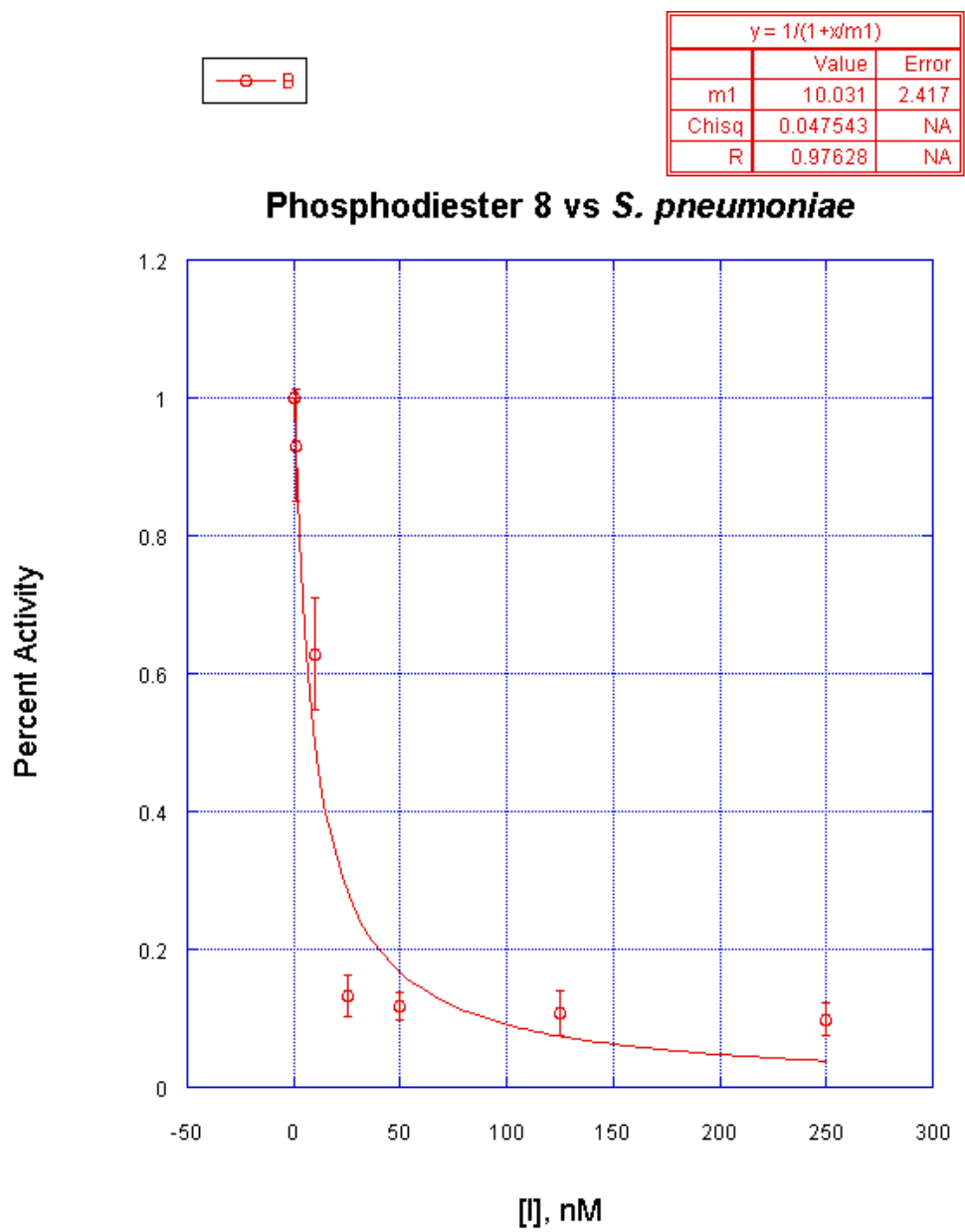


Figure 2.11: IC₅₀ plot for phosphodiester **8** vs. spPPCS

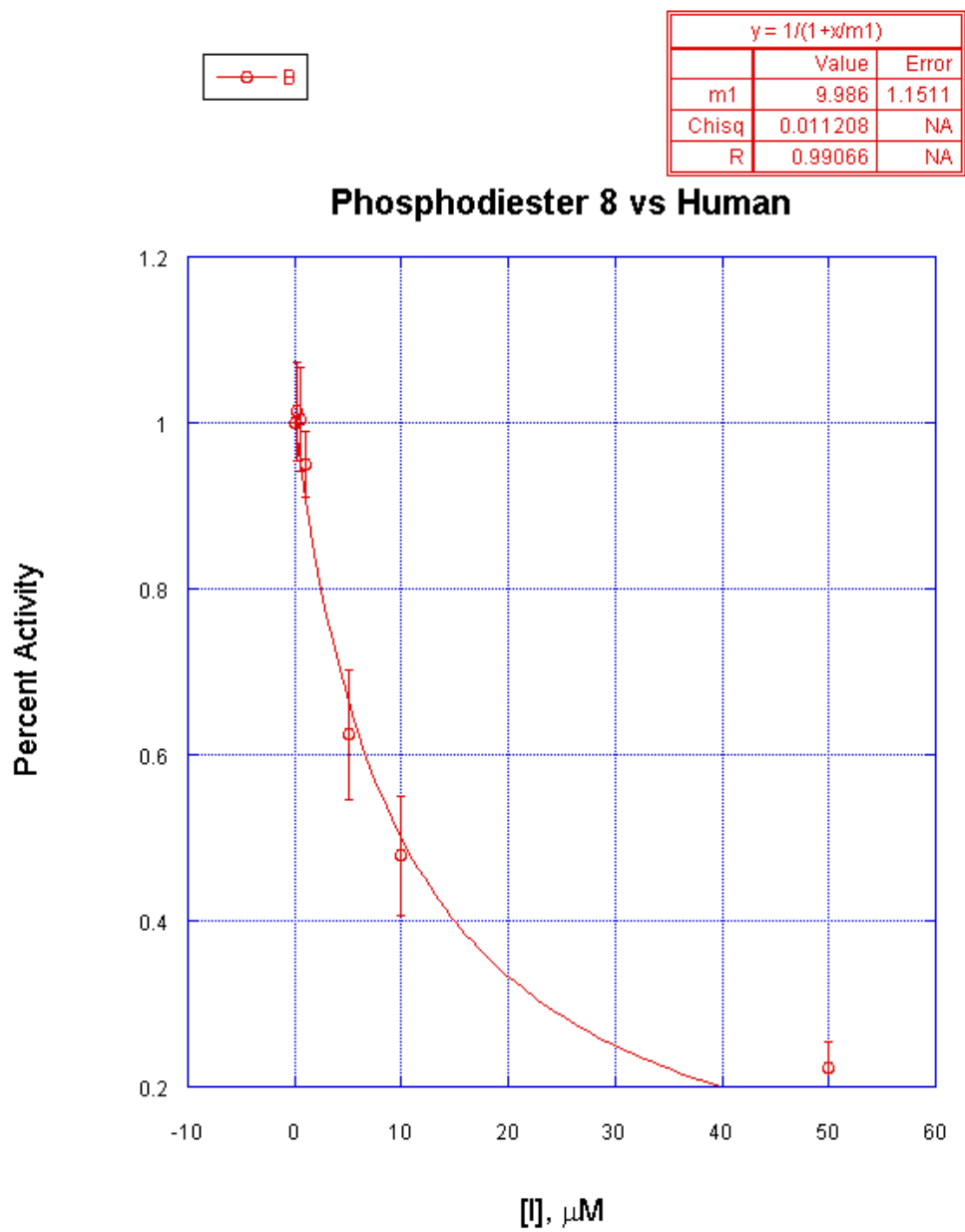


Figure 2.12: IC₅₀ plot for phosphodiester **8** vs. hPPCS

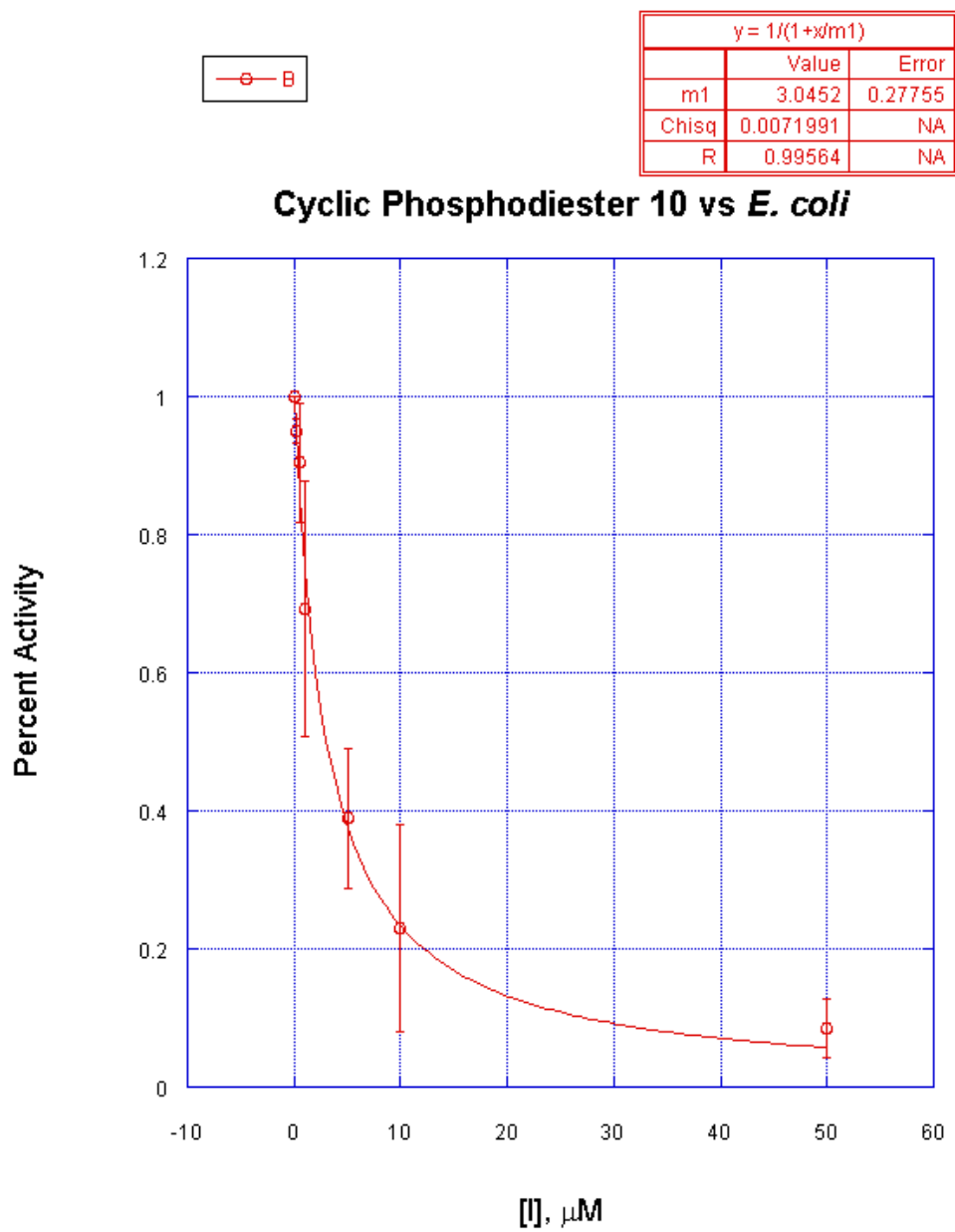


Figure 2.13: IC₅₀ plot for cyclic phosphodiester **10** vs. ecPPCS

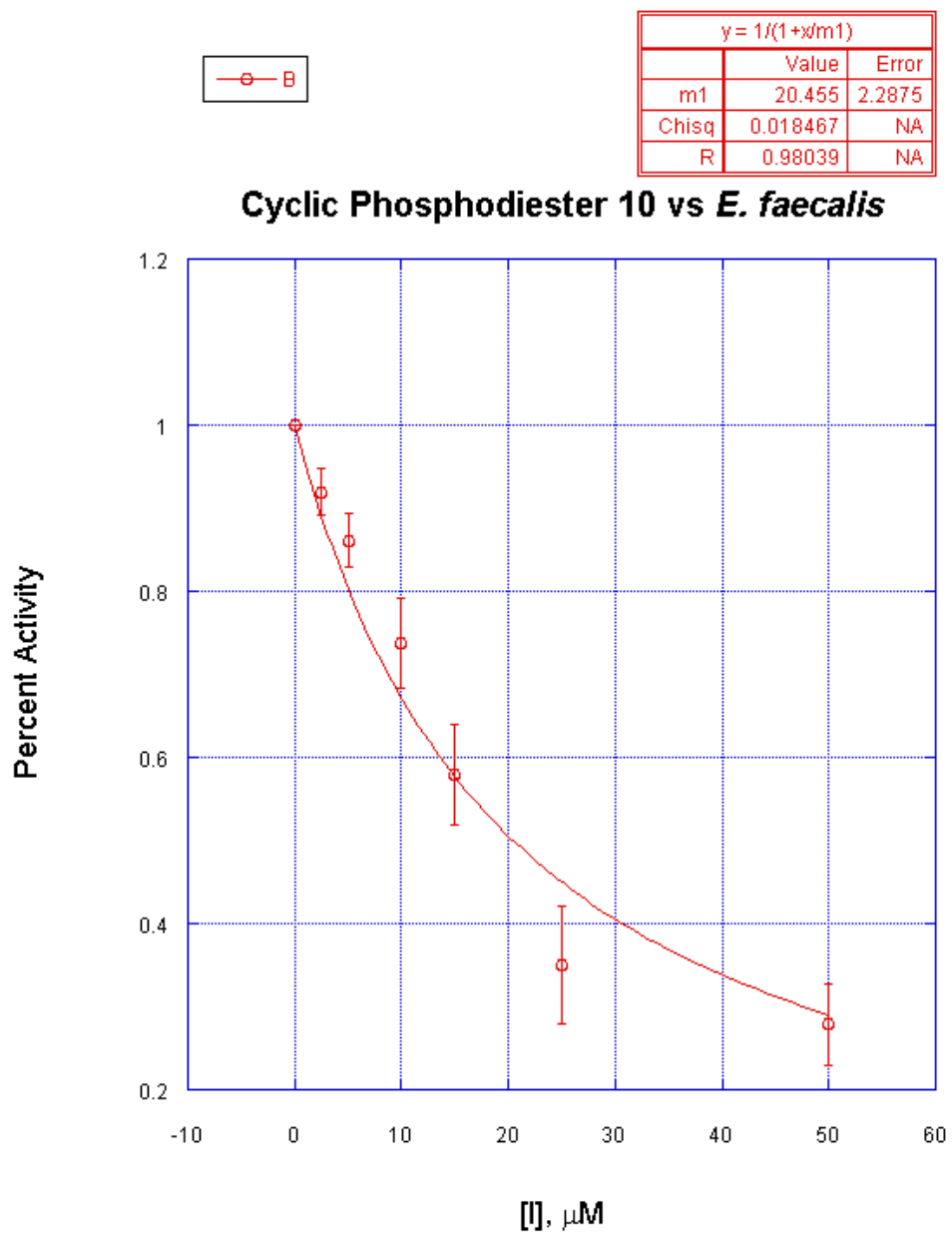


Figure 2.14: IC₅₀ plot for cyclic phosphodiester **10** vs. efPPCS

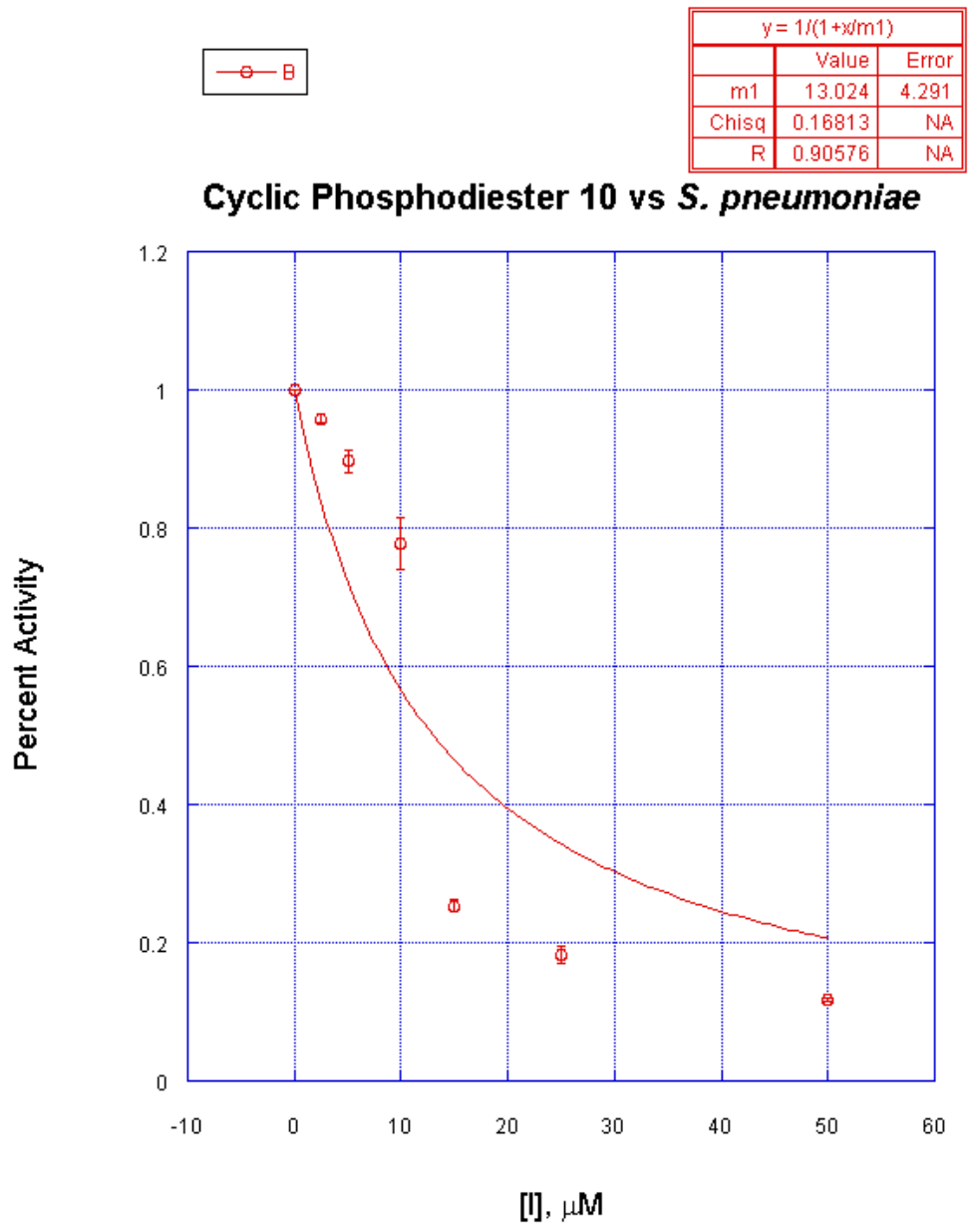


Figure 2.15: IC₅₀ plot for cyclic phosphodiester **10** vs. spPPCS

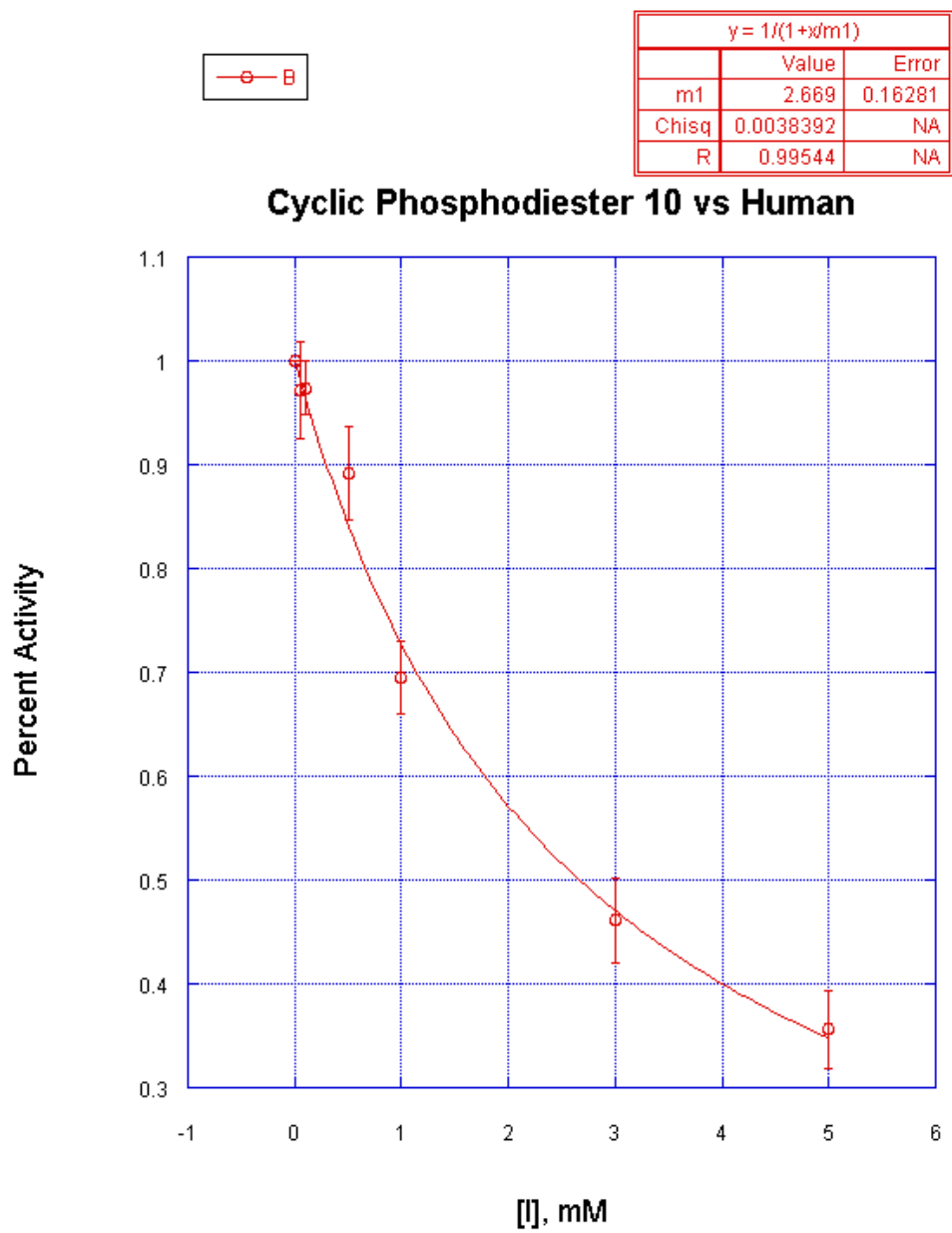


Figure 2.16: IC₅₀ plot for cyclic phosphodiester **10** vs. hPPCS

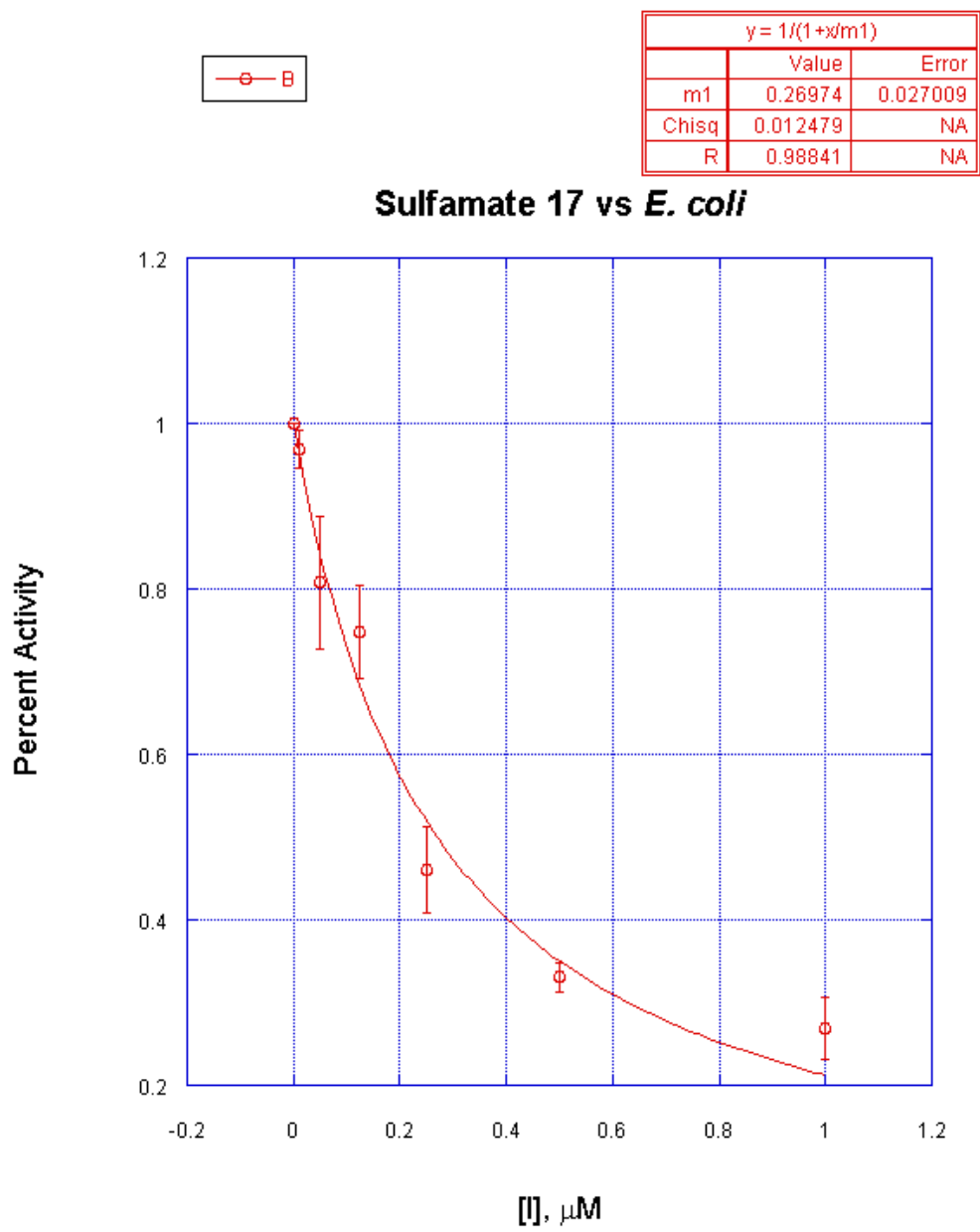


Figure 2.17: IC₅₀ plot for sulfamate **17** vs. ecPPCS

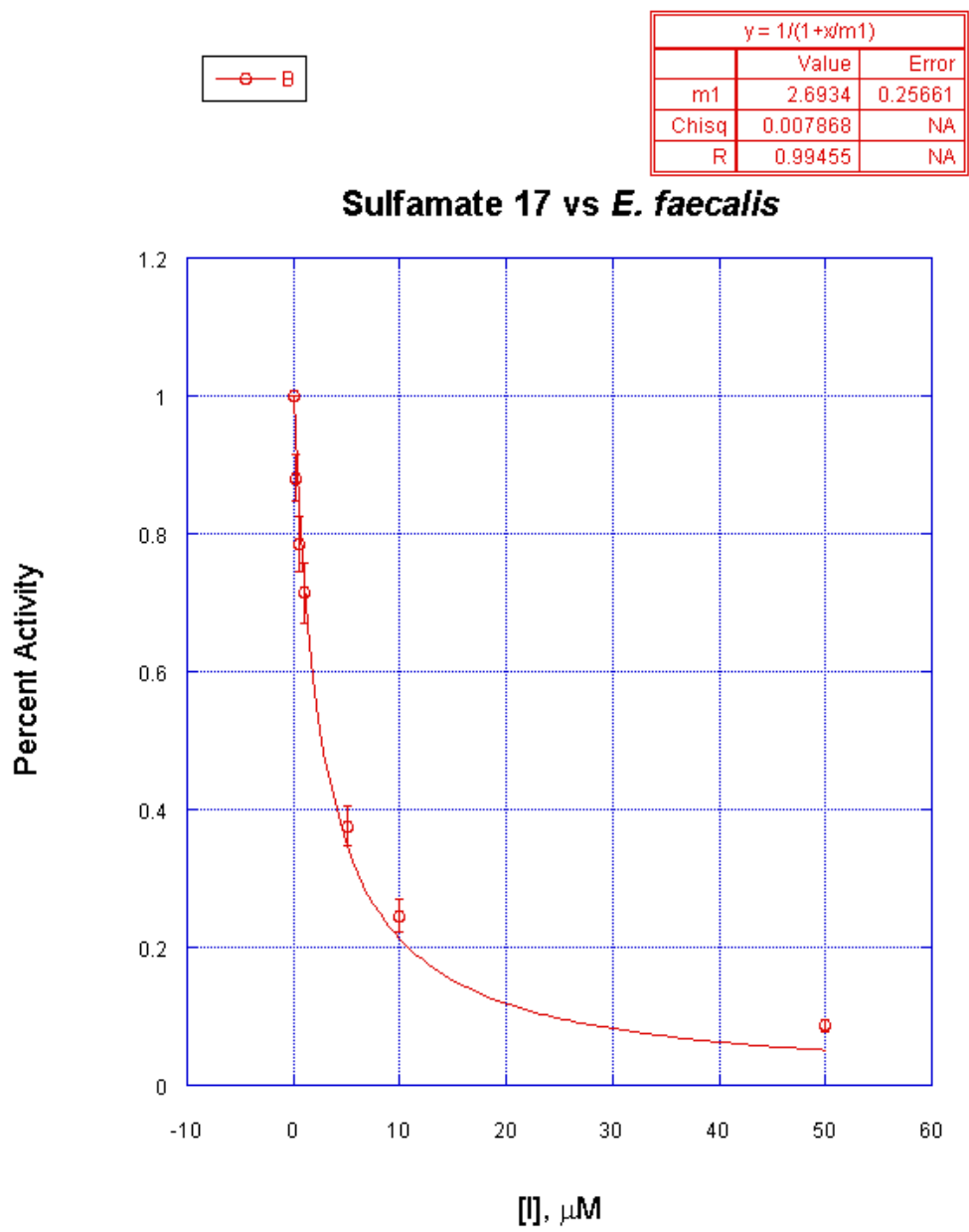


Figure 2.18: IC₅₀ plot for sulfamate **17** vs. efPPCS

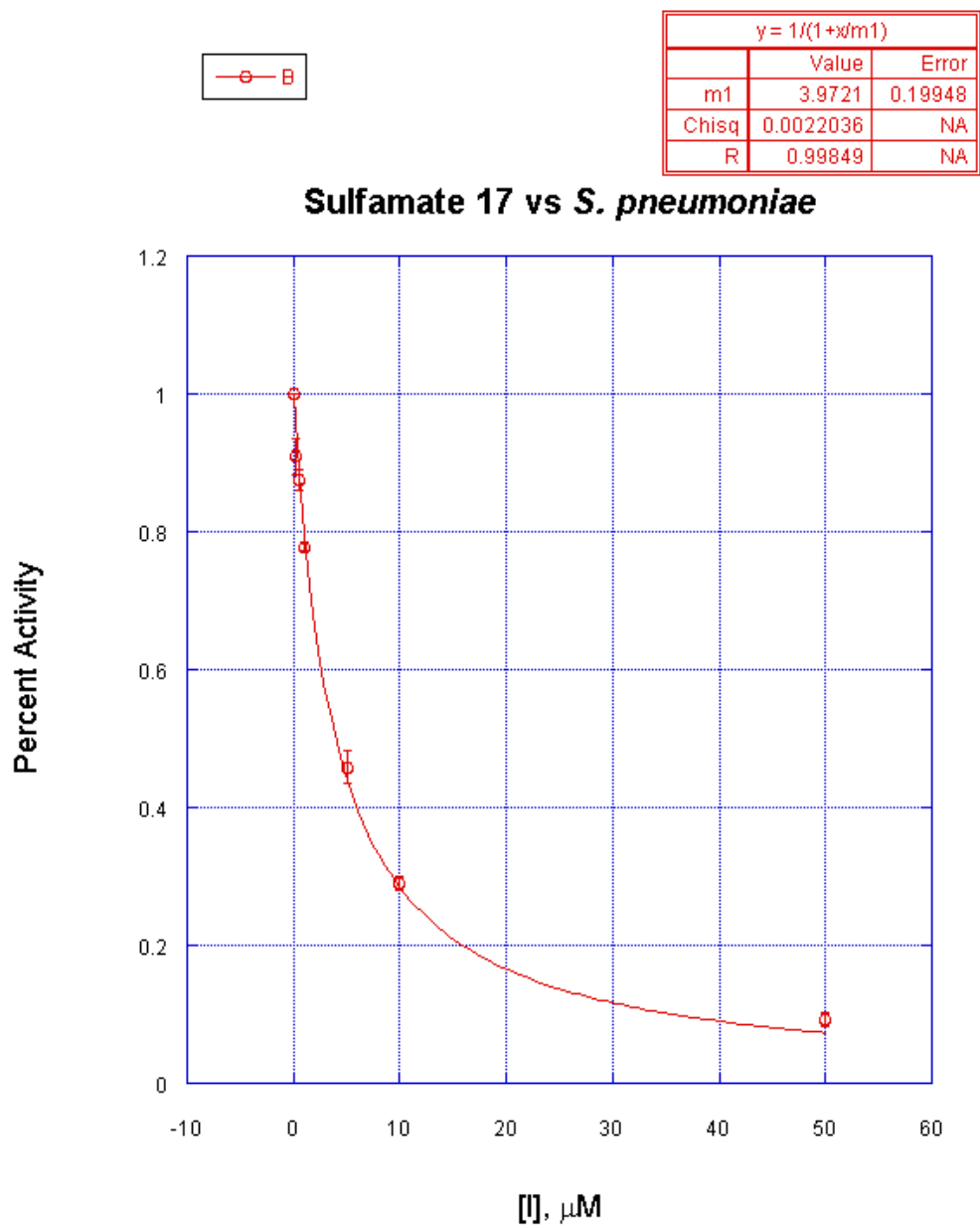


Figure 2.19: IC₅₀ plot for sulfamate **17** vs. spPPCS

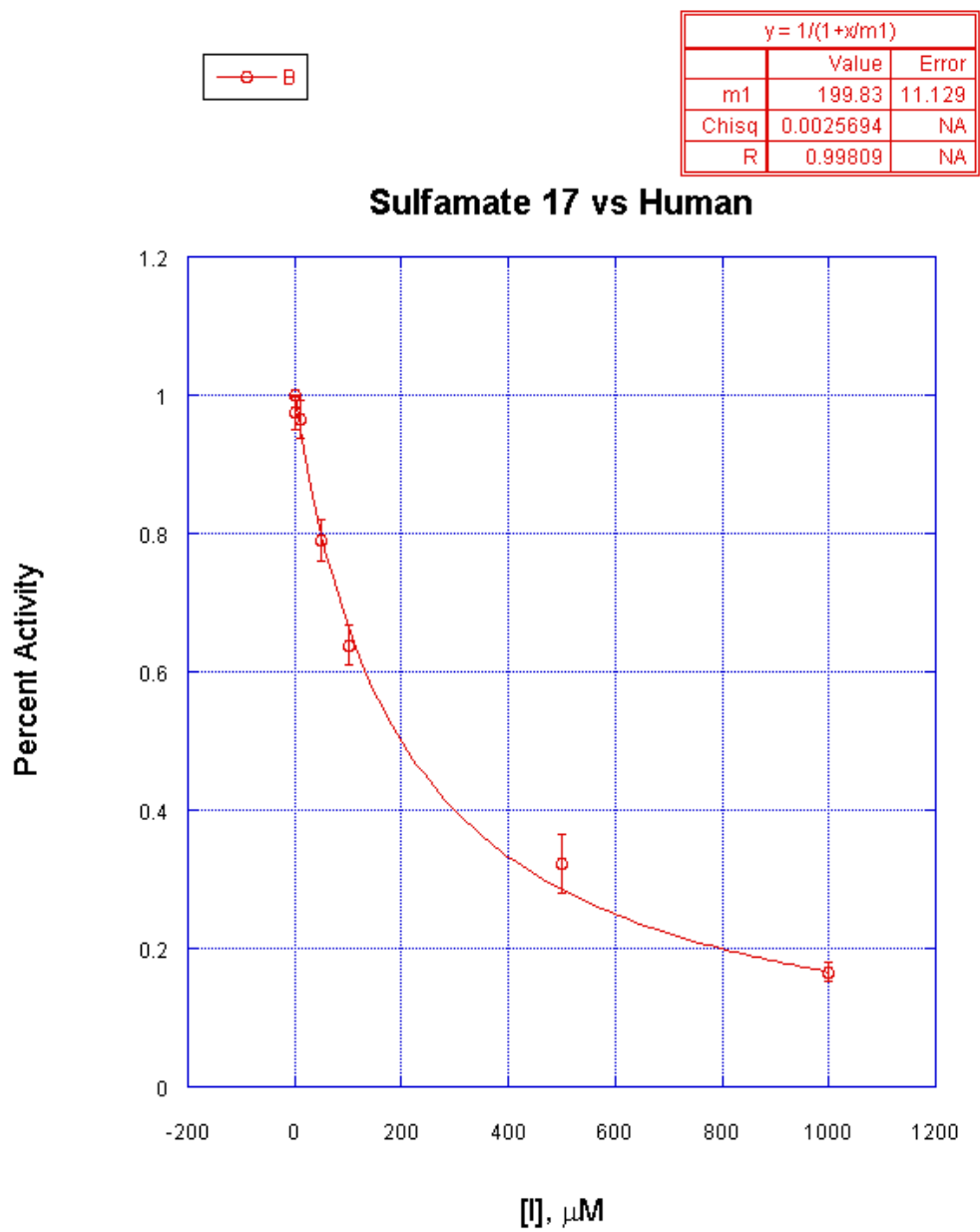


Figure 2.20: IC₅₀ plot for sulfamate **17** vs. hPPCS

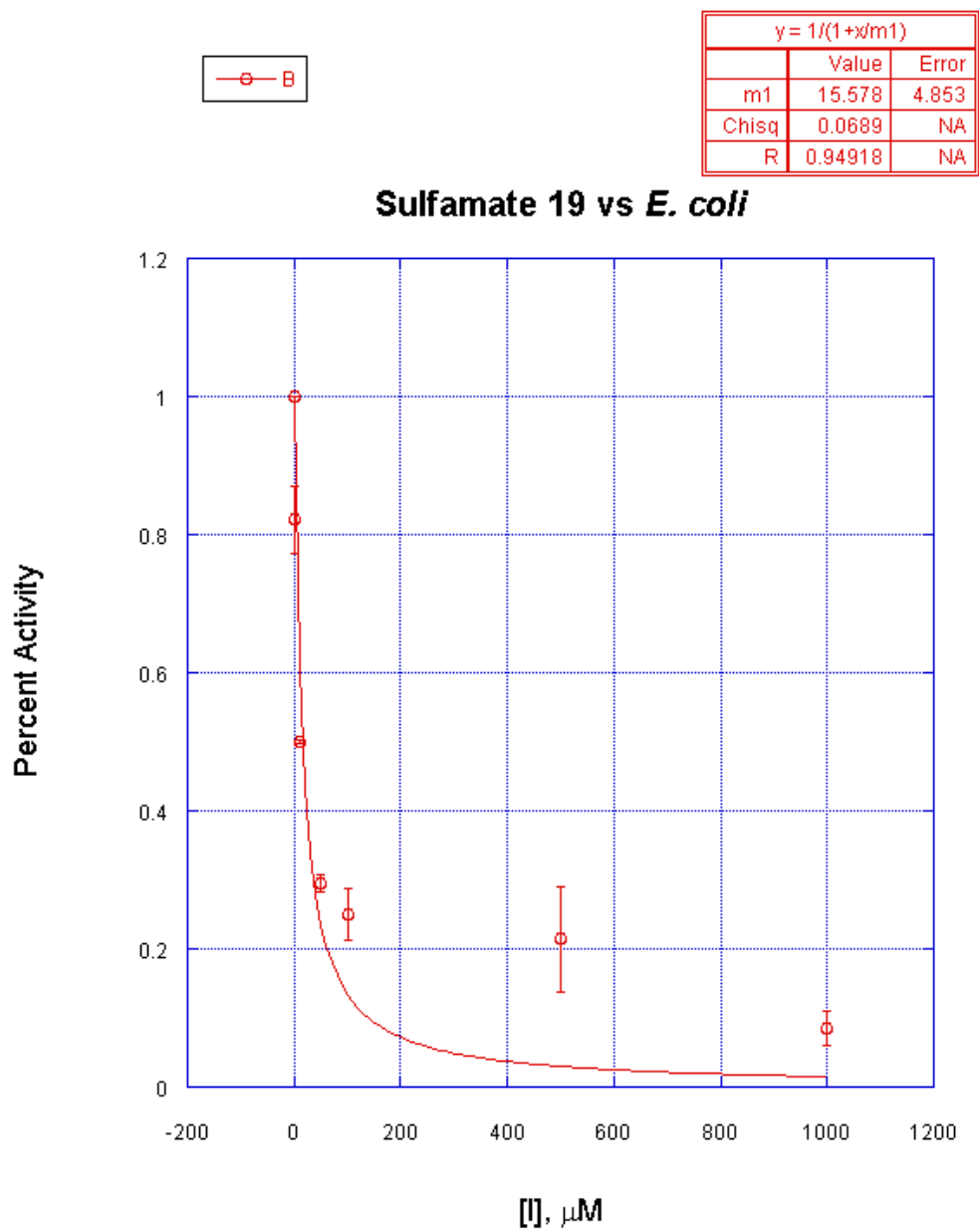


Figure 2.21: IC₅₀ plot for sulfamate **19** vs. ecPPCS

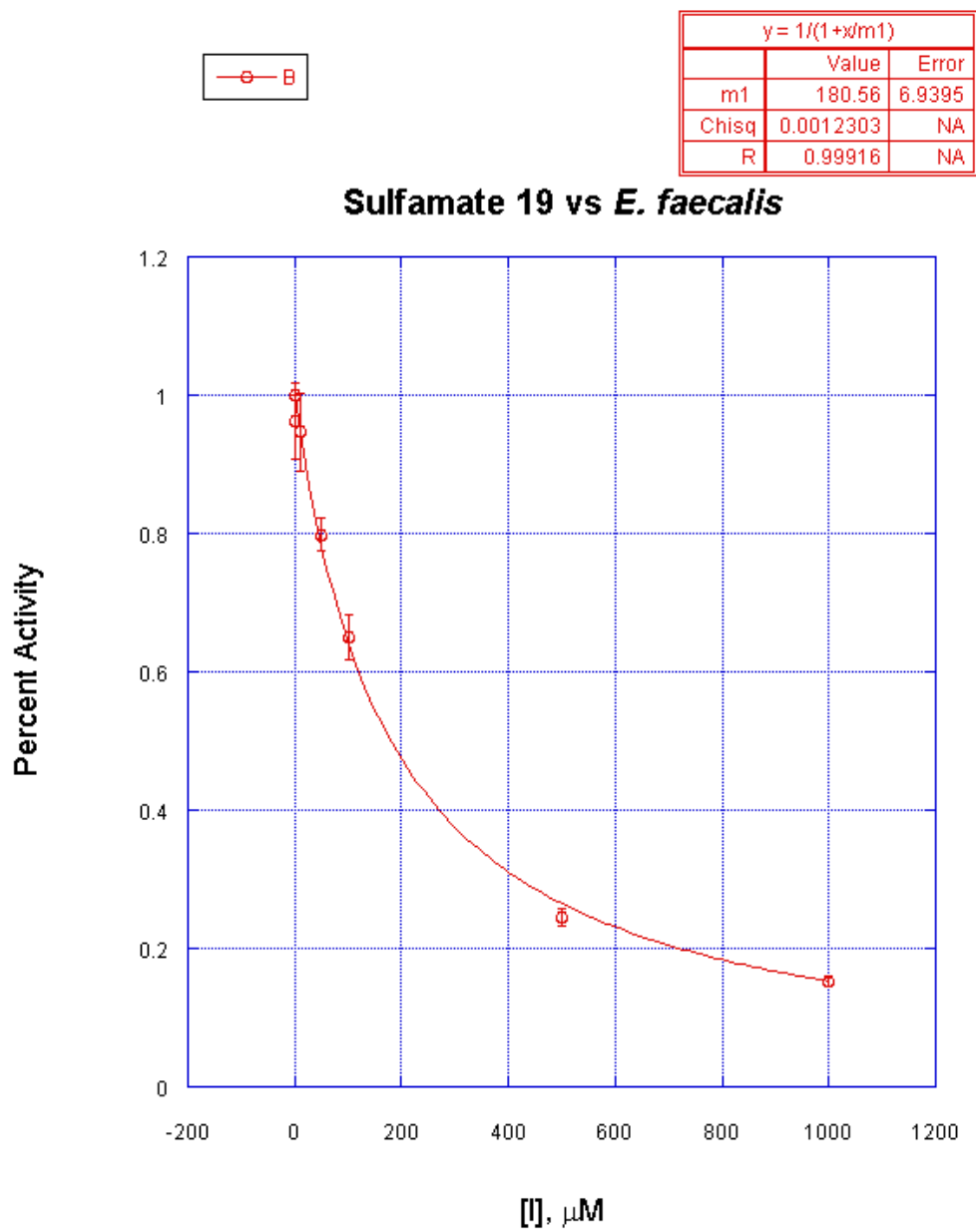


Figure 2.22: IC₅₀ plot for sulfamate **19** vs. efPPCS

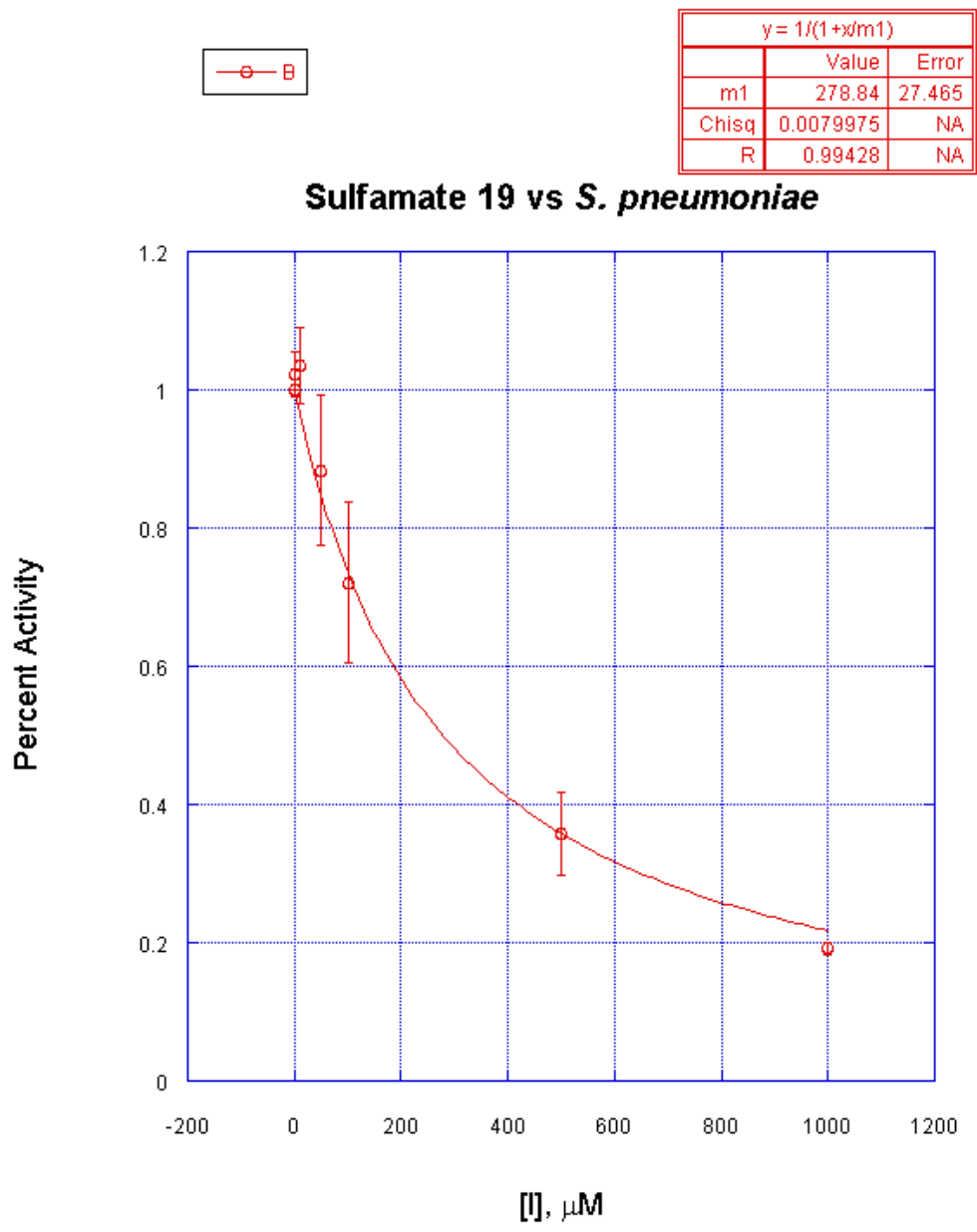


Figure 2.23: IC₅₀ plot for sulfamate **19** vs. spPPCS

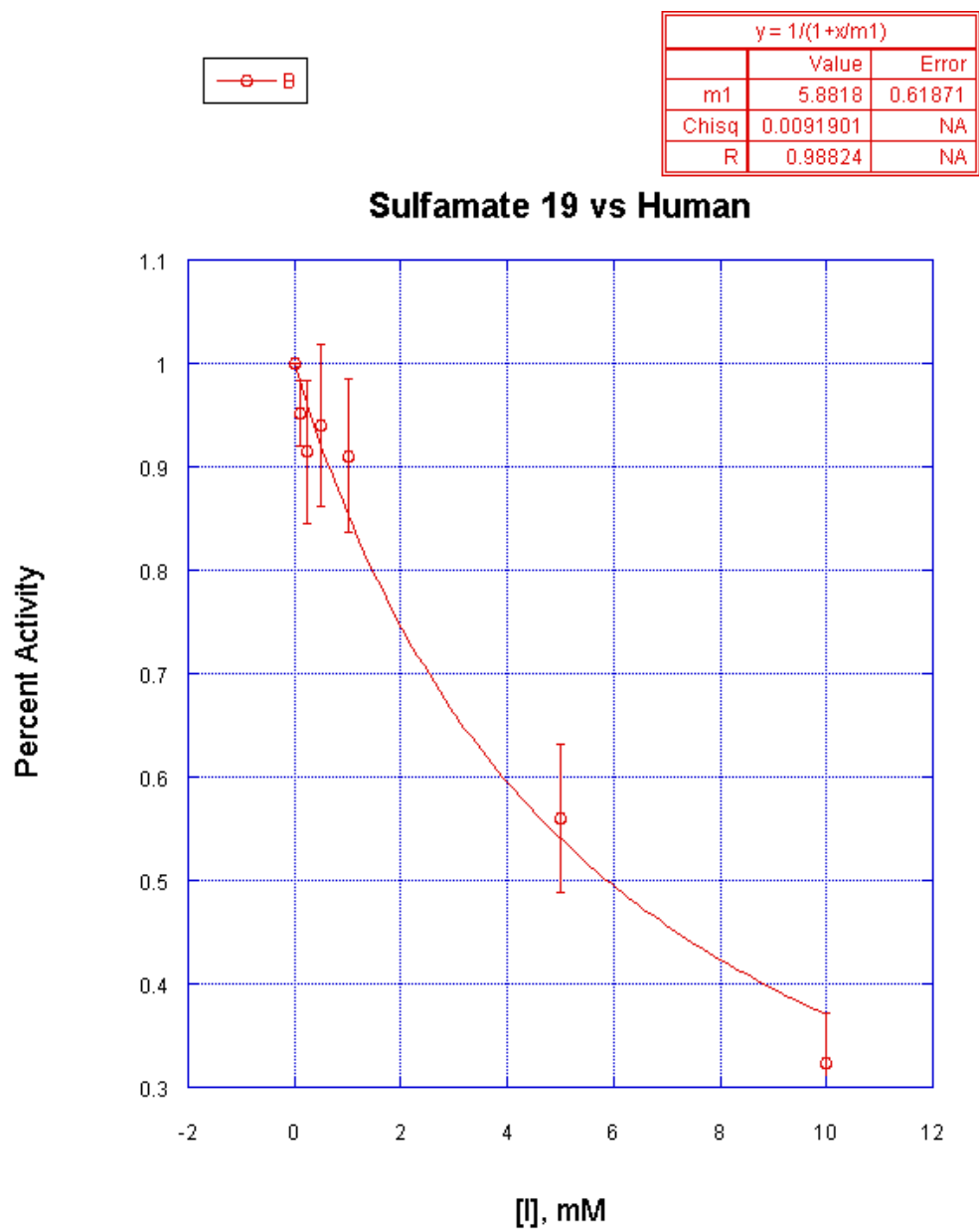


Figure 2.24: IC₅₀ plot for sulfamate **19** vs. hPPCS

References

1. Magnuson, K. J., Suzanne; Rock, Charles O.; Cronan, John E., Jr., Regulation of fatty acid biosynthesis in *Escherichia coli*. *Microbiological Reviews* **1993**, *57*, (3), 522-42.
2. Nicely, N. I.; Parsonage, D.; Paige, C.; Newton, G. L.; Fahey, R. C.; Leonardi, R.; Jackowski, S.; Mallett, T. C.; Claiborne, A., Structure of the Type III Pantothenate Kinase from *Bacillus anthracis* at 2.0 Å Resolution: Implications for Coenzyme A-Dependent Redox Biology. *Biochemistry* **2007**, *46*, (11), 3234-3245.
3. Brown, G. M., The Metabolism of Pantothenic Acid. *Journal of Biological Chemistry* **1959**, *234*, (2), 370-378.
4. Stanitzek, S.; Augustin, M. A.; Huber, R.; Kupke, T.; Steinbacher, S., Structural Basis of CTP-Dependent Peptide Bond Formation in Coenzyme A Biosynthesis Catalyzed by *Escherichia coli* PPC Synthetase. *Structure* **2004**, *12*, (11), 1977-1988.
5. Strauss, E.; Kinsland, C.; Ge, Y.; McLafferty, F. W.; Begley, T. P., Phosphopantothenoylcysteine Synthetase from *Escherichia coli*. Identification and characterization of the last unidentified Coenzyme A biosynthetic enzyme in bacteria. *J. Biol. Chem.* **2001**, *276*, (17), 13513-13516.
6. Blaesse, M.; Kupke, T.; Huber, R.; Steinbacher, S., Crystal structure of the peptidyl-cysteine decarboxylase EpiD complexed with a pentapeptide substrate. *EMBO J* **2000**, *19*, (23), 6299-6310.
7. Gerdes, S. Y.; Scholle, M. D.; D'Souza, M.; Bernal, A.; Baev, M. V.; Farrell, M.; Kurnasov, O. V.; Daugherty, M. D.; Mseeh, F.; Polanuyer, B. M.; Campbell, J. W.; Anantha, S.; Shatalin, K. Y.; Chowdhury, S. A. K.; Fonstein, M. Y.; Osterman, A. L., From genetic Footprinting to antimicrobial drug targets: Examples in cofactor biosynthetic pathways. *Journal of Bacteriology* **2002**, *184*, (16), 4555-4572.
8. Strauss, E.; Kinsland, C.; Ge, Y.; McLafferty, F. W.; Begley, T. P., Phosphopantothenoylcysteine synthetase from *Escherichia coli*. Identification and characterization of the last unidentified coenzyme A biosynthetic enzyme in bacteria. *J Biol Chem* **2001**, *276*, (17), 13513-6.
9. Kupke, T.; Schwarz, W., 4'-phosphopantetheine biosynthesis in Archaea. *J Biol Chem* **2006**, *281*, (9), 5435-44.
10. Daugherty, M.; Polanuyer, B.; Farrell, M.; Scholle, M.; Lykidis, A.; de Crecy-Lagard, V.; Osterman, A., Complete reconstitution of the human coenzyme A biosynthetic pathway via comparative genomics. *J Biol Chem* **2002**, *277*, (24), 21431-9.
11. Manoj, N.; Strauss, E.; Begley, T. P.; Ealick, S. E., Structure of human phosphopantothenoylcysteine synthetase at 2.3 Å resolution. *Structure* **2003**, *11*, (8), 927-36.
12. Yao, J.; Patrone, J. D.; Dotson, G. D., Characterization and Kinetics of Phosphopantothenoylcysteine Synthetase from *Enterococcus faecalis*. *Biochemistry* **2009**, *48*, (12), 2799-2806.
13. Heacock, D.; Forsyth, C. J.; Shiba, K.; Musier-Forsyth, K., Synthesis and Aminoacyl-tRNA Synthetase Inhibitory Activity of Prolyl Adenylate Analogs. *Bioorganic Chemistry* **1996**, *24*, (3), 273-289.
14. Lee, J.; Kang, S. U.; Kang, M. K.; Chun, M. W.; Jo, Y. J.; Kkwak, J. H.; Kim, S., Methionyl adenylate analogues as inhibitors of methionyl-tRNA synthetase. *Bioorganic & Medicinal Chemistry Letters* **1999**, *9*, (10), 1365-1370.

15. Somu, R. V.; Boshoff, H.; Qiao, C.; Bennett, E. M.; Barry, C. E.; Aldrich, C. C., Rationally Designed Nucleoside Antibiotics That Inhibit Siderophore Biosynthesis of *Mycobacterium tuberculosis*. *Journal of Medicinal Chemistry* **2005**, 49, (1), 31-34.
16. Ferreras, J. A.; Ryu, J.-S.; Di Lello, F.; Tan, D. S.; Quadri, L. E. N., Small-molecule inhibition of siderophore biosynthesis in *Mycobacterium tuberculosis* and *Yersinia pestis*. *Nat Chem Biol* **2005**, 1, (1), 29-32.
17. Tian, Y.; Suk, D.-H.; Cai, F.; Crich, D.; Mesecar, A. D., Bacillus anthracis o-Succinylbenzoyl-CoA Synthetase: Reaction Kinetics and a Novel Inhibitor Mimicking Its Reaction Intermediate. *Biochemistry* **2008**, 47, (47), 12434-12447.
18. Koroniak, L.; Ciustea, M.; Gutierrez, J. A.; Richards, N. G. J., Synthesis and Characterization of an N-Acylsulfonamide Inhibitor of Human Asparagine Synthetase. *Organic Letters* **2003**, 5, (12), 2033-2036.
19. Meier, J. L.; Mercer, A. C.; Rivera, H.; Burkart, M. D., Synthesis and evaluation of bioorthogonal pantetheine analogues for in vivo protein modification. *Journal of the American Chemical Society* **2006**, 128, (37), 12174-12184.
20. Mercer, A. C.; Meier, J. L.; Hur, G. H.; Smith, A. R.; Burkart, M. D., Antibiotic evaluation and in vivo analysis of alkynyl Coenzyme A antimetabolites in *Escherichia coli*. *Bioorganic & Medicinal Chemistry Letters* **2008**, 18, (22), 5991-5994.
21. Kocienski, P., *Protecting Groups*. 3rd ed.; 2005; p 119-180, 451-483.
22. Greene, T., Wuts, P., *Protective Groups in Organic Synthesis*. 1999; p 201-246, 660-701.
23. Cohen, S. B.; Halcomb, R. L., Synthesis and Characterization of an Anomeric Sulfur Analogue of CMP-Sialic Acid. *The Journal of Organic Chemistry* **2000**, 65, (19), 6145-6152.
24. Michalski, J.; Dabkowski, W., State of the Art. Chemical Synthesis of Biophosphates and their Analogues via P III Derivatives. In *New Aspects in Phosphorus Chemistry IV*, 2004; pp 43-47.
25. Dellinger, D. J.; Sheehan, D. M.; Christensen, N. K.; Lindberg, J. G.; Caruthers, M. H., Solid-Phase Chemical Synthesis of Phosphonoacetate and Thiophosphonoacetate Oligodeoxynucleotides. *Journal of the American Chemical Society* **2003**, 125, (4), 940-950.
26. Evans, D. A.; Gage, J. R.; Leighton, J. L., Asymmetric synthesis of calyculin A. 3. Assemblage of the calyculin skeleton and the introduction of a new phosphate monoester synthesis. *The Journal of Organic Chemistry* **1992**, 57, (7), 1964-1966.
27. Manoharan, M.; Lu, Y.; Casper, M. D.; Just, G., Alkyl Group as a Protecting Group for Internucleotide Phosphate and Thiophosphate Linkages in Oligonucleotide Synthesis: Facile Oxidation and Deprotection Conditions. *Organic Letters* **2000**, 2, (3), 243-246.
28. Imoto, S.; Patro, J. N.; Jiang, Y. L.; Oka, N.; Greenberg, M. M., Synthesis, DNA Polymerase Incorporation, and Enzymatic Phosphate Hydrolysis of Formamidopyrimidine Nucleoside Triphosphates. *Journal of the American Chemical Society* **2006**, 128, (45), 14606-14611.
29. Worthington, A.; Burkart, M. D., One-pot chemo-enzymatic synthesis of reporter-modified proteins. *Organic & biomolecular chemistry* **2006**, 4, (1), 44.
30. Rolf Appel, G. B., Hydrazinsulfonsäure-amide, I. Über das Hydrazodisulfamid. *Chemische Berichte* **1958**, 91, (6), 1339-1341.

31. Okada, M., Efficient general method for sulfamoylation of a hydroxyl group. *Tetrahedron letters*; **2000**, 41, (36), 7047.
32. Cheng, Y.; Prusoff, W. H., Relationship between inhibition constant (K₁) and concentration of inhibitor which causes 50 percent inhibition (I₅₀) of an enzymatic-reaction. *Biochemical Pharmacology* **1973**, 22, (23), 3099-3108.
33. Yao, J. W.; Dotson, G. D., Kinetic characterization of human phosphopantothenoylcysteine synthetase. *Biochimica Et Biophysica Acta-Proteins and Proteomics* **2009**, 1794, (12), 1743-1750.
34. Kupke, T., Molecular Characterization of the 4'-Phosphopantothenoylcysteine Synthetase Domain of Bacterial Dfp Flavoproteins. *J. Biol. Chem.* **2002**, 277, (39), 36137-36145.
35. Copeland, R. A., *Evaluation of enzyme inhibitors in drug discovery : a guide for medicinal chemists and pharmacologists*. Wiley-Interscience: Hoboken, N.J., 2005.

Chapter 3

Co-Crystallization of Intermediate Mimics with *E. coli* PPCS

Introduction

The crystal structures of Human PPCS and a mutant (Asn210Asp) *E. coli* PPCS domain containing a N-terminal hexa-His tag, have been published.^{1, 2} Both mammalian and bacterial PPCS are dimers in solution. Their structures contain a Rossmann fold, which is typical of nucleotide binding enzymes.^{1, 2} Dimerization of the two subunits is via interactions between the four stranded antiparallel β sheets, one contributed from each monomer. In addition to dimerization functions, the β sheet is also positioned over the active site of the partner subunit, suggesting cooperativity between the two subunits for both the eukaryotic and the prokaryotic enzymes. The eukaryotic PPCS protein has an additional dimerization domain, consisting of a helix- β strand-helix motif. The significance of this extra dimerization domain is unclear.

The structures of the *E. coli* PPCS in complex with CTP, phosphopantothenoyl cytidylate, and CMP have been determined.¹ From the CTP bound structure, the protein interacts with the phosphates of the CTP via a bound divalent metal ligand, which is common for many enzymes that bind NTP. Interaction with the ribose and nucleotide ring is primarily through hydrogen bonds with the protein backbone, involving the residues Ala98, Pro128, and Val131 for the cytidine as well as Phe147 and Ala95 for the ribose. Upon soaking the crystals with both CTP and phosphopantothenate, phosphopantothenoyl cytidylate is bound to the active site of the enzyme. The pantothenate chain extends through a groove formed from two β strands and binds to the protein mostly via charged and hydrogen bond interactions.

The cysteine binding pocket of the second half reaction has been hypothesized to involve binding contacts with Asn210, Arg206, and Ala276 based upon mutagenesis studies. However, no one has confirmed these binding contacts and the cysteine binding pocket has not been explored or used in inhibitor design. Identification of the cysteine

binding site and the orientation of cysteine binding to the PPCS-acyl cytidylate complex, also has mechanistic implications toward the ability of PPCS to discriminate between cysteine and serine. This discrimination has critical biological implications, since incorporation of serine would lead to the production of potentially toxic CoA antimetabolites.³

Having successfully synthesized the first selective inhibitors of PPCS (**Figure 3.1**), we were interested in using these chemical probes to glean more information about the active site of the native *E. coli* PPCS domain.⁴ The purpose of this study was to further explore the binding contacts within the active site of PPCS by elucidating the differences in the binding contacts made by the cyclic terminal phosphate of compound **10** versus the non-cyclic phosphate of compound **8** and the internal sulfamate linkage of compound **17** versus the phosphodiester of compound **8**, and exploring the cysteine binding pocket.

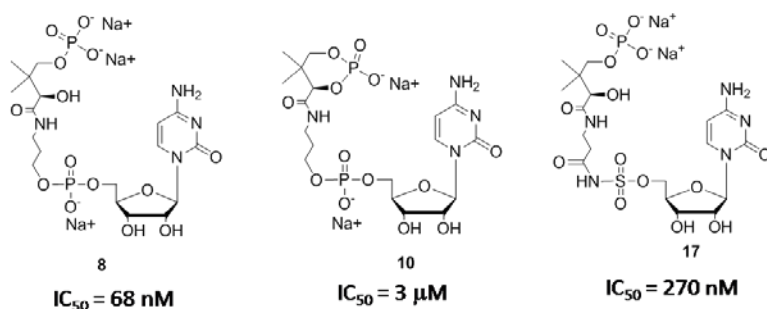


Figure 3.1: First Inhibitors of PPCS

Co-Crystallization of *E. coli* PPCS Domain with Phosphodiester Inhibitor

The IC_{50} values of the intermediate mimics **8**, **10**, and **17**, indicated that the terminal and bridging phosphates were important for potency and that changing either resulted in a reduction in potency.⁴ The loss in potency of intermediate mimics **10** and **17**, in comparison to that of the phosphodiester mimic, are most likely due to loss of key binding contacts in the phosphate binding sites of PPCS. As well, intermediate mimics **10** and **17** could also be making unique binding contacts due to their differences in geometry and electronics. Such differences may point the way to new avenues for structure-based drug design of PPCS inhibitors.

Based upon the crystallization conditions reported in literature, an initial 96 well PEG sitting drop screen was set up.¹ The commercially available Nextall 96 well PEG

screen allows for screening different PEGs starting at low molecular weight PEGs (200 amu) all the way up to high molecular weight PEGs of 4000 amu while varying pH, buffer system, and salts. The initial screen was conducted using *E. coli* 1) apo PPCS, 2) PPCS with inhibitor **8**, and 3) PPCS with inhibitor **8**, and cysteine. Within 7 days, several different sets of conditions out of the initial screen afforded diffraction quality crystals (**Figure 3.2**).

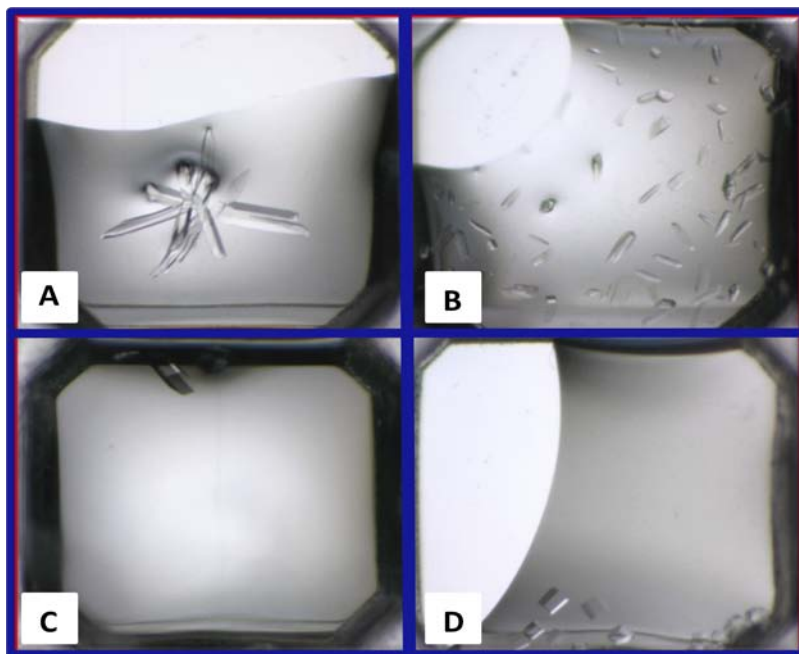


Figure 3.2: Co-crystals of PPCS [15 mg/mL] and Inhibitor **8** from Nextall PEG screen. Crystallization conditions as follows: (A) 0.2 M Ammonium chloride 20% PEG 3350 (B) 0.2 M K/Na tartrate 20% PEG 3350 (C) 0.1 M Sodium acetate pH 4.6 30% PEG 300 (D) 0.2 M Potassium thiocyanate 20% PEG 3350

The crystallization conditions were then further optimized using a focused grid hanging drop screen of 24 wells varying the pH and buffer concentration around the conditions of 0.1 M sodium acetate pH 4.6 30% PEG 300 and 0.2 M potassium thiocyanate 20% PEG 3350..

Diffraction crystals of PPCS and phosphodiester **8** were harvested within 14 days. Upon harvesting the crystals, the cryo-protective conditions were explored using the well solution, the well solution plus 40% PEG 400, the well solution plus 10% glycerol, and paraffin oil. Once cryoprotected, the crystals were flash frozen using liquid N₂ and stored in liquid N₂. X-ray diffraction data was taken at the advanced photon source (APS) in Argonne National Laboratory. Due to the size of the asymmetric unit of

the crystal of the PPCS domain with phosphodiester **8**, the x-ray detector had to be moved back to a distance of 250 mm and offset 150 mm in order to resolve the very close together spots of the diffraction pattern. While offsetting the detector allowed for the diffraction pattern to be resolved, moving the x-ray detector away from the x-ray source led to the higher resolution diffraction data being lost. Despite this obstacle, several data sets were obtained of sufficient quality to be processed.

Data Collection	
Space Group	C222(1)
Unit Cell	45.615, 141.081, 240.799
	90, 90, 90
Wave length (Å)	1.1271
Resolution (Å)	2.45-2.37
R_{sym} (%)	6.6 (31.4)
<I/σI>	20 (2)
Completeness (%)	98.5 (94.6)
Redundancy	3.3 (2.6)

Table 3.1: Data collection statistics for structure of phosphodiester **8** bound PPCS

The diffraction data was indexed, integrated, and scaled using HKL2000.⁵ The best data set came from crystals grown using 0.1 M NaOAc, pH 5.5, and 24% PEG 400 using paraffin oil as the cryoprotective solution, giving a resolution of 2.37 Å and a redundancy of 3.1 (**Table 3.1**). The crystals were of space group C222(1) and contained 3 monomers in the asymmetric unit. This data set has been solved using molecular replacement using ccp4 software suite with the published activated intermediate bound mutant (1u7z) as the model (**Figure 3.3**).^{1,6} The structure of PPCS with phosphodiester **8** was overlaid with the structure of the PPCS mutant with the activated intermediate to confirm the validity of the structure and the binding mode of the intermediate-based inhibitor (**Figure 3.4**). The overlay reveals that the intermediate mimic binds to PPCS similar to the activated intermediate, as designed. The most notable difference between the two structures is the lack of a carbonyl on phosphodiester **8** leading to the loss of a hydrogen bonding contact with Ala275 and slightly different orientations of the phosphopantothenate arm.

Both the N- and C-terminal amino acids are solvent exposed with the first three N-terminal amino acids and the C-terminal arginine unresolved. The N-terminal region of the PPCS domain in its native form would be attached to the PPCDC domain.

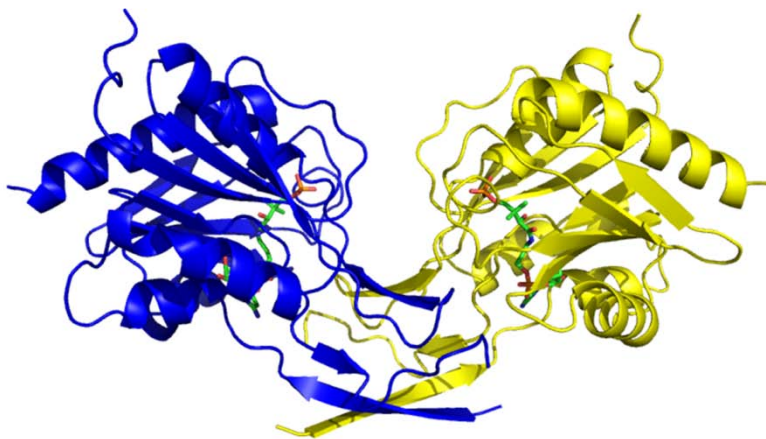


Figure 3.3: Phosphodiester mimic **8** bound to PPCS domain

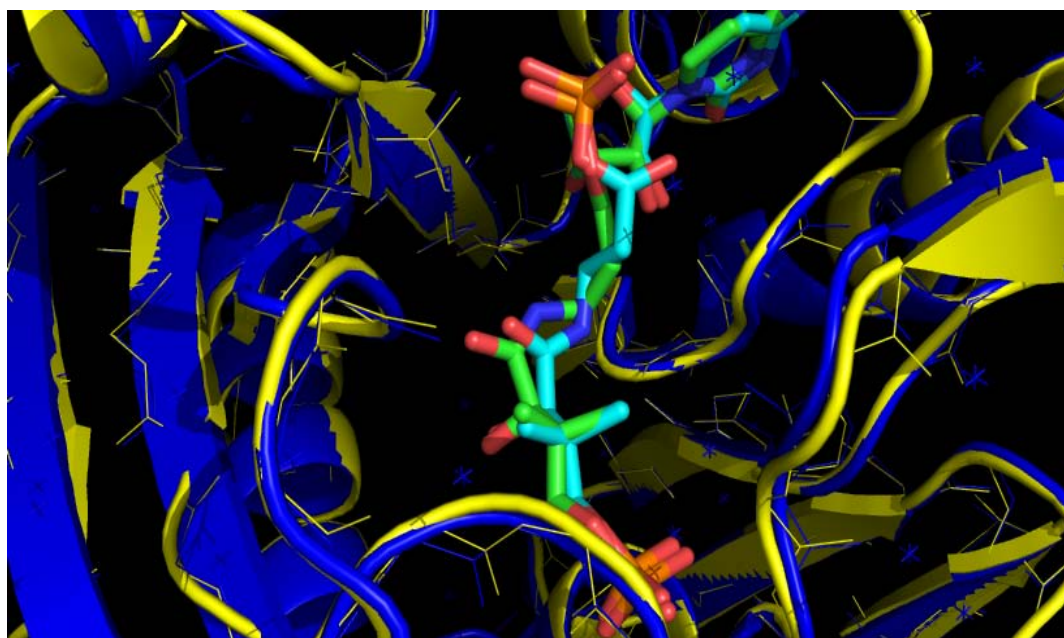


Figure 3.4: Overlay of phosphodiester **8** and PPCS (blue) with 1U7Z (yellow)

A closer look at phosphodiester **8** in the active site of PPCS shows that the molecule takes advantage of almost all of the binding contacts of the activated intermediate in PPCS (**Figure 3.5**). Within the nucleotide binding pocket, the cytidine portion of inhibitor **8** forms hydrogen bond contacts with Pro308, Ile310, and Val311.

The ring oxygen of the ribose ring forms a hydrogen bond with lysine 345 while the 2' and 3' alcohols form a hydrogen bonding network with the backbone of Ala275, Ala273, and Phe327. The internal phosphate forms a salt bridge with Lys341 and has a hydrogen bond to the backbone of Ala329. The internal phosphate also forms a binding contact with Lys289 from the other monomer. This binding contact is important because it was shown in previous site directed mutagenesis studies that Lys289 was critical for enzymatic catalysis of PPCS. Lys289 from the other monomer binding to the internal phosphate of the bound molecule is similar in the structure of the mutant; however, this contact is only briefly mentioned in the crystallographic study and there is no mention of the implications this contact may have on dimerization based upon the molecule bound in the active site. One subtle difference between the phosphodiester 8 bound structure and the activated intermediate bound PPCS mutant is the orientation of the side chain on Val205. Val205 is important because it is believed that the Val205 of one monomer interacts at the active site of the other monomer and helps to create the cysteine binding pocket. In literature, the side chain of Val205 adopts different conformation within the

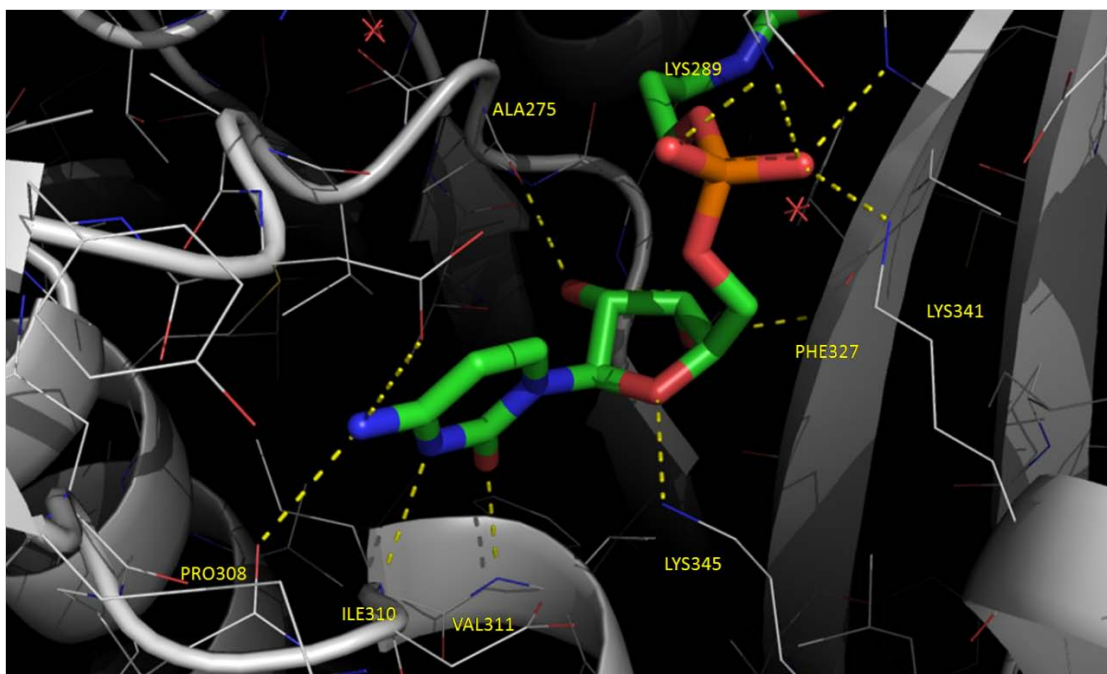


Figure 3.5: Nucleotide binding pocket of PPCS with phosphodiester 8 different monomers of the dimer with the different conformations being responsible for allowing access of the cysteine into the active site to react with the intermediate by either

allowing space for its side chain in one conformation or creating a steric hindrance and disallowing entrance in the other conformation. In our structure both Val205 of the dimer adopt the same conformation and form an open binding cavity that should allow for unhindered access to the bound molecule in the active site. The other difference between the structure of the intermediate bound PPCS mutant and our current structure is the mutation from Asn210 to Asp210 in the mutant enzyme. In the mutant structure, Asp210

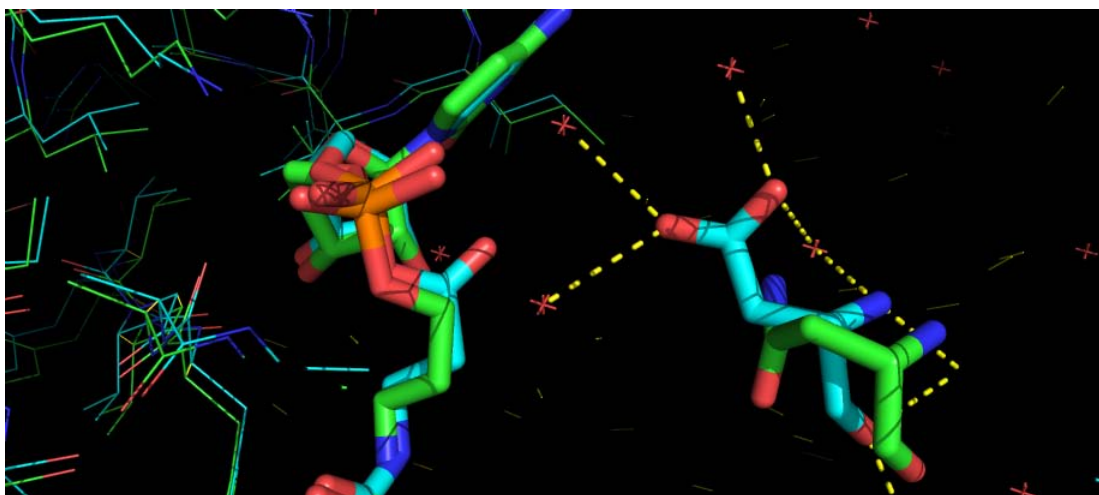


Figure 3.6: Asn210Asp mutation in the active site

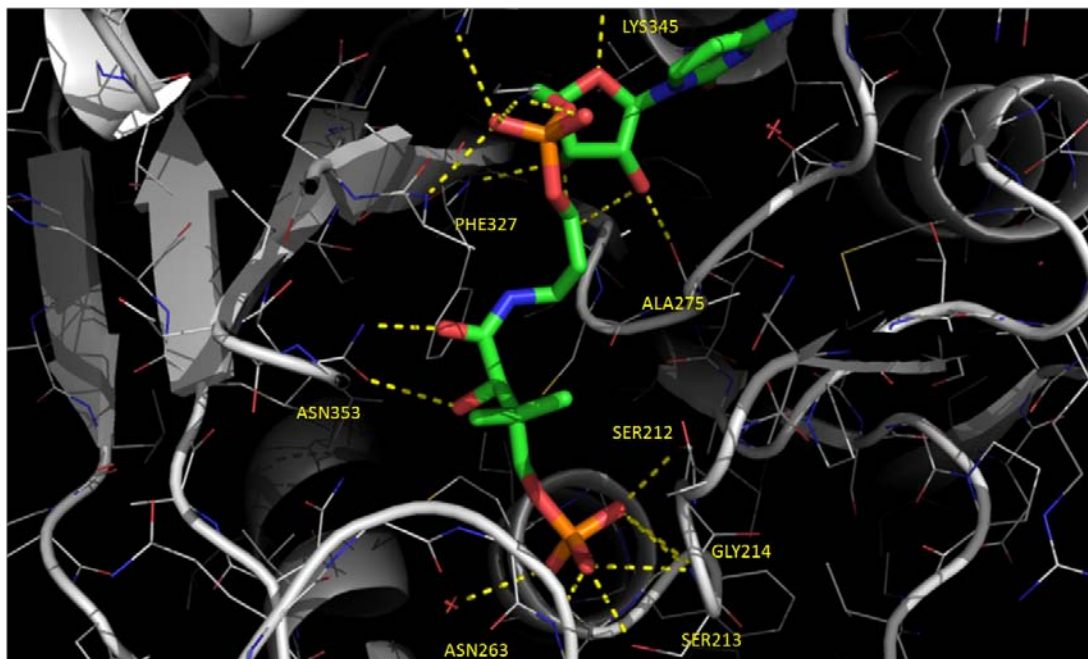


Figure 3.7: Phosphopantothenate binding pocket of PPCS with phosphodiester 8

adopts a different conformation than the Asn210 in our native PPCS structure, and forms a hydrogen bond with a water molecule not present in our structure. It has been speculated that this mutation either causes a perturbation to the oxyanion hole of the enzyme or forms an undesirable salt bridge with substrate cysteine, resulting in a decreased rate in the second half reaction of the mutant PPCS.¹

The phosphopantothenol binding pocket is a long narrow channel that is covered by a flexible binding clamp that extends from Asp354 to Ala368 (**Figure 3.7**). Within the binding pocket, the 4' phosphate of the inhibitor extends into the phosphate cradle composed of residues Ser212, Ser213, Gly214, Met216, and a water molecule. This phosphate binding pocket forms an elaborate hydrogen bonding network to the negatively charged terminal phosphate and constitutes the majority of the binding contacts in the phosphopantothenate binding pocket. Asn353 is an important residue in the binding pocket because it is responsible for hydrogen bonding to both the carbonyl of the amide bond in panthenol and the secondary alcohol of the pantooyl portion of the molecule. Phosphodiester **8** lacks a hydrogen bond from the amide nitrogen to the backbone carbonyl of Cys274. As can be seen from the overlay of the two molecules, phosphodiester **8** does not possess the carbonyl present in the active intermediate which due to its sp² hybridization is not as easily rotatable as the methylene of mimic **8** and most likely responsible for the differences in location and orientation of the amide nitrogen.

Co-Crystallization of *E. coli* PPCS Domain with Sulfamate Inhibitor

The hanging drop conditions used for the co-crystallization of PPCS and phosphodiester **8** were then used as the basis for the co-crystallography study of inhibitors **10** and **17**. Co-crystals of both compounds **10** and **17** had formed within two weeks. These crystals were of a lesser quality than the co-crystals of PPCS and **8** (**Figure 3.8**). From **Figure 3.8**, it can be seen that the co-crystals with both **10** and **17** are not of uniform width with thicker portions and softer edges. Nevertheless, the crystals were harvested, cryoprotected, and flash frozen. These crystals produced low quality and low resolution diffraction patterns that could not be used.

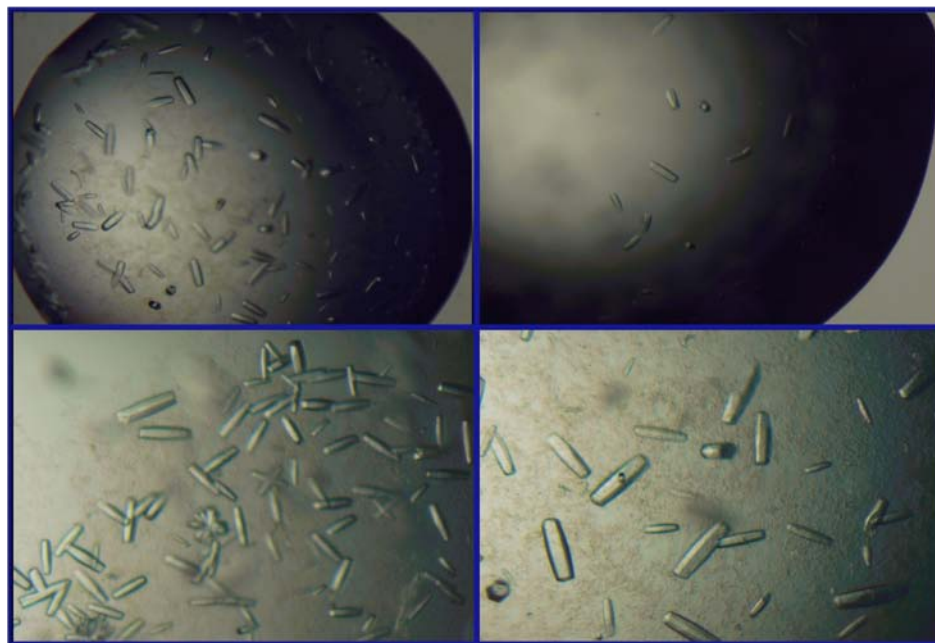


Figure 3.8: Crystals of PPCS and **10** (left) and PPCS and **17** (right)

To improve the quality of the co-crystals with inhibitors **10** and **17**, a Nextall 96 well PEG screen and an Emerald 96 well wizard screen were performed incubating with 2.5 mM of the appropriate inhibitor overnight. The Emerald wizard screen produced a new set of crystallization conditions very similar to the original crystallization conditions but with $\text{Ca}(\text{OAc})_2$ as additive (**Figure 3.9**). All crystals from these conditions were harvested and the cryoprotective solution was varied from no cryoprotection, 15% glycerol in the well solution, and 40% PEG 400.

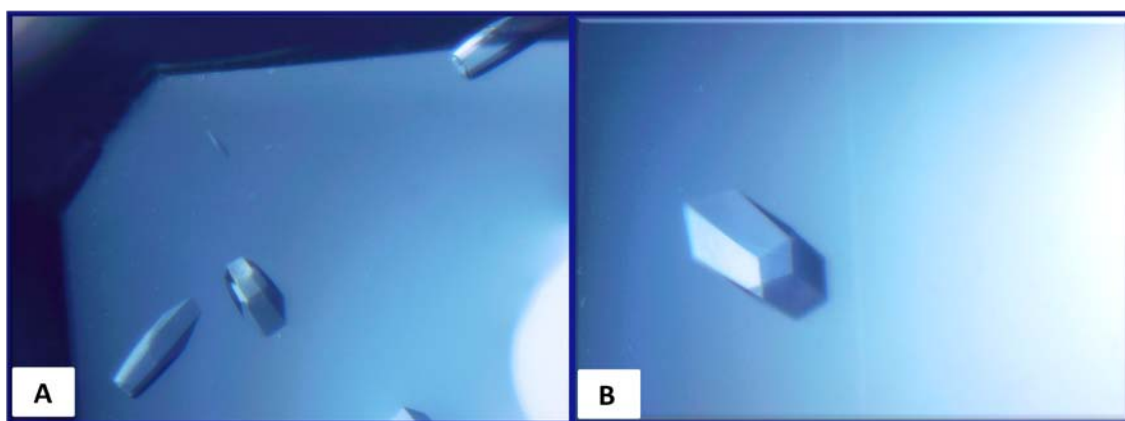


Figure 3.9: Emerald Wizard Screen. Conditions: (left) 0.1 M Sodium acetate pH 4.5, 0.1 M $\text{Ca}(\text{OAc})_2$ 30% PEG 300 and 2.5 mM **10** (right) 0.1 M Sodium acetate pH 4.5, 0.1 M $\text{Ca}(\text{OAc})_2$ 30% PEG 300 and 2.5 mM **17**

Data Collection	
Space Group	P6 ₁ 22
Unit Cell	44.038, 44.038, 390.47
	90, 90, 120
Wave length (Å)	1.1271
Resolution (Å)	2.15-2.11
R_{sym} (%)	7.3 (33.3)
<I/σI>	>20 (5)
Completeness (%)	99.7 (100)
Redundancy	17.7 (13.8)

Table 3.2: Data collection statistics for structure of sulfamate **17** bound PPCS

The best data set for the co-crystal of PPCS and sulfamate **17** was obtained from 32% PEG 300 0.1M sodium acetate pH 5.2 with the well solution plus 40% PEG 300 as the cryoprotectant. The data was collected at APS shifting the X-ray detector back 250 mm and offsetting it by 150 mm. The crystal gave a resolution of 2.11 Å, and belonged to space group P6₁22 with one monomer in the asymmetric unit (**Table 3.2**). This data set has been solved using molecular replacement using the ccp4 software suite with the structure of phosphodiester **8** bound PPCS as the model and the dimer being generated from the symmetry related molecule along the crystallographic 2 fold axis (**Figure 3.10**).^{1, 6} It is known that the native domain of *E. coli* PPCS is a dimer in solution, but it should be noted that both the structure of the PPCS Asn210Asp mutant from literature and the structure of sulfamate **17** bound PPCS, crystallized as monomers with residues Thr284 to 299 being disordered.¹ This is significant because within this loop is Lys289, which as previously mentioned is crucial for PPCS catalysis and forms a binding contact with the internal phosphate of either the bound intermediate or phosphodiester **8**.

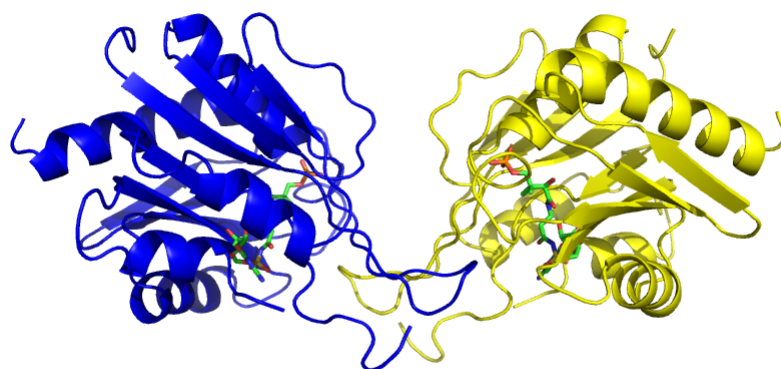


Figure 3.10: Sulfamate mimic **17** bound to PPCS domain

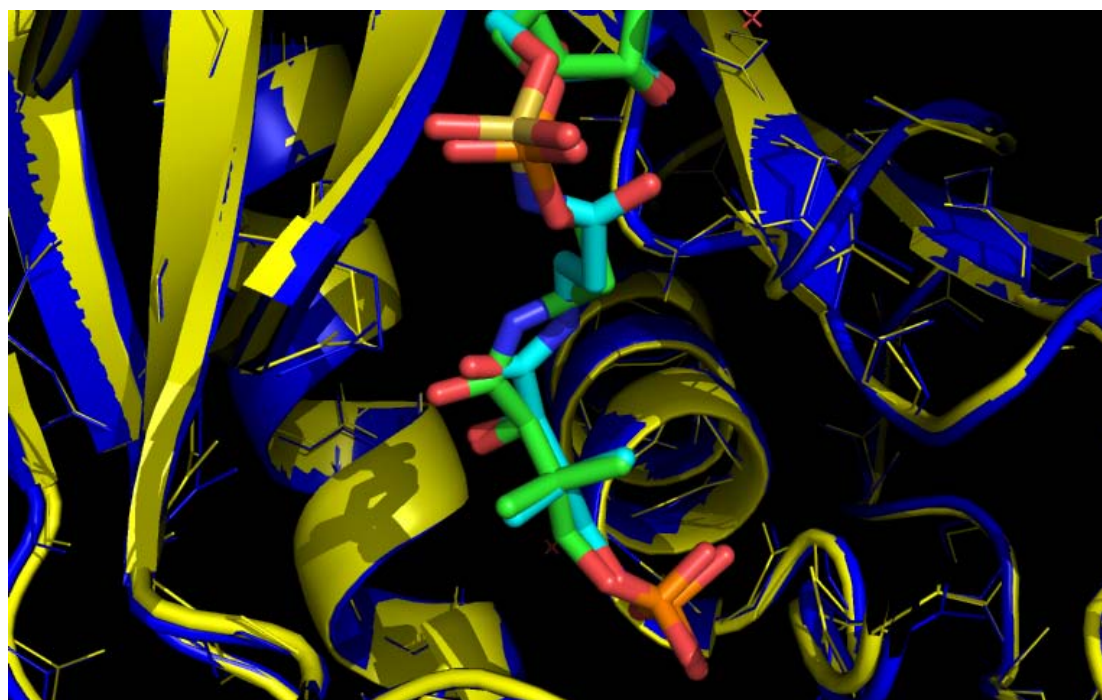


Figure 3.11: Overlay of phosphodiester **8** and sulfamate **17**

An overlay of the structure of PPCS and phosphodiester **8** (the model) and PPCS and the sulfamate mimic **17** was generated (**Figure 3.11**). From this overlay, it is apparent that the phosphodiester **8** and sulfamate **17** bind in an almost identical manner and that the difference in potency must be explained by very subtle differences in the binding contacts.

Investigating the nucleotide binding pocket, the majority of the binding contacts for the sulfamate **17** are the same as the phosphodiester inhibitor **8** (**Figure 3.12**). The

exocyclic amine on the cytidine ring forms a hydrogen bond with Pro308 while the carbonyl on the cytidine ring forms hydrogen bonds with Ile310 and Val311. The 2' and 3' hydroxyl groups on the ribose ring form a hydrogen bond with Ala275 and Ala273

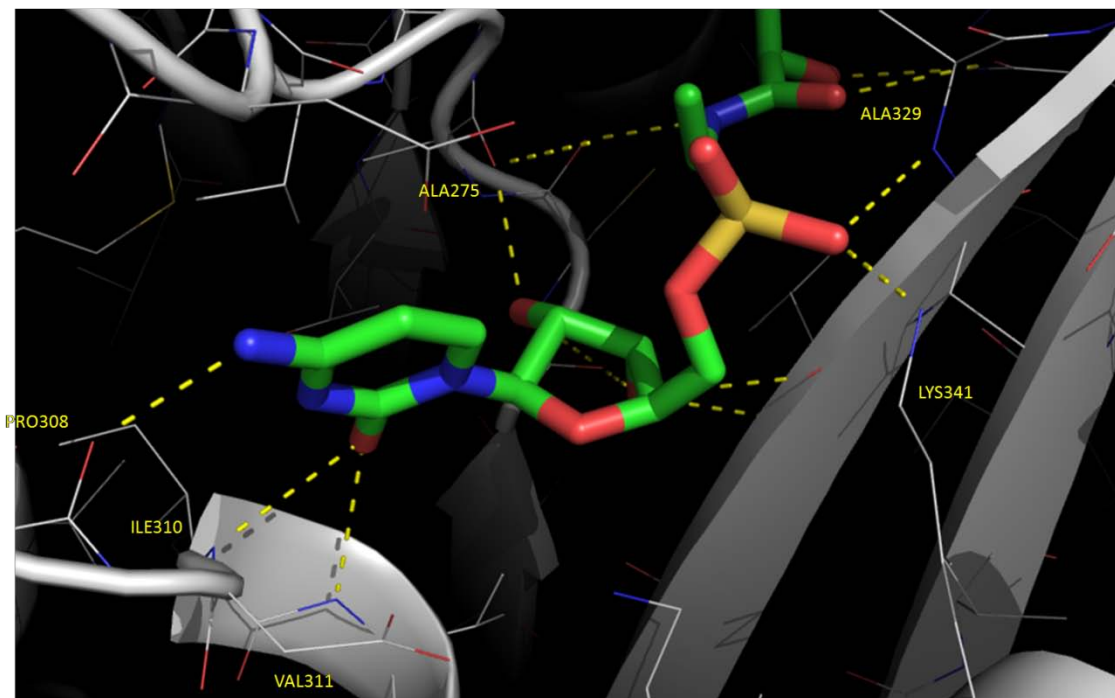


Figure 3.12: Nucleotide binding pocket of PPCS with sulfamate 17

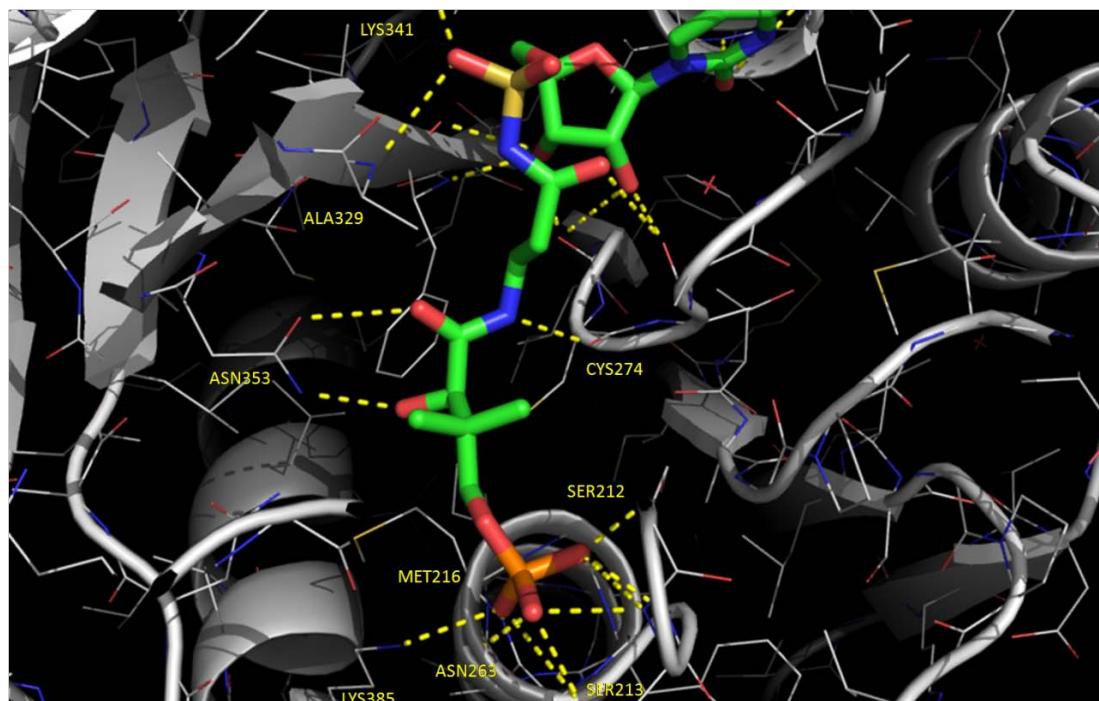


Figure 3.13: Phosphopantothenate binding pocket of PPCS with sulfamate 17

and Phe327, respectively. The ring oxygen in sulfamate **17** does not form a hydrogen bond with Lys345, as is the case with both the activated intermediate and phosphodiester inhibitor **8**. Also, the sulfamate makes a hydrogen bond with Lys341 as opposed to the salt bridge that the negatively charged phosphate of the phosphodiester **8** makes.

Within the phosphopantothenate binding pocket, sulfamate **17** binds very similarly to phosphodiester **8**. The 4' phosphate of the sulfamate extends into the phosphate cradle consisting of Ser212 and 213, Gly214, and Met216. The secondary alcohol and the carbonyl of the amide bond, both form a hydrogen bond to Asn263. The geometry of the sulfamate twists the β -alanine portion of the molecule in order for the nitrogen of the amide bond to hydrogen bond with the backbone carbonyl of Cys274. The sulfamate oxygen forms a hydrogen bond with Ala329 along with the hydrogen bond to Lys345.

Phosphodiester **8** and sulfamate **17** have IC_{50} s within 4 fold of each other with phosphodiester **8** having an IC_{50} of 68 nM and sulfamate **17** having an IC_{50} of 270 nM which explains their very similar mode of binding and common binding contacts. There are several differences in the binding that can explain the differences in the IC_{50} s of the two compounds. The main difference in the binding of the two compounds is how the two compounds bind at the edge of the ribose binding pocket through the internal linkage of the molecule, and at the carbonyl of the amide bond in the panthenol arm. The sulfamate cannot form an ionic interaction with Lys341 and does not form a hydrogen bond with its ribose ring oxygen with Lys345. Despite the carbonyl in the sulfamate being able to form a hydrogen bond and the nitrogen in the amide bond forming a hydrogen bond with Cys274, these added binding contacts are not able to counteract the loss of the ionic interaction of the negatively charged phosphate.

Co-Crystallization of *E. coli* PPCS Domain with Cyclic Phosphodiester Inhibitor

The best data set for the co-crystal of PPCS and cyclic phosphodiester **10** was obtained from 30% PEG 400 0.1 M sodium acetate pH 4.5 0.2 M calcium acetate with the well solution plus 40% PEG 400 as the cryoprotectant. The data was collected at APS shifting the X-ray detector back 250mm and offsetting it by 150 mm. The crystal gave a resolution of 2.30 Å, and belonged to space group $P6_122$ with one monomer in the asymmetric unit (**Table 3.3**). This data set has been solved using molecular replacement

using the ccp4 software suite with the structure of PPCS and phosphodiester **8** as the model (**Figure 3.14**).⁶ A brief investigation of this structure shows that there is a major difference in the structure of PPCS when the cyclic phosphodiester **10** is bound in the active site as compared to the non-cyclic inhibitors **8** and **17**. Looking at the yellow monomer in **Figure 3.14**, one can see that the flexible binding clamp composed of the residues Asp354 to Ala368 is disordered and not making contact with the PPA binding pocket. An overlay of cyclic phosphodiester **10** and the non-cyclic phosphodiester **8** show that there is also a difference in the orientation of the panthenol arm within the binding pocket (**Figure 3.15**).

Data Collection	
Space Group	P6 ₁ 22
Unit Cell	43.891, 43.891, 386.951
	90, 90, 120
Wave length (Å)	1.1271
Resolution (Å)	2.34-2.30
R_{sym} (%)	8.4 (49.7)
<I/σI>	>20 (5)
Completeness (%)	99.6 (99.6)
Redundancy	17.6 (18.2)

Table 3.3: Data collection statistics for structure of phosphodiester **10** bound PPCS

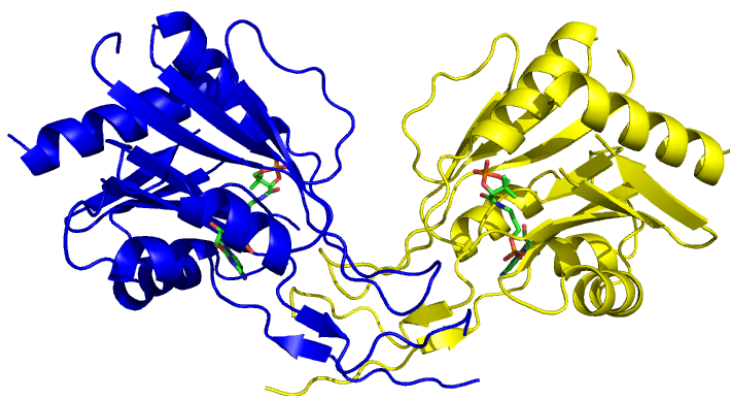


Figure 3.14: Cyclic phosphodiester **10** bound to PPCS domain

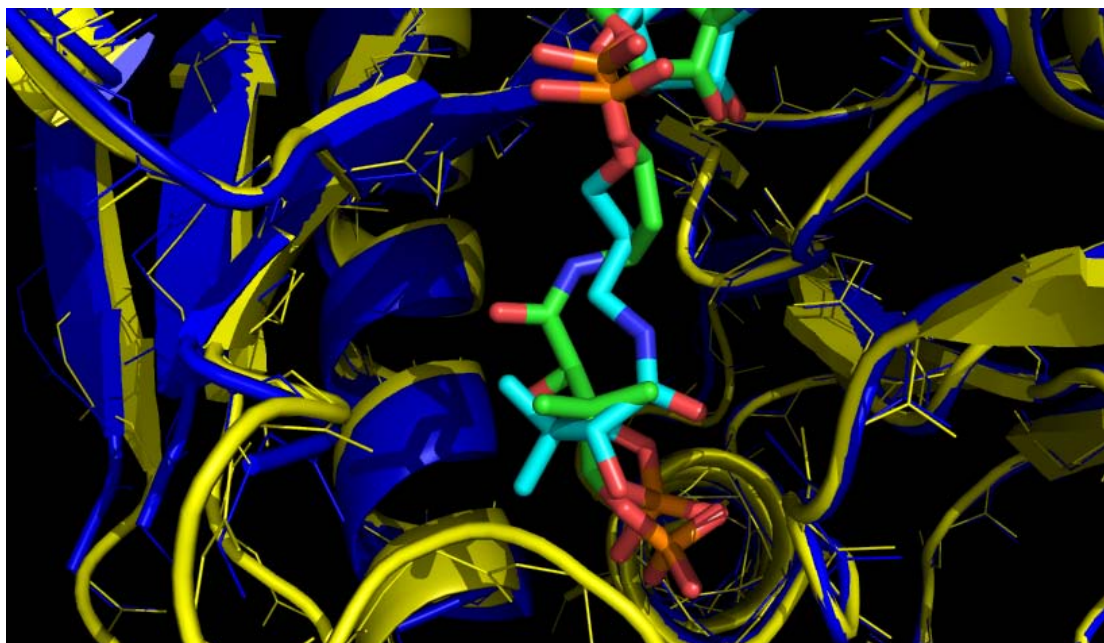


Figure 3.15: Overlay of cyclic phosphodiester **10** and phosphodiester **8**

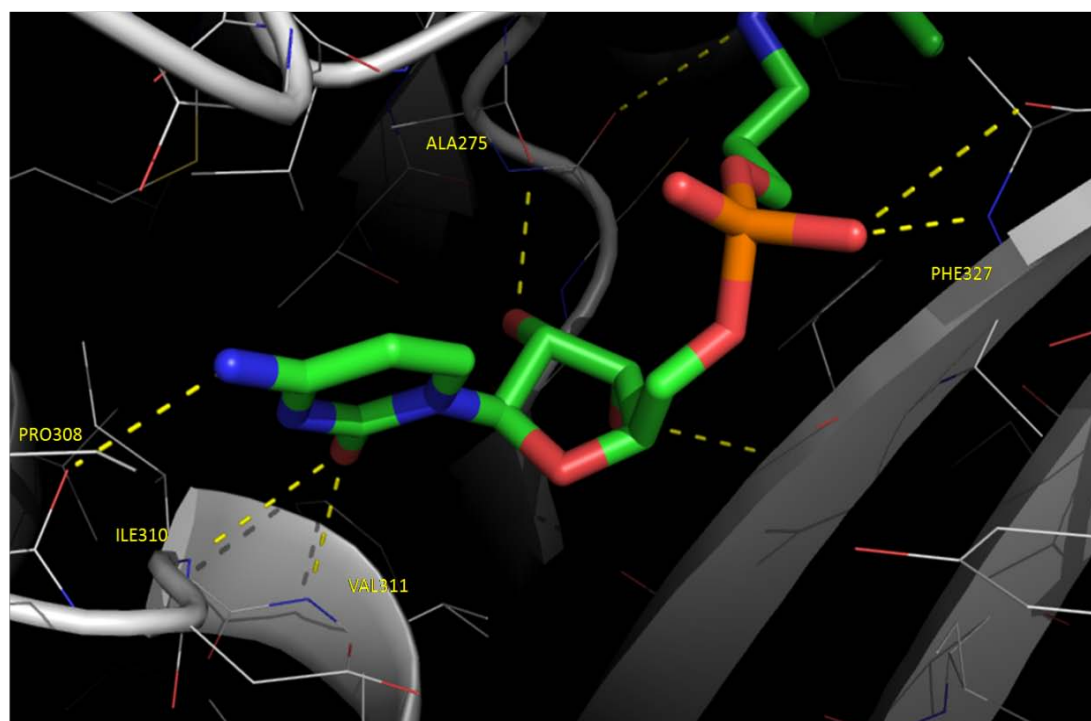


Figure 3.16: Nucleotide binding pocket with cyclic phosphodiester **10**

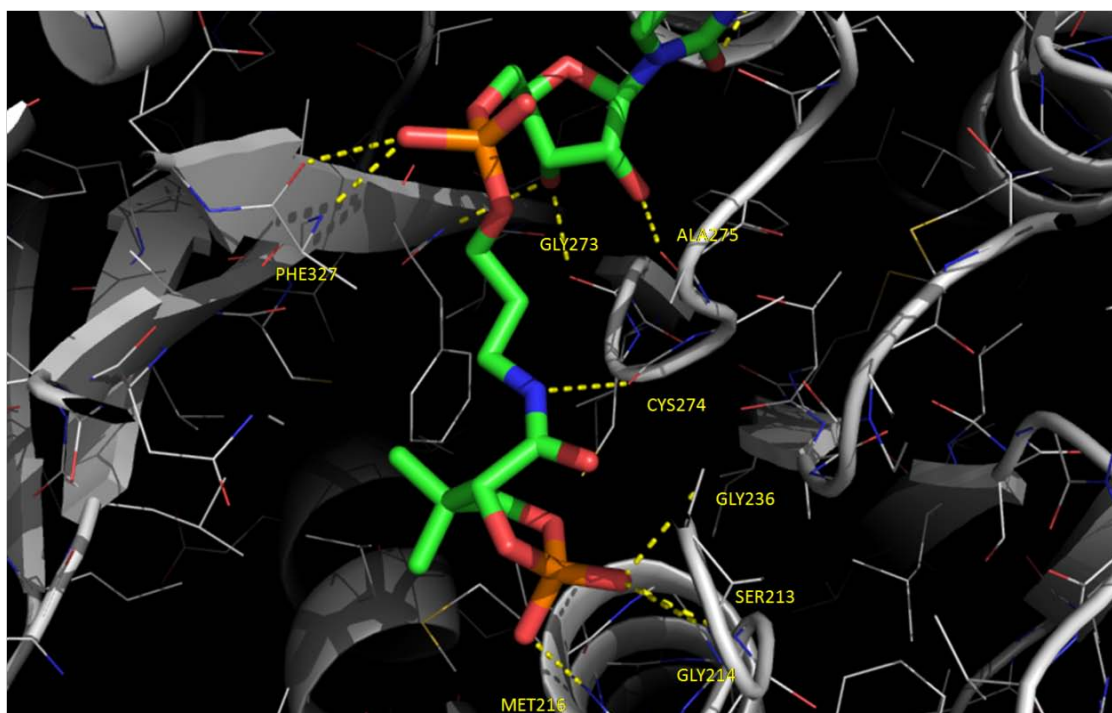


Figure 3.17: Phosphopantothenate binding pocket with cyclic phosphodiester **10**

Within the nucleotide binding pocket, the cytidine nucleobase is bound in the same fashion as the other inhibitors with a hydrogen bonding network to Pro308, Ile310, and Val311. The 2' and 3' alcohols form hydrogen bonds with Ala275, Ala273 and Phe327. However, it can be seen that the internal phosphate does not form a salt bridge with Lys341 and there is no binding contact with the ring oxygen on the ribose ring.

The most drastic difference in the binding of the cyclic phosphodiester mimic **17** with PPCS can be seen within the PPA binding pocket (**Figure 3.17**). In order for the terminal cyclic phosphate to reach into the phosphate cradle, the panthenol arm must twist and place the gem dimethyl group toward Asn353. Despite this adjustment the terminal cyclic phosphate cannot reach into the phosphate cradle very well and only makes a few hydrogen bonds in the cradle. This orientation of the gem dimethyl group does not allow for a hydrogen bond to form to Asn353 and more importantly the gem dimethyl creates a large steric clash which keeps the Asp354 to Ala368 binding flap from closing on the PPA binding pocket.

There is an interesting trend between the crystal structures that form a dimer in the asymmetric unit and the ability of the molecule within the active site in these structures to interact with Lys289. Both phosphodiester **8** bound to native PPCS and the

activated intermediate bound to the mutant PPCS are able to interact with Lys289 and form crystallographic dimers. Whereas the apo form of the Asn210Asp mutant and native PPCS structures with inhibitors **10** and **17** do not have molecules that interact with Lys289 and form monomers in the asymmetric unit. Site directed mutagenesis studies have shown that mutation of certain residues such as Asn210, Thr194 and 198, Ala275 diminish the ability of PPCS to form a dimer and in these cases PPCS elutes as a monomer in gel filtration experiments.⁷ In the structures with the activated intermediate or phosphodiester **8** bound to the active site, Lys289 is able to interact with the internal phosphate of the two molecules keeping the monomers of the dimer closer together increasing the overlap of the dimerization domain thus stabilizing the dimer. Mutation of Lys289 did not cause PPCS to run as a monomer in the literature report most likely due to the fact that the dimerization domain was not mutated and there was no molecule in the active site to perturb the protein.⁷ It was determined in the mutagenesis study that the Asn210Asp mutant ran closer to the monomer, so it is not surprising that its crystal structure was a monomer in the asymmetric unit.⁷ The structure of PPCS with sulfamate **17** may have been a monomer because sulfamate **17** has no phosphate to interact with Lys289. Without the added stability of the Lys289 contact to counteract the disturbance to the dimerization domain due to the molecule bound in the active site the overlap of the dimerization domain may not have been sufficient to keep the dimer. The cyclic phosphate **10** has the necessary phosphate for binding to Lys289, but due to the binding mode of the cyclic phosphate moiety, the active site and protein are so perturbed that Lys289 cannot form a binding contact and the dimerization domain does not have the necessary overlap to give a dimer. To test if PPCS is really a monomer in solution when bound to mimics **10** and **17** and a dimer when bound to mimic **8**, a set of gel filtration experiments should be run.

Based upon the differences in the three structures it is possible to use this information to design 2nd generation inhibitors. The nucleotide binding pocket showed very little difference among the three structures, except that phosphodiester **8** could form an extra hydrogen bond between the ring oxygen of the ribose ring and Lys345. This difference does not seem to account for a large difference in potency. However if taking advantage of this contact is the goal, then the cytidine portion of the molecule should be

replaced with isosteres of the same size or smaller. The internal phosphate linkage and its ability to form an ionic interaction with Lys341 and Lys289 from the other monomer are quite important and it will be difficult to replace. The sulfamate in inhibitor **17** does an adequate job as a geometric and electronic isostere in the *E. coli* PPCS structure; however, the sulfamate does not interact with Lys289. This replacement is better tolerated in *E. coli* PPCS as compared to the other PPCSs tested *in vitro*.⁴ If the sulfamate linkage is taken forward as the isosteric replacement for the phosphate then it will be necessary to take advantage of other binding contacts within the active site to increase inhibitor potency.

The PPA binding pocket and the binding contacts made by the intermediate mimics **8**, **10**, and **17** provide an opportunity for more chemical diversity in inhibitor design. The amine on Asn353 is a hydrogen bond donor to the amide carbonyl on the pantothenate arm, while the carbonyl on Asn353 is hydrogen bond acceptor to the secondary alcohol. The other important binding contact in this region of the binding pocket is the carbonyl oxygen of Cys274, which forms a hydrogen bond with the hydrogen on the nitrogen of the amide. These contacts should be accessible to any carbonyl compound such as an amide, ester, urea, or a ketone with either an alcohol or an amine in the α position. An α hydroxy ketone should be an interesting isostere. The α hydroxy ketone would not contact Cys274, but neither does phosphodiester **8**, which is the most potent molecule to date. However, it is essential that there be little steric bulk on this side of the PPA binding pocket. While it should be easy to take advantage of Asn353, it must be done with a linear molecule. A non-linear molecule will cause a steric clash with the binding clamp in the same manner that the gem dimethyl of cyclic phosphodiester **10** and cause a drastic drop in potency.

The final binding pocket is the phosphate cradle consisting of amino acids Ser212 through Met216. The terminal phosphate is crucial for binding to PPCS. Both phosphodiester **8** and sulfamate **17** bind very tightly within this binding pocket. However, cyclic phosphate **10** cannot fully extend into the phosphate cradle due to steric hindrance and the effective shortening of the panthenol arm due to the cyclized phosphate. The cyclized phosphate moiety still forms hydrogen bonds with Ser213, Gly214, and Met216, which shows the potential for a cyclic phosphate isostere to bind within the phosphate

cradle as long as there is a long enough linker that does not contain sterically bulky groups on the edge of the phosphate binding cradle. A neutral isostere such as triazole or a tetrazole attached with at least one or two methylene groups between it and any other functional groups would be ideal for fitting into the phosphate cradle.

Co-Crystallization of *E. coli* PPCS Domain with Phosphodiester **8 and Cysteine**

To complete the second goal of the structural study and investigate the cysteine binding pocket, the crystallographic conditions obtained from the Nextall 96 well PEG screen and explored using focused hanging drop screens. Unfortunately the co-crystallographic study with PPCS, phosphodiester **8**, and cysteine did not yield a crystal structure that included cysteine in the active site. Initial attempts involving the focused hanging drop screens focused around 0.1 M sodium acetate pH 4.6 30% PEG 300 and 0.2 M potassium thiocyanate 20% PEG 3350 with 15 mg/ml PPCS, 0.93 mM inhibitor **8**, and 2mM cysteine yielded less crystals and crystals of a poorer quality than drops without cysteine. These crystals were harvested, cryoprotected, and flash frozen using liquid N₂. Most of the crystals did not diffract beyond 4Å resolution and those that had a higher resolution did not give quality diffraction patterns that could be indexed and integrated using HKL2000.

To overcome the poor quality of the crystals with cysteine, co-crystals of PPCS and phosphodiester **8** were grown without cysteine according to the focused screen and cysteine was soaked into the pre-established crystal. At first, 1, 10, or 100 mM cysteine was placed in the cryoprotective solution used during the flash freezing process. Low resolution screening of these crystals revealed quality diffraction patterns, but when the data was processed there was no cysteine in the active site. The study was continued by extending the soaking time of the co-crystals of PPCS and phosphodiester **8** with the cryoprotective solution containing 1, 10, and 100 mM cysteine to 1 min, 15 min, 1 hour, 2 hours, and 24 hours. The concentration of the cysteine in the solution had no effect on the crystals, however, longer incubation times tended to crack and dissolve the pre-grown crystals containing PPCS and phosphodiester **8**. Despite this exhaustive screen, no structures with phosphodiester **8** and cysteine were obtained.

Unfortunately, phosphodiester **8** is not able to stabilize the PPCS active site enough to allow cysteine to bind to PPCS on the timescale that is visible by

crystallography. It is possible that the cysteine is able to enter the active site of PPCS and with no electrophile present; the cysteine diffuses back out into the solution. Stanitzek et al. observed catalytic turnover when the PPCS mutant with the activated intermediate in the active site showing that cysteine is free to enter the active site and react with the activated intermediate on the crystallographic timescale.¹ In order to crystallize cysteine with PPCS and explore its binding pocket, it is necessary to employ a mechanistic trap with an electrophilic functionality such as a Michael acceptor or an epoxide.

Acknowledgements

I would like to thank and acknowledge Nicole Scott for cloning ecPPCS. I would like to thank and acknowledge Jeanne Stuckey and Jennifer Meagher for allowing me to work in their laboratory and their help and guidance with the crystallographic study.

Materials and Methods

Cloning, Overexpression, and Purification of *E. coli* PPCS: The *coaB* coding region of the *dfp* gene (encoding ser181-arg406 of the *E. coli* CoaBC protein)^{1, 8} was PCR amplified using *E. coli* MG1655 genomic DNA as a template, and the primers, *coabecl*(forward primer), 5' – CGCGCATA TGTCGCCCCGTCAACGACCTGAAACATCTG-3' and *dfp3* (reverse primer), 5'-GCGCCTCGAGACGTCGATTTTTTTCATCATAACGGG-3'. The forward primer introduces an *NdeI* site (shown underlined) to provide a start codon for the *coaB* coding region, and the reverse primer creates a *XhoI* site (shown underlined) downstream of the stop codon of the open reading frame. The PCR products were digested with *NdeI* and *XhoI*, and ligated into pET23a(+) (Novagen) cut with *NdeI* and *XhoI*. The resulting plasmid was designated pUMDOT3 and the insert was confirmed by DNA sequencing.

E. coli BL21 AI (Invitrogen) harboring the plasmid pUMDOT3 were grown in 500 mL LB-ampicillin media (5 g of NaCl, 5 g of yeast extract, 10 g of tryptone, and 100 mg of ampicillin per L) at 37°C and 250 rpm to a OD600 of 0.6. The cells were then cooled by shaking at 16°C for 10-15 min, induced with 0.07% L-arabinose, and continued to grow at 16°C and 250 rpm for 12-16 hours. The cells were harvested at 6000 x g for 10 minutes at 4°C, washed, and then suspended in 12 ml of 20 mM HEPES pH 8.0. Cells were lysed by French Press and crude cytosol obtained by centrifugation at 20,000 x g for 25 minutes at 4°C.

ecPPCS was purified using a tandem anion exchange column (Source 15Q (GE Healthcare); 20 mL) and cation exchange column (Source 15S (GE Healthcare); 8 mL). The 12 mL of crude cytosol was loaded onto the tandem chromatography columns which had been pre-equilibrated with 20 mM HEPES pH 8.0. The columns were then washed with another 40 mL of equilibration buffer and the anion exchange column was removed. Under these conditions the ecPPCS does not bind to the anion exchange resin, but does bind to the cation exchange resin. The cation exchange column was eluted with a linear gradient of 0-0.4 M NaCl in 20 mM HEPES pH 8.0, with a total gradient volume of 100 mL. ecPPCS eludes as a single peak at 75 mM NaCl and was greater than 98 % pure as determined by SDS-PAGE. The fractions were combined and diluted with 20 mM TrisHCl pH 8.0 with 10 mM NaCl to a total volume of 15 mL. The solution was concentrated to a volume of 1 mL using a Centricon 10,000 MW cutoff centrifugal filter device. This process was repeated and the buffer exchange was complete. The concentration of PPCS was adjusted to 15 mg/mL.

Synthesis of compounds 8, 10, and 17: Compounds 8, 10, and 17 were synthesized as previously described.

96 Well sitting drop robotic screens: 96 Well crystallization screens with three crystallization wells per each of the 96 reservoir wells. The Nextall PEG and Emerald Wizard screens were set up using Honeybee 961 crystallization robot. The crystal trays were incubated at 20°C for 3-14 days until crystals were mature and ready for harvest.

24 Well focused hanging drop screens: Focused hanging drop screens were set up using Hampton 1.5 mL capacity hanging drop trays. The drops contained 15 mg/mL PPCS and the appropriate compound. The pH was varied across the row and concentration of PEG was varied down the columns. The trays were set up and incubated at 20°C for 3-14 days until crystals were mature and ready for harvest.

References

1. Stanitzek, S.; Augustin, M. A.; Huber, R.; Kupke, T.; Steinbacher, S., Structural Basis of CTP-Dependent Peptide Bond Formation in Coenzyme A Biosynthesis Catalyzed by Escherichia coli PPC Synthetase. *Structure* **2004**, 12, (11), 1977-1988.
2. Manoj, N.; Strauss, E.; Begley, T. P.; Ealick, S. E., Structure of Human Phosphopantothenoylecysteine Synthetase at 2.3 Å Resolution. *Structure* **2003**, 11, (8), 927-936.
3. Strauss, E.; Tadhg, P. B., The Selectivity for Cysteine over Serine in Coenzyme A Biosynthesis. *ChemBioChem* **2005**, 6, (2), 284-286.
4. Patrone, J. D.; Yao, J.; Scott, N. E.; Dotson, G. D., Selective Inhibitors of Bacterial Phosphopantothenoylecysteine Synthetase. *Journal of the American Chemical Society* **2009**, 131, (45), 16340-16341.
5. Otwinowski, Z.; Minor, W.; Charles W. Carter, Jr., Processing of X-ray diffraction data collected in oscillation mode. In *Methods in Enzymology*, Academic Press: 1997; Vol. Volume 276, pp 307-326.
6. Phaser crystallographic software. *Journal of Applied Crystallography* **2007**, 40, (4), 658-674.
7. Kupke, T., Molecular Characterization of the 4'-Phosphopantothenoylecysteine Synthetase Domain of Bacterial Dfp Flavoproteins. *Journal of Biological Chemistry* **2002**, 277, (39), 36137-36145.
8. Kupke, T., Molecular Characterization of the 4'-Phosphopantothenoylecysteine Synthetase Domain of Bacterial Dfp Flavoproteins. *J. Biol. Chem.* **2002**, 277, (39), 36137-36145.

Chapter 4

Probes of the individual half reactions of PPCS

Introduction

In the first half reaction catalyzed by PPCS, CTP binds and then PPA enters the active site. The carboxylate of PPA then attacks the α phosphate on CTP to generate an activated intermediate and release pyrophosphate (**Figure 4.1**).^{1, 2} The second half reaction involves cysteine entering the active site and initiating amide bond formation via nucleophilic attack on the carbonyl of the mixed anhydride of the activated cytidylate intermediate. With this mechanistic information, it should be possible to design probes that will mimic the PPA substrate to probe and exploit the first half reaction. Likewise,

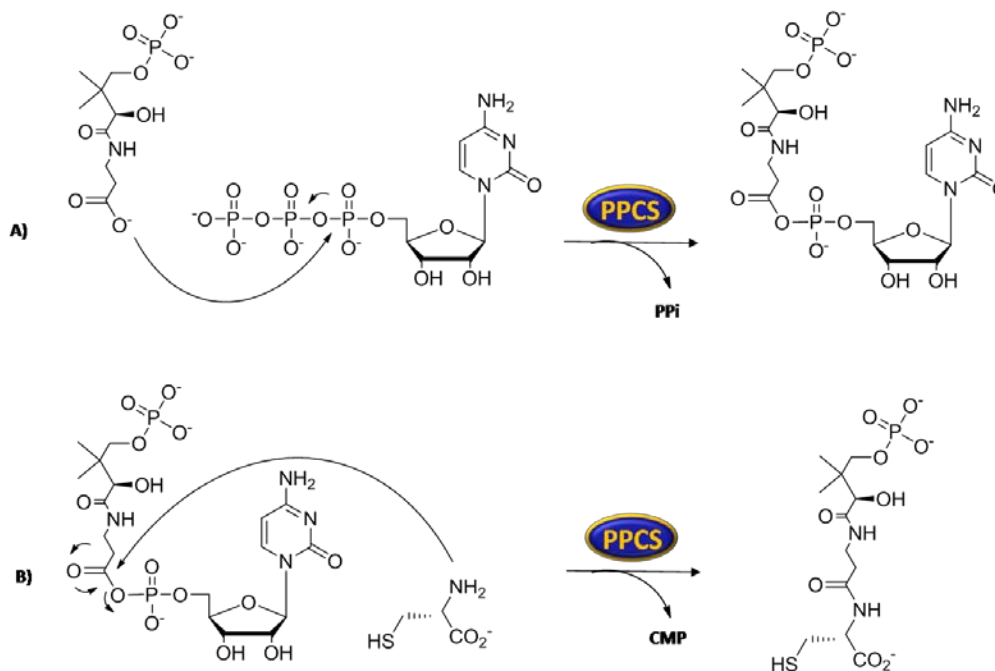


Figure 4.1: Mechanism of both half reactions of PPCS. A) Mechanism of first half reaction B) Mechanism of second half reaction

intermediate mimics containing an electrophilic functionality could be used to exploit the mechanism of the second half reaction and trap substrate cysteine in the active site.

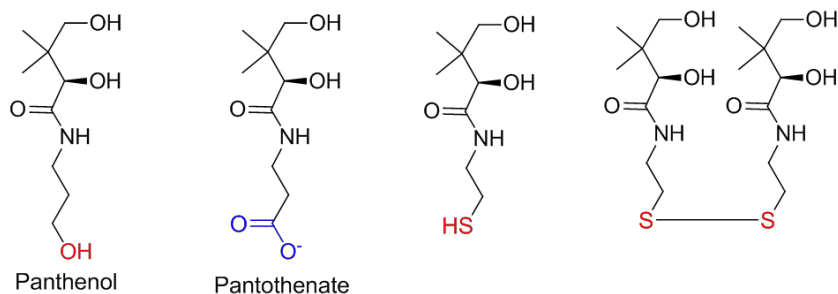


Figure 4.2: Known inhibitors of bacterial and malarial growth

Several pantothenate analogs are known to inhibit both malarial and bacterial growth *in vitro* and are thought to inhibit and/or serve as alternate substrates for pantothenate kinase (**Figure 4.2**).³ Panthenol is commercially available and the thiol and disulfide molecules can be readily made from pantolactone and cystamine. Unfortunately, due to a lack of commercial availability, there are no pantothenate or PPA mimics with a three carbon unit to mimic the β -alanine portion of the molecule other than panthenol. Herein, we have constructed PPA and pantothenate based probes which keep the three

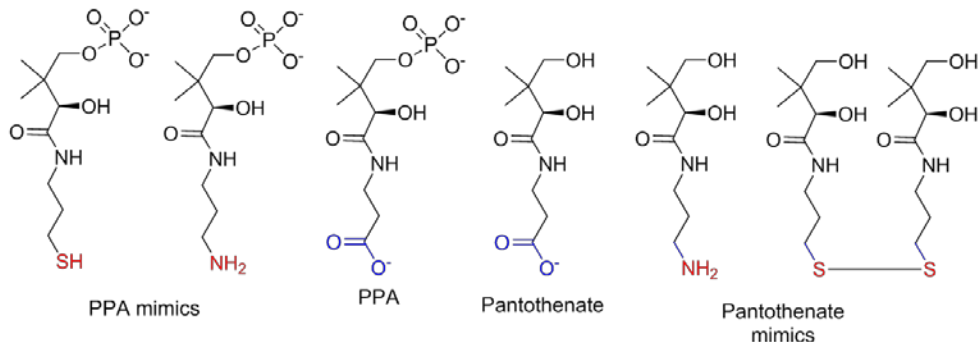


Figure 4.3: Proposed PPA analogs

carbon unit of β -alanine, but replace the carboxylate with a nucleophilic thiol or amine (**Figure 4.3**). The PPA mimics should either act as competitive inhibitors with regard to PPA or act as mechanism-based inhibitors that are able to utilize PPCS and CTP to form an intermediate mimic *in situ*. If the mechanism of inhibition conforms to the latter, then pre-incubating these substrate analogs with CTP and PPCS would allow the thiol or amine to attack the α phosphate of CTP and synthesize a cytidylate mimic analog within the active site of PPCS (**Figure 4.4**).

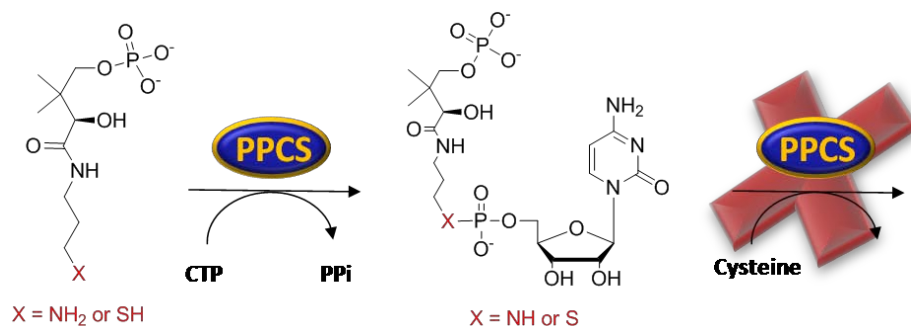


Figure 4.4: Mechanism of proposed PPA analog inhibitors

The second class of probes was designed to be an intermediate mimic mechanism based probe with a vinyl sulfone built into the pantothenate portion of the molecule. Vinyl sulfones have found great utility in the study of enzyme mechanisms and interactions because of their ability to act as Michael acceptors and crosslink the mechanism-based probe to the enzyme being studied, usually via cysteine attack on the vinyl sulfone.⁴⁻⁷ It has been shown that various vinyl sulfones react with the active site cysteine of cysteine proteases, such as Cruzain, ketosynthases, such as KASI and KASII, as well as the cystamine functionality of the phosphopantetheine arm of carrier proteins (**Figure 4.5**). The carrier protein mechanism-based probe was shown to specifically irreversibly label an acyl carrier protein from *Mycobacterium tuberculosis* as shown by mass spectrometry, and the ketosynthase mechanism-based probe was able to crosslink acyl carrier protein and KASI as analyzed by SDS-PAGE analysis (**Figure 4.5**).^{5,7}

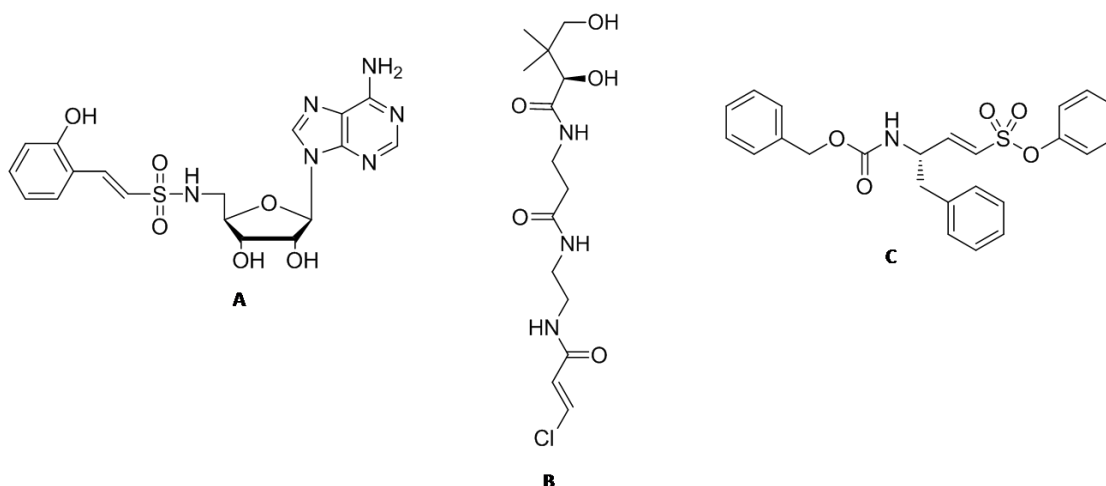


Figure 4.5: Examples of vinyl sulfones in literature. A) Carrier protein mechanism-based probe⁵ B) Ketosynthase mechanism-based probe⁷ C) Cruzain mechanism-based probe⁶

Based upon the ability of these vinyl sulfones to act as Michael acceptors and the ability to characterize the resulting irreversibly labeled product, an intermediate mimic was designed with a vinyl sulfone functionality in place of the electrophilic carbonyl of the activated intermediate. The vinyl sulfone intermediate mimic would be attacked by the cysteine that enters PPCS as the third substrate rather than by a cysteine embedded within the enzyme of interest. Once cysteine attacks the vinyl sulfone it should be possible to isolate and characterize the ternary complex and identify whether the amine or thiol of cysteine is the nucleophile in the second half reaction catalyzed by PPCS (**Figure 4.6**).

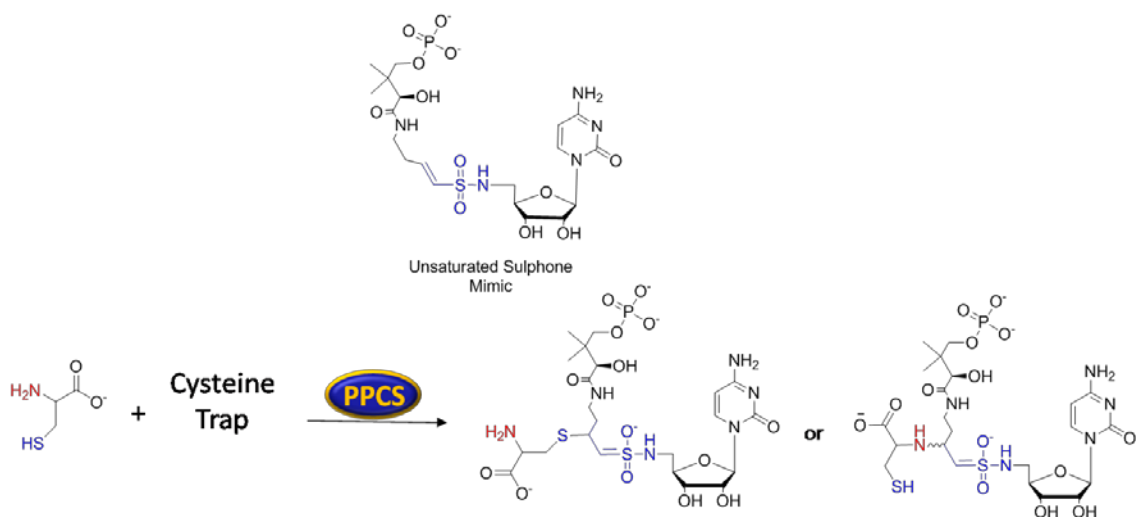
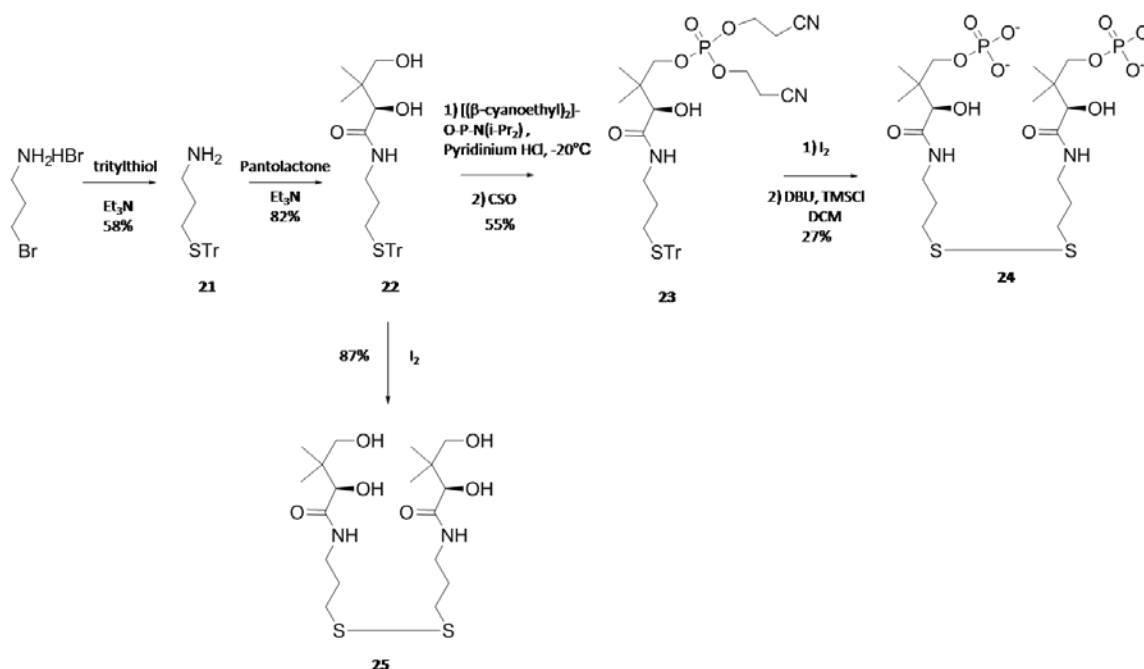


Figure 4.6: Mechanism of vinyl sulfone intermediate mimic

Phosphopantothenate and pantothenate based probes

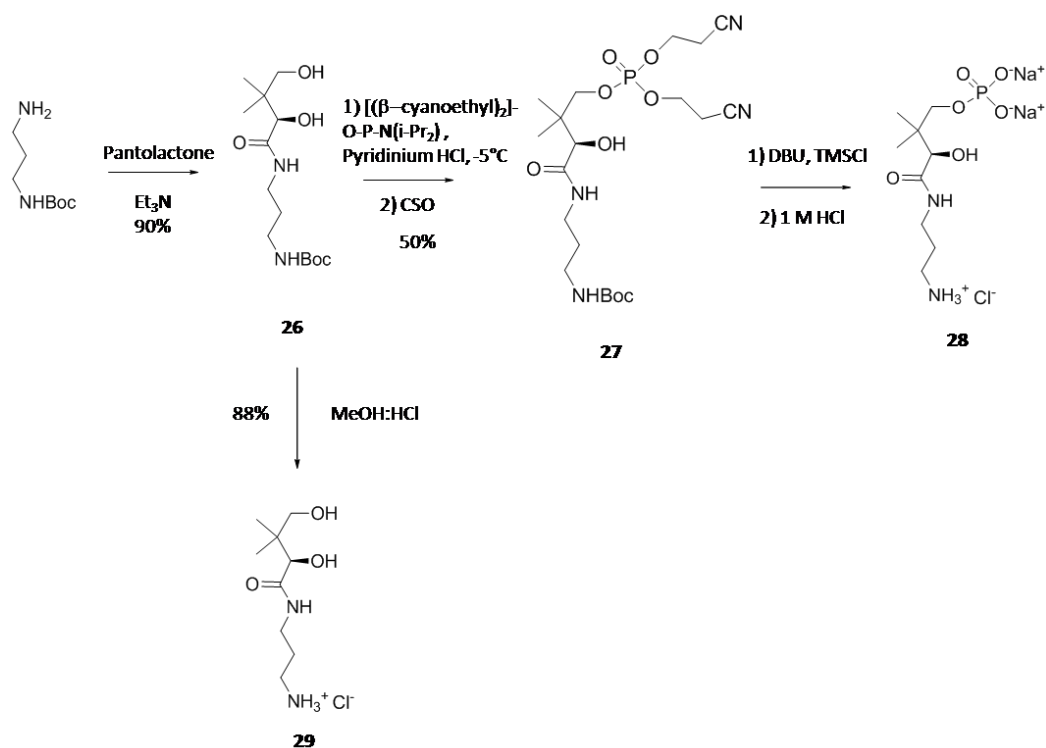
The synthesis of the proposed thiol analog of PPA begins with the nucleophilic displacement of the bromide on 3-bromopropylamine hydrobromide with trityl thiol in 58%. The propyl amine **21** was used to open pantolactone to yield the desired diol **22**.⁸ The choice of the protecting groups on the phosphate proved to be very important as the deprotection was more difficult than initially anticipated. Originally, ethyl protecting groups were used based upon the commercial availability of chlorodiethyl phosphate and ease of the phosphorylation which proceeded in 87% yield.⁹ All attempts to deprotect the ethyl groups with TMSBr or under acidic conditions resulted in degradation of the molecule with only 1.6 mg of the desired phosphate ever recovered. Alternatively, the

diol was then phosphitylated with pyridinium HCl as the activator at -20°C to yield the protected phosphodiester. Phosphodiester **23** was deprotected by oxidatively cleaving the trityl group to yield the disulfide followed by deprotecting the phosphodiester by treating with DBU and TMSCl. After purification by anion exchange column and P2 sizing column, the disulfide **24** was obtained in 27% yield as the tetrasodium salt.^{9, 10} The non-phosphorylated analog of the desired mimic was synthesized from the protected diol **22** by oxidatively deprotected the thiol group to give diol **25**.



Scheme 4.1: Synthesis of proposed thiol PPA analog

The synthesis of the proposed amine analog of PPA is similar to thiol mimic and begins with the opening of pantolactone with tert-butyl (3-aminopropyl)carbamate (**Scheme 4.2**). The phosphitylation and oxidation of diol **26** was not as straightforward as initially anticipated. Standard phosphitylation and oxidation conditions led to no reaction in the case of diol **26**. In order to get the desired β -cyanoethyl protected phosphate, diol **26** was treated with bis(β -cyanoethyl) diisopropylphosphoramidite and pyridinium HCl as the activator at -5°C in DMF. The protected phosphate **27** was deprotected in two steps to yield the desired phosphate **28**; however, the phosphorylated compound was not recovered after anion exchange chromatography. The non-phosphorylated analog **29** was obtained in 88% by treating the protected diol **29** with methanolic HCl.



Scheme 4.2: Synthesis of amine PPA analog

The first assay performed was to test whether the non-phosphorylated analogs **25** and **29** would be substrates for the kinase PanK, the first enzymatic step in CoA synthesis. The kinase assay consists of coupling PanK to pyruvate kinase (PK) and lactate dehydrogenase (LDH), and following the oxidation of NADH to NAD, which can be monitored by the disappearance of UV absorbance at 340 nm (**Figure 4.7**). The disulfide **25** had a K_m of 500 μM and the amine compound **29** showed no phosphorylation (**Figure 4.8**). It is known that the carbonyl group of the carboxylate of vitamin B₅ is important for binding to the kinase. Despite not possessing a carbonyl functionality at this position, the oxidized and reduced forms of **25** were still able to be phosphorylated by *E. coli* PanK. The amine **29**, however, does not only lack the carbonyl, but also possesses a positive charge on the amine. This positive charge probably forms unfavorable interactions in the carboxyl binding pocket of PanK and thus it is not phosphorylated in any appreciable amount.

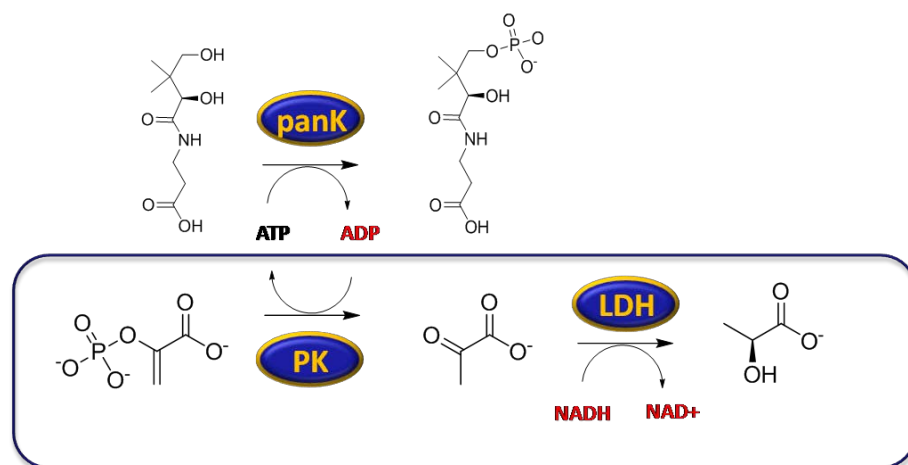


Figure 4.7: Kinase assay

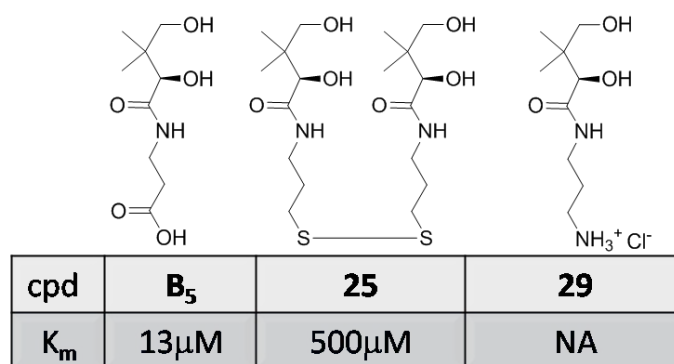


Figure 4.8: Kinase assay results

The phosphorylated disulfide **24** was then tested for time dependent PPCS inactivation using the pyrophosphate reagent coupled PPCS assay. Compound **24** was pre-incubated with one equivalent of dithiothreitol (DTT) at 37°C for one hour. The reduced version of compound **24** was then incubated with PPCS and CTP for various times. The other substrates were then added to the assay mixture and PPCS activity was monitored. Unfortunately, compound **24** did not display any inhibition of PPCS activity in this manner and as such compound **24** was not a time dependent mechanism-based inhibitor. This result maybe due to the thiol not being placed at the proper geometry in relation to the α phosphate of CTP in the active site of PPCS. To try and increase the nucleophilicity of the thiol by biasing the equilibrium towards the thiolate, the pH of the pre-incubation solution was varied from 7.5 to 8.5. Even at the elevated pHs the thiol mimic did not display any time dependent inhibition.

Disulfide **24** was then tested as a competitive inhibitor of PPCS with respect to PPA. The inhibitor concentration was varied along with the concentration of PPA while the other substrate concentrations were fixed. The velocity of the reaction was plotted against PPA concentration for the different disulfide concentrations (**Figure 4.9**).

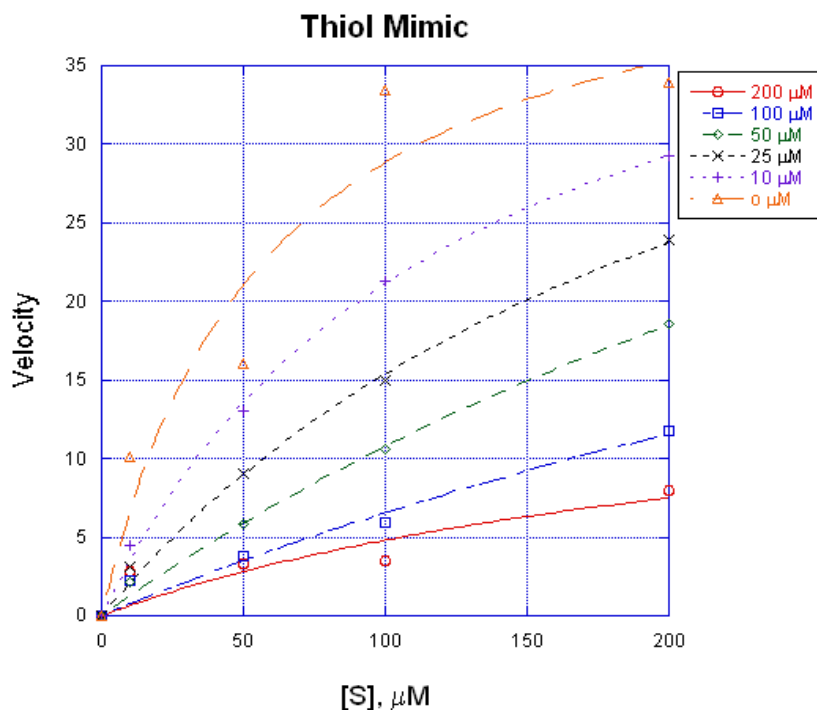


Figure 4.9: Velocity versus PPA concentration

The curves from **Figure 4.9** were fit using the following equation:

$$v = \frac{V_{max}}{1 + \frac{K_m}{[S]}}$$

and solving for K_m^{app} . The K_m^{app} values were then replotted against disulfide concentration to give a straight line with an x intercept equal to negative K_i , which in this case was based on the two initial runs and was equal to 12 μM +/- 2.

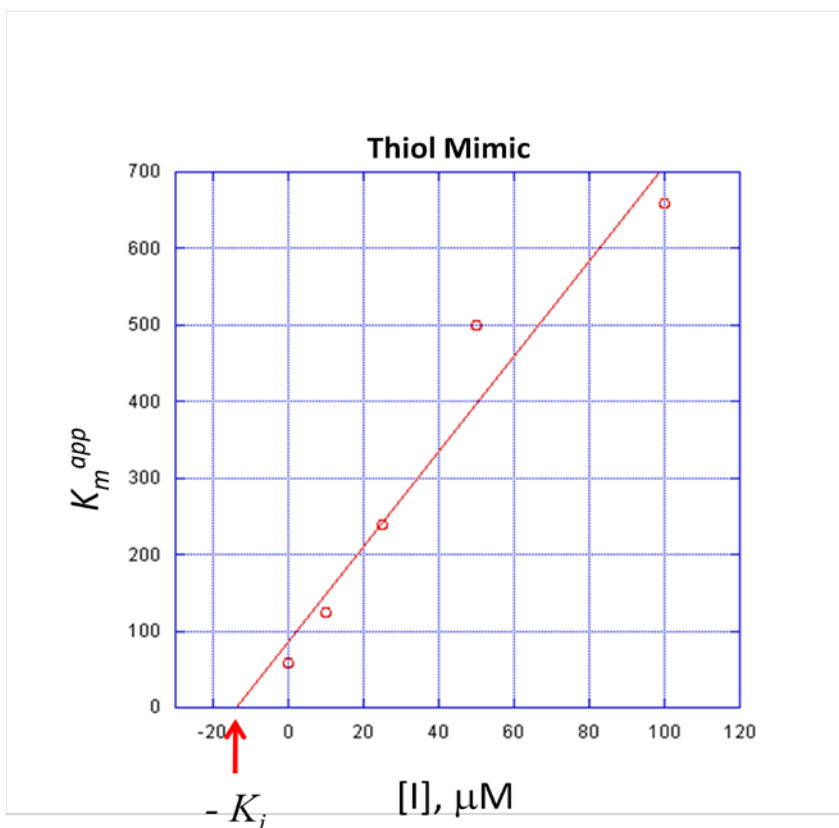


Figure 4.10: K_m^{app} versus [I]

Vinyl Sulfone mechanism-based probes

Retrosynthetic analysis of the vinyl sulfone mimic reveals that the first disconnection is the terminal phosphate on the 1,3 diol of the panthenol portion (**Figure 4.9**). This phosphate will be installed last in the synthetic sequence using the phosphitylation/oxidation methodology previously used on intermediate mimic **8**. The second disconnection was the nitrogen sulfur bond of the vinyl sulfonate dissecting the molecule into two halves consisting of an amino cytidine portion and the panthenol portion with the vinyl sulfone. The vinyl sulfone can be installed via a Horner Wadsworth Emmons (HWE) reaction using ethyl methanesulfonate and an aldehyde derived from β -alanine or from panthenol itself.

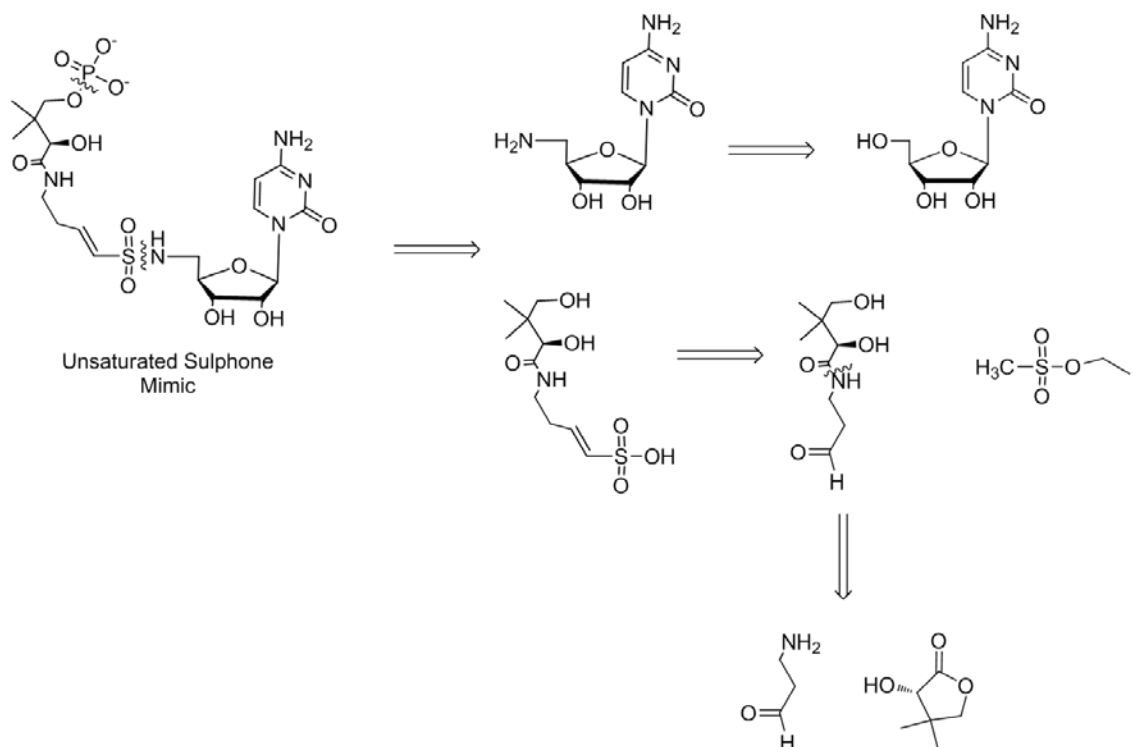
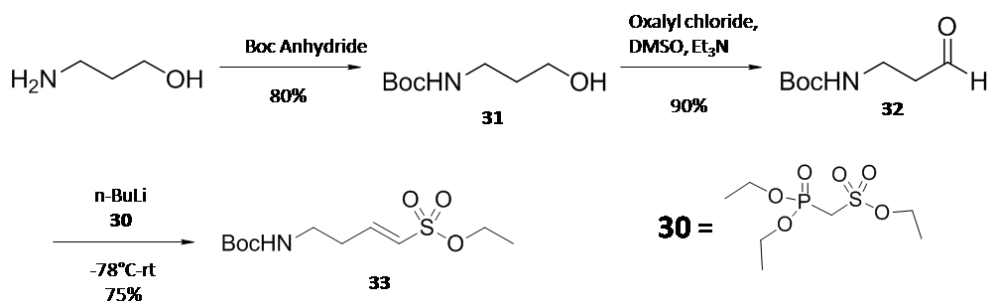


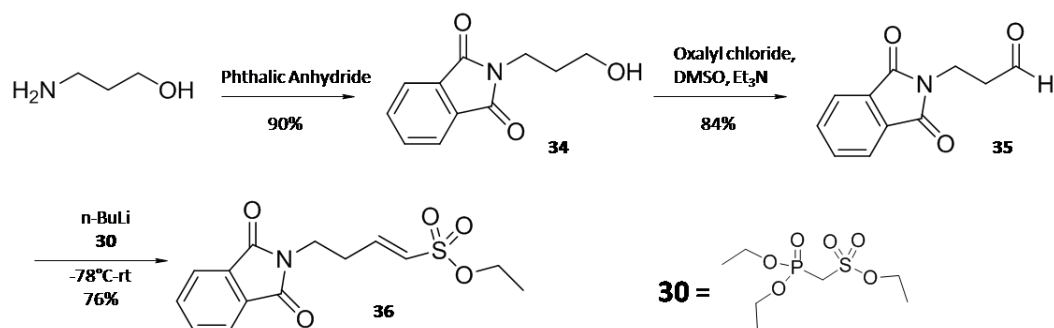
Figure 4.11: Retrosynthetic analysis of vinyl sulfone intermediate mimic

In the forward direction, several aldehydes were constructed in order to probe which aldehyde was most suited for the HWE reaction and subsequent coupling to the amino cytidine molecule. The synthesis of the boc protected vinyl sulfone begins with the selective protection of the amine on 3-aminopropanol with boc anhydride in 80% (**Scheme 4.3**).¹¹ The alcohol is then subjected to standard Swern oxidation to yield the aldehyde **32**. The aldehyde is then converted to the vinyl sulfone by coupling compound **32** to the sulfone **30** via a HWE reaction in 75% yield.⁴ The phthalate protected vinyl sulfone is synthesized in a similar fashion as vinyl sulfone **33** (**Scheme 4.4**). The amine on 3-aminopropanol was selectively protected using phthalic anhydride in 90% yield.¹²⁻¹⁴

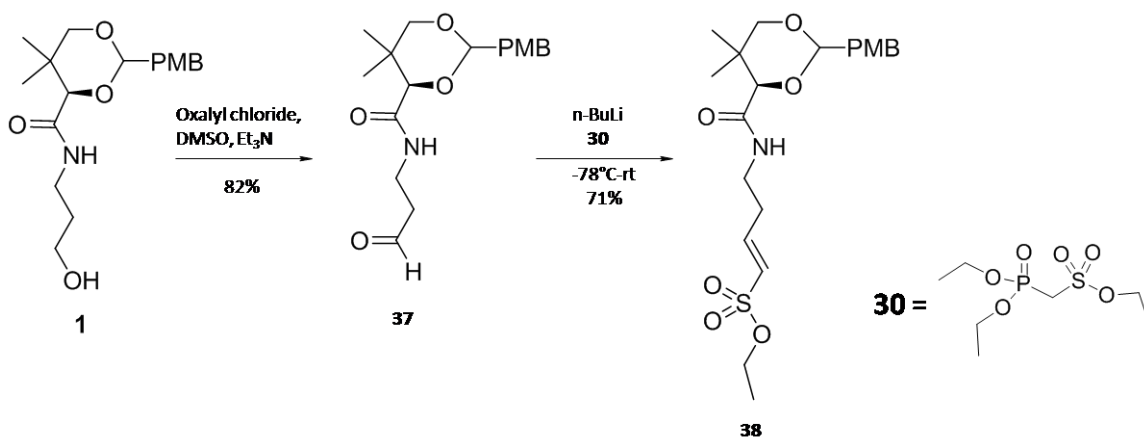


Scheme 4.3: Synthesis of Boc protected vinyl sulfone

Alcohol **34** was then subjected to standard Swern oxidation conditions to yield aldehyde **35**.^{13, 15} The vinyl sulfone was then obtained by coupling aldehyde **35** to sulfone **30** via a HWE reaction in 65%. The third vinyl sulfone synthesized was the PMB acetal vinyl sulfone derived from the PMB acetal of panthenol (**Scheme 4.5**). The previously synthesized PMB protected panthenol **1** was oxidized to the aldehyde in 82% yield. The aldehyde was then coupled to sulfone **30** under standard HWE conditions to yield the desired vinyl sulfone **38**.

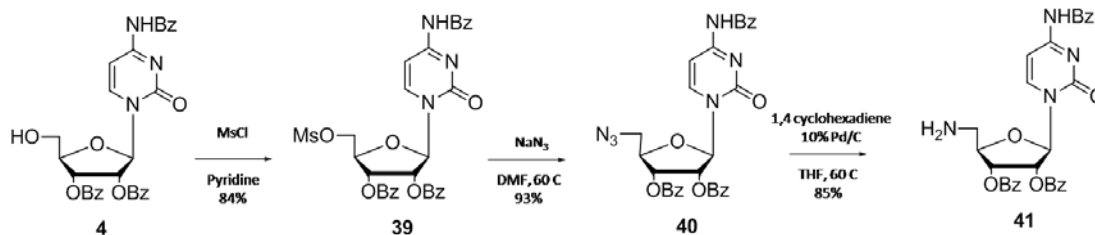


Scheme 4.4: Synthesis of phthaloyl protected vinyl sulfone



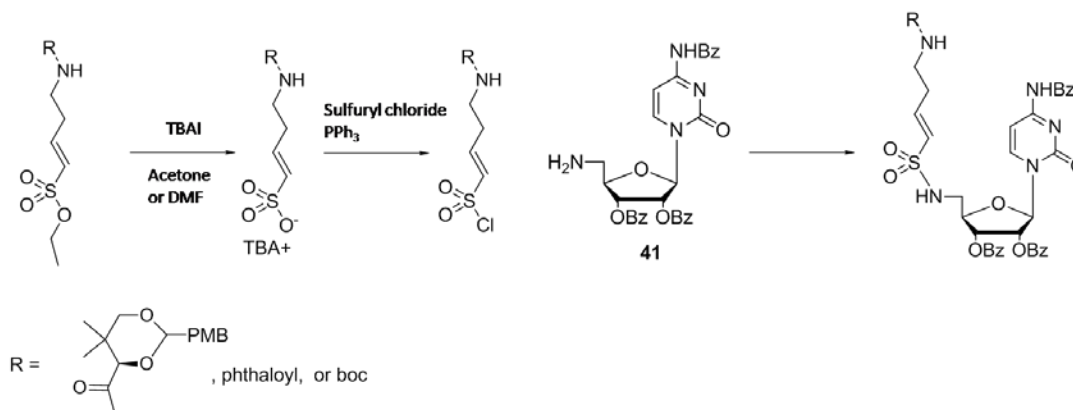
Scheme 4.5: Synthesis of PMB protected vinyl sulfone

The amine group was installed on the cytidine portion of the molecule starting from the previously synthesized tribenzoyl cytidine. Tribenzoyl cytidine **5** was treated with mesyl chloride to yield the mesylated tribenzoyl cytidine **39**. Displacement of the mesylate of compound **39** was accomplished using excess sodium azide to give tribenzoyl cytidine azide **40** in 93%.¹⁶ Reduction of the azide to the amine was accomplished by either Staudinger reduction or transfer hydrogenation to afford the desired amine **41**.^{4, 16}



Scheme 4.6: Synthesis of tribenzoyl cytidine amine

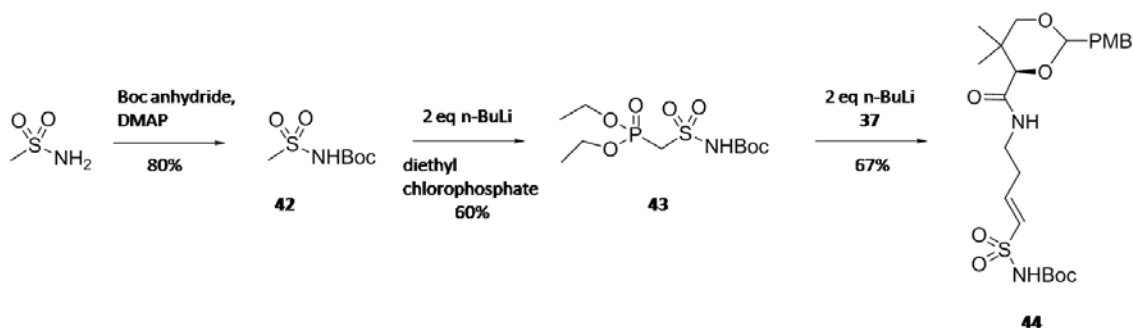
With the tribenzoyl cytidine amine **41** and the protected vinyl sulfonate esters **33**, **36**, and **38** in hand, the next step was to couple the two fragments. The ethyl ester of the vinyl sulfone was deprotected using tetrabutylammonium iodide (TBAI).^{4, 6, 17, 18} In the case of the phthaloyl protected sulfonate and the PMB protected sulfonate the resulting tetrabutylammonium (TBA) salt were chromatographable via silica column, however, the boc protected TBA salt was used without further purification. Initial attempts involved subjected the TBA salt to the chlorination conditions of triphenylphosphine and sulfonyl chloride to generate the sulfonyl chloride in situ and then addition of the tribenzoyl cytidine amine **41** or tribenzoyl cytidine **4**. Under these conditions, the tribenzoyl cytidine analogs **41** and **4** were recovered in 80% or greater and no productive coupling was detected whether the boc, phthaloyl, or PMB vinyl sulfonate was used.



Scheme 4.7: Coupling of two fragments

The Boc protected sulfonate was used in model reactions for probing the chlorination and coupling conditions because it was most analogous to molecules successfully coupled in literature.¹⁷ The Boc protected sulfonate TBA salt was exposed to one to ten equivalents of freshly distilled sulfonyl chloride and one to three equivalents of triphenylphosphine. Based upon literature precedent, the reaction mixture was purified

over oven dried silica gel.^{4, 17} However, the desired sulfonyl chloride was not recovered. Triphenylphosphine oxide and TBA were recovered off the column, but no species containing the Boc protecting group and the vinyl group were recovered. The chlorination conditions were then varied using Oxalyl chloride, thionyl chloride, and phosphorous trichloride; however, the sulfonyl chloride was not isolatable. Investigating the PMB protected sulfonate TBA salt using the various chlorinating conditions resulted in up to 50% deprotection of the PMB acetal and no chlorinated product.



Scheme 4.8: Synthesis of N-Boc sulfones

Based upon literature reports that N-Boc protected mesylates and tosylates can be coupled to various alcohols through the Mitsunobu reaction, an alternative route utilizing a Mitsunobu reaction to install either the vinyl sulfone or the sulfonyl phosphonate was also explored.¹⁹ Methanesulfonamide is protected with Boc anhydride in the presence of catalytic DMAP (Scheme 4.8).²⁰ Treating sulfone **42** with two equivalents of n-butyl lithium and diethyl chlorophosphate yielded the desired phosphonate smoothly in 60%.²⁰ The Boc protected phosphonate was then coupled via a HWE reaction to the PMB protected aldehyde **37**. The Mitsunobu reaction conditions were explored treating triphenylphosphine with diisopropyl azodicarboxylate (DIAD) to pre-form the betaine and then tribenzoyl cytidine **4** and the various N-Boc sulfones **42-44** were added and allowed to stir for 24 hrs. Under these conditions only sulfone **42** was successful in forming the cytidine sulfone in 53% by NMR. Numerous attempts to isolate the desired cytidine sulfone via column chromatography, inseparable mixtures contaminated with tribenzoyl cytidine and triphenylphosphine oxide were obtained. Varying the reaction conditions did not allow for the successful addition of either sulfone **43** or **44** with tribenzoyl cytidine being isolated as the major product in all cases. The optimized conditions of pre-forming the betaine and accelerating the reaction using sonication

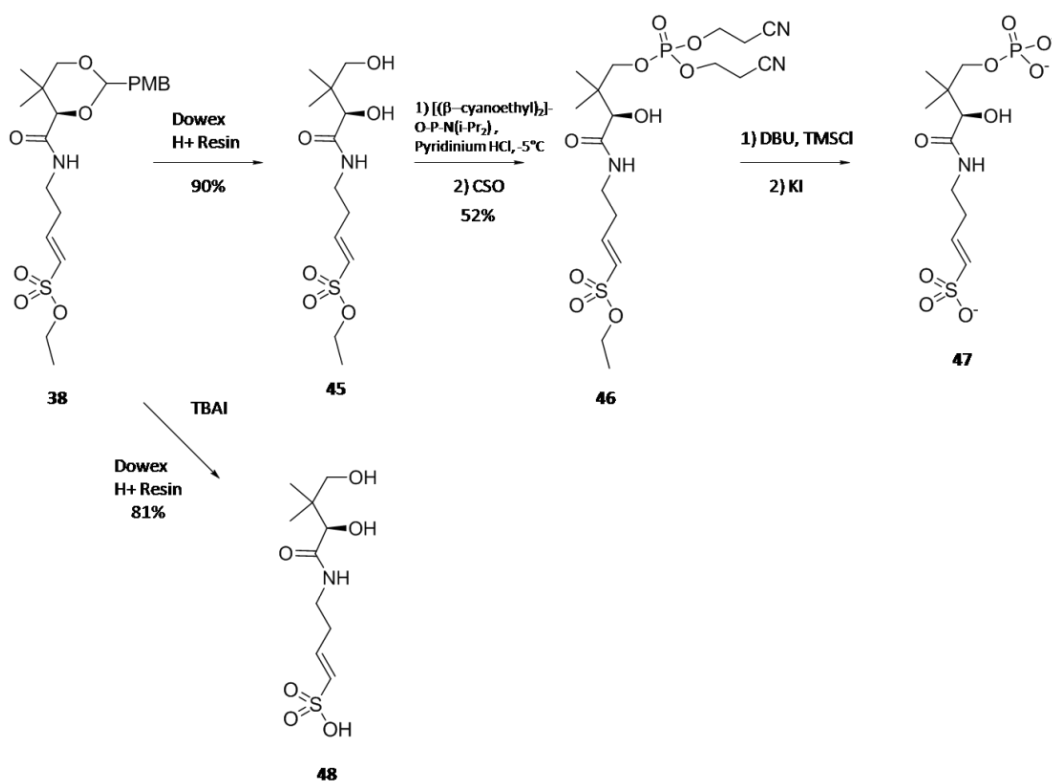
allowed for the reaction time of sulfone **42** to be reduced to 15 min, but there was no improvement in yield or purification.

The final attempt to install the desired vinyl sulfone on the intermediate mimic was to build the sulfonyl phosphonate required for the HWE reaction off of the cytidine portion of the molecule. Mesityl tribenzoyl cytidine **39** was treated with either two or three equivalents of sodium hydride, LDA, or *n*-BuLi at -78°C for thirty minutes and diethyl chlorophosphate was added. Upon workup and purification greater than 75% of the starting mesylate was recovered along with 10% tribenzoyl cytidine but none of the desired product. The stir time was extended and the reaction was allowed to warm to room temperature, 0°C, and -48°C with the same results.

Installing the vinyl sulfone in an intermediate mimic of PPCS proved more difficult than initially anticipated due to the inability to link the two fragments of the intermediate mimic. The vinyl sulfone moiety was readily installed in a PMB protected panthenol molecule and in both a Boc and phthaloyl protected β -alanine molecule. However, converting these molecules to the necessary sulfonyl chlorides was never accomplished. This reaction was difficult due to the inability to properly monitor the reaction as TLC was inconclusive at best. Crude ^1H NMRs conclusively showed decomposition products during some reactions, but did not conclusively show conversion to the desired product under any circumstances. The phthaloyl protected β -alanine was the most promising based on the fact that despite not yielding the sulfonyl chloride the phthaloyl protecting group was never deprotected *in situ* under the chlorination conditions and the phthaloyl protected β -alanine was converted successfully to the acid chloride.

The alternative route of installing the vinyl sulfone on the cytidine portion of the molecule was promising because it eliminated the need to generate the sulfonyl chloride and utilized previously made intermediates. Installing the sulfonyl phosphonate required for the HWE reaction on the cytidine portion via the Mitsunobu reaction was unsuccessful using the desired phosphonate nucleophile. Tribenzoyl cytidine had proven to be an efficient nucleophile under all other reaction conditions, but its steric hindrance may have prevented its activation under the Mitsunobu conditions or once activated may have been too sterically hindered to allow nucleophilic attack by the phosphonate.

Deprotonation of mesyl tribenzoyl cytidine and subsequent nucleophilic attack of diethyl chlorophosphate was also surprisingly unsuccessful. Extra equivalents of base were employed due to the acidic amide proton on the benzoyl protecting group of the exocyclic amine, but the reaction was still unsuccessful. The recovered starting material means that the deprotonated mesylate was not nucleophilic enough to attack the chlorophosphate or the mesylate was not properly deprotonated. While unsuccessful to this point, the route of installing the sulfonyl phosphonate on the cytidine portion of the molecule is promising and more straightforward to monitor and thus troubleshoot as compared to the sulfonyl chloride route.



Scheme 4.9: Synthesis of vinyl sulfone PPA analog

An alternative smaller vinyl sulfone based upon the PPA portion of the intermediate mimic was also pursued. The PMB acetal of the ethyl sulfonate **38** can be cleanly removed by passing the molecule through a Dowex 100 H^+ anion exchange column. The primary alcohol is selectively phosphitylated using pyridinium HCl in DMF at -5°C and oxidized in situ using hydrogen peroxide to give the crude protected phosphate **45**. The crude protected phosphate **45** was deprotected in a two step sequence using DBU and TMSCl to deprotect the terminal phosphate, followed by potassium

iodide to remove the ethyl ester. Crude NMR after passing the reaction mixture through a C18 sep prep column revealed pantolactone and other degradation products. The non-phosphorylated analog **48** was obtained by simply treating ethyl ester **38** with tetrabutyl ammonium iodide followed by passing the crude reaction mixture through a Dowex 100 column followed by a C18 sep prep column.

Conclusion

Disulfide **24** was the first PPA mimic synthesized and evaluated as an inhibitor of PPCS. Compound **24** was synthesized as the tetrasodium salt in four steps from commercially available material. Deprotection of the final product proved to be the most difficult step due to decomposition of the final product under the deprotection conditions. The disulfide in compound **24** was reduced prior to pre-incubation with PPCS and CTP. Under these conditions, the sulfur analog of PPA did not display time dependent inactivation of PPCS. The reduced form of disulfide **24** was shown to be a competitive inhibitor with respect to PPA of PPCS with an initial K_i of 12 μM . This molecule was the first PPA competitive inhibitor of PPCS and proved low micromolar inhibition could be achieved with a low molecular weight molecule. In order to take the PPA mimic **24** forward, the terminal phosphate must either be replaced by a neutral isostere or masked as a labile phosphodiester prodrug.

The mechanistic probe designed with a vinyl sulfone installed in an intermediate mimic to trap cysteine in the second half reaction of PPCS was not synthesized due to the difficulty of linking the cytidine portion and the vinyl sulfone installed within the β -alanine portion of the molecule. The first route consisted of installing the vinyl sulfone on the β -alanine portion of panthenol and then generating a sulfonyl chloride to be linked to tribenzoyl cytidine. This strategy was hampered by the inability to monitor the chlorination of the vinyl sulfone. Alternatively, installing the prerequisite sulfonyl phosphonate for the HWE reaction on the cytidine portion of the molecule was much more straightforward to monitor, but was as yet unsuccessful. The PMB protected vinyl sulfone **38** was successfully deprotected to yield both the ethyl ester and the sulfonic acid. Current attempts to chemically phosphorylate the diol on the ethyl ester **45** were successful, but it was not possible to purify the product. The PMB protected vinyl sulfone was successfully deprotected to yield the diol **48**.

Acknowledgements

I would like to thank and acknowledge Nicole Scott for cloning ecPPCS, Kyle Heslip for performing the time dependence and competition assays for the PPA analogs and Dr. Garry Dotson for cloning and expressing PanK as well as performing the PanK assays.

Materials and Methods

General Methods: All chemicals were used as purchased from Acros, Fisher, Fluka, Sigma-Aldrich, or Specialty Chemicals Ltd. and used without further purification unless otherwise noted. ^1H NMR, ^{13}C NMR, and ^{31}P NMR spectra were recorded on a Bruker Avance DRX 500MHz spectrometer or Bruker Avance DPX 300MHz spectrometer. Proton assignments are reported in ppm from an internal standard of TMS (0.0ppm), and phosphorous assignments are reported relative to an external standard of 85% H_3PO_4 (0.0ppm). Proton chemical data are reported as follows: chemical shift, multiplicity (ovlp = overlapping, s = singlet, d = doublet, t = triplet, q = quartet, p = pentet, m = multiplet, br = broad), coupling constant in Hz, and integration. All high resolution mass spectra were acquired from the Mass Spectrometry facility in the Chemistry Department at The University of Michigan using either positive-ion or negative-ion mode ESI-MS. Thin layer chromatography was performed using Analtech GHLF 250 micron silica gel TLC plates. All flash chromatography was performed using grade 60 Å 230-400 mesh silica purchased from Fisher.

3-(tritylthio)propan-1-amine (21) 3-bromopropan-1-amine hydrobromide (2.38 g, 10.85 mmol) was dissolved in anhydrous THF (8 mL). DBU (5.83 mL, 32.56 mmol) was added dropwise and stirred for 15 min. Trityl thiol (3 g, 10.85 mmol) was added and stirred at room temperature for 24 hrs. The solvents were removed *in vacuo* and the resulting syrup was purified over silica (50 mL) eluting with 25% EtOAc in hexanes (150 mL), 50% EtOAc in hexanes (150 mL), 75% EtOAc in hexanes (150 mL), and 100% EtOAc to yield desired product as a yellow oil (2.12g, 58%). ^1H NMR ($\text{DMSO}-d_6$) δ 7.92 (s, 1H), 7.37 – 7.29 (m, 12H), 7.25 (t, $J = 6.7$, 3H), 2.98 (dd, $J = 12.9, 6.4$, 2H), 2.10 (t, $J = 7.4$, 2H), 1.47 – 1.38 (m, 2H). ^{13}C NMR ($\text{DMSO}-d_6$): δ 145.07, 129.57, 128.45, 127.11, 66.41, 41.25, 32.38, 29.45. HR-ESI-MS: calcd for $[\text{M}+\text{H}]^+$, 334.1624; found 334.1632.

(R)-2,4-dihydroxy-3,3-dimethyl-N-(3-(tritylthio)propyl)butanamide (22) 3-(tritylthio)propan-1-amine **1** (1.40 g, 4.19 mmol) was dissolved in ethanol (10 mL). Triethylamine (1.75 mL, 12.57 mmol) was added and stirred for 10 min. Pantolactone (1.60 g, 12.57 mmol) was added and the reaction was heated to 120°C and stirred overnight. Solvents were removed *in vacuo* and the resulting syrup was purified over silica (75 mL) eluting with DCM (300 mL), 1% MeOH in DCM (225 mL), 2% MeOH in DCM (300 mL) to yield desired product as a clear oil (1.59 g, 82%). ¹H NMR (DMSO-*d*₆) δ 7.64 (t, *J* = 5.7 Hz, 1 H), 7.36 – 7.14 (m, 15H), 5.29 (d, *J* = 5.5, 1H), 4.46 (t, *J* = 5.6, 1H), 3.65 (d, *J* = 5.6, 1H), 3.28-3.23 (m, 2H), 3.10 – 3.02 (m, 1H), 3.01-2.92 (m, 1H), 2.07 (t, *J* = 7.44 Hz, 2H), 1.44 (t, *J* = 7.05 Hz, 2H), 0.74 (s, 3H), 0.72 (s, 3H). ¹³C NMR (DMSO-*d*₆) δ 173.30, 144.95, 129.51, 128.47, 127.14, 75.45, 68.48, 66.38, 49.06, 37.99, 29.49, 28.61, 21.44, 20.79. HR-ESI-MS: calcd for [M+Na]⁺, 486.2074; found 486.2080.

(R)-biscyanoethyl (3-hydroxy-2,2-dimethyl-4-oxo-4-((3-(tritylthio)propyl)amino)butyl) phosphate (23) The protected thiol **2** (200 mg, 0.432 mmol) and *O,O*-bis(cyanoethyl)-*N*-diisopropylamine phosphoramidite (178 mg, 0.648 mmol) was dissolved in anhydrous pyridine (2 mL) and cooled to -20°C. Pyridinium HCl (78 mg, 0.648 mmol) was added and stirred at -20°C for 2 hrs. 5 M *t*-butyl hyperperoxide (130 mL, 0.648 mmol) was added dropwise and stirred for 2 hrs. Solvents were removed *in vacuo* and the resulting syrup was purified over silica (25 mL) eluting with 50% EtOAc in hexanes (75 mL), 75% EtOAc in hexanes (150 mL), and 100% EtOAc, and 10% MeOH in EtOAc (75 mL) to yield desired product as a clear oil (154 mg, 55%). ¹H NMR (DMSO-*d*₆) δ 7.72 (s, 1H), 7.40 – 7.27 (m, 12H), 7.25 (d, *J* = 7.5, 3H), 5.64 (d, *J* = 5.8, 1H), 4.01 (m, 4H), 3.84-3.80 (m, 1H), 3.95-3.93 (m, 2H), 3.63 (d, *J* = 5.46 Hz, 1H), 3.47-3.40 (m, 2H), 2.94-2.87 (m, 4H), 2.07 (t, *J* = 7.35 Hz, 2H), 1.45 (t, *J* = 2.7, 2H), 0.83 (s, 3H), 0.80 (s, 3H). ¹³C NMR (DMSO-*d*₆) δ 172.30, 144.94, 129.51, 128.48, 127.14, 118.17, 74.33, 66.41, 62.81, 60.83, 38.87, 38.02, 29.48, 28.60, 21.00, 20.19, 19.57. ³¹P NMR (DMSO-*d*₆): δ -2.11 (s, 1P).

(3R,3'R)-((disulfanediylobis(propane-3,1-diyl))bis(azanediyl))bis(3-hydroxy-2,2-dimethyl-4-oxobutane-4,1-diyl) bis(phosphate) tetrasodium salt (24) The protected phosphate **23** (65 mg, 0.099 mmol) was dissolved in MeOH (5 mL) and the solution was cooled to 0°C. I₂ (25 mg, 0.10 mmol) was added and the reaction was stirred at 0°C for

15 min. The reaction was then diluted to a volume of 15 mL of MeOH and passed through AGMP anion exchange column (12 mL). The solvents were removed in vacuo. The resulting paste was taken up in anhydrous THF (3 mL). DBU (0.120 mL, 0.80 mmol) was added followed by TMSCl (0.065 mL, 0.50 mmol) and allowed to stir for 6 hrs. The solvents were removed in vacuo and the resulting paste was taken up in 1:1 pyridine:H₂O (5 mL) and stirred for 3 hrs. The reaction was partitioned between DCM and H₂O. The H₂O layer was washed with DCM (2x) and the loaded onto a 15 mL AMGP anion exchange resin. The column was eluted with a gradient of 1M NaCl with the UV active fractions at 420 mM NaCl collected and passed through a P2 sizing column eluting with H₂O. The UV active fractions (16-20) were pooled and lyophilized to yield the desired compound as a fluffy white solid (18.5 mg, 27%). ¹H NMR (D₂O-*d*₂) δ 3.94 (s, 1H), 3.70 (dd, J = 2.2, 6.9 Hz, 1H), 3.45 (dd, J = 4.74, 9.09 Hz, 1H), 3.22 (t, J = 6.51 Hz, 2H), 2.63 (t, J = 7.0 Hz, 2H), 1.81 (t, J = 6.50 Hz, 2H), 0.87 (s, 3H), 0.79 (s, 3H). ¹³C NMR (D₂O-*d*₂) δ 174.80, 74.36, 70.97, 38.27, 38.17, 37.41, 35.10, 28.00, 20.75, 18.42. ³¹P NMR (DMSO-*d*₆) δ 0.51 (s, 1P). ESI-MS calcd for [M+3Na]⁻ 665.07; found 665.1.

(2R,2'R)-N,N'-(disulfanediybis(propane-3,1-diyl))bis(2,4-dihydroxy-3,3-

dimethylbutanamide) (25) The protected thiol **22** (50 mg, 0.108 mmol) was dissolved in MeOH (5 mL). The solution was cooled to 0°C and I₂ (27 mg, 0.108 mmol) was added and the reaction was stirred at 0°C for 15 min. The reaction was diluted with DCM and then washed with H₂O. The H₂O layer was then passed through a 12 mL AMGP anion exchange column. The eluent was collected and lyophilized to give the desired compound as a white solid (41 mg, 87%). ¹H NMR (D₂O-*d*₂) δ 3.85 (s, 1H), 3.48 (d, J = 11.25 Hz, 1H), 3.25 (d, ovlp, 1H), 3.23-3.15 (m, ovlp, 2H), 2.62 (t, J = 7.13 Hz, 2H), 1.79 (t, J = 7.13 Hz, 2H), 0.80 (s, 3H), 0.77 (s, 3H). ¹³CNMR (D₂O-*d*₂) δ 174.97, 75.73, 68.38, 38.60, 37.48, 36.27, 28.20, 20.57, 19.16. ESI-MS: calcd for [M+H]⁺, 440.21; found 440.2.

(R)-tert-butyl (3-(2,4-dihydroxy-3,3-dimethylbutanamido)propyl)carbamate (26)

tert-Butyl (3-aminopropyl)carbamate (500 mg, 2.87 mmol) was dissolved in ethanol (10 mL). Triethylamine (1.20 mL, 8.61 mmol) was added and stirred for 10 min. Pantolactone (1.12 g, 8.61 mmol) was added and the reaction was heated to 120°C and stirred overnight. Solvents were removed *in vacuo* and the resulting syrup was purified

over silica (75 mL) eluting with DCM (300 mL), 1% MeOH in DCM (225 mL), 2% MeOH in DCM (300 mL), 4% MeOH in DCM (300 mL) to yield desired product as a clear oil (786 mg, 90%). ^1H NMR (DMSO- d_6) δ 7.75 (t, J = 5.7, 1H), 6.79 (t, J = 5.6, 1H), 5.37 (d, J = 5.5, 1H), 4.48 (t, J = 5.6, 1H), 3.69 (d, J = 5.5, 1H), 3.34 (s, 1H), 3.30 (dd, J = 10.4, 5.8, 1H), 3.17 (dd, J = 10.4, 5.4, 1H), 3.09 (dd, J = 11.7, 5.3, 1H), 3.02 (dt, J = 13.2, 6.6, 1H), 2.91 (dd, J = 12.7, 6.4, 2H), 1.48 (dt, J = 12.7, 6.2, 2H), 1.37 (s, 9H), 0.80 (s, 3H), 0.79 (s, 3H). ^{13}C NMR (DMSO- d_6) δ 173.41, 156.08, 77.91, 75.57, 68.49, 39.47, 37.78, 36.06, 30.17, 28.70, 21.43, 20.88. HR-ESI-MS: calcd for $[\text{M}+\text{Na}]^+$, 327.1891; found 327.1887.

(R)-tert-butyl (3-(4-((bis(2-cyanoethoxy)phosphoryl)oxy)-2-hydroxy-3,3-dimethylbutanamido)propyl)carbamate (27) The protected amine **26** (80 mg, 0.432 mmol) and *O,O*-bis(cyanoethyl)-*N*-diisopropylamine phosphoramidite (178 mg, .648 mmol) was dissolved in anhydrous DMF (2 mL) and cooled to -5°C . Pyridinium HCl (78 mg, .648 mmol) was added and stirred at -5°C for 4 hrs. 5 M *t*-butyl hyperperoxide (0.130 mL, 0.648 mmol) was added dropwise and stirred for 2 hrs. Solvents were removed *in vacuo* and the resulting syrup was purified over silica (15 mL) eluting with EtOAc (50 mL), 5% MeOH in EtOAc (50 mL) to yield desired product as a clear oil (64 mg, 50%). ^1H NMR (DMSO- d_6) δ 7.84 (t, J = 5.64 Hz, 1H), 6.79 (t, J = 5.58 Hz, 1H), 5.71 (d, J = 5.13 Hz, 1H), 4.19-4.15 (m, 4H), 3.98-3.94 (m, 1H), 3.88-3.83 (m, 1H), 3.70 (d, J = 4.80 Hz, 1H), 2.96-2.92 (m, 4H), 1.47 (t, J = 6.48 Hz, 2H), 1.37 (s, 9H), 3.17-3.05 (m, 4H), 0.91 (s, 3H), 0.88 (s, 3H). ^{13}C NMR (DMSO- d_6) δ 172.41, 162.77, 156.09, 118.71, 77.93, 74.18, 73.89, 62.82, 60.83, 37.79, 36.13, 31.22, 28.70, 20.87, 20.19, 19.57. ^{31}P NMR (DMSO- d_6) δ -2.11 (s, 1P).

sodium (R)-4-((3-ammoniopropyl)amino)-3-hydroxy-2,2-dimethyl-4-oxobutyl phosphate chloride (28) The protected phosphorylated amine **27** (45 mg, 0.092 mmol) was dissolved in anhydrous DCM (2 mL). DBU (0.11 mL, 0.736 mmol) was added followed by TMSCl (0.60 mL, 0.50 mmol). The reaction was stirred for 6 hrs. The solvents were removed *in vacuo*. The resulting residue was dissolved in 1:1 pyridine:H₂O (5 mL) and stirred at rt for 4 hrs. The solvents were removed *in vacuo*. The resulting residue was dissolved in 1M HCl (5 mL) and stirred for 12 hrs. The solvents were removed *in vacuo* and the resulting paste was dissolved in water and passed through a

C18 sep prep column. Fractions 3-5, which were positive by I₂ staining, were combined and solvents were removed in vacuo. Crude NMR and mass spectrometry revealed desired product contaminated with pyridine and another undetermined contaminant. Crude ¹H NMR (D₂O- *d*₂) δ 3.81 (s, 1H), 3.69-3.67 (m, 1H), 3.55 -3.53 (m, 1H), 2.83 (t, *J* = 7.26 Hz, 2H), 1.72-1.67 (m, ovlp, 2H), 0.78 (s, 3H), 0.73 (s, 3H). ³¹P NMR (DMSO-*d*₆) δ -0.34 (s, 1P). ESI-MS: calcd for [2M+H]⁺, 567.22; found 567.2.

(R)-N-(3-aminopropyl)-2,4-dihydroxy-3,3-dimethylbutanamide hydrochloride salt (29) The protected amine **26** (15 mg, 0.049 mmol) was dissolved in 1.25 M MeOH:HCl (5 mL) and stirred at rt for 8 h. Solvents were removed in vacuo and desired product was dried on high vac overnight to yield the desired product as white crystalline solid (10 mg, 88%). ¹H NMR (D₂O- *d*₂) δ 3.85 (s, 1H), 3.37 (d, *J* = 11.3, 1H), 3.25 (d, *J* = 11.2, 1H), 3.19 (t, *J* = 6.9, 2H), 2.87 (t, *J* = 7.6, 2H), 1.76 (dd, *J* = 14.6, 7.2, 2H), 0.79 (s, 3H), 0.75 (s, 3H). ¹³C NMR (D₂O- *d*₂): δ 175.58, 75.69, 68.20, 38.55, 36.99, 35.56, 26.66, 20.46, 19.08.

ethyl (diethoxyphosphoryl)methanesulfonate (30) Ethyl methane sulfonate (1 mL, 9.6 mmol) was dissolved in anhydrous THF (5 mL). The solution was cooled to -78°C for 30 min. 1.6 M *n*-BuLi (6.2 mL, 10.12 mmol) was added dropwise and the solution was stirred for 15 min. Diethyl chlorophosphate (0.775 mL, 5.34 mmol) was added dropwise and stirred at -78°C. This reaction was then warmed up to -48°C and stirred for 1.5 hrs. The reaction was quenched with saturated ammonium chloride and allowed to warm to rt. The solvents were removed in vacuo and the resulting syrup was purified over silica (50 mL) eluting with 25% EtOAc in hexanes (150 mL), 50% EtOAc in hexanes (150 mL), and EtOAc (150 mL) to yield the desired phosphonate as a clear oil (776 mg, 55%). ¹H NMR (DMSO-*d*₆): δ 4.43 (d, *J* = 18 Hz, 2H), 4.32 (q, *J* = 6.0 Hz, 2H), 4.09 (q, *J* = 7.02 Hz, 4H), 1.25 (t, *J* = 7.05 Hz, 6Hz). ¹³C NMR (DMSO-*d*₆): δ 68.54, 63.11, 47.03, 45.25, 16.54, 15.13. ³¹P NMR (DMSO-*d*₆): δ 12.43 (s, 1P).

tert-butyl (3-hydroxypropyl)carbamate (31) Boc anhydride (6.15 g, 28.18 mmol) was dissolved in anhydrous THF (50 mL). The solution was cooled to 0°C and 3-aminopropanol (1.95 mL) was added slowly and stirred for 15 min. Triethylamine (8.9 mL, 64 mmol) was added and the reaction was allowed to warm to rt and stirred overnight. Solvents were removed *in vacuo* and the resulting syrup was partitioned

between DCM and H₂O. The DCM layer was dried (Na₂SO₄) and concentrated in vacuo to give the desired product as a clear oil (3.63 g, 80%). ¹H NMR (DMSO-*d*₆): δ 4.39 (t, *J* = 3.09 Hz, 1 H), 3.38 (q, *J* = 3.66 Hz, 2 H), 2.95 (q, *J* = 3.96 Hz, 2 H), 1.51 (p, *J* = 4.05 Hz, 2 H), 1.37 (s, 9 H). ¹³C NMR (DMSO-*d*₆): δ 156.08, 77.83, 58.96, 37.62, 33.20, 28.83. . HR-ESI-MS: calcd for [M+Na]⁺, 198.1101; found 198.1117.

tert-butyl (3-oxopropyl)carbamate (32) Oxalyl chloride (0.91 mL, 10.4 mmol) was dissolved in anhydrous DCM (7 mL) and cooled to -78°C. A solution of DMSO (1.6 mL, 22.8 mmol) in anhydrous DCM (3 mL) was added dropwise and then stirred at -78°C for 15 min. A solution of the protected alcohol **31** (1 g, 5.7 mmol) in anhydrous DCM (3 mL) was added dropwise and stirred at -78°C for 4 hr. Triethylamine (3 mL, 22.8 mmol) was added and the reaction was warmed to rt over 2 hr. The reaction was diluted using DCM and washed with H₂O (3x). Solvents were removed *in vacuo* and the resulting syrup was purified over silica (75 mL) eluting with 25% EtOAc in hexanes (250 mL) and 50% EtOAc in hexanes to yield 891 mg of the desired product as a pale yellow oil (90%). ¹H NMR (DMSO-*d*₆): δ 9.62 (s, 1 H), 3.21 (q, *J* = 3.77 Hz, 2 H), 2.52 (m, ovlp, 2 H), 1.37 (s, 9 H). ¹³C NMR (DMSO-*d*₆): δ 202.88, 155.99, 78.17, 53.00, 34.44, 28.65.

(E)-ethyl 4-((tert-butoxycarbonyl)amino)but-1-ene-1-sulfonate (33) Ethyl (diethoxyphosphoryl)methanesulfonate (499 mg, 1.87 mmol) was dissolved in anhydrous THF (4 mL) and cooled to -78°C. n-BuLi (1.6M, 1.25 mL, 2 mmol) was added dropwise and stirred for 30 min. The aldehyde **32** (270 mg, 1.55 mmol) in anhydrous THF (2 mL) was added dropwise and stirred at -78°C for 2h and then warmed to rt and stirred for 48h. Solvents were removed *in vacuo* and the resulting syrup was purified over silica (50 mL) and eluted with 25% EtOAc in hexanes (150 mL), 50% EtOAc in hexanes (150 mL), 75% EtOAc in hexanes (150 mL) to yield the desired product as a pale yellow oil (325 mg, 75%). ¹H NMR (DMSO-*d*₆): δ 7.12 (t, *J* = 5.52, 1 H), 5.85 (dt, *J* = 5.25, 20.52 Hz, 1 H), 5.48 (dt, *J* = 5.25, 15.36 Hz, 1 H), 4.24 (q, *J* = 7.08 Hz, 2 H), 4.10 (d, *J* = 7.20 Hz, 2 H), 3.57 (t, *J* = 5.10 Hz, 2 H), 1.38 (s, 9 H), 1.27 (t, *J* = 7.02 Hz, 3 H). ¹³C NMR (DMSO-*d*₆): δ 156.10, 137.58, 117.34, 78.19, 67.91, 52.50, 41.50, 28.68, 15.30. HR-ESI-MS: calcd for [M+Na]⁺, 302.1033; found 302.1034.

2-(3-hydroxypropyl)isoindoline-1,3-dione (34) 3-aminopropanol (10g, 131 mmol) and phthalic anhydride (19.46g, 131 mmol) were placed in an open flask with a magnetic stir

bar. The two solids were heated to 150°C for 2 hrs. The reaction was cooled to rt and H₂O was added. The reaction was filtered and dried under vacuum to yield the desired product as a white crystalline solid (23.77g, 90%). ¹H NMR (DMSO-*d*₆): δ 7.79 (s, 4H), 4.53 (t, *J* = 5.04 Hz, 1H), 3.61 (t, *J* = 7.20 Hz, 2H), 3.43 (q, *J* = 6.06 Hz, 2H), 1.73 (p, *J* = 6.21 Hz, 2H). ¹³C NMR (DMSO-*d*₆): δ 168.31, 162.33, 134.67, 132.07, 123.31, 59.02, 35.61, 31.64.

3-(1,3-dioxoisindolin-2-yl)propanal (35) Oxalyl chloride (1.75 mL, 20 mmol) was dissolved in anhydrous DCM (30 mL) and cooled to -78°C. A solution of DMSO (2.84 mL, 40 mmol) in anhydrous DCM (5 mL) was added dropwise and then stirred at -78°C for 15 min. A solution of the protected alcohol **34** (2.05 g, 10 mmol) in anhydrous DCM (10 mL) was added dropwise and stirred at -78°C for 4 hr. Triethylamine (3.17 mL, 22.8 mmol) was added and the reaction was warmed to rt over 2 hr. The reaction was diluted using DCM and washed with H₂O (3x). Solvents were removed *in vacuo* and the resulting syrup was purified over silica (75 mL) eluting with 25% EtOAc in hexanes (250 mL) and 50% EtOAc in hexanes to yield 1.70 g of the desired product as a pale yellow oil (84%). ¹H NMR (DMSO-*d*₆): δ 9.84 (s, 1H), 7.89-7.84 (m, 2H), 7.77-7.72 (m, 2H), 4.06 (t, *J* = 6.90 Hz, 2H), 2.90 (td, *J* = 6.96, 1.26 Hz, 2H). ¹³C NMR (DMSO-*d*₆): δ 199.41, 134.13, 131.97, 42.38, 31.68.

(E)-ethyl 4-(1,3-dioxoisindolin-2-yl)but-1-ene-1-sulfonate (36) Ethyl (diethoxyphosphoryl)methanesulfonate (98 mg, 0.378 mmol) was dissolved in anhydrous THF (2.5 mL) and cooled to -78°C. n-BuLi (1.6M, 0.225 mL, 0.41 mmol) was added dropwise and stirred for 30 min. The aldehyde **35** (64 mg, 0.315 mmol) in anhydrous THF (2 mL) was added dropwise and stirred at -78°C for 2h and then warmed to rt and stirred for 48h. Solvents were removed *in vacuo* and the resulting syrup was purified over silica (25 mL) and eluted with 25% EtOAc in hexanes (75 mL), 50% EtOAc in hexanes (75 mL), 75% EtOAc in hexanes (75 mL) to yield the desired product as a pale yellow oil (75 mg, 76%). ¹H NMR (DMSO-*d*₆): δ 7.89-7.84 (m, 2H), 7.78-7.73 (m, 2H), 6.90 (dt, *J* = 7.08, 15.24 Hz, 1H), 6.33 (dt, *J* = 1.44, 15.24 Hz, 1H), 4.16 (q, *J* = 2.9 Hz), 3.90 (t, *J* = 6.87 Hz, 2H), 2.71 (qd, *J* = 1.38, 6.93 Hz, 2H), 1.33 (t, *J* = 6.12 Hz, 3H). ¹³C NMR (DMSO-*d*₆): δ 168.03, 144.32, 134.29, 131.81, 126.97, 123.48, 66.89, 35.85, 30.61, 14.84.

(4R)-2-(4-methoxybenzyl)-5,5-dimethyl-N-(3-oxopropyl)-1,3-dioxane-4-carboxamide (37) Oxalyl chloride (1.08 mL, 12.38 mmol) was dissolved in anhydrous DCM (10 mL) and cooled to -78°C. A solution of DMSO (1.76 mL, 24.75 mmol) in anhydrous DCM (5 mL) was added dropwise and then stirred at -78°C for 15 min. A solution of the protected alcohol **1** (2.0 g, 6.19 mmol) in anhydrous DCM (10 mL) was added dropwise and stirred at -78°C for 4 hr. Triethylamine (3.5 mL, 24.75 mmol) was added and the reaction was warmed to rt over 2 hr. The reaction was diluted using DCM and washed with H₂O (3x). Solvents were removed *in vacuo* and the resulting syrup was purified over silica (75 mL) eluting with 25% EtOAc in hexanes (250 mL), 50% EtOAc in hexanes (250 mL), and 75% EtOAc (250 mL) to yield 1.63 g of the desired product as a pale yellow oil (82%). ¹H NMR (DMSO-*d*₆): δ 9.62 (s, 1H), 7.57 (t, J = 5.25 Hz, 1H), 7.44 (d, J = 8.61 Hz, 2H), 6.93 (d, J = 8.64 Hz, 2H), 5.51 (s, 1H), 4.08 (s, 1H), 3.76 (s, 3H), 3.67-3.62 (m, 2H), 3.58-3.44 (m, 1H), 3.38-3.29 (m, 1H), 2.57 (t, J = 6.45 Hz, 2H), 0.97 (s, 3H), 0.93 (s, 3H). ¹³C NMR (DMSO-*d*₆): δ 203.00, 168.89, 128.24, 113.78, 83.69, 77.83, 60.22, 55.59, 43.95, 32.88, 21.96, 19.47, 14.55.

(E)-ethyl 4-((4R)-2-(4-methoxybenzyl)-5,5-dimethyl-1,3-dioxane-4-carboxamido)but-1-ene-1-sulfonate (38) Ethyl (diethoxyphosphoryl)methanesulfonate (250 mg, 0.964 mmol) was dissolved in anhydrous THF (5 mL) and cooled to -78°C. *n*-BuLi (1.6M, 0.625 mL, 1 mmol) was added dropwise and stirred for 30 min. The aldehyde **37** (311 mg, 0.964 mmol) in anhydrous THF (3 mL) was added dropwise and stirred at -78°C for 2h and then warmed to rt and stirred for 48h. Solvents were removed *in vacuo* and the resulting syrup was purified over silica (25 mL) and eluted with 25% EtOAc in hexanes (75 mL), 50% EtOAc in hexanes (75 mL), 75% EtOAc in hexanes (75 mL) to yield the desired product as a pale yellow oil (292 mg, 71%). ¹H NMR (DMSO-*d*₆): δ 7.44 (d, J = 8.52 Hz, 2H), 6.93 (d, J = 8.50 Hz, 2H), 5.86 (dt, J = 6.10, 15.20 Hz, 1H), 5.53 (s, 1H), 5.50-5.45 (m, ovlo, 1H), 4.23 (m, 2H), 4.13-4.07 (m, 2H), 3.76 (s, 3H), 3.66-3.58 (m, 2H), 1.24 (td, J = 2.2, 7.0 Hz, 3H), 1.03 (s, 3H), 0.95 (s, 3H).

O-Mesyl-tribenzoyl cytidine (39) Tribenzoyl cytidine (1.29 g, 2.25 mmol) was dissolved in anhydrous pyridine (8 mL) and cooled to 0°C. Mesyl chloride (0.261 mL, 3.38 mmol) was added dropwise and stirred at 0°C for 2 h. The reaction was allowed to warm to rt and then stirred overnight. The solvents were removed *in vacuo* and the

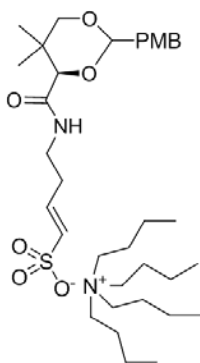
resulting syrup was purified over silica (100 mL) eluting with 25% EtOAc in hexanes (300 mL), 50% EtOAc in hexanes (300 mL), 75% EtOAc in hexanes (300 mL), and 100% EtOAc (300 mL) to yield 1.23 g of the desired compound as a white solid (84%). ^1H NMR (DMSO- d_6): δ 11.43 (s, 1 H), 8.31 (d, $J = 4.50$ Hz, 1 H), 8.03 (d, $J = 4.86$ Hz, 2 H), 7.94 (d, $J = 4.80$ Hz, 2 H), 7.88 (d, $J = 4.77$ Hz, 2H), 7.69-7.65 (m, 3 H), 7.55-7.44 (m, 6 H), 6.26 (d, $J = 2.13$ Hz, 1 H), 5.97 (t, $J = 2.99$ Hz, 1 H), 5.83 (t, $J = 3.65$ Hz, 1 H), 4.77 (s, 1 H), 4.65 (t, ovlp, 1 H), 4.63 (m, 1 H), 3.28 (s, 3 H). ^{13}C NMR (DMSO- d_6): δ 165.09, 165.00, 164.42, 154.80, 147.66, 134.44, 134.44, 134.38, 133.45, 133.34, 129.84, 129.22, 128.99, 128.94, 97.33, 91.83, 79.81, 73.96, 70.90, 69.30, 37.35. HR-ESI-MS: calcd for $[\text{M}+\text{Na}]^+$, 656.1309; found 656.1332.

5'-Azido-5'-deoxy-tribenzoyl cytidine (40) The mesylate **39** (850 mg, 1.3 mmol) was dissolved in anhydrous DMF (7 mL). Sodium azide (425 mg, 6.5 mmol) was added and the reaction was heated to 60°C and stirred for 16h. Solvents were removed *in vacuo* and the resulting paste was purified over silica (50 mL) eluting with 25% EtOAc in hexanes (150 mL), 50% EtOAc in hexanes (150 mL) to yield the desired product as a white solid (702 mg, 93%). ^1H NMR (DMSO- d_6): δ 11.42 (s, 1 H), 8.34 (d, $J = 6.63$ Hz, 1 H), 8.02 (d, $J = 7.77$ Hz, 2 H), 7.92 (d, $J = 8.07$ Hz, 2 H), 7.87 (d, $J = 7.92$ Hz, 2 H), 7.68-7.63 (m, 3 H), 7.55-7.44 (m, 6 H), 6.21 (s, 1 H), 5.99 (s, 1 H), 5.76 (t, $J = 7.32$ Hz, 1 H), 4.68-4.63 (m, 1 H), 3.90-3.84 (m, 2 H). ^{13}C NMR (DMSO- d_6): δ 165.13, 165.05, 162.76, 147.85, 134.41, 134.33, 133.56, 133.30, 129.82, 129.20, 129.06, 129.00, 128.92, 97.37, 91.89, 80.80, 73.95, 71.53, 51.38. ^1H NMR (DMSO- d_6): δ 1HR-ESI-MS: calcd for $[\text{M}+\text{H}]^+$, 581.1785; found 581.1785.

5'-Amino-5'-deoxy-tribenzoyl cytidine (41) The azide **40** (100 mg, 0.172 mmol) was dissolved in anhydrous THF (2 mL) and degassed with Ar. Pd/C (10%, 53 mg, 0.05 mmol) was added followed by 1,4 cyclohexadiene (0.2 mL, 1.72 mmol). The reaction was heated to 60°C and stirred overnight. The reaction was filtered through a celite plug. The solvents were removed *in vacuo*. The resulting residue was purified over silica (25 mL) eluting with 50% EtOAc in hexanes (50 mL), 75% EtOAc in hexanes (50 mL), EtOAc (50 mL), 10% MeOH in EtOAc (50 mL), and 20% MeOH in EtOAc (100 mL) to yield the desired product as a white solid (81 mg, 85%). ^1H NMR (DMSO- d_6): δ 11.52 (1s, 1H), 8.52 (d, $J = 7.00$ Hz, 1H), 8.02 (d, $J = 7.25$ Hz, 2H), 7.93 (d, $J = 8.05$ Hz, 2H),

7.83 (d, $J = 7.15$, 2H), 7.68-7.58 (m, 3H), 7.53-7.39 (m, 7H), 5.98 (m, br, 2H), 5.71 (m, br, 1H), 4.53 (q, $J = 3.65$ Hz, 1H), 3.64-3.59 (m, 1H), 3.51-3.45 (m, 1H). ^{13}C NMR (DMSO- d_6): δ 167.243, 164.65, 164.40, 163.54, 154.46, 145.65, 133.97, 133.68, 133.00, 132.71, 129.27, 129.26, 128.76, 128.63, 128.45, 128.32, 96.82, 88.38, 83.15, 74.39, 71.44, 50.11. HR-ESI-MS: calcd for $[\text{M}+\text{H}]^+$, 555.1874; found 555.1891.

Representative TBAI deprotection



tetraethylammonium (E)-4-((4R)-2-(4-methoxybenzyl)-5,5-

dimethyl-1,3-dioxane-4-carboxamido)but-1-ene-1-sulfonate The PMB protected vinyl sulfonate **38** (200 mg, 0.45 mmol) was dissolved in anhydrous acetone (5 mL). TBAI (251 mg, 0.679 mmol) was added and the reaction was heated to 55°C for 12 hrs. The solvents were removed in vacuo and the resulting residue was purified over silica (30 mL) eluting with 50% EtOAc in hexanes (100 mL), 75% EtOAc in hexanes (100 mL), EtOAc (100 mL), 10% MeOH in EtOAc (100 mL), and 20% MeOH in EtOAc (100 mL) to yield the desired product as a extremely hygroscopic white solid (250 mg, 85%). ^1H NMR (CDCl_3-d_1): δ 7.37-7.34 (m, 2H), 6.85-6.82 (m, 2H), 5.80-5.73 (m, 1H), 5.52-5.45 (m, 1H), 5.35 (s, 1H), 3.70 (t, $J = 2.67$ Hz, 2H), 3.56 (t, $J = 6.60$ Hz, 2H), 3.43 (d, $J = 3.90$ Hz, 1H), 3.18 (t, $J = 4.86$ Hz, 9H), 1.57-1.51 (m, 8H), 1.38-1.32 (m, 8H), 1.01 (s, 3H), 0.98 (s, 3H), 0.91 (t, $J = 4.41$ Hz, 12H). ^{13}C NMR (CDCl_3-d_1): δ 171.07, 160.05, 130.17, 127.59, 113.64, 101.30, 83.81, 78.40, 60.30, 58.55, 55.25, 33.04, 23.88, 21.83, 20.99, 19.64, 19.14, 14.13, 13.65.

tert-butyl methylsulfonylcarbamate (42) Methanesulfonamide (3.80 g, 40 mmol) was suspended in anhydrous DCM (50 mL). Triethylamine (6.06 mL, 44 mmol) and DMAP (0.49 g, 4.0 mmol) were added and stirred for 15 min. Di-(*t*-butyl)dicarbonate (10 g, 46 mmol) in anhydrous DCM (50 mL) was added dropwise over 10 min. The reaction was stirred for 6 hrs. The solvents were removed in vacuo and the resulting syrup was

dissolved in EtOAc. The EtOAc was washed with 1 M HCl, water, and brine. The organic layer was then dried (Na_2SO_4) and concentrated in vacuo leave a white solid. ^1H NMR ($\text{DMSO}-d_6$): δ 11.23 (s, 1H), 3.20 (s, 3H), 1.43 (s, 9H). ^{13}C NMR ($\text{DMSO}-d_6$): δ 151.16, 82.53, 41.20, 28.12.

***tert*-butyl ((diethoxyphosphoryl)methyl)sulfonylcarbamate (43)** Diisopropylamine (4.48 mL, 31.76 mmol) was dissolved in anhydrous THF (30 mL) and cooled to -78°C for 15 min. *n*-BuLi (12.30 mL, 30.73 mmol) was added dropwise and stirred at -78°C for 30 min. *tert*-butyl methylsulfonylcarbamate **42** (2.00 g, 10.24 mmol) in anhydrous THF (20 mL) was added dropwise over 10 min and the reaction was stirred at 78°C for 30 min. The reaction was then warmed to -48°C and stirred for 1 hr. The reaction was quenched with saturated ammonium chloride and warmed to rt. The solvents were removed in vacuo. The resulting syrup was purified over silica (50 mL) eluting with 50% EtOAc in hexanes (150 mL), 75% EtOAc in hexanes (150 mL), EtOAc (150 mL), 10% MeOH in EtOAc (150 mL), and 20% MeOH in EtOAc (150 mL) to yield the desired product as a white solid (2.04 g, 60%). ^1H NMR ($\text{DMSO}-d_6$): δ 11.57 (s, 1H), 4.23 (d, $J = 16.74$ Hz, 2H), 4.08 (p, $J = 7.11$ Hz, 4H), 1.43 (s, 9H), 1.25 (t, $J = 6.99$ Hz, 6H). ^{13}C NMR ($\text{DMSO}-d_6$): δ 151.50, 82.51, 63.05, 62.97, 28.18, 16.59. ^{31}P NMR ($\text{DMSO}-d_6$): δ 12.43 (s, 1P).

***tert*-butyl ((E)-4-((4R)-2-(4-methoxybenzyl)-5,5-dimethyl-1,3-dioxane-4-carboxamido)but-1-en-1-yl)sulfonylcarbamate (44)** *tert*-butyl ((diethoxyphosphoryl)methyl)sulfonylcarbamate **43** (331 mg, 1.0 mmol) was dissolved in anhydrous THF (3 mL) and cooled to -78°C . *n*-BuLi (1.6M, 0.625 mL, 1 mmol) was added dropwise and stirred for 30 min. The aldehyde **37** (323 mg, 1.0 mmol) in anhydrous THF (2 mL) was added dropwise and stirred at -78°C for 2h and then warmed to rt and stirred for 48h. Solvents were removed *in vacuo* and the resulting syrup was purified over silica (50 mL) and eluted with 25% EtOAc in hexanes (150 mL), 50% EtOAc in hexanes (150 mL), 75% EtOAc in hexanes (150 mL) to yield the desired product as a wax (313 mg, 71%). ^1H NMR (CDCl_3-d_1): δ 7.42 (dd, $J = 5.51, 8.64$ Hz, 2H), 6.92 (d, $J = 6.78$ Hz, 2H), 6.70 (dt, $J = 5.61, 18.45$ Hz, 1H), 6.52-6.47 (m, 1H), 5.45 (d, $J = 4.38$ Hz, 1H), 3.81 (s, 3H), 3.71 (d, $J = 4.80$ Hz, 2H), 3.48-3.39 (m, 2H), 3.25 (s, 1H), 3.02-2.95 (m, 1H), 2.85-2.77 (m, 1H), 1.48-1.45 (m, 9H), 1.10 (s, 3H), 1.09 (s,

3H). ^{13}C NMR (DMSO- d_6): δ 171.62, 160.02, 130.92, 128.26, 113.78, 100.97, 83.76, 82.27, 78.01, 55.64, 33.17, 28.12, 22.07, 19.58.

(R,E)-ethyl 4-(2,4-dihydroxy-3,3-dimethylbutanamido)but-1-ene-1-sulfonate (45)

The PMB acetal **38** (50 mg, 0.097 mmol) was dissolved in 1:1 MeOH:H₂O (10 mL) and passed through a Dowex 100 (H⁺ form) anion exchange column (12 mL). The first 12 mL of eluent was collected and combined. The volume was reduced in vacuo to ~2 mL and passed through a C18 Sep prep column. Fractions 3-5, which tested positive by I₂ staining, were combined and lyophilized to yield the desired product as a hygroscopic white solid (27 mg, 90%). ^1H NMR (D₂O- d_2) δ 5.87 (dt, J = 5.88, 15.30 Hz, 1H), 5.57-5.50 (m, 1H), 4.28-4.21 (m, 2H), 3.95 (d, J = 7.14 Hz, 2H), 3.89 (s, 1H), 3.78-3.72 (m, 2H), 3.39 (d, J = 11.25 Hz, 1H), 3.27 (d, J = 11.13 Hz, 1H), 1.24 (t, J = 6.87 Hz, 3H), 0.81 (s, 3H), 0.78 (s, 3H). ^{13}C NMR (D₂O- d_2) δ 175.09, 136.26, 117.00, 75.70, 69.38, 68.34, 52.39, 39.88, 38.61, 20.49, 19.08, 14.32.

(R,E)-ethyl 4-(4-((bis(2-cyanoethoxy)phosphoryl)oxy)-2-hydroxy-3,3-dimethylbutanamido)but-1-ene-1-sulfonate (46)

The diol **45** (75 mg, 0.242 mmol) and *O,O*-bis(cyanoethyl)-*N*-diisopropylamine phosphoramidite (100 mg, 0.363 mmol) was dissolved in anhydrous DMF (2 mL) and cooled to -5°C. Pyridinium HCl (43 mg, 0.363 mmol) was added and stirred at -5°C for 4 hrs. 5 M *t*-butyl hyperperoxide (0.075 mL, 0.363 mmol) was added dropwise and stirred for 2 hrs. Solvents were removed *in vacuo* and the resulting syrup (62 mg, 52%) was taken forward.

(R,E)-4-(2,4-dihydroxy-3,3-dimethylbutanamido)but-1-ene-1-sulfonic acid (48)

The PMB acetal **38** (50 mg, 0.117 mmol) was dissolved in anhydrous acetone (5 mL). TBAI (65 mg, 0.176 mmol) was added and the reaction was heated to 55°C for 12 hrs. The solvents were removed in vacuo and the resulting residue was purified over silica (30 mL) eluting with 50% EtOAc in hexanes (60 mL), 75% EtOAc in hexanes (60 mL), EtOAc (60 mL), 10% MeOH in EtOAc (100 mL), and 20% MeOH in EtOAc (100 mL) to yield the desired product as a extremely hygroscopic white solid. The white solid was then dissolved in 1:1 MeOH:H₂O (10 mL) and passed through a Dowex 100 (H⁺ form) anion exchange column (12 mL). The first 12 mL of eluent was collected and combined. The volume was reduced in vacuo to ~2 mL and passed through a C18 Sep prep column. Fractions 3-5, which tested positive by I₂ staining, were combined and lyophilized to

yield the desired product as a wax (26 mg, 81%). ^1H NMR (D_2O - d_2) δ 6.41-6.24 (m, ovlp, 2H), 3.84 (s, 1H), 3.35 (d, J = 6.81 Hz, 1H), 3.29-3.21 (m, ovlp, 3H), 2.30 (q, J = 6.51 Hz, 2H), 0.88 (s, 3H), 0.80(s, 3H).

Growing and Culturing of Cells

Escherichia coli BL21-AI/pUMDOT2 was used for the expression of *E. coli* PanK. The construct contains the *coaA* gene of *E. coli* under the control of viral T7 RNA promoter and overall expression controlled by L-arabinose induction. Cell cultures were grown in 250 ml LB broth containing ampicillin (50 $\mu\text{g}/\text{ml}$) at 37° C until it reached an optical density of 0.6 – 0.8 at 600 nm. One mL of 20% (w/v) L-arabinose was added to the culture to induce protein expression. The induced culture was allowed to grow at 37° C for 3 hours post induction. The cells were harvested by centrifuged for 10 minutes at 10,000 x g. The cells were then washed and suspended in 10 ml of 20 mM HEPES pH 8.0 buffer, and subsequently lysed by French Press. The resulting suspension was centrifuged at 4° C and 20,000 rpm for 30 minutes. The lysate containing soluble protein was collected and purified through a 2 ml Ni^{+2} -NTA column. All fractions containing the protein of interest were pooled together and desalted using Bio-Gel P-2 resin. The purified proteins were stored in aliquots at -80° C.

PanK Assays

Continuous spectrophotometric measurements of the conversion of NADH to NAD^+ were performed in a pyruvate kinase/lactate dehydrogenase coupled assay. The oxidation of NADH was monitored by the decreasing absorbance at 340 nm at 10 second intervals over 5 minutes. Assays were performed in a 96 well plate in a final volume of 100 μl (80 μl from assay mix + 10 μl of enzyme + 10 μl of PA or PA analogs). PanK was at a concentration of 50 mg/mL and PA analog concentrations varied from 3 μM to 3 mM. The reactions were started by adding the enzyme and substrate to the assay mix. The assay mix contained a final concentration of 50 mM HEPES pH 8.0, 2 mM MgCl_2 , 1 mM ATP, 1 mM PEP, 0.4 mM NADH, 100 units/ml pyruvate kinase, 80 units/ml of lactic dehydrogenase, and H_2O to a final volume of 100 μL .

Cloning, Overexpression, and Purification of *E. coli* PPCS

The *coaB* coding region of the *dfp* gene (encoding ser181-arg406 of the *E. coli* CoaBC protein)^{21, 22} was PCR amplified using *E. coli* MG1655 genomic DNA as a template, and

the primers, coabec1(forward primer), 5' – CGCGCATA TGTCGCCCCGTCAACGACCTGAAACATCTG-3' and dfp3 (reverse primer), 5'- GCGCCTCGAGACGTCGATTTTTTTCATCATAACGGG-3'. The forward primer introduces an *NdeI* site (shown underlined) to provide a start codon for the *coaB* coding region, and the reverse primer creates a *XhoI* site (shown underlined) downstream of the stop codon of the open reading frame. The PCR products were digested with *NdeI* and *XhoI*, and ligated into pET23a(+) (Novagen) cut with *NdeI* and *XhoI*. The resulting plasmid was designated pUMDOT3 and the insert was confirmed by DNA sequencing.

E. coli BL21 AI (Invitrogen) harboring the plasmid pUMDOT3 were grown in 500 mL LB-ampicillin media (5 g of NaCl, 5 g of yeast extract, 10 g of tryptone, and 100 mg of ampicillin per L) at 37°C and 250 rpm to a OD600 of 0.6. The cells were then cooled by shaking at 16°C for 10-15 min, induced with 0.07% L-arabinose, and continued to grow at 16°C and 250 rpm for 12-16 hours. The cells were harvested at 6000 x g for 10 minutes at 4°C, washed, and then suspended in 12 ml of 20 mM HEPES pH 8.0. Cells were lysed by French Press and crude cytosol obtained by centrifugation at 20,000 x g for 25 minutes at 4°C.

ecPPCS was purified using a tandem anion exchange column (Source 15Q (GE Healthcare); 20 mL) and cation exchange column (Source 15S (GE Healthcare); 8 mL). The 12 mL of crude cytosol was loaded onto the tandem chromatography columns which had been pre-equilibrated with 20 mM HEPES pH 8.0. The columns were then washed with another 40 mL of equilibration buffer and the anion exchange column was removed. Under these conditions the ecPPCS does not bind to the anion exchange resin, but does bind to the cation exchange resin. The cation exchange column was eluted with a linear gradient of 0-0.4 M NaCl in 20 mM HEPES pH 8.0, with a total gradient volume of 100 mL. ecPPCS eludes as a single peak at 75 mM NaCl and was greater than 98 % pure as determined by SDS-PAGE.

Time Dependence Assay

The disulfide **24** (1mM stock) was preincubated with equimolar DTT for 1h at 37°C. Assays were performed in a 96 well plate in a final volume of 100 µl. ecPPCS (12.9 µL of 310nM stock), the reduced thiol mimic (4.5 µL of 1 mM stock), of MgCTP (2.7 µL of 20mM stock), and water (9.9 µL) were preincubated at time intervals ranging from 15

min-4hrs. A solution containing Pyrophosphate reagent (40 μL), PDK (5 μL), DTT (14 μL of 100mM stock), cysteine (1.4 μL of 100 mM stock), PPA (2 μL , of 30 mM stock), and water (7.6 μL) was added to the pre-incubated PPCS/inhibitor solution and then continuous spectrophotometric measurements of the conversion of NADH to NAD⁺ were performed via the Pyrophosphate reagent coupled assay. The oxidation of NADH was monitored by the decreasing absorbance at 340 nm at 10 second intervals over 10 minutes.

References

1. Yao, J.; Dotson, G. D., Kinetic characterization of human phosphopantothienoylcysteine synthetase. *Biochimica et Biophysica Acta (BBA) - Proteins & Proteomics* **2009**, 1794, (12), 1743-1750.
2. Yao, J.; Patrone, J. D.; Dotson, G. D., Characterization and Kinetics of Phosphopantothienoylcysteine Synthetase from *Enterococcus faecalis*. *Biochemistry* **2009**, 48, (12), 2799-2806.
3. Spry, C.; Kirk, K.; Saliba, K. J., Coenzyme A biosynthesis: an antimicrobial drug target. *Fems Microbiology Reviews* **2008**, 32, (1), 56-106.
4. Lu, X. Q.; Olsen, S. K.; Capili, A. D.; Cisar, J. S.; Lima, C. D.; Tan, D. S., Designed Semisynthetic Protein Inhibitors of Ub/Ubl E1 Activating Enzymes. *Journal of the American Chemical Society* 132, (6), 1748-1749.
5. Qiao, C. H.; Wilson, D. J.; Bennett, E. M.; Aldrich, C. C., A mechanism-based aryl carrier protein/thiolation domain affinity probe. *Journal of the American Chemical Society* **2007**, 129, (20), 6350-6351.
6. Reddick, J. J.; Cheng, J.; Roush, W. R., Relative Rates of Michael Reactions of (Phenethyl)thiol with Vinyl Sulfones, Vinyl Sulfonate Esters, and Vinyl Sulfonamides Relevant to Vinyl Sulfonyl Cysteine Protease Inhibitors. *Organic Letters* **2003**, 5, (11), 1967-1970.
7. Worthington, A. S.; Rivera, H.; W., J.; AlexanderTorpey, M. D.; Burkart, M. D., Mechanism-Based Protein Cross-Linking Probes To Investigate Carrier Protein-Mediated Biosynthesis. *ACS Chemical Biology* **2006**, 1, (11), 687-691.
8. Mercer, A. C.; Meier, J. L.; Hur, G. H.; Smith, A. R.; Burkart, M. D., Antibiotic evaluation and in vivo analysis of alkynyl Coenzyme A antimetabolites in *Escherichia coli*. *Bioorganic & Medicinal Chemistry Letters* **2008**, 18, (22), 5991-5994.
9. Li, K. W.; Wu, J.; Xing, W.; Simon, J. A., Total Synthesis of the Antitumor Depsipeptide FR-901,228. *Journal of the American Chemical Society* **1996**, 118, (30), 7237-7238.
10. Evans, D. A.; Gage, J. R.; Leighton, J. L., Asymmetric synthesis of calyculin A. 3. Assemblage of the calyculin skeleton and the introduction of a new phosphate monoester synthesis. *The Journal of Organic Chemistry* **1992**, 57, (7), 1964-1966.
11. Majik, M. S.; Parameswaran, P. S.; Tilve, S. G., Total Synthesis of (-)and (+) Tedanalactam. *The Journal of Organic Chemistry* **2009**, 74, (16), 6378-6381.
12. Pierwocha, A. W.; Walczak, K., The use of tri-O-acetyl-d-glucal and -d-galactal in the synthesis of [omega]-aminoalkyl 2-deoxy- and 2,3-dideoxy-d-hexopyranosides. *Carbohydrate Research* **2008**, 343, (15), 2680-2686.
13. Zhang, J.; Xiong, C.; Ying, J.; Wang, W.; Hruby, V. J., Stereoselective Synthesis of Novel Dipeptide β -Turn Mimetics Targeting Melanocortin Peptide Receptors. *Organic Letters* **2003**, 5, (17), 3115-3118.
14. Nugent, B. M.; Williams, A. L.; Prabhakaran, E. N.; Johnston, J. N., Free radical-mediated vinyl amination: a mild, general pyrrolidinyl enamine synthesis. *Tetrahedron* **2003**, 59, (45), 8877-8888.
15. Reggelin, M.; Junker, B.; Heinrich, T.; Slavik, S.; Buhle, P., Asymmetric Synthesis of Highly Substituted Azapolycyclic Compounds via 2-Alkenyl Sulfoximines

Potential Scaffolds for Peptide Mimetics. *Journal of the American Chemical Society* **2006**, 128, (12), 4023-4034.

16. Winans, K. A.; Bertozzi, C. R., An Inhibitor of the Human UDP-GlcNAc 4-Epimerase Identified from a Uridine-Based Library: A Strategy to Inhibit O-Linked Glycosylation. *Chemistry & Biology* **2002**, 9, (1), 113-129.

17. Gennari, C.; Salom, B.; Potenza, D.; Williams, A., Synthesis of Sulfonamido-Pseudopeptides - New Chiral Unnatural Oligomers. *Angewandte Chemie-International Edition in English* **1994**, 33, (20), 2067-2069.

18. Roush, W. R.; Gwaltney, S. L.; Cheng, J.; Scheidt, K. A.; McKerrow, J. H.; Hansell, E., Vinyl Sulfonate Esters and Vinyl Sulfonamides: Potent, Irreversible Inhibitors of Cysteine Proteases. *Journal of the American Chemical Society* **1998**, 120, (42), 10994-10995.

19. Campbell, J. A.; Hart, D. J., tert-Butyl [[2-(trimethylsilyl)ethyl]sulfonyl]carbamate: a new reagent for use in Mitsunobu reactions. *The Journal of Organic Chemistry* **1993**, 58, (10), 2900-2903.

20. Reuter, D. C.; McIntosh, J. E.; Guinn, A. C.; Madera, A. M., Synthesis of Vinyl Sulfonamides Using the Horner Reaction. *Synthesis* **2003**, 2003, (15), 2321-2324.

21. Kupke, T., Molecular Characterization of the 4'-Phosphopantothienoylcysteine Synthetase Domain of Bacterial Dfp Flavoproteins. *J. Biol. Chem.* **2002**, 277, (39), 36137-36145.

22. Stanitzek, S.; Augustin, M. A.; Huber, R.; Kupke, T.; Steinbacher, S., Structural Basis of CTP-Dependent Peptide Bond Formation in Coenzyme A Biosynthesis Catalyzed by Escherichia coli PPC Synthetase. *Structure* **2004**, 12, (11), 1977-1988.

Chapter 5

Difluorophosphonate Mechanistic Probe

Introduction

Phosphonates have become increasingly useful as chemically stable isosteres for phosphates in medicinal chemistry. It has been shown that due to the increased electronegativity of fluorine, α,α difluorophosphonates more closely mimic the electronics of the oxygen atom in the naturally occurring phosphate as compared to the methylene of a non-fluorinated phosphonate.¹⁻³ Difluorophosphonates also have lower pKa values for the phosphonic acid protons, which are more in line with a phosphate.¹⁻³ Recently, a difluorophosphonate analog of diaminopelic acid (DAP) was designed to react with an active site cysteine of aspartate semi-aldehyde dehydrogenase (ASA-DH) (**Figure 5.1**).^{4,5} The difluorophosphonate was shown to be a time dependent slow binding inhibitor most likely due to covalent linkage of cysteine to the molecule.^{4,5}

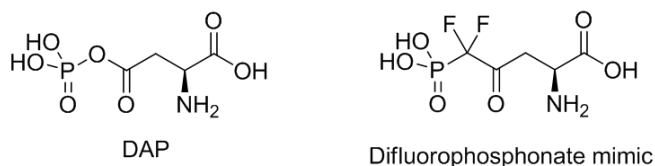


Figure 5.1: Difluorophosphonate inhibitor of ASA-DH

It can be reasoned from these results that a difluorophosphonate analog designed to mimic the activated intermediate of PPCS should behave in a similar fashion. Pre-incubating PPCS, cysteine, and the difluorophosphonate intermediate mimic should allow for binding of the intermediate mimic followed by cysteine entering the active site of PPCS, attacking the carbonyl of the mimic, and forming a tetrahedral ternary complex (**Figure A.2**). Forming a ternary complex with cysteine would allow the proposed compound to be a potent inhibitor because it would be able to take advantage of the binding contacts in the binding pockets of all three enzyme substrates. Beyond being a

potent inhibitor, the proposed molecule having trapped cysteine during the second half reaction would allow us to study the yet unexplored cysteine binding pocket by co-crystallizing PPCS, the difluorophosphonate mimic, and cysteine.

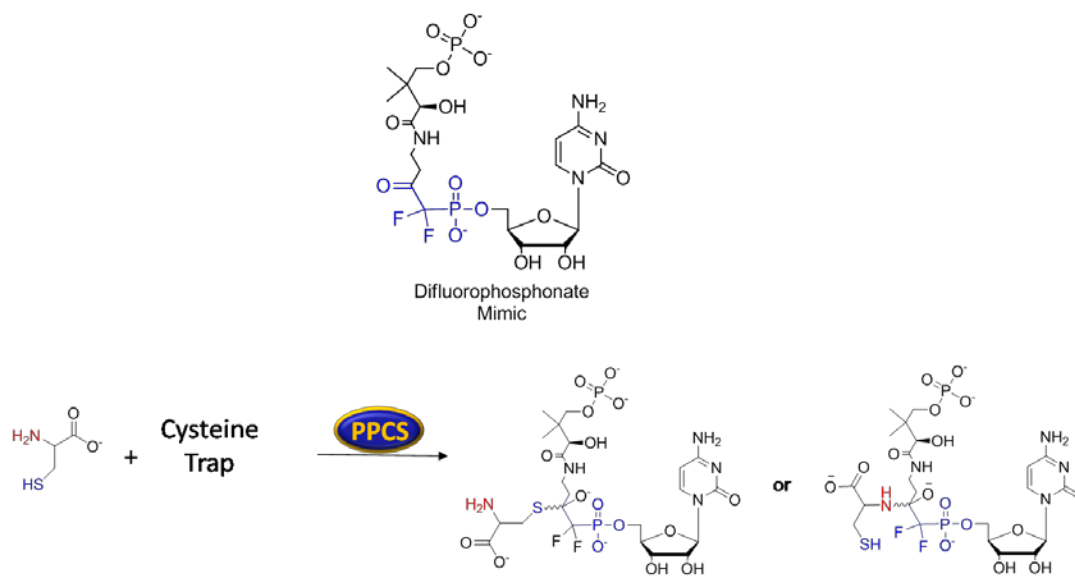


Figure 5.2: Proposed difluorophosphonate electrophilic trap and its mechanism of action

Aside from studying the binding pocket, the proposed difluorophosphonate inhibitor would allow for the elucidation of the mechanism of the second half reaction. To date, the mechanism of the second half reaction has not been proven. When entering the active site, cysteine can either attack via the more nucleophilic thiol or less nucleophilic amine. The proposed difluorophosphonate trap can be attacked by either of the two nucleophilic functional groups of cysteine (**Figure 5.2**). Upon attack and trapping of cysteine, the ternary complex can be studied by crystallography within the active site or isolated and characterized by 2D NMR studies.

Synthesis of difluorophosphonate probe

A retrosynthetic analysis shows that the 4' terminal phosphate on the pantothenic acid portion of the proposed difluorophosphonate is the first disconnection and can be installed last via phosphorylation and in situ oxidation (**Figure 5.3**). The disconnection that dissects the molecule in two halves consists of a DCC coupling between an appropriately protected cytosine fragment and a pantothenate fragment with a difluorophosphonate moiety. The pantothenate portion of the molecule can be further

fragmented to a pantothenate portion and the commercially available diethyl (difluoromethyl)phosphonate.

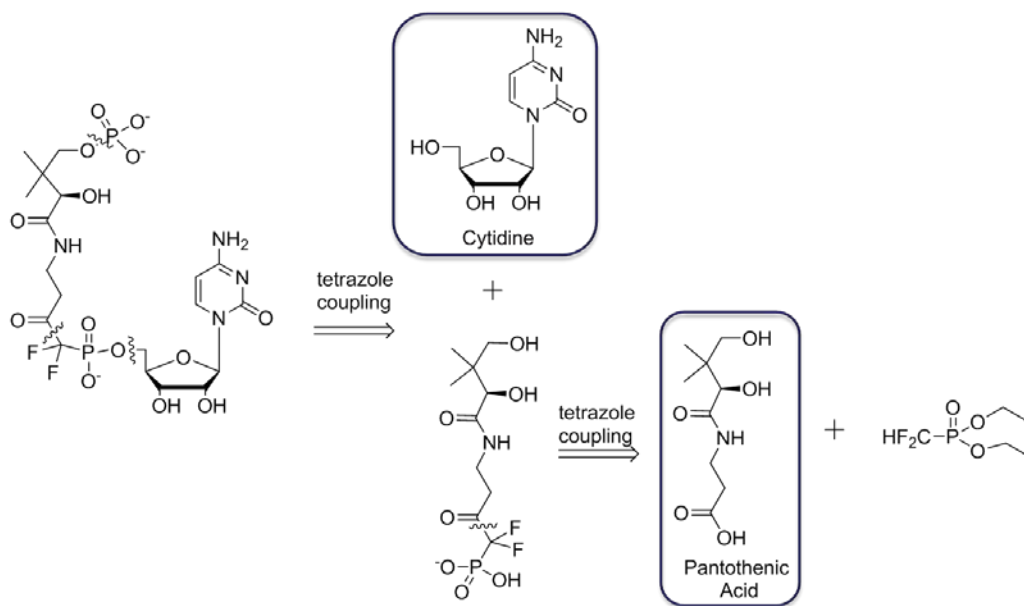
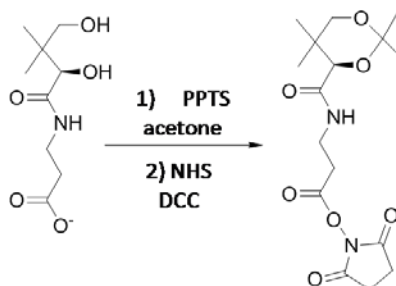


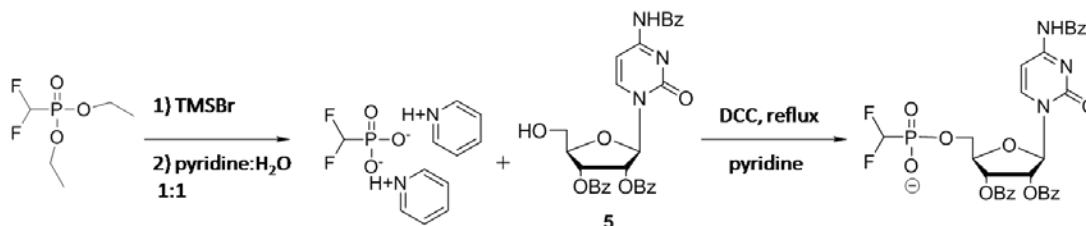
Figure 5.3: Retrosynthetic analysis of proposed difluorophosphonate mimic

The synthesis of the difluorophosphonate mimic begins with the protonation of pantothenate followed by protection of the 1,3 diol as an acetonide (**Scheme 5.1**). The acetonide was then activated as the NHS ester. Due to a lack of literature precedent for coupling of this type, the coupling of the difluorophosphonate to tribenzoyl cytidine before attempting the C-C bond formation involving the difluoromethyl phosphonate.⁶⁻⁹ The commercially available diethyl difluoromethyl phosphonate is treated with 4 equivalents of TMSBr for 18h followed by stirring in a 1:1 mixture of pyridine and water for 1h (**Scheme 5.2**). The resulting mixture was



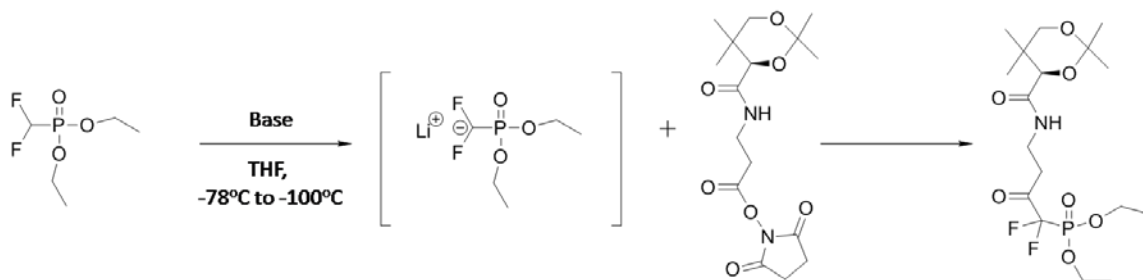
Scheme 5.1: Synthesis of NHS ester

azeotropically distilled with toluene (3 x 10mL).⁸ The deprotected phosphonate was then treated with tribenzoyl cytidine **5** and DCC in refluxing pyridine for 72 h.⁶ While the crude product was not isolated, the desired product was confirmed by 2D ³¹P, ¹H HMBC by the presence of a phosphorous signal that showed cross peaks with both the α proton of the phosphonate and the two 5' protons on the ribose ring of tribenzoyl cytidine

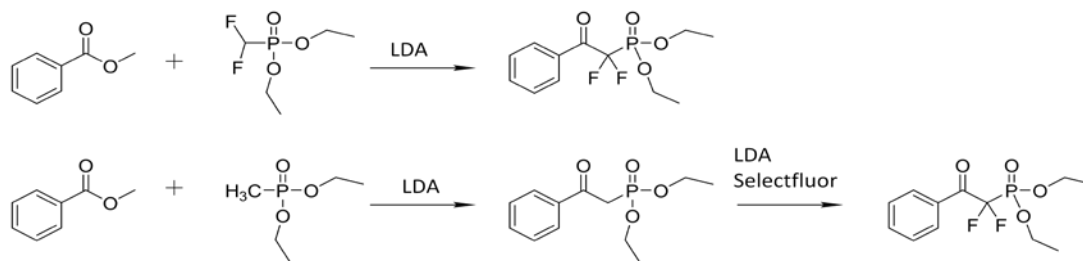


Scheme 5.2: Model reaction of DCC coupling

Having shown that a model difluorophosphonate could be coupled to tribenzoyl cytidine, the next goal was to form the C-C bond between the protected pantothenate molecule and the difluorophosphonate. The initial attempts to form the C-C bond, involved generating the lithium anion of the difluorophosphonate at -78°C and then dropwise addition of the electrophilic NHS ester.^{1-3, 5, 10-20} Anion generation with n-BuLi resulted in phosphonate degradation as seen by ³¹P NMR. However, anion generation at -78°C or -100°C followed by addition of the electrophile resulted in starting phosphonate by ³¹P NMR and the free acid on the pantothenate electrophile from the aqueous quench (**Scheme 5.3**). The base used to generate the difluorophosphonate anion was varied using LDA, n-BuLi, NaH, LiH, KHMDS, and Cs₂CO₃ along with the stir time of both the anion generation and nucleophilic attack, but none of these attempts were successful. The protecting group on the 1,3 diol was changed to a PMB acetal and the activated ester was changed to a pentafluorophenol ester. This electrophile was also unsuccessful.



Scheme 5.3: C-C bond forming reaction



Scheme 5.4: Model reaction of phosphonate linkage

In order to more systematically evaluate synthetic viability of this reaction, a very simplified model reaction employing methyl benzoate as the electrophilic ester and both the difluorinated and non-fluorinated diethyl methyl phosphonate (**Scheme 5.4**). Using this model system, I was able to link the non-fluorinated diethyl methyl phosphonate to methyl benzoate in 49.8% isolated yield, but was unable to link the difluorinated diethyl methyl phosphonate to methyl benzoate in any detectable amount.²¹ The phenylethylphosphonate was then taken forward and treated with two equivalents of LDA and 2 equivalents of Selectfluor for 2 h at room temperature yielding 10% of the desired difluorinated model phosphonate.²¹

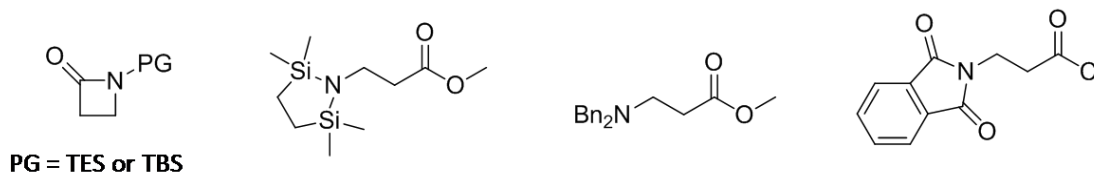
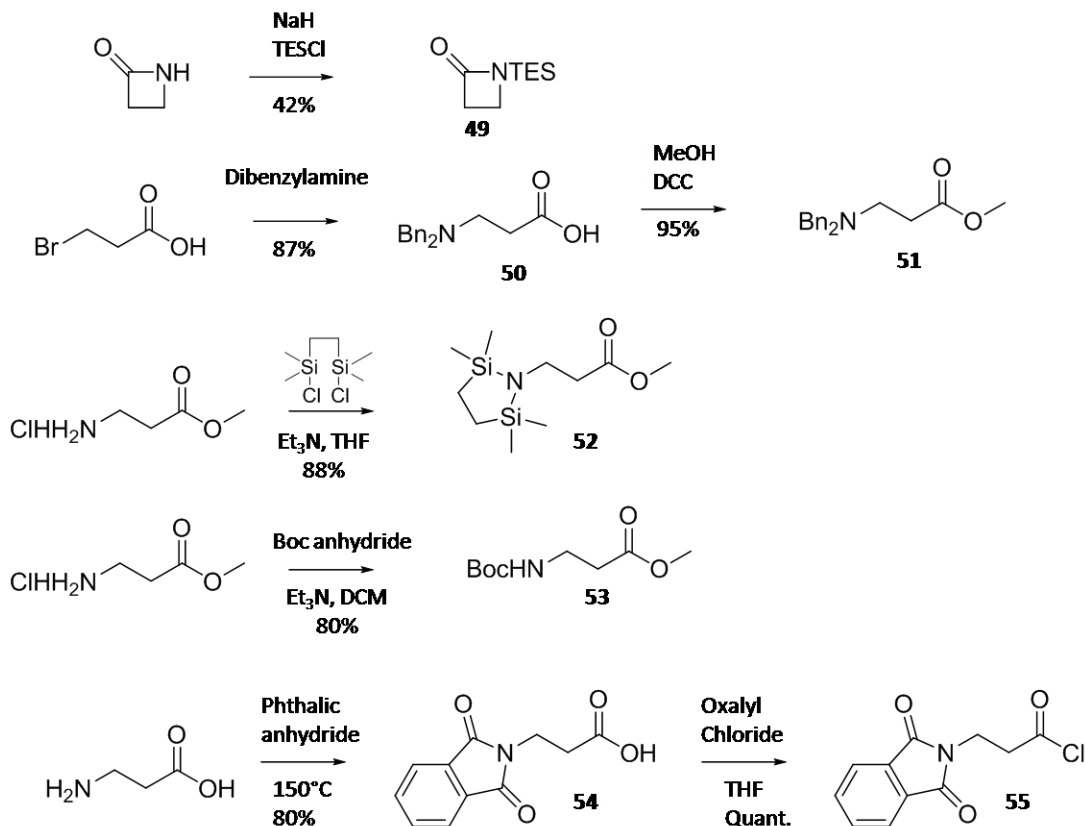


Figure 5.4: Alternative esters

Based upon the results from the model study, smaller and less functionalized esters of β -alanine were chosen to move forward with as the electrophile in the C-C bond forming reaction (**Figure 5.4**). The various β -alanine derivatives in **Figure 5.4** were synthesized from the appropriate starting materials (**Scheme 5.5**). Treating azetidinone with NaH and TESCl yielded the protected β -lactam **49**.²² 3-Bromopropionic acid was converted to methyl ester **51** by displacement of the bromide by dibenzylamine followed by standard esterification using DCC and methanol.²³ Protected methyl esters **52** and **53**



Scheme 5.5: Synthesis of β -alanine fragments

were made simply by protecting β -alanine methyl ester with 1,2-Bis(chlorodimethylsilyl)ethane and boc anhydride respectively.^{24, 25} Treating β -alanine with phthalic anhydride at 150°C and oxalyl chloride yielded the protected acyl chloride **55**.²⁶

Three equivalents of the lithium anion of methyl diethylphosphonate was generated at -78°C and then treated with the protected β -alanine derivatives **49**, **51**, **52**, **53**, and **55**. Compounds **49** and **55** did not yield the desired phosphonates under these conditions with **49** not reacting and **55** showing degradation of starting material. Methyl ester **51** provided less than 10% yield under the standard conditions, however, replacing the methyl ester with an activated pentafluorophenol (pfp) gave a 22% yield (**Figure 5.5**). The boc protected **53** gave a modest 52% yield of the desired phosphonate. Methyl ester **52** reacted smoothly under these conditions and upon the acidic work up of the reaction produced the diethyl phosphonate with the deprotected HCl salt of the amine in 82%.

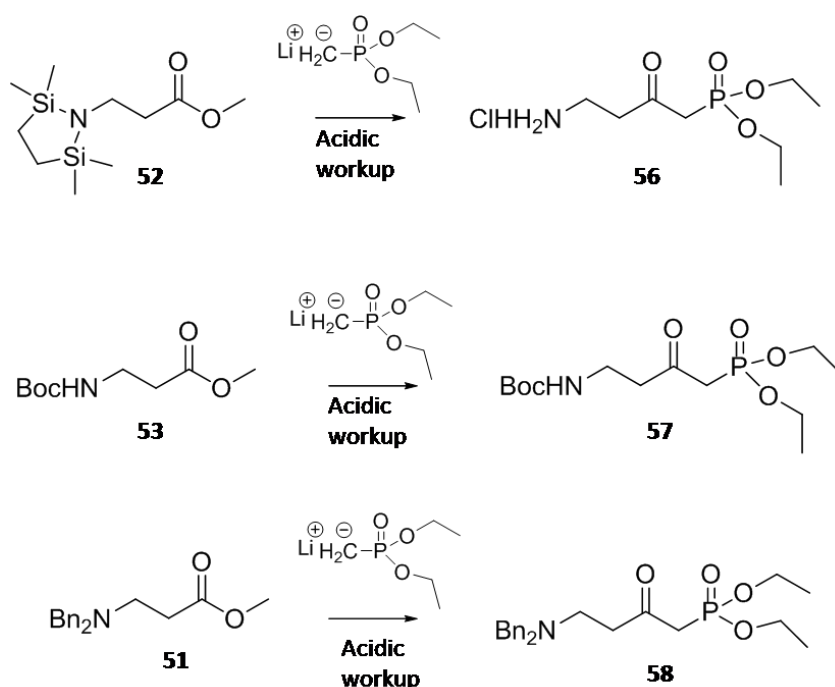


Figure 5.5: Synthesis of phosphonates

With the phosphonates in hand, the next step was the installation of the α difluoro functionality. In the case of phosphonate **56**, the primary amine had to be protected after the protecting group was lost during the acidic workup. Attempts to protect phosphonate A8 with either the original silyl protecting group or a boc group failed and resulted in degradation of the starting material. Alternatively, phosphonate **56** was taken forward and used to open pantolactone with intention of then protecting the diol. However, due to the acidic nature of the α protons and the electron withdrawing capability of the phosphonate the desired diol was only produced in less than 10%.

At this point focus was shifted to working with the already protected phosphonates **57** and **58**. Phosphonates **57** and **58** were treated with two equivalents of base and two equivalents of Selectfluor and N-fluorobenzenesulfonimide as the electrophilic source of fluorine (**Table 5.1**). The reactions were monitored by ^{31}P and ^{19}F NMR. None of the conditions tested yielded the desired difluorophosphonate. Treating both the boc protected and dibenzyl protected phosphonates **57** and **58** with the bases listed in **Table 5.1** with Selectfluor yielded no reaction by both ^{31}P and ^{19}F NMR and the starting phosphonate was recoverable. Exposing phosphonates **57** and **58** to similar reaction conditions except with N-fluorobenzenesulfonimide as the electrophilic source

of fluorine and DBU as the base, NMR showed no reaction had occurred.²⁷ However, when the stronger bases were employed the reaction conditions led to decomposition of the starting material. ³¹P NMR showed the disappearance of the starting phosphonate and the appearance of a new phosphorous peak that was not split into a triplet indicative of the phosphorous being coupled to fluorine. ¹⁹F NMR showed the starting material and several other fluorinated species. The only species that was isolated after column chromatography was the N-fluorobenzenesulfonimide. Attempts to shorten the reaction time or use only one equivalent of base in the fluorination were unsuccessful and led to no reaction with recovery of starting materials.

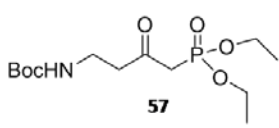
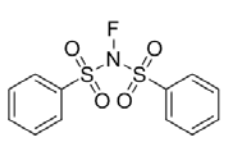
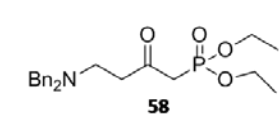
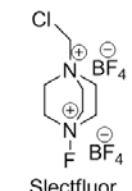
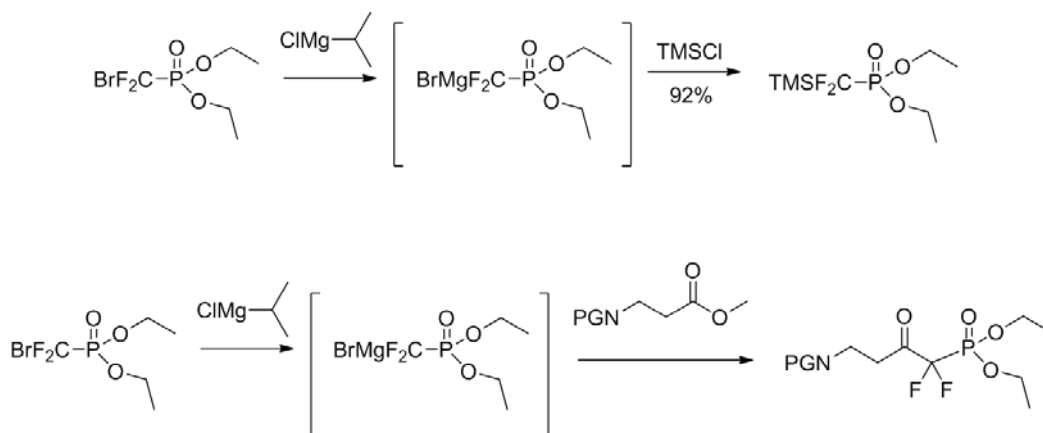
Phosphonate	Fluorine Source	Base
 <p>57</p>	 <p>N-Fluorobenzenesulfonimide</p>	<p>LDA, NaH, t-BuONa, DBU</p>
 <p>58</p>	 <p>Slectfluor</p>	<p>LDA, NaH, t-BuONa, DBU</p>

Table 5.1: Attempts to install electrophilic fluorine



Scheme 5.6: Alternative difluorophosphonate strategy

An alternative strategy was explored in which magnesium was inserted into carbon bromine bond of diethyl (bromodifluoromethyl)phosphonate and this species can be used as a nucleophile (**Scheme 5.5**).²⁸ According to the literature procedure, the silyl phosphonate was made in 92% yield.²⁸ This method was advantageous because of the ability to monitor the reaction progress by ¹⁹F NMR. The starting diethyl (bromodifluoromethyl)phosphonate gives a ¹⁹F doublet at -60 ppm while the quenched protonated difluorophosphonate gives a doublet at -130 ppm, and the difluorophosphonate a to a carbonyl gives a doublet at approximately -110 ppm. Two equivalents of the magnesium phosphonate species was generated in situ at -78°C for five minutes and then methyl esters **51-53** and acyl chloride **55** were added dropwise. ¹⁹F NMR revealed the protonated quenched phosphonates in all cases. This result could have been due to acidic protons on the β-alanine derivatives such as the benzylic protons on **51** or the amide proton on the boc protecting group on **53**, but the silyl derivative **52** and the acyl chloride **55** do not have these acidic protons.

To ascertain if the protonation event was caused by the β-alanine derivatives, a control reaction was run in which the magnesium phosphonate species was generated and then quenched using D₂O. In this case if the magnesium species was generated and sustained for five minutes and then quenched with D₂O, then the ¹⁹F NMR would have shown a doublet of triplets caused by the deuterium splitting the fluorine signal. However, the ¹⁹F NMR revealed only approximately 10% of the deuterated species and 90% of the protonated phosphonate. This result coupled with the fact that the magnesium phosphonate species should be stable at -78°C for several hours according to the literature report points to the fact that the reaction is being quenched before the addition of the electrophile presumably by a proton most likely due to moisture.²⁸ Great care was taken in an attempt to exclude moisture from the reaction, but I was not able to improve upon the amount of deuterated phosphonate generated and based upon the inability to generate the stable magnesium phosphonate species this synthetic strategy was abandoned.

Since the magnesium phosphonate species was not stable in our hands, the less reactive but more stable zinc phosphonate was explored as a more suitable nucleophile. In this methodology, zinc is inserted in the carbon bromide bond and this species is then

treated with an acyl chloride. This method has the advantage that the zinc inserted species is stable at room temperature for days.^{29, 30 31, 32} The zinc phosphonate species was generated in diglyme and then treated with freshly distilled acetyl chloride for 24 hrs. ¹⁹F NMR revealed a complex mixture of fluorinated species of which approximately 30% was the desired acylated difluorophosphonate. The desired product was not separable from the rest of the complicated mixture. The reaction was repeated with acyl chloride **55**. In this case, ¹⁹F NMR revealed a mixture of the starting diethyl (bromodifluoromethyl)phosphonate, the protonated difluorophosphonate, and several other fluorinated species that were not α to a carbonyl based upon the chemical shift.

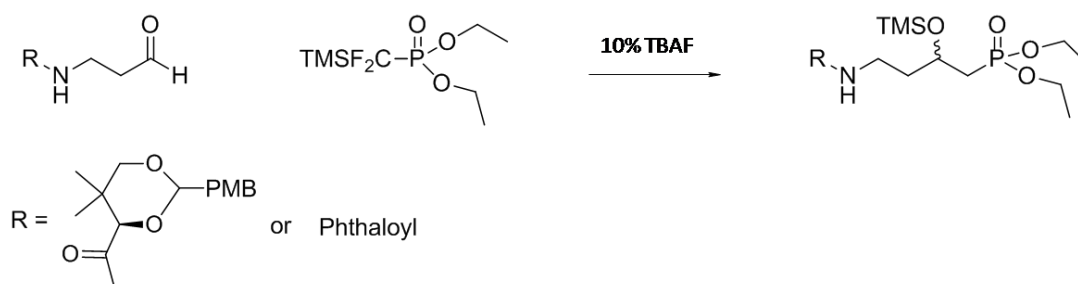


Figure 5.6: TBAF method of installing difluorophosphonate

The final attempt to install the α difluorophosphonate functionality was to use catalytic TBAF and the silyl difluorophosphonate (**Figure 5.6**). In this strategy, the TMS group on the difluorophosphonate is deprotected by the 10% TBAF. The generated anion can then attack the aldehyde and produce an oxyanion. The oxyanion can then attack the TMS group on another molecule of the silyl difluorophosphonate and allow the phosphonate to attack another molecule of the aldehyde. This method was attempted using both the PMB protected aldehyde **37** and the phthaloyl protected β -alanine derivative **35**. In both cases the reaction was stirred from 24 hrs to 72 hrs and the TBAF was varied from 10% up to 50%. Monitoring the reaction by ¹H NMR showed that the aldehyde signal persisted and thus no reaction had taken place.

At this point, the difluorophosphonate was abandoned due to the difficulty encountered installing the desired functionality. The difluorophosphonate is still an attractive target for a mechanism-based probe; however, installing the functionality was not feasible at this time. Using isopropyl magnesium chloride and forming the magnesium phosphonate species was the method that displayed the most success and was easily monitored by ¹⁹F NMR. This method may still be optimized in the future if the

magnesium phosphonate species can be generated and persist at -78°C . Conducting the reaction in a glove box may provide a more anhydrous environment and thus allow for the magnesium insertion and productive bond formation.

Materials & Methods

General Methods: All chemicals were used as purchased from Acros, Fisher, Fluka, Sigma-Aldrich, or Specialty Chemicals Ltd. and used without further purification unless otherwise noted. ^1H NMR, ^{13}C NMR, and ^{31}P NMR spectra were recorded on a Bruker Avance DRX 500MHz spectrometer or Bruker Avance DPX 300MHz spectrometer. Proton assignments are reported in ppm from an internal standard of TMS (0.0ppm), and phosphorous assignments are reported relative to an external standard of 85% H_3PO_4 (0.0ppm). Proton chemical data are reported as follows: chemical shift, multiplicity (ovlp = overlapping, s = singlet, d = doublet, t = triplet, q = quartet, p = pentet, m = multiplet, br = broad), coupling constant in Hz, and integration. All high resolution mass spectra were acquired from the Mass Spectrometry facility in the Chemistry Department at The University of Michigan using either positive-ion or negative-ion mode ESI-MS. Thin layer chromatography was performed using Analtech GHLF 250 micron silica gel TLC plates. All flash chromatography was performed using grade 60 Å 230-400 mesh silica purchased from Fisher.

1-(triethylsilyl)azetidin-2-one (49) 60% NaH (80 mg, 2 mmol) was suspended in anhydrous THF (2 mL). Azetidinone (142 mg, 2 mmol) in anhydrous THF (2 mL) was added dropwise and stirred for 5 min. TESC1 (0.352 mL, 2.1 mmol) was added dropwise and the reaction was stirred for 4 hrs. The reaction was quenched with water (1 mL) and then solvents were removed *in vacuo*. The resulting yellow syrup was purified over silica (25 mL) eluting with 25% EtOAc in hexanes (100 mL) and 50% EtOAc in hexanes (100 mL) to yield the desired product as a clear oil (214 mg, 42%). ^1H NMR ($\text{DMSO}-d_6$): δ 3.32 (t, $J = 5.10$ Hz, 2H), 3.06 (t, $J = 5.10$ Hz, 2H), 1.09 (t, $J = 6.10$ Hz, 6H), 0.88 (q, $J = 6.10$ Hz, 9H).

3-(dibenzylamino)propanoic acid (50) Dibenzylamine (0.961 mL, 5mmol) was dissolved in anhydrous toluene (7 mL). Triethylamine (1.4 mL, 10 mmol) was added and stirred for 15 min. 3-Bromopropionic acid (765 mg, 5 mmol) was added and the reaction

was heated to reflux for 12 hrs. The reaction was cooled to rt and then filtered. The solvents were removed in vacuo and the resulting syrup was purified over silica (50 mL) eluting with 25% EtOAc in hexanes (150 mL), 50% EtOAc in hexanes (50 mL), and EtOAc (150 mL) to yield the desired product as an oil (1.17 g, 87%). ¹H NMR (DMSO-*d*₆): δ 7.36-7.31 (m, 6H), 7.25 (t, *J* = 6.50 Hz, 2H), 3.34 (s, 4H), 2.65 (t, *J* = 7.40 Hz, 2H), 2.43 (t, *J* = 7.30 Hz, 2H). ¹³C NMR (DMSO-*d*₆): δ 174.13, 139.59, 128.98, 128.64, 127.33, 57.54, 49.00, 32.39, 14.55.

methyl 3-(dibenzylamino)propanoate (51) 3-(dibenzylamino)propanoic acid (**50**) (383 mg, 1.42 mmol) was dissolved in anhydrous THF (5 mL). DCC (293 mg, 1.42 mmol) was added and stirred for 15 min. Anhydrous MeOH (0.18 mL, 4.27 mmol) was added and the reaction was allowed to stir for 4 hrs. The reaction was filtered and the solvents were removed in vacuo to yield the desired product (381 mg, 95%). ¹H NMR (DMSO-*d*₆): δ 7.35-7.29 (m, 6H), 7.26-7.23 (m, 2H), 3.57 (s, 3H), 3.34 (s, 4H), 2.65 (t, *J* = 7.40 Hz, 2H), 2.43 (t, *J* = 7.30 Hz, 2H). ¹³C NMR (DMSO-*d*₆): δ 174.13, 139.59, 128.98, 128.64, 127.33, 57.54, 55.41, 49.00, 32.39, 14.55. ESI-MS: calcd for [M+H]⁺, 284.15; found 284.1.

methyl 3-(2,2,5,5-tetramethyl-1,2,5-azadisilolidin-1-yl)propanoate (52) β-alanine methyl ester was dissolved in anhydrous DCM (10 mL). Triethylamine (4.17 mL) was added and stirred at rt for 30 min. The solution was cooled to 0°C for 30 min. 1,2-Bis(chlorodimethylsilyl)ethane (2.15g, 10 mmol) in anhydrous DCM (10 mL) was added dropwise. The reaction was stirred at 0°C for 2 hrs and then warmed to rt for 1 hr. The reaction was diluted into 125 mL DCM and then washed with H₂O) (2 x 25 mL). The organic layer was dried (Na₂SO₄) and evaporated in vacuo to yield the desired product as 2.28 g of a clear oil (88%). ¹H NMR (DMSO-*d*₆): δ 3.59 (s, 3H), 3.06 (t, *J* = 4.5 Hz, 2H), 2.37 t, *J* = 7.1 Hz, 2H), 0.65 (s, 4H), 0.04 (s, 12H). ¹³C NMR (DMSO-*d*₆): δ 172.55, 51.61, 39.06, 38.24, 8.16, 0.29.

methyl 3-((tert-butoxycarbonyl)amino)propanoate (53) β-Alanine methyl ester (1g, 7.16 mmol) was dissolved in anhydrous DCM (15mL). Triethylamine (3.0 mL, 21.48 mmol) was added and allowed to stir for 15 min. Boc anhydride (1.72g, 7.88 mmol) was added and the reaction was allowed to stir overnight. The reaction was partitioned between DCM and H₂O. The DCM layer was dried (Na₂SO₄) and evaporated in vacuo

to yield the desired product as a clear oil (1.15g, 80%). ^1H NMR (DMSO- d_6): δ 6.87 (s, 1H), 3.58 (s, 3H), 3.14 (q, $J = 5.65, 7.00$ Hz, 2H), 2.42 (t, $J = 6.95$ Hz, 2H), 1.37 (s, 9H). ^{13}C NMR (DMSO- d_6): δ 172.16, 155.92, 78.15, 51.80, 36.54, 34.55, 28.67.

3-(1,3-dioxoisindolin-2-yl)propanoic acid (54) β -Alanine (4.49g, 52.16 mmol) and phthalic anhydride (7.4g, 52.16 mmol) were placed in an open flask with a magnetic stir bar. The two solids were heated to 150°C for 2 hrs. The reaction was cooled to rt and H₂O was added. The reaction was filtered and dried under vacuum to yield the desired product as a white crystalline solid (9.1g, 80%). ^1H NMR (DMSO- d_6): δ 12.39 (s, 1H) 7.80 (s, 4H), 3.77 (d, $J = 7.26$ Hz, 2H), 2.60 (d, $J = 7.26$ Hz, 2H). ^{13}C NMR (DMSO- d_6): δ 172.61, 168.00, 162.34, 134.76, 131.99, 123.39, 32.99, 32.79.

3-(1,3-dioxoisindolin-2-yl)propanoyl chloride (55) Phthathoyl β -alanine (1g, 4.58 mmol) was dissolved in anhydrous DCM (10 mL). To this heterogeneous mixture was added anhydrous dioxane (2 drops). Oxalyl chloride (0.52 mL, 5.96 mmol) was added and the reaction was stirred overnight. The solvents were removed in vacuo to yield the desired acyl chloride as a white solid (quantitative). ^1H NMR (DMSO- d_6): δ 7.90-7.86 (m, 2H), 7.79-7.75 (m, 2H), 4.06 (t, $J = 6.96$ Hz, 2H), 3.36 (t, $J = 6.96$ Hz, 2H). ^{13}C NMR (DMSO- d_6): δ 1171.43, 167.70, 134.31, 131.80, 123.56, 44.96, 33.21.

diethyl (4-amino-2-oxobutyl)phosphonate hydrochloride (56) Diethyl methylphosphonate (1.07 mL, 7.1 mmol) and 3Å molecular sieves were dissolved in anhydrous THF (2 mL) and the solution was cooled to -78°C. n-BuLi (4.4 mL, 7.1 mmol) was added dropwise and allowed to stir for 45 min. Methyl ester **52** (580 mg, 2.37 mmol) in anhydrous THF (2 mL) was added dropwise and the reaction was stirred for 2 hrs. The reaction was quenched with saturated ammonium chloride. The reaction was diluted with ether and portioned between ether and saturated ammonium chloride. The ethereal extract was then washed with 1M HCl (2.4 mL). The water layer was then concentrated in vacuo to yield the HCl salt of the desired product. ^1H NMR (DMSO- d_6): δ 7.99 (s, br, 3H), 4.05 (p, $J = 7.20$ Hz, 4H), 3.35 (d, $J = 22.20$ Hz, 2H), 2.98 (d, $J = 6.1$ Hz, 2H), 2.94 (t, $J = 5.70$ Hz, 2H), 1.25 (t, $J = 7.0$ Hz, 6H). ^{31}P NMR (DMSO- d_6): δ 20.12 (s, 1P).

diethyl (4-(dibenzylamino)-2-oxobutyl)phosphonate (57) Diethyl methylphosphonate (1.65 mL, 11.27 mmol) and 3Å molecular sieves were dissolved in anhydrous THF (3

mL) and the solution was cooled to -78°C . n-BuLi (7.0 mL, 11.27 mmol) was added dropwise and allowed to stir for 45 min. The pfp ester of 3-(dibenzylamino)propanoic acid (1.64 g, 3.75 mmol) in anhydrous THF (3 mL) was added dropwise and the reaction was stirred for 2 hrs. The reaction was quenched with saturated ammonium chloride. Solvents were removed in vacuo and the resulting syrup was purified over silica (50 mL) eluting with 25% EtOAc in hexanes (150 mL), 50% EtOAc in hexanes (150 mL), and 75% EtOAc in hexanes (150 mL) to yield the desired product (340 mg, 22%). ^1H NMR (DMSO- d_6): δ 7.36-7.32 (m, 6H), 7.26-7.23 (m, 2H), 4.02-3.99 (m, 4H), 3.12 (d, $J = 22.05$ Hz, 2H), 2.82 (t, $J = 7.05$ Hz, 2H), 2.62 (t, $J = 7.05$ Hz, 2H), 1.20 (t, $J = 7.00$ Hz, 6H). ^{13}C NMR (DMSO- d_6): δ 202.21, 139.56, 129.03, 128.68, 127.38, 62.17, 57.58, 47.50, 41.24, 16.59.

References

1. Blackburn, G. M. B., David; Martin, Stephen J.; Parratt, Martin J., Studies on selected transformations of some fluoromethanephosphonate esters. *J. Chem. Soc. Perk. Trans. I* **1987**, 181-187.
2. Hakogi, T.; Hakogi, T., Synthesis of sphingomyelin difluoromethylene analog. *Tetrahedron letters* **2006**, 47, (15), 2627.
3. Yokomatsu, T.; Yokomatsu, T., Synthesis of non-competitive inhibitors of Sphingomyelinases with significant activity. *Bioorganic & medicinal chemistry letters* **2003**, 13, (2), 229.
4. Cox, R. J.; Hadfield, A. T.; Mayo-Martin, M. B., Difluoromethylene analogues of aspartyl phosphate: the first synthetic inhibitors of aspartate semi-aldehyde dehydrogenase. *Chemical Communications* **2001**, (18), 1710-1711.
5. Cox, R. J.; Cox, R., Aspartyl phosphonates and phosphoramidates: the first synthetic inhibitors of bacterial aspartate-semialdehyde dehydrogenase. *Chembiochem* **2002**, 3, (9), 874.
6. Myers, T. C.; Myers, T., Phosphonic acid analogs of nucleoside phosphates. III. The synthesis of adenosine 5'-methylendiphosphonate, a phosphonic acid analog of adenosine 5'-diphosphate. *Journal of organic chemistry* **1965**, 30, (5), 1517.
7. Casara, P. J.; Casara, P., Synthesis of acid stable 5'-O-fluoromethyl phosphonates of nucleosides. Evaluation as inhibitors of reverse transcriptase. *Bioorganic & medicinal chemistry letters* **1992**, 2, (2), 145.
8. Shirokova, E. A.; Jasko, M. V.; Khandazhinskaya, A. L.; Ivanov, A. V.; Yanvarev, D. V.; Skoblov, Y. S.; Pronyaeva, T. R.; Fedyuk, N. V.; Pokrovskii, A. G.; Kukhanova, M. K., New Phosphonoformic Acid Derivatives of 3'-Azido-3'-Deoxythymidine. *Russian journal of bioorganic chemistry* **2004**, 30, (3), 242.
9. Jasko, M. V.; Shipitsyn, A. V.; Khandazhinskaya, A. L.; Shirokova, E. A.; Solyev, P. N.; Plyasunova, O. A.; Pokrovskii, A. G., New derivatives of alkyl- and aminocarbonylphosphonic acids containing 3'-azido-3'-deoxythymidine. *Russian journal of bioorganic chemistry* **2006**, 32, (6), 542.
10. Berkowitz, D. B.; Berkowitz, D., Ready Access to Fluorinated Phosphonate Mimics of Secondary Phosphates. Synthesis of the (α,α -Difluoroalkyl)phosphonate Analogs of L-Phosphoserine, L-Phosphoallothreonine, and L-Phosphothreonine. *Journal of organic chemistry* **1996**, 61, (14), 4666.
11. Liu, H.; Liu, H.-J., Organocerium compounds in synthesis. *Tetrahedron* **1999**, 55, (13), 3803.
12. Blades, K.; Blades, K., A reproducible and high-yielding cerium-mediated route to α,α -difluoro- β -ketophosphonates. *Tetrahedron* **1997**, 53, (30), 10623.
13. Pham, V.; Pham, V., Design and Synthesis of Novel Pyridoxine 5'-Phosphonates as Potential Antiischemic Agents. *Journal of medicinal chemistry* **2003**, 46, (17), 3680.
14. Maring, C. J.; Maring, C., Structure-Based Characterization and Optimization of Novel Hydrophobic Binding Interactions in a Series of Pyrrolidine Influenza Neuraminidase Inhibitors. *Journal of medicinal chemistry* **2005**, 48, (12), 3980.
15. Pan, Y.; Pan, Y., Design, Synthesis, and Biological Activity of a Difluoro-Substituted, Conformationally Rigid Vigabatrin Analogue as a Potent- γ -Aminobutyric Acid Aminotransferase Inhibitor. *Journal of medicinal chemistry* **2003**, 46, (25), 5292.

16. Rajwanshi, V. K.; Rajwanshi, V., Synthesis of 5'-triphosphate mimics (P3Ms) of 3'-azido-3',5'-dideoxy-thymidine and 3',5'-dideoxy-5'-difluoromethylene-thymidine as HIV-1 reverse transcriptase inhibitors. *Nucleosides, nucleotides & nucleic acids* **2005**, 24, (3), 179.
17. Fox, D. T.; Fox, D., Synthesis and Evaluation of 1-Deoxy-D-xylulose 5-Phosphoric Acid Analogues as Alternate Substrates for Methylerythritol Phosphate Synthase. *Journal of organic chemistry* **2005**, 70, (6), 1978.
18. Pfund, E.; Lequeux, T.; Masson, S.; Vazeux, M.; Cordi, A.; Pierre, A.; Serre, V.; Hervé, G., Efficient synthesis of fluorothiosparfosic acid analogues with potential antitumoral activity. *Bioorganic & medicinal chemistry* **2005**, 13, (16), 4921.
19. Li, X.; Li, X., α,α -Difluoro- β -ketophosphonates as potent inhibitors of protein tyrosine phosphatase 1B. *Bioorganic & medicinal chemistry letters* **2004**, 14, (16), 4301.
20. Liu, H. J. a. n. g.; Liu, H., Efficient addition of cerium(III) enolate of ethyl acetate to ketones: application to the synthesis of β -ethoxycarbonylmethyl α,β -unsaturated ketones. *Canadian Journal of Chemistry* **1991**, 69, (12), 2008.
21. Sylvain, L.; Michèle, W.; Jacques, P., A Convenient Synthesis of Dibenzyl α,α -Difluoromethyl- β -ketophosphonates. *European Journal of Organic Chemistry* **2002**, 2002, (15), 2640-2648.
22. Urbach, A.; Muccioli, G. G.; Stern, E.; Lambert, D. M.; Marchand-Brynaert, J., 3-Alkenyl-2-azetidiones as fatty acid amide hydrolase inhibitors. *Bioorganic & medicinal chemistry letters* **2008**, 18, (14), 4163-4167.
23. Erhardt, P. W., Benzylamine and dibenzylamine revisited. Syntheses of N-substituted aryloxypropanolamines exemplifying a general route to secondary aliphatic amines. *Synthetic Communications* **1983**, 13, (2), 103-113.
24. Djuric, S.; Venit, J.; Magnus, P., Silicon in synthesis: stabase adducts - a new primary amine protecting group: alkylation of ethyl glycinate. *Tetrahedron letters* **1981**, 22, (19), 1787-1790.
25. Hattori, K.; Yamamoto, H., Highly selective enolization method for heteroatom substituted esters; its application to the Ireland ester enolate Claisen rearrangement. *Tetrahedron* **1994**, 50, (10), 3099-3112.
26. Gérald, L.; Peter, M.; Delphine, J.-L.; Francesco, R.; Dieter, S., Preparation of Protected β -Homocysteine, β -Homohistidine, and β -Homoserine for Solid-Phase Syntheses. *Helvetica Chimica Acta* **2004**, 87, (12), 3131-3159.
27. Differding, E. D., Rudolf O.; Krieger, Arlette; Rueegg, Gabriela M.; Schmit, Chanta, Electrophilic fluorinations with N-fluorobenzenesulfonimide: convenient access to α -fluoro- and α,α -difluorophosphonates. *Synlett* **1991**, 6, 395-6.
28. Waschbüsch, R.; Samadi, M.; Savignac, P., A useful magnesium reagent for the preparation of 1,1-difluoro-2-hydroxyphosphonates from diethyl bromodifluoromethylphosphonate via a metal-halogen exchange reaction. *Journal of Organometallic Chemistry* **1997**, 529, (1-2), 267-278.
29. Han, S.; Moore, R. A.; Viola, R. E., A Facile Synthesis of a Difluoromethylene Analog of β -Aspartyl Phosphate as an Inhibitor of L-Aspartate- β -semialdehyde Dehydrogenase. *Synlett* **2003**, 2003, (06), 0845-0846.
30. Burton, D. J., Ishihara, T., Maruta, M., A useful zinc reagent for the preparation of 2-oxo-1,1-difluoroalkylphosphonates. *Chemistry Letters* **1982**, 5, 755-758.

31. Burton, D. J.; Sprague, L. G.; Pietrzyk, D. J.; Edelmuth, S. H., A safe practical synthesis of difluorophosphonoacetic acid. *The Journal of Organic Chemistry* **1984**, 49, (18), 3437-3438.
32. Burton, D. J.; Sprague, L. G., Preparation of difluorophosphonoacetic acid and its derivatives. *The Journal of Organic Chemistry* **1988**, 53, (7), 1523-1527.

Chapter 6

Conclusion

PPCS is the second enzyme in the CoA biosynthetic pathway and catalyzes the amide bond formation between PPA and L-cysteine, which is responsible for the installation of the biologically active thiol of phosphopantetheine.^{1, 2} PPCS is broadly classified into three types (Type I-III) based upon nucleotide triphosphate preference and whether it is expressed as fusion protein with PPCDC or as a monofunctional enzyme. Type I PPCSs are found in a majority of bacteria and archaea, utilize CTP for activation of PPA in the first half reaction, and are expressed as the C-terminal domain of a fusion protein with PPCDC. Type II PPCSs are found in eukaryotes, utilize both CTP and ATP, and expressed separately from PPCDC as a monofunctional enzyme. Type III PPCSs are found in certain bacteria, utilize CTP in the first half reaction of PPCS, and are expressed as a monofunctional enzyme.³ Based upon the difference in PPCS type, nucleotide triphosphate preference, sequence similarity between human and bacteria, and the fact that PPCS is essential for bacterial growth, PPCS was chosen for exploration as a potential novel antibacterial target.

Initially four intermediate mimics were designed based upon the activated cytidylate intermediate formed during bacterial PPCS catalysis (**Figure 6.1**). These

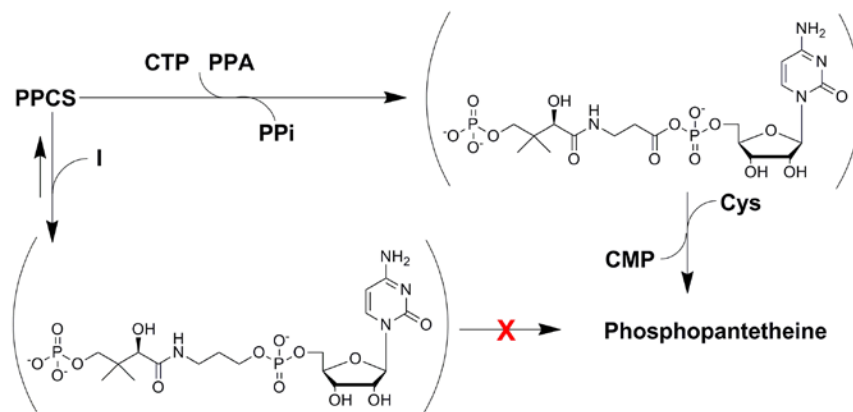
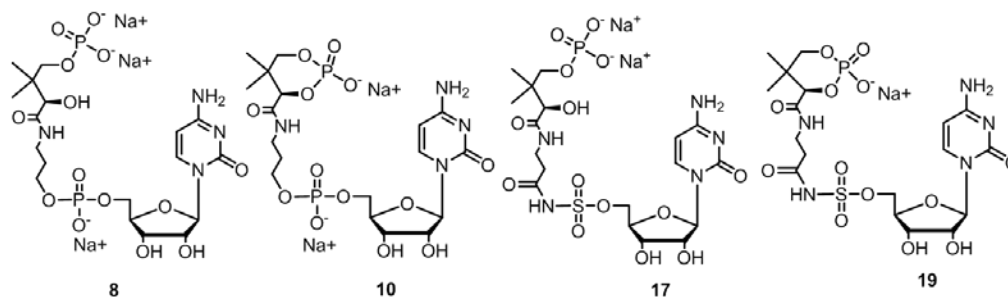


Figure 6.1: Mechanism of intermediate mimic inhibition.

intermediate mimics were designed to take advantage the natural binding contacts of the activated intermediate and utilize the cytidine portion of the molecule as a selectivity handle for bacterial PPCS over human PPCS. The two phosphodiester mimics (**8** and **10**) and the two sulfamate mimics (**17** and **19**) were synthesized in twelve steps with an average yield of 18%. The intermediate mimics were evaluated as inhibitors against PPCS from *E. coli*, *E. faecalis*, *S. pneumoniae*, and human (**Figure 6.2**). Phosphodiester **8** was the most potent inhibitor with IC₅₀ values ranging from 10-68 nM and 100-1000 fold selectivity for bacterial PPCS over human PPCS. The most potent compound was also shown to be a tight binding, slow onset inhibitor with respect to efPPCS with a *K_i* of 24 nM. These molecules were the first selective inhibitors of bacterial PPCS and provide the foundation for further exploration of PPCS as antibacterial target.



	<i>E. Coli</i> (I)	<i>E. Faecalis</i> (III)	<i>S. Pneumoniae</i> (III)	Human (II)
8	68 nM (9)	65 nM (9)	10 nM (2)	10 μM (1)
10	3.0 μM (0.3)	18 μM (5)	13 μM (4)	3 mM (0.2)
17	270 nM (3)	2.7 μM (0.3)	3.9 μM (0.2)	200 μM (11)
19	16 μM (5)	180 μM (7)	280 μM (27)	5.9 mM (0.6)

Figure 6.2: Selective inhibitors of PPCS. Standard error in parentheses

These first generation inhibitors were used as probes in a crystallographic study to establish the binding determinants of inhibitor potency. The structures of phosphodiester **8**, cyclic phosphodiester **10**, and sulfamate **17** mimics bound to PPCS were solved to 2.37 Å, 2.30 Å, and 2.11 Å, respectively. The structure of phosphodiester **8** bound to wild type *E. coli* PPCS domain was very similar to the intermediate bound PPCS mutant structure reported in literature. Sulfamate **17** binds to PPCS in the same manner as phosphodiester **8** with the decrease in potency most likely due to the lack of Lys289 forming a contact with sulfamate **17**. The structure of cyclic phosphodiester **10** bound PPCS varied greatly

from the other structures. In order for the cyclic phosphate moiety to bind in the terminal phosphate binding cradle, the gem dimethyl group must orient itself towards Asn353 and prevent the flexible binding clamp from closing on the inhibitor.

While there are many known mimics of pantothenate, there are few known mimics of PPA.⁶ The disulfide compound **24** was the first PPA mimic chemically synthesized and shown to be an inhibitor of PPCS. The reduced form of PPA mimic **24** was shown to be competitive with respect to PPA and have a K_i of 12 μM . Although this molecule does not contain a moiety designed to give it selectivity for bacterial PPCS over human PPCS, this mimic proves that low micromolar inhibition is possible with a low molecular weight molecule and that the whole active site does not have to be occupied in order to inhibit PPCS catalysis.

Attempts to synthesize mechanistic traps designed to react with substrate cysteine in the second half reaction of PPCS were unsuccessful. A difluorophosphonate and a vinyl sulfone were designed to undergo nucleophilic attack of cysteine in the second half reaction. However, the difluorophosphonate moiety was not able to be installed into a panthenol or β -alanine portion of the intermediate mimic. The targeted vinyl sulfone compound synthesis seems more obtainable with a vinyl sulfone being installed into three different β -alanine/panthenol molecules. Although these vinyl sulfones were not successfully coupled to a cytidine moiety, they may prove useful as PanK inhibitors or PanK-activated inhibitors.

This study was significant because it produced the first selective inhibitors of PPCS and the first synthetic PPA mimic to inhibit PPCS. These inhibitors of PPCS provide a proof of concept that PPCS can be selectively inhibited at a low micromolar to low nanomolar potency, and up to 1000 fold selectivity for the bacterial PPCS over human PPCS. Going forward, the information gathered from the crystal structures of our various intermediate mimics bound to PPCS, coupled with the *in vitro* PPCS inhibition results, provide the foundation for the design of 2nd generation inhibitors with improved physiochemical properties to allow cellular entry. It may be possible to modify several of these molecules by replacing the terminal phosphate moiety with a neutral isostere, such as a triazole, in order to improve their chances of cellular entry and allow for the first inhibitor of PPCS to prevent bacterial growth

References

1. Brown, G. M., The Metabolism of Pantothenic Acid. *Journal of Biological Chemistry* **1959**, 234, (2), 370-378.
2. Stanitzek, S.; Augustin, M. A.; Huber, R.; Kupke, T.; Steinbacher, S., Structural Basis of CTP-Dependent Peptide Bond Formation in Coenzyme A Biosynthesis Catalyzed by Escherichia coli PPC Synthetase. *Structure* **2004**, 12, (11), 1977-1988.
3. Yao, J. W.; Dotson, G. D., Kinetic characterization of human phosphopantothenoylcysteine synthetase. *Biochimica Et Biophysica Acta-Proteins and Proteomics* **2009**, 1794, (12), 1743-1750.
4. Kupke, T., Molecular Characterization of the 4'-Phosphopantothenoylcysteine Synthetase Domain of Bacterial Dfp Flavoproteins. *J. Biol. Chem.* **2002**, 277, (39), 36137-36145.
5. Yao, J.; Patrone, J. D.; Dotson, G. D., Characterization and Kinetics of Phosphopantothenoylcysteine Synthetase from Enterococcus faecalis. *Biochemistry* **2009**, 48, (12), 2799-2806.
6. Spry, C.; Kirk, K.; Saliba, K. J., Coenzyme A biosynthesis: an antimicrobial drug target. *Fems Microbiology Reviews* **2008**, 32, (1), 56-106.